

# **BIODEGRADABLE MULTIFUNCTIONAL NANOCARRIERS FOR pDNA and siRNA DELIVERY**

Dissertation

zur Erlangung des Doktorgrades der Naturwissenschaften (Dr. rer. nat.)

dem

Fachbereich Pharmazie der Philipps-Universität Marburg

vorgelegt von

Mengyao Zheng  
aus Beijing, China

Marburg/Lahn 2012

Vom Fachbereich Pharmazie der Philipps-Universität Marburg als Dissertation am 02.07.2012  
angenommen.

Erstgutachter: Prof. Dr. Thomas Kissel

Zweitgutachterin: Prof. Dr. Seema Agarwal

Tag der mündlichen Prüfung: 04.07.2012

Die vorliegende Arbeit entstand auf Anregung und unter Leitung von

*Herrn Prof. Dr. Thomas Kissel*

am Institut für Pharmazeutische Technologie und Biopharmazie  
der Philipps-Universität Marburg.

# TABLE OF CONTENTS

<b>1</b>	<b>INTRODUCTION.....</b>	<b>8</b>
1.1	Nanomedicine and Non-Viral Delivery of Nucleic Acids.....	9
1.2	Targeted Gene Delivery Using Cell Specific Ligands.....	10
1.3	Polymers and Dendrimers in Gene Delivery .....	11
1.4	Pulmonary Gene Delivery .....	14
1.5	Structure of the Thesis: Aims and Outline .....	15
1.6	References .....	16
<b>2</b>	<b>TARGETING THE BLIND SPOT OF POLYCATIONIC NANOCARRIER-BASED SIRNA DELIVERY .....</b>	<b>19</b>
2.1	Abstract.....	20
2.2	Introduction.....	20
2.3	Results and Discussion.....	23
2.4	Conclusion .....	28
2.5	Materials and Methods.....	28
2.6	Acknowledgements.....	29
2.7	Supporting informations.....	29
2.8	References .....	33
<b>3</b>	<b>AMPHIPHILIC AND BIODEGRADABLE hy-PEI-g-PCL-b-PEG COPOLYMERS EFFICIENTLY MEDIATE TRANSGENE EXPRESSION DEPENDING ON THEIR GRAFT DENSITY .....</b>	<b>36</b>
3.1	Abstract.....	37
3.2	Introduction .....	37

<b>3.3</b>	<b>Methods and Materials .....</b>	<b>39</b>
<b>3.4</b>	<b>Results and Discussion.....</b>	<b>43</b>
<b>3.5</b>	<b>Conclusion.....</b>	<b>50</b>
<b>3.6</b>	<b>Acknowledgements .....</b>	<b>51</b>
<b>3.7</b>	<b>References .....</b>	<b>51</b>
<b>4</b>	<b>ENHANCING IN VIVO CIRCULATION AND SIRNA DELIVERY WITH BIODEGRADABLE POLYETHYLENIMINE-GRAFT-POLYCAPROLACTONE-BLOCK-POLY(ETHYLENE GLYCOL) COPOLYMERS .....</b>	<b>54</b>
<b>4.1</b>	<b>Abstract .....</b>	<b>55</b>
<b>4.2</b>	<b>Introduction .....</b>	<b>55</b>
<b>4.3</b>	<b>Methods and materials .....</b>	<b>57</b>
<b>4.4</b>	<b>Results and Discussion.....</b>	<b>60</b>
<b>4.5</b>	<b>Conclusion.....</b>	<b>70</b>
<b>4.6</b>	<b>Acknowledgements .....</b>	<b>71</b>
<b>4.7</b>	<b>References .....</b>	<b>71</b>
<b>5</b>	<b>MODULAR SYNTHESIS OF FOLATE CONJUGATED TERNARY COPOLYMERS: POLYETHYLENIMINE-GRAFT-POLYCAPROLACTONE-BLOCK-POLY(ETHYLENE GLYCOL)-FOLATE FOR TARGETED GENE DELIVERY DELIVERY .....</b>	
<b>5.1</b>	<b>Abstract .....</b>	<b>75</b>
<b>5.2</b>	<b>Introduction .....</b>	<b>75</b>
<b>5.3</b>	<b>Experimental Section.....</b>	<b>77</b>
<b>5.4</b>	<b>Results and Discussion.....</b>	<b>84</b>

<b>5.5</b>	<b>Conclusion.....</b>	<b>93</b>
<b>5.6</b>	<b>Acknowledgment.....</b>	<b>93</b>
<b>5.7</b>	<b>Supporting Information .....</b>	<b>93</b>
<b>5.8</b>	<b>References .....</b>	<b>93</b>
<b>6</b>	<b>MOLECULAR MODELING AND IN VIVO IMAGING CAN IDENTIFY SUCCESSFUL FLEXIBLE TRIAZINE DENDRIMER-BASED SIRNA DELIVERY SYSTEMS.....</b>	<b>97</b>
<b>6.1</b>	<b>Abstract .....</b>	<b>98</b>
<b>6.2</b>	<b>Introduction .....</b>	<b>99</b>
<b>6.3</b>	<b>Experimental Section.....</b>	<b>100</b>
<b>6.4</b>	<b>Results and Discussion.....</b>	<b>105</b>
<b>6.5</b>	<b>Conclusion.....</b>	<b>118</b>
<b>6.6</b>	<b>Acknowledgements .....</b>	<b>119</b>
<b>6.7</b>	<b>References .....</b>	<b>119</b>
<b>7</b>	<b>DESIGN AND BIOPHYSICAL CHARACTERIZATION OF BIORESPONSIVE DEGRADABLE POLY(DIMETHYLAMINOETHYL METHACRYLATE) BASED POLYMERS FOR IN VITRO DNA TRANSFECTION .....</b>	<b>123</b>
<b>7.1</b>	<b>Abstract .....</b>	<b>124</b>
<b>7.2</b>	<b>Introduction .....</b>	<b>124</b>
<b>7.3</b>	<b>Experimental Part.....</b>	<b>126</b>
<b>7.4</b>	<b>Results and Discussion.....</b>	<b>132</b>
<b>7.5</b>	<b>Conclusion.....</b>	<b>145</b>
<b>7.6</b>	<b>References.....</b>	<b>146</b>
<b>8</b>	<b>SUMMARY.....</b>	<b>147</b>

<b>8.1</b>	<b>Summary .....</b>	<b>147</b>
<b>8.2</b>	<b>Perspectives.....</b>	<b>150</b>
<b>8.3</b>	<b>Zusammenfassung .....</b>	<b>151</b>
<b>9</b>	<b>APPENDICES .....</b>	<b>155</b>
<b>9.1</b>	<b>Abbreviations .....</b>	<b>155</b>
<b>9.2</b>	<b>List of Publications .....</b>	<b>156</b>
9.2.1	Articles .....	156
9.2.2	Poster Presentations .....	157
9.2.3	Lectures .....	158
9.2.4	Abstracts.....	158
<b>9.3</b>	<b>Curriculum Vitae .....</b>	<b>159</b>
<b>9.4</b>	<b>Danksagung .....</b>	<b>160</b>

# Chapter 1 INTRODUCTION



## 1.1 Nanomedicine and Delivery of Nucleic Acids

Nanomedicine is the engineering, manufacturing and application of nanotechnology for medical applications especially in terms of drug or nucleic acids delivery.<sup>1,2</sup> Nanomedicine is expected to become a revolutionary class of therapeutics to improve human health at the atomic and molecular scale. Especially concerning advanced drug and gene delivery systems, the use of nanotechnology can improve the delivery of macromolecular drug substances (for example nucleic acids) and help them to cross cellular barriers. Not only soluble drug carriers, but also insoluble drug carriers can be formulated as nanoparticles using techniques such as the solvent displacement<sup>4</sup> or solvent evaporation/emulsion technique.<sup>5</sup> With one to several hundred nanometers in size, it is also widely believed that drug delivery systems prepared by nanotechnology may also make targeted delivery and co-delivery of two or more therapeutic agents in “multifunctional” carriers possible.<sup>6,7</sup>

One of the important applications of nanomedicine is gene therapy, a powerful approach for the treatment of cancer and genetic diseases by the transfer of genetic material into specific cells of the patient.<sup>8</sup> For high therapeutic efficacy, gene delivery systems need to be directed to their target region and specifically taken up by the target cell populations through an initial set of barriers from the test tube to the membrane of a target cell. These include physico-chemical challenges, such as binding and condensing gene materials, as well as *in vitro* barriers such as cell uptake, protecting the gene materials against enzymatic degradation and other competing polyanions (serum stability), transport through the cytoplasm, endolysosomal escape and unpackaging of gene materials from the delivery agents.<sup>9</sup> Additionally, for efficient gene delivery vector accumulation, long circulation time *in vivo* is of critical importance and requires efficient particle evasion from the clearing organs including the liver, which is largely mediated by the physicochemical properties of the gene delivery vectors.<sup>10</sup>

siRNA are a double-stranded RNAs of 21–23 nucleotides with two-nucleotide 3' overhangs and 5'-phosphorylated ends<sup>11, 12</sup> and can be delivered into target cells by gene delivery agents. Although the delivery of siRNA faces many of the same barriers and intracellular steps as delivery of plasmid DNA, the delivery of siRNA appears more difficult than DNA delivery. Differences between pDNA and siRNA delivery are for example that the final target destination of siRNA is the cytoplasm, whereas plasmid DNA must be transported into the nucleus. In other words, to achieve successful siRNA delivery, the siRNA must be delivered and released rapidly from its carrier upon endosomal escape into the cytoplasm. Secondly, a recent report showed that siRNA is less flexible<sup>13, 14</sup> and the knowledge on structural conformation of cationic polymers reacting with nucleic acids is still limited. Due to rigidity, the condensation of siRNA within cationic polymers is assumed to be more difficult. For the above reasons, the design of high

affinity, good protection agents is a key point in the development of nanocarriers for siRNA delivery systems.<sup>3</sup> Moreover, novel design and development of next-generation of biocompatible and biodegradable siRNA delivery vectors with controlled release and molecular targeting properties is also a big challenge, especially for the therapeutic benefit in the clinical applications.

## 1.2 Targeted Gene Delivery Using Cell Specific Ligands

**Active vs passive targeting.** The term “passive targeting” is usually defined as a method to

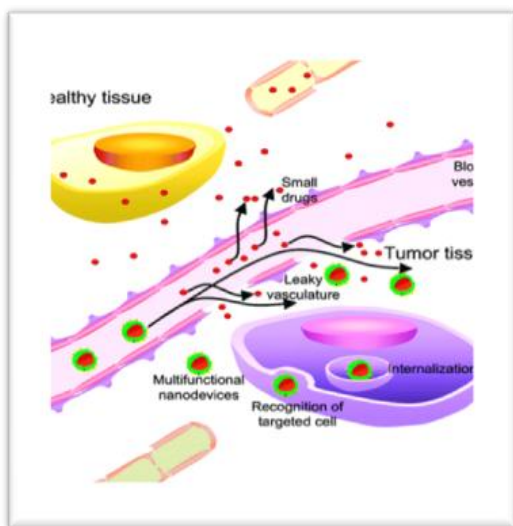


Figure 1. Enhanced permeability and retention (EPR) effect.<sup>14</sup>

deliver drugs based on the ability of the drug carrier to circulate for longer times in the bloodstream and accumulate in pathological tissues. “Active targeting” is also called ligand based targeting, which is based on the ligand-receptor recognition to recognize and bind the ligand-conjugated carriers on the target tissues. In the case of cancer therapy, the delivery of gene materials with non-targeted agents (passive targeting) is achieved mainly passive by the enhanced permeability and retention (EPR) effect (Figure 1)<sup>15</sup>: the endothelial cells of tumor neo-vasculature are poorly disorganized with large

fenestrations, causing macromolecules to leak extensively into the tumor tissue. Additionally, macromolecules are retained easily in the tumors because of the low venous return in the tumor and poor lymphatic clearance.<sup>16</sup> This preferential accumulation through the EPR effect is the so-called “passive targeting”, which is characteristic of non-targeted agents. On the other hand, active targeting describes the active binding of the drug or gene delivery vectors to cell surface through receptor-mediated endocytosis, facilitating the retention and cellular uptake (Figure 2).<sup>10</sup> The introduction of targeting ligands should enhance the tissue-, cell-, or subcellular-specific delivery efficiency through the active targeting, as compared to corresponding non-targeted gene delivery agents. To achieve the cell-specific active targeting, a great number of systems with ligands are designed and determined to target certain cancer cells.<sup>17</sup> This is particularly important for gene materials that require intracellular delivery for bioactivity.

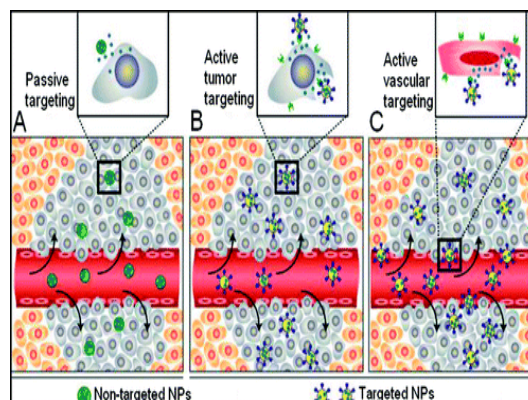


Figure 2. Passive vs active targeting. (A) Non-targeted NPs (B) The presence of targeting ligands on the surface of NPs (C) Targeted NPs.<sup>15</sup>

The successful targeting includes at first the identification of the structures on the cell surface which could provide a selective uptake into the cell. Secondly, for active targeting, gene delivery agents are coupled with a ligand which is expected to interact with a specific target on the cell surface.<sup>3</sup> For example, folate was used as a targeting moiety for lung targeting, which is the key point of the administration of biomacromolecules to the pulmonary epithelium and could therefore be an attractive approach for local and systemic therapies. In our workgroup, we have successfully synthesized and determined Folate-conjugated ternary copolymer PEI-g-PCL-b-PEG-Fol, which performed effective DNA and siRNA delivery not only *in vitro* but also *in vivo* (data will be shown in the following).

### 1.3 Polymers and Dendrimers in Gene Delivery

**Polymeric Delivery Vectors.** With development in nanotechnology several distinct gene delivery system, including liposome, albumin NP, polymeric NP, and dendrimer have been approved or entered clinical development (Figure 3). Polymeric nonviral vectors have been developed for gene transfection since the 1990s. They have the additional advantage of lower toxicity and immunogenicity than their viral counterparts and have been gradually considered as more promising vectors than their viral counterparts. Polymeric vectors also offer the possibility of industrial production following good manufacturing practice. Moreover, the gene-packaging-capacity of synthetic polymeric nonviral vectors is unlimited concerning the amount of genetic material. So far, various potential polymeric nonviral vectors have been described especially for gene delivery as shown in Figure 4.

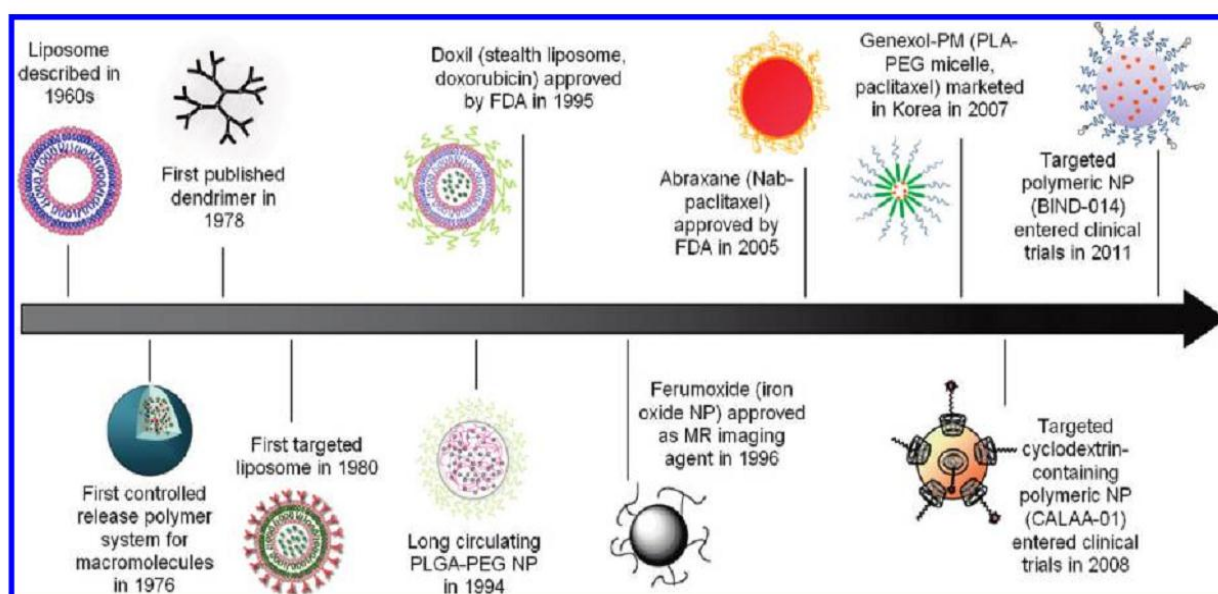


Figure 3. Historical timeline of clinical-stage nanoparticle technologies.<sup>15</sup>

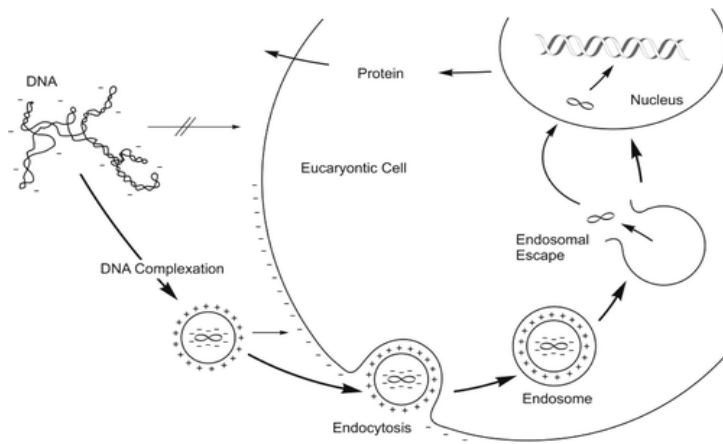


Figure 5. Since negatively charged nucleic acids are not efficiently taken up by cells, they require formulation. After adsorptive endocytosis of the gene delivery vector, therapeutic DNA needs to be released from the endosome, translocated into the nucleus where it is transcribed, and translated in the cytosol for successful transgene expression.<sup>3</sup>

**Poly(ethylene imine) (PEI)-Based Gene Carriers.** In the past decade, the cationic polymer poly(ethylene imine) (PEI) has been regarded to play the most important role in nonviral gene delivery. In 1995, the potential of PEI as a gene delivery vector was first discussed.<sup>18</sup> The investigated molecular weights of PEI range from 1 kDa to  $1.6 \times 10^3$  kDa.<sup>19</sup> Due to results from a transfection study with L929 cells, researchers

found that the most suitable molecular weight of PEI for gene delivery ranges from 5 to 25 kDa. Higher molecular weight PEI can increase cytotoxicity due to cell-surface aggregation of the polymer.<sup>20</sup> Low molecular weight PEI is less toxic but is usually less effective as a gene delivery vector. PEI carries protonable amino groups, which confers the ability for PEI to change its conformation with the pH change in the cytosol and to have a high endosomal buffering capacity, the so-called “proton-sponge” effect. This property of PEI is described to cause osmotic swelling and endosomal escape of complexes (Figure 5).<sup>18</sup> PEI polymers can be classified into (hyper)branched and linear architectures. Highly branched PEI showed stronger complexation with DNA and formed smaller complexes than linear PEI.<sup>21</sup> The condensation behavior of branched PEI with DNA is less dependent on the preparation buffer conditions<sup>21</sup> than high molecular weight linear, which is distinctly dependent on the buffer condition. For example, complexes of linear PEI 22 kDa with DNA (1  $\mu$ m) in a high ionic strength solution were larger than the complexes prepared in a low ionic strength 5% glucose solution (30–60 nm).<sup>18, 22</sup> Interestingly, the transfection efficiency of linear PEI22 kDa/DNA complexes *in vitro* was higher than that of branched PEI800/DNA and branched PEI25 kDa/DNA complexes when complexes were prepared in a salt-containing buffer.<sup>21</sup> However, further *in vivo* investigations showed that linear PEI22 kDa/DNA complexes prepared in high salt condition were less active than the complexes formed

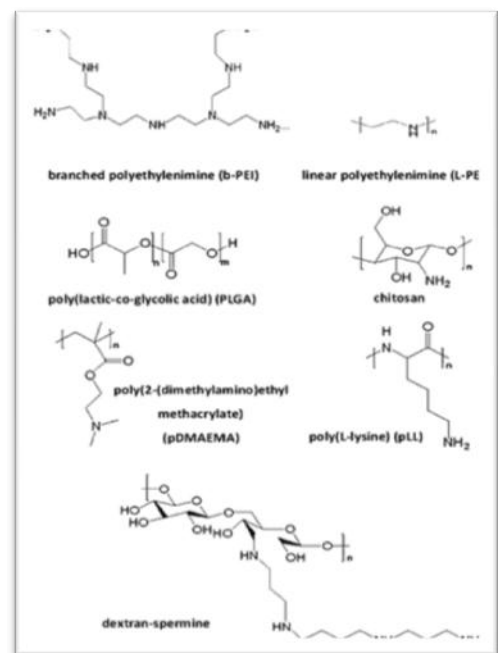


Figure 4. Polymeric vectors employed for pulmonary gene delivery.<sup>12</sup>

in low salt condition (100-fold less). This indicates that efficient transgene expression strongly depends on the size of the complexes.

**Dendritic Delivery Vectors.** Dendrimers are globular, hyperbranched macromolecules with precise core-shell nanostructures in which every repeated sequence represents a higher generation.<sup>23</sup> Due to their hypothetical monodispersity, dendrimers are interesting carriers for small molecule drugs<sup>24</sup> and nucleic acids.<sup>25</sup> Before dendrimers were first employed for pulmonary gene delivery, the stability of DNA complexes of polyamidoamine (PAMAM) of unspecified core composition and generation was characterized in the presence of pulmonary surfactant.<sup>26</sup> The authors found that dendriplexes stably protected DNA from degradation by DNase I in the presence of phospholipids alone or Alveofact. Their transfection efficiency was not affected in pulmonary cell lines in the presence of the natural surfactant Alveofact and in none of the cell lines tested in the presence of the synthetic surfactant Exosurf.<sup>26</sup> In a study comparing the biodistribution of transgene expression as a function of administration route, DNA complexes of Starburst G9 EDA PAMAM were administered intratracheally, intranasally, and intravenously. Surprisingly, transgene expression after local administration of dendriplexes was even lower than compared with naked DNA, while the opposite was true for systemic administration. Additionally, dendriplex-mediated reporter gene expression after local administration was limited to the lung.<sup>27</sup> Comparably, SuperFect, a generation 4 fractured PAMAM dendrimer,<sup>28</sup> also generated only very low luciferase reporter gene expression in the lung, although its *in vitro* efficacy was not inhibited by the presence of mucin or  $\alpha$ 1-glycoprotein.<sup>29</sup> In recent years, PAMAM and diaminobutane (DAB) dendrimers were described to up- and down regulate hundreds of genes in treated cells.<sup>30</sup> Interestingly, generation 3 polypropylenimine diaminobutane (DAB) dendrimers with 16 protonable peripheral amines mediated high transfection efficiencies in A431 and A549 cells; however, both the dendrimer alone and the dendriplexes caused upregulation of epidermal growth factor receptor (EGFR) expression and activated its downstream Akt signaling.<sup>31</sup> Comparably, Starburst PAMAM was shown to induce acute lung injury *in vivo* triggered by activation of autophagic cell death by deregulation of the Akt-TSC2-mTOR signaling pathway.<sup>32</sup> Therefore novel, biocompatible dendritic vectors need to be developed.

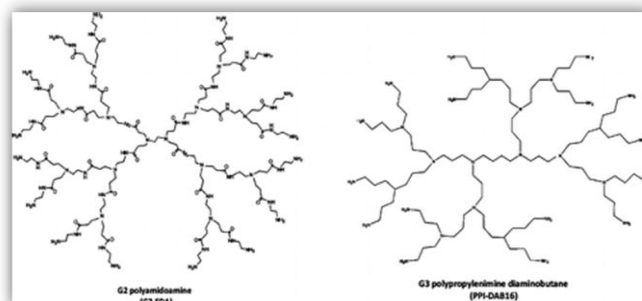


Figure 6. Chemical structures of generation 2 ethylene diamine core PAMAM and generation 3 DAB core PPI with 16 primary amines.<sup>12</sup>

## 1.4 Pulmonary Gene Delivery

The potential of pulmonary gene delivery was reported in a large number of studies.<sup>33-36</sup> Because of the high affinity between the airway epithelium cells with the targeted delivery vectors, the lung is a promising target organ for gene delivery. The administration of biomacromolecules like DNA or siRNA to the pulmonary epithelium could be an attractive approach for local passive targeting but systemic therapies. Compared with hydrophilic macromolecules like nucleic acids, small and hydrophobic molecules lead to more rapid local and systemic effects because of the air-blood-barrier.<sup>37</sup> Therefore, for successful pulmonary gene delivery, formulation of the therapeutic nucleic acids into nanosized carrier systems is necessary. Furthermore, successful pulmonary gene delivery must overcome a number of biological barriers, which includes anatomic, physical, immunologic, and metabolic barriers.<sup>3</sup> In the two last decades, various potential polymeric nonviral vectors have been developed for pulmonary gene transfection, such as poly(ethylene imine) (PEI), poly(2-(dimethylamino)ethyl methacrylate) (pDMAEMA), the polysaccharide chitosan, the biologically occurring polyamine spermine, and the biodegradable noncationic polymer PLGA.<sup>38</sup> For in vitro pulmonary gene delivery experiments, the application of lung epithelial cells cannot be replaced by conventional cell culture, because the epithelium differentiates in layers of cells with a distinct apical and basolateral side and connects each other by tight junctions. The Calu-3 cell line, A549 epithelial cells and human primary small airway epithelial cells (HSAEC) are classic models of airway epithelium. Although intratracheal instillation was frequently applied in lab-scale with animals, clinical success was still not achieved, which depends not only on the development of effective, biocompatible, and targeted gene delivery vectors, but also requires deeper understanding of the mechanisms of pulmonary gene delivery.

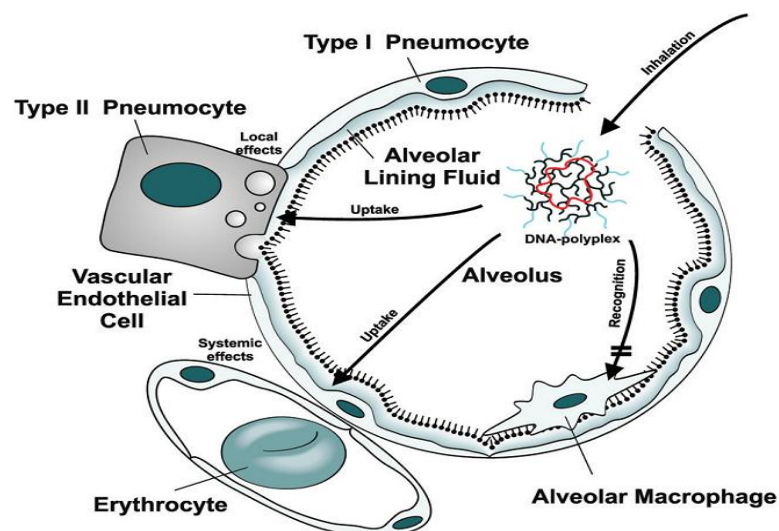


Figure 7: After entering the alveoli, gene delivery systems can possibly interact with the alveolar lining fluid or can be taken up by various cell types. Recognition by and uptake into macrophages should be avoided, for example, by adjusting the size and surface of nanoparticles. Uptake into pneumocytes could lead to local therapeutic effects, and transcytosis into the systemic circulation could lead to systemic wanted or unwanted effects.<sup>3</sup>

## 1.5 Structure of the Thesis: Aims and Outline

This thesis focuses on a number of issues in non-viral polymeric delivery of nucleic acids concerning biophysicochemical parameters *in vitro* and *in vivo* application.

The investigations in *chapters 2-5* were gene delivery study with the use of PEI-based polymeric gene delivery systems. We should answer the questions: why the principle of DNA transfection cannot be directly applied for siRNA transfection and to search for the development of better siRNA delivery systems, our work began with the study of the binding mechanism of nucleic acids/polycations complexation and aggregation through different levels of hierarchy on the atomic and molecular scale, with the novel synergistic use of molecular modeling, molecular dynamics simulation, isothermal titration calorimetry and other characterization techniques (*chapter 2*). These data were expected to explain the different nature and the different hierarchical mechanism of formation of related polycation-siRNA and polycation-pDNA complexes, which is the important base of the following research of the effective nucleic acids, especially siRNA delivery.

*Chapter 3* concentrates on *in vitro* pDNA delivery with biodegradable amphiphilic copolymers hy-PEI-g-(PCL-b-PEG)<sub>n</sub>, which was grafted with PCL-b-PEG chains onto hyper-branched poly(ethylene imine). In this copolymer, poly(caprolactone) (PCL) acts as a linker between PEI and PEG to increase the biodegradability of the copolymers and the permeability of the complexes through the cell membranes. So far, the investigations about these copolymers were limited to the discussion of the influence of PEI, PCL and PEG chain lengths. Therefore in this section, our study focused on the influence of graft density by correlating physic-chemical and biological *in vitro* properties of the complexes and expected that with the introduction of the grafted PCL-b-PEG chains, the *in vitro* DNA delivery efficiency with the grafted PCL-b-PEG chains could be improved.

*Chapter 4* continues to describe the siRNA delivery efficiency of these biodegradable amphiphilic grafted copolymers hy-PEI-g-PCL-b-PEG *in vitro* and *in vivo*. The purpose of this study was to enhance the *in vivo* blood circulation time and siRNA delivery efficiency of the same copolymers in *chapter 3*, by introducing high graft densities of PCL-PEG chains. We assumed that the effect of PEG on prolonged circulating depends not only on its length or percentage, but also on the structure or the shape of the amphiphilic copolymers, which have advantages especially for *in vivo* siRNA delivery.

Following the successful design and characterization of biodegradable amphiphilic copolymers hy-PEI-g-(PCL-b-PEG)<sub>n</sub> (*chapter 3, 4*), in *chapters 5*, we successfully synthesized and characterized folate-conjugated ternary copolymers based on polyethylenimine-graft-polycaprolactone-block-poly(ethylene glycol) (PEI-g-PCL-b-PEG-Fol) as targeted DNA delivery system. We hypothesized that these conjugated copolymer would

efficiently transfect folate-overexpressing cells via folate receptor-mediated endocytosis, which is especially meaningful for the pulmonary gene delivery.

The aim of *Chapter 6* study was to identify suitable siRNA delivery systems based on hyperflexible generation 2-4 triazine dendrimers by correlating physico-chemical and biological *in vitro* and *in vivo* properties of the complexes with their thermodynamic interaction features simulated by molecular modeling.

*Chapter 7* is the research about novel water soluble, degradable polymers based on poly(*N,N*-dimethylaminoethyl methacrylate) (PDMAEMA) p-DNA delivery system. We expected lower cytotoxicity but efficiently transfect of pDNA with these degradable polymers.

All results are summarized in *Chapter 8*, where an outlook also provides information on further possible applications and developments.

## 1.6 References

1. Riehemann, K.; Schneider, S. W.; Luger, T. A.; Godin, B.; Ferrari, M.; Fuchs, H., Nanomedicine--challenge and perspectives. *Angew Chem Int Ed Engl* **2009**, *48* (5), 872-97.
2. Petros, R. A.; DeSimone, J. M., Strategies in the design of nanoparticles for therapeutic applications. *Nat Rev Drug Discov* **2010**, *9* (8), 615-27.
3. Merkel, O. M.; Zheng, M.; Debus, H.; Kissel, T., Pulmonary gene delivery using polymeric nonviral vectors. *Bioconjug Chem* **2011**, *23* (1), 3-20.
4. Nguyen, J.; Steele, T. W. J.; Merkel, O.; Reul, R.; Kissel, T., Fast degrading polyesters as siRNA nano-carriers for pulmonary gene therapy. *Journal of Controlled Release* **2008**, *132* (3), 243-251.
5. Yan, F.; Zhang, C.; Zheng, Y.; Mei, L.; Tang, L. N.; Song, C. X.; Sun, H. F.; Huang, L. Q., The effect of poloxamer 188 on nanoparticle morphology, size, cancer cell uptake, and cytotoxicity. *Nanomedicine-Nanotechnology Biology and Medicine* **2010**, *6* (1), 170-178.
6. Ferrari, M., Cancer nanotechnology: opportunities and challenges. *Nat Rev Cancer* **2005**, *5* (3), 161-71.
7. Zhang, L.; Gu, F. X.; Chan, J. M.; Wang, A. Z.; Langer, R. S.; Farokhzad, O. C., Nanoparticles in medicine: therapeutic applications and developments. *Clin Pharmacol Ther* **2008**, *83* (5), 761-9.
8. Mulligan, R. C., The basic science of gene therapy. *Science* **1993**, *260* (5110), 926-32.
9. Pack, D. W.; Hoffman, A. S.; Pun, S.; Stayton, P. S., Design and development of polymers for gene delivery. *Nat Rev Drug Discov* **2005**, *4* (7), 581-93.
10. Farokhzad, O. C.; Langer, R., Impact of nanotechnology on drug delivery. *ACS Nano* **2009**, *3* (1), 16-20.
11. Bernstein, E.; Caudy, A. A.; Hammond, S. M.; Hannon, G. J., Role for a bidentate ribonuclease in the initiation step of RNA interference. *Nature* **2001**, *409* (6818), 363-366.
12. Zamore, P. D.; Tuschl, T.; Sharp, P. A.; Bartel, D. P., RNAi: double-stranded RNA directs the ATP-dependent cleavage of mRNA at 21 to 23 nucleotide intervals. *Cell* **2000**, *101* (1), 25-33.
13. Merkel, O. M.; Mintzer, M. A.; Librizzi, D.; Samsonova, O.; Dicke, T.; Sproat, B.; Garn, H.; Barth, P. J.; Simanek, E. E.; Kissel, T., Triazine dendrimers as nonviral vectors for *in vitro* and *in vivo* RNAi: the effects of peripheral groups and core structure on biological activity. *Mol Pharm* **2010**, *7* (4), 969-83.
14. Pavan, G. M.; Mintzer, M. A.; Simanek, E. E.; Merkel, O. M.; Kissel, T.; Danani, A., Computational insights into the interactions between DNA and siRNA with "rigid" and "flexible" triazine dendrimers. *Biomacromolecules* **2010**, *11* (3), 721-30.



15. Matsumura, Y.; Maeda, H., A new concept for macromolecular therapeutics in cancer chemotherapy: mechanism of tumor-tropic accumulation of proteins and the antitumor agent smancs. *Cancer Res* **1986**, *46* (12 Pt 1), 6387-92.
16. Cabral, H.; Nishiyama, N.; Kataoka, K., Supramolecular Nanodevices: From Design Validation to Theranostic Nanomedicine. *Accounts of Chemical Research* **2011**, *44* (10), 999-1008.
17. Shi, J. J.; Xiao, Z. Y.; Kamaly, N.; Farokhzad, O. C., Self-Assembled Targeted Nanoparticles: Evolution of Technologies and Bench to Bedside Translation. *Accounts of Chemical Research* **2011**, *44* (10), 1123-1134.
18. Boussif, O.; Lezoualc'h, F.; Zanta, M. A.; Mergny, M. D.; Scherman, D.; Demeneix, B.; Behr, J. P., A versatile vector for gene and oligonucleotide transfer into cells in culture and in vivo: polyethylenimine. *Proc Natl Acad Sci U S A* **1995**, *92* (16), 7297-301.
19. Meunier-Durmort, C.; Grimal, H.; Sachs, L. M.; Demeneix, B. A.; Forest, C., Adenovirus enhancement of polyethylenimine-mediated transfer of regulated genes in differentiated cells. *Gene Ther* **1997**, *4* (8), 808-14.
20. Fischer, D.; Bieber, T.; Li, Y.; Elsassner, H. P.; Kissel, T., A novel non-viral vector for DNA delivery based on low molecular weight, branched polyethylenimine: effect of molecular weight on transfection efficiency and cytotoxicity. *Pharm Res* **1999**, *16* (8), 1273-9.
21. Wightman, L.; Kircheis, R.; Rossler, V.; Carotta, S.; Ruzicka, R.; Kurs, M.; Wagner, E., Different behavior of branched and linear polyethylenimine for gene delivery in vitro and in vivo. *J Gene Med* **2001**, *3* (4), 362-72.
22. Goula, D.; Remy, J. S.; Erbacher, P.; Wasowicz, M.; Levi, G.; Abdallah, B.; Demeneix, B. A., Size, diffusibility and transfection performance of linear PEI/DNA complexes in the mouse central nervous system. *Gene Ther* **1998**, *5* (5), 712-7.
23. Boas, U.; Heegaard, P. M., Dendrimers in drug research. *Chem Soc Rev* **2004**, *33* (1), 43-63.
24. D'Emanuele, A.; Attwood, D., Dendrimer-drug interactions. *Adv Drug Deliv Rev* **2005**, *57* (15), 2147-62.
25. Shcharbin, D. G.; Klajnert, B.; Bryszewska, M., Dendrimers in gene transfection. *Biochemistry (Mosc)* **2009**, *74* (10), 1070-9.
26. Ernst, N.; Ulrichskotter, S.; Schmalix, W. A.; Radler, J.; Galneder, R.; Mayer, E.; Gersting, S.; Plank, C.; Reinhardt, D.; Rosenecker, J., Interaction of liposomal and polycationic transfection complexes with pulmonary surfactant. *J Gene Med* **1999**, *1* (5), 331-40.
27. Kukowska-Latallo, J. F.; Raczka, E.; Quintana, A.; Chen, C.; Rymaszewski, M.; Baker, J. R., Jr., Intravascular and endobronchial DNA delivery to murine lung tissue using a novel, nonviral vector. *Hum Gene Ther* **2000**, *11* (10), 1385-95.
28. Tang, M. X.; Redemann, C. T.; Szoka, F. C., Jr., In vitro gene delivery by degraded polyamidoamine dendrimers. *Bioconjug Chem* **1996**, *7* (6), 703-14.
29. Rosenecker, J.; Naundorf, S.; Gersting, S. W.; Hauck, R. W.; Gessner, A.; Nicklaus, P.; Muller, R. H.; Rudolph, C., Interaction of bronchoalveolar lavage fluid with polyplexes and lipoplexes: analysing the role of proteins and glycoproteins. *J Gene Med* **2003**, *5* (1), 49-60.
30. Akhtar, S.; Benter, I., Toxicogenomics of non-viral drug delivery systems for RNAi: potential impact on siRNA-mediated gene silencing activity and specificity. *Adv Drug Deliv Rev* **2007**, *59* (2-3), 164-82.
31. Omid, Y.; Barar, J., Induction of human alveolar epithelial cell growth factor receptors by dendrimeric nanostructures. *Int J Toxicol* **2009**, *28* (2), 113-22.
32. Li, C.; Liu, H.; Sun, Y.; Wang, H.; Guo, F.; Rao, S.; Deng, J.; Zhang, Y.; Miao, Y.; Guo, C.; Meng, J.; Chen, X.; Li, L.; Li, D.; Xu, H.; Li, B.; Jiang, C., PAMAM nanoparticles promote acute lung injury by inducing autophagic cell death through the Akt-TSC2-mTOR signaling pathway. *J Mol Cell Biol* **2009**, *1* (1), 37-45.
33. Kinsey, B. M.; Densmore, C. L.; Orson, F. M., Non-viral gene delivery to the lungs. *Current Gene Therapy* **2005**, *5* (2), 181-194.
34. Aneja, M. K.; Geiger, J. P.; Himmel, A.; Rudolph, C., Targeted gene delivery to the lung. *Expert Opin Drug Deliv* **2009**, *6* (6), 567-83.

35. Griesenbach, U.; Alton, E. W. F. W.; Co, U. C. F. G. T., Gene transfer to the lung: Lessons learned from more than 2 decades of CF gene therapy. *Advanced Drug Delivery Reviews* **2009**, *61* (2), 128-139.
36. Sanders, N.; Rudolph, C.; Braeckmans, K.; De Smedt, S. C.; Demeester, J., Extracellular barriers in respiratory gene therapy. *Adv Drug Deliv Rev* **2009**, *61* (2), 115-27.
37. Cryan, S. A.; Sivadas, N.; Garcia-Contreras, L., In vivo animal models for drug delivery across the lung mucosal barrier. *Adv Drug Deliv Rev* **2007**, *59* (11), 1133-51.
38. Park, T. G.; Jeong, J. H.; Kim, S. W., Current status of polymeric gene delivery systems. *Adv Drug Deliv Rev* **2006**, *58* (4), 467-86.

## Chapter 2

# TARGETING THE BLIND SPOT OF POLYCATIONIC NANOCARRIER-BASED SIRNA DELIVERY

Submitted to ACS Nano

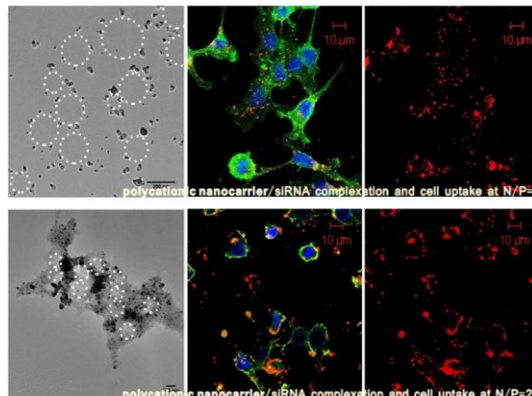
**Mengyao Zheng<sup>†</sup>, Giovanni M. Pavan<sup>‡</sup>, Manuel Neeb<sup>§</sup>, Andreas K. Schaper<sup>||</sup>, Andrea Danani<sup>‡</sup>, Gerhard Klebe<sup>§</sup>, Olivia M. Merkel<sup>†,⊥</sup> and Thomas Kissel<sup>†,\*</sup>**

### Author contributions

T. K. guided and directed the research. O. M. M. and M. Z. designed the measurements. M. Z. prepared the polyplexes for isothermal titration calorimetry and TEM. M.Z. carried out the SYBR® Gold assay, heparin assay, dye quenching assay, dynamic light scattering/zeta potential analysis, *in vitro* cell uptake (CLSM) and knockdown experiments (RT-PCR). M. Z., O. M. M. and G. M. P. analysed the experimental data.

## 2.1 Abstract

Polycationic nanocarriers attract increasing attention to the field of siRNA delivery. We investigated the mechanism of nucleic acids/polycations complexation and aggregation through different levels of hierarchy on the atomic and molecular scale with the novel synergistic use of molecular modeling, molecular dynamics simulation, isothermal titration calorimetry and other characterization techniques. These data suggest the different nature and the different hierarchical mechanism of formation of related polycation-siRNA and polycation-pDNA complexes. The results of fluorescence quenching assays indicated a biphasic behavior of siRNA



Abstract graphic: polycationic nanocarrier/siRNA complexation and cell uptake at different N/P ratios.

binding with polycations where molecular reorganization of the siRNA within the polycations occurred at lower N/P-ratios (nitrogen/phosphorus). Additionally, heparin assays showed that the stability of siRNA/polymer complexes is especially good at a rather lower N/P-ratio of 2. Interestingly, with the following study of the relationship between nucleic acids/polycations aggregation mechanism and *in vitro* siRNA delivery efficiency, which is performed by RT-PCR and confocal laser scanning microscopy, we found that not only PEI25kDa but also the PCL-PEG-modified copolymer showed the best knockdown effect with siRNA at N/P=2, although higher N/P ratios were believed to be necessary until now by most of the researchers in the area of polycationic nanocarrier-based siRNA delivery. Our results emphasize the importance of low N/P ratios, which allow for excellent siRNA delivery efficiency, but have been disregarded like a “blind spot” in previous reports on siRNA delivery. Our investigation highlights the formulation of siRNA complexes from a thermodynamic point of view and opens new perspectives to advance the rational design of new siRNA delivery systems.

**KEYWORDS:** siRNA delivery ·DNA delivery ·Polyethylenimine ·Molecular modeling · Isothermal titration calorimetry ·RT-PCR ·Supramolecular complexation

## 2.2 Introduction

Nanomedicine is the engineering, manufacturing and application of nanotechnology for medical applications, amongst others for drug or nucleic acids delivery.<sup>1, 2</sup> One of the most important applications of nanomedicine is gene delivery, a powerful approach for the treatment of cancer and genetic diseases. Compared with viral counterparts and liposomes, polymeric gene delivery

systems have the advantages of lower toxicity and immunogenicity by design, and allow for industrial production involving good manufacturing practice.<sup>3</sup> A wide range of polymeric vectors were designed and developed based on the complexation of nucleic acids via electrostatic interaction between the negatively charged phosphates along the nucleic acid backbone with the positive charges on the cationic polymers.<sup>4</sup> The cationic polymer poly(ethylenimine) (PEI) is one of the best studied vectors for non-viral gene delivery. Starting in the 1990s, the polymeric non-viral vector PEI has been developed to achieve successful delivery of nucleic acids like plasmid DNA, antisense oligonucleotides, ribozymes, and siRNA.<sup>2</sup> Since the discovery of gene silencing by introduction of double-stranded RNA,<sup>5</sup> RNA interference is widely used in functional genomics and drug development.<sup>6, 7</sup> Although the delivery of siRNA faces many of the same barriers and intracellular steps as delivery of plasmid DNA, the delivery of siRNA appears more difficult than DNA delivery, and the design of high affinity, good protection agents is a key point in the development of nanocarriers for siRNA delivery systems. In this study, we used isothermal titration calorimetry (ITC) to investigate the complexation behavior of siRNA and DNA with polycations. These thermodynamic parameters also allow for the study of the hierarchical aggregation phenomena which result from the biomolecular interactions between nucleic acids and cationic polymers.<sup>8</sup> Because the knowledge on structure conformation of cationic polymers and genetic materials is limited, molecular dynamics (MD) simulation was used to investigate the local mechanism of binding between pDNA or siRNA molecules and cationic polymers, providing detailed insight into the structural conformations and binding behavior.<sup>9-11</sup> This synergetic use of MD simulation and ITC provides a complete description not only of the local binding between polymers and nucleic acids but also of the hierarchical aggregation steps which occur during polyplex formation. Additionally, the complexation of DNA and siRNA was also studied using heparin assays and dye quenching assays, and subsequently *in vitro* transfection experiments were conducted with both siRNA and pDNA. Our investigations are focused on the study of binding mechanisms, the different location of plasmid DNA and siRNA within complexes of cationic polymers, their different structural conformations and biophysical parameters as well as the size and surface charge of the final polyplexes. By investigating these parameters and correlating them to functional studies including knockdown of glyceraldehyde 3-phosphate dehydrogenase (GAPDH) gene expression measured by RT-PCR, we try to find distinguishing features of siRNA complexation and to explain why the principle of DNA transfection cannot generally be directly applied to siRNA transfection.<sup>12</sup>

Our study of the complexation mechanism between nucleic acids and polycationic nanocarriers describes the very different nature of polycation-siRNA and polycation-DNA hierarchical aggregation. We demonstrate that siRNA complexation can be schematized into two “rigid” steps,

namely (i) polycation-siRNA primary complexation, followed by the (ii) hierarchical association of multiple nanocomplexes into larger polyplexes (Figure 1A). DNA condensation, however, involves three steps: after the (i) primary electrostatic interactions between polycations and DNA, the saturated polycation-DNA complex can undergo (ii) structural rearrangement (folding), followed by the (iii) hierarchical association of multiple nanocomplexes into larger polyplexes (Figure 1B). In this hierarchical framework, siRNA aggregation results in a more uniform and stable complex formation, at low N/P ratios already, which lead to increased siRNA delivery efficiency. Interestingly, with the following study of the relationship between nucleic acids/polycations aggregation mechanism and *in vitro* siRNA delivery efficiency, which is performed by RT-PCR and confocal laser scanning microscopy, the polycationic nanocarriers based siRNA delivery system showed the best knockdown effect with siRNA at N/P=2, although higher N/P ratios were believed to be necessary until now by most of the researchers in the area of polycationic nanocarrier-based siRNA delivery.

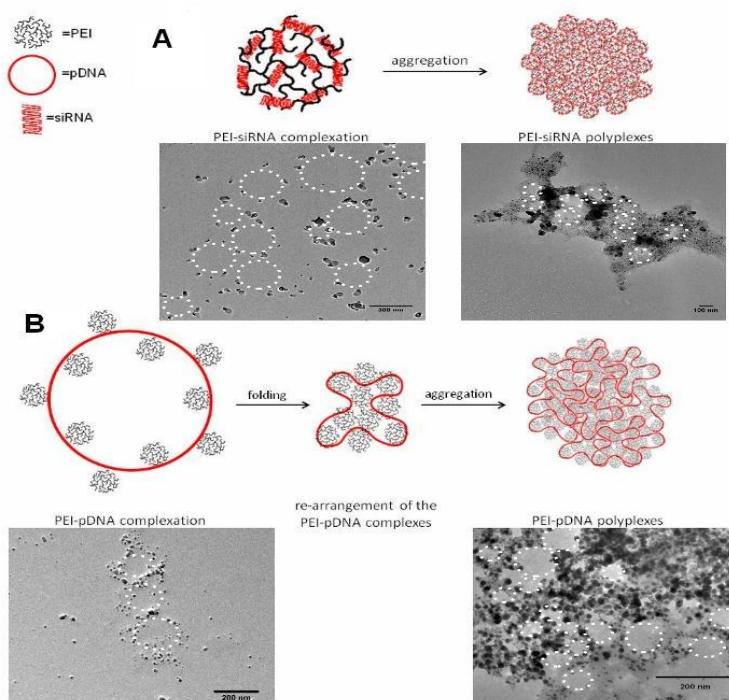


Figure 1. Model for different hierarchical aggregation mechanism. (A) PEI/siRNA. (B) PEI/pDNA. The synergic use of MD simulations, ITC and dye quenching assays provides us a complete description not only of the local binding between polymers and nucleic acids but also of the hierarchical aggregation steps which occur during polyplex formation. TEM: during reduction of the silver cations into silver nanoparticles on the negatively charged sugar-phosphate backbone of the nucleic acids, siRNA and DNA were stained with Ag (black) and then condensed with polycations at low and high N/P ratios.

## 2.3 Results and Discussion

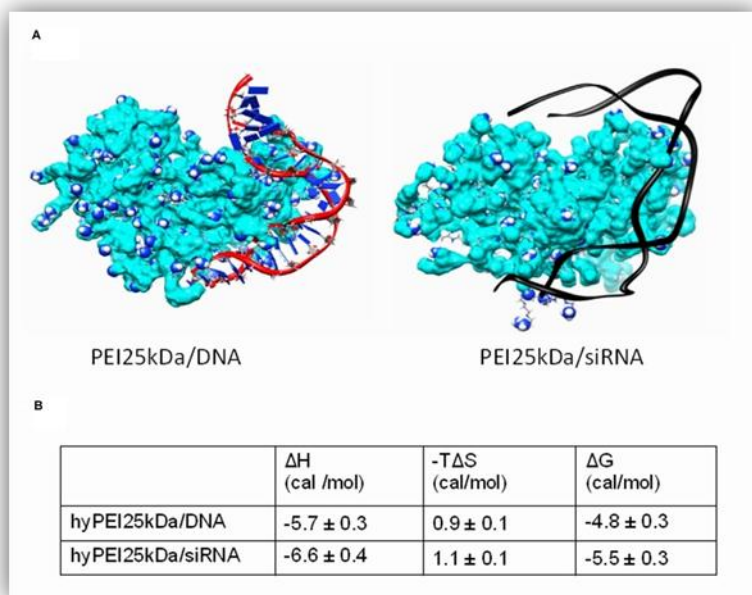


Figure 2. Molecular modeling and MD simulations. (A) Equilibrated configurations of the MD simulations of nucleic acids/PEI25kDa polyplexes. (B) Simulated  $\Delta G$  energies and the contributing potentials of the binding between branched PEI25kDa and DNA or DsiRNA normalized to energy per charged surface amine expressed in kcal mol<sup>-1</sup>.

binding entropy ( $\Delta S$ ) related to the siRNA and DNA complexation with PEI25kDa was practically the same, while the enthalpy ( $\Delta H$ ) of siRNA/PEI25kDa binding ( $-6.6$  kcal mol<sup>-1</sup>) was higher than that of DNA/PEI25kDa ( $\Delta H = -5.7$  kcal mol<sup>-1</sup>). As a consequence, the normalized free energy of binding of PEI25kDa with siRNA ( $\Delta G = -5.5$  kcal mol<sup>-1</sup>) was more favorable than that of DNA complexation ( $\Delta G = -4.8$  kcal mol<sup>-1</sup>), indicating that PEI25kDa polymers are slightly more strongly attracted by siRNA than by DNA. This can be explained with a more consistent curvature and a higher local flexibility of siRNA with respect to DNA, which facilitates the uniform binding between the negative charges present on the nucleic acid with the positive ones of the polymer. The models in figure 2 were designed and simulated to study the possible presence of differences in the binding of PEI25kDa with DNA and siRNA. While Dicer substrate interfering RNA (DsiRNA) molecules are double-strands of 25/27mer, the plasmid DNA used in the experiments presented in this work contains about 4400 base pairs. The DNA model used for simulations is just a portion of the complete plasmid, and the simulation is thus representative of the local interactions between the polymers and the DNA double strands. Under physiological conditions, plasmid DNA exists usually as an elongated helix as B-form, while RNA exists as more compact and curved double helix which is known as A-form.<sup>13</sup> That makes RNA locally more flexible in the case of local roll and tilt deformations<sup>14</sup> and more adaptable<sup>15</sup> in case of binding with a charged spherical polymer than DNA.<sup>10</sup> For PEI25kDa, not all of the charged surface groups are sterically available

### Molecular dynamics (MD) simulation study of PEI25kDa binding with DNA and siRNA

With the use of MD simulation, we aimed to compare the behavior of PEI25kDa while binding DNA vs. siRNA according to a 1:1 complexation model. All of the thermodynamic energies obtained from MD simulations were normalized per charge (and expressed in kcal mol<sup>-1</sup>) to allow for the comparison between the different nucleic acids (Figure 2). Interestingly, the

to bind a single strand of nucleic acids because a large part of charged amines is back folded. During the binding between PEI25kDa and DNA/siRNA, parts of the positive surface charges of the polymer establish strong electrostatic interactions with the nucleic acid. At the binding interface, positive and negative charges neutralize each other. But moving away from the binding site on the polymer surface, there are several other positively charged surface groups which do not participate actively in the binding with the nucleic acid (“primary complexes” in figure 2).

These free charges can potentially lead to inter-particle electrostatic attractions with other siRNA/DNA molecules giving rise to hierarchical aggregation phenomena. In fact, primary complexes can aggregate further and re-organize into larger polyplexes.<sup>16</sup> Therefore, there is a balance that needs to be considered between the amount of charges and the ability to use these charges. In this framework, it is evident that the pure binding between the polymer and the nucleic acid which is depicted by MD simulation constitutes only the first, and most immediate step in a complex hierarchical aggregation phenomenon which involves different scales and types of interactions, from strong electrostatic to weaker hydrophobic intermolecular forces. This hierarchy emerges when binding data from MD simulation are compared with the thermodynamic values calculated based on ITC measurements. The consequent molecular complexes can potentially undergo further structural reorganization and can interact with other polyplexes in solution. This causes slower complexation as compared to siRNA, where a consistent structural rearrangement is not expected due to the limited length of the nucleic acids. Moreover, DNA molecules need more polycations to achieve complete condensation and to form stable polyplexes. This hypothesis was challenged with the following ITC results.

### **Isothermal titration calorimetry (ITC)**

The atomic binding results of local interactions from MD simulation are complemented by results from isothermal titration calorimetry (ITC) experiments, which provide reliable thermodynamic interpretation<sup>17</sup> of the aggregation of multiple polycation/nucleic acid nanocomplexes into higher-scale polyplexes. The ITC results are supported by the data from MD modeling and showed the same tendency of the binding behavior between polycations and different nucleic acids: the affinity between polycations and siRNA is higher than that between polycations and plasmid DNA, and the formation of hierarchical polycation/siRNA polyplexes is much easier and more stable than the complexation with plasmid DNA (Table 1). Even if the interaction between PEI25kDa and DNA or siRNA is locally very similar, the flexible PEI25kDa/DNA nanocomplexes can undergo structural rearrangement (folding), resulting in less uniform aggregation of multiple nanocomplexes into larger polyplexes (Figure 1B). Moreover, ITC indicates also that DNA molecules need a larger excess of polycations than siRNA to achieve complete condensation and to



form stable polyplexes (Table 1). If on an atomic level the pure polymer-nucleic acid molecular recognition is controlled by electrostatic forces, on a higher-scale level, the inter-polyplex interactions are also consistently characterized by hydrophobic forces, as is evidenced by data from ITC (Table 1). Hydrophobic aggregation is assumed to be typically an entropy-driven assembly phenomenon, accompanied by a lower favorable enthalpy (Table 1).<sup>18</sup> This is particularly evident in the case of DNA. In fact, if PEI is modified with hydrophobic poly(caprolactone) segments, DNA/PEI25k-PCL1500-PEG2k nanocomplexes aggregate stronger due to increased hydrophobicity<sup>19</sup> and condense DNA more effectively. Concerning modified PEI25kDa, only about 5 PEI25k-PCL1500-PEG2k molecules are required to condense one DNA molecule (N-value or site), whereas 11 molecules unmodified PEI25kDa are needed for the same effect.

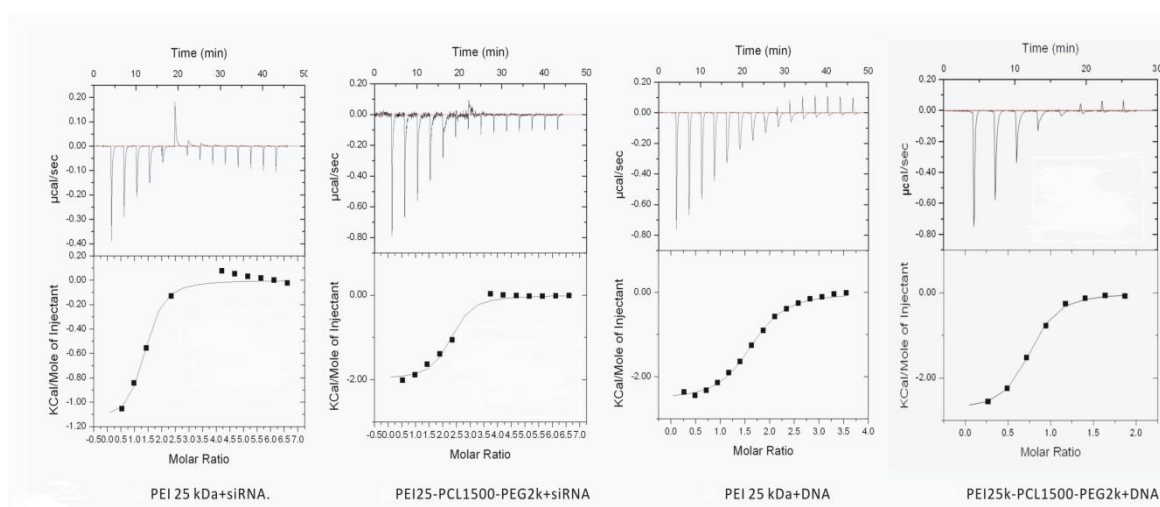


Figure 3. Thermodynamic interpretation was provided during Isothermal titration calorimetry. Standard binding isotherm curve of siRNA and pDNA with polycations. The siRNA reorganization from the saturated complex into aggregates is an endothermic process, reflected in an endothermic peak at N/P=1 in the ITC measurements.

Table 1. Thermodynamic parameters for the specific binding between polycations and DNA or siRNA.

	N	K	$\Delta H$	$\Delta S$	$\Delta G$
	(sites)	( $M^{-1}$ )	(cal/mol)	(cal/mol/deg)	(cal/mol)
hyPEI25k/DNA	1.59 $\pm$ 0.02	1.29E5 $\pm$ 1.37E4	-2569 $\pm$ 40.96	14.8	-6979.4
hyPEI25k/siRNA	2.26 $\pm$ 0.03	2.23E6 $\pm$ 9.28E5	-2172 $\pm$ 48.09	21.8	-8668.4
hyPEI25k-PCL1500-PEG2k/DNA	0.683 $\pm$ 0.01	2.58E5 $\pm$ 3.20E4	-2795 $\pm$ 57.88	15.4	-7384.2
hyPEI25k-PCL1500-PEG2k/siRNA	2.23 $\pm$ 0.05	2.80E5 $\pm$ 7.40E4	-2063 $\pm$ 53.96	18.0	-7427.0

All binding parameters are reliable experimental thermodynamic data calculated based on ITC. The larger dissociation constant K of siRNA/polycation complexation reflects that the affinity

between polycations with siRNA is higher than that with pDNA. Concerning modified PEI, only about 5 PEI25k-PCL1500-PEG2k molecules were required to condense one pDNA molecule (N-value or site), whereas 11 PEI molecules were needed.

## Fluorescence Quenching Assay

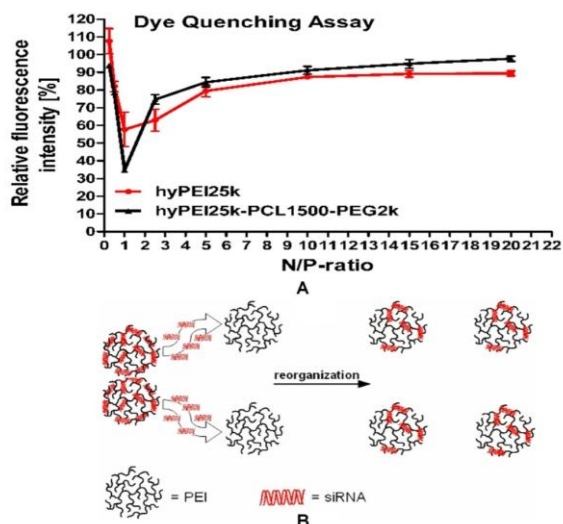


Figure 4. Dye quenching assay. (A) The fluorescence of Tye563-labeled siRNA molecules is quenched by each other in a “multi-molecular complex” due to close spatial proximity. Each curve had a minimum of fluorescence at N/P-ratio=1, after which the fluorescence increased again due to a decreased number of siRNA molecules per polyplex, resulting in less proximity of the labeled siRNA and thus in lower quenching. This special phenomenon of short nucleic acids condensation can be understood as a reorganization of the polyplexes. (B) Molecular reorganization of the siRNA within the polycations at lower N/P-ratios.

The dye quenching assay is another method to investigate the binding behavior of nucleic acids by polycations: the fluorescence of labeled siRNA molecules will be quenched by each other due to close spatial proximity in complexes where many siRNA molecules are compacted. Although we have used different polycations to condense siRNA, each curve has a minimum of fluorescence at N/P-ratio=1. After this minimum, the fluorescence increases again with increasing of N/P-ratio (Figure 4A). Interestingly, an equilibrium in ITC is also reached at remarkably lower N/P ratios for siRNA than for DNA, highlighting the

noteworthiness of this low N/P ratio. The endothermic peaks of siRNA binding isotherm curves close to N/P=1 (Figure 3), together with the dye quenching assay (Figure 4A) reveal a special condensation phenomenon of siRNA: siRNA molecules “escape” from saturated “primary multi-molecular nanocomplexes” at N/P=1 and reorganize into more stable nanocomplexes with a lower energy level (N/P=2) (Figure 4B). This trend was already observed with siRNA<sup>20</sup> and oligonucleotides<sup>21</sup>. Moreover, the particle size distribution (polydispersity index, PDI) measurements indicate that siRNA can be condensed into more ordered and uniform polyplexes with the lowest PDI at N/P=2 (Figure S2). Additionally, heparin assays confirmed that siRNA polyplexes at N/P=2 are particularly stable against competing polyanions (Figure S1). Therefore, we assumed that lower N/P-ratios (N/P=2 in case of PEI) are especially effective for siRNA delivery.

## ***In vitro* uptake and gene Knockdown effect**

Interestingly, with the following study of the relationship between nucleic acids/polycations aggregation mechanism and *in vitro* siRNA delivery efficiency, which is performed by RT-PCR (Figure 5A, 5B) and confocal laser scanning microscopy (Figure 5C), we found that not only PEI25kDa but also the PCL-PEG-modified copolymer hyPEI25k-PCL1500-PEG2k showed the best intracellular delivery and knockdown effect with siRNA at N/P=2, although higher N/P ratios were believed to be necessary until now by most of the researchers in the area of polycationic nanocarrier-based siRNA delivery<sup>22-25</sup>. In case of PEI25kDa, by increasing the N/P ratio, the hGAPDH gene expression decreased from N/P 1 (53.26% knockdown) to N/P 2 (72.29% knockdown) and increased again with the increasing of N/P ratios. The knockdown effect in the graph is better at N/P 30 than at N/P 2, but the negative control at N/P 30 is also very low, which indicates that at higher N/P-ratio, the knockdown effect is not only caused by gene silencing, but also the cytotoxicity of the polycations. The CLSM micrographs reflected the same tendency: although the siRNA could be delivered effectively into the cytosol at N/P 20, a less vital cell morphology with partially dilapidated cellular membranes was observed, which indicated a high cytotoxicity of these polycationic delivery agents at high N/P ratios. On the other hand, the siRNA delivery efficiency at N/P 2 was as good as at N/P 20, but with a vital cell morphology (Figure 5C), as a result of more uniform and stable complex formation and lower cytotoxicity.

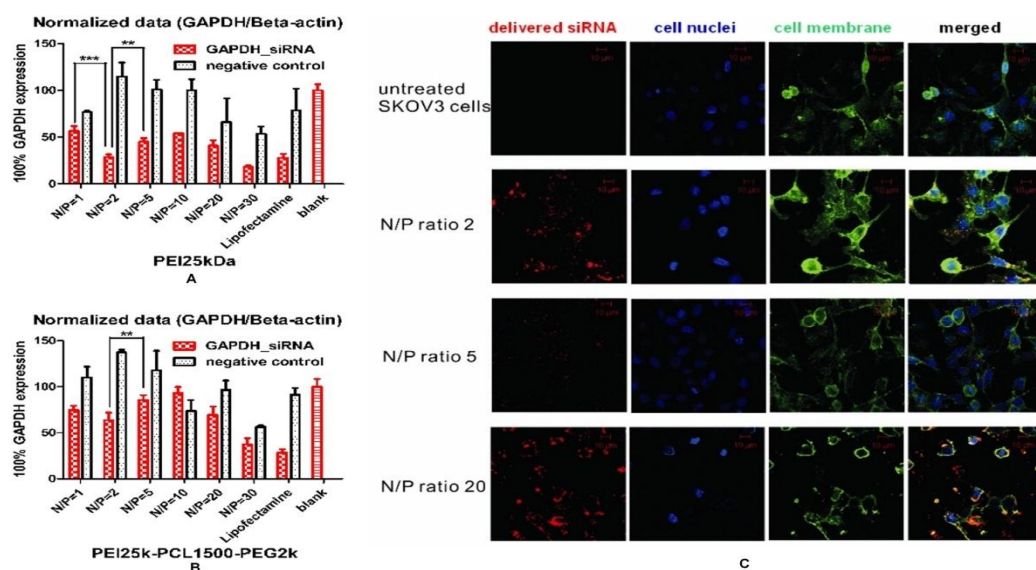


Figure 5. *In vitro* cell uptake and knockdown at different N/P-ratios. (A) Knockdown effect of siRNA/PEI25kDa polyplexes using RT-PCR. (B) Knockdown effect of siRNA/PEI25k-PCL1500-PEG2k polyplexes using RT-PCR: polycations showed the best knockdown effect with siRNA at N/P-ratio 2. In case of PEI25kDa, by increasing the N/P ratio, the GAPDH gene expression decreased from N/P 1 (53.26% knockdown) to N/P 2 (72.29% knockdown) and increased again. The knockdown effect at N/P 20 and 30 seems better than at N/P 2, but the lower negative control bar indicated the toxicity at higher N/P ratio. (C) Confocal laser scanning microscopy (CLSM) showed the cell uptake at different N/P ratios: both the uptake efficiency at N/P 2 and N/P 20 were good, but N/P 20 was too toxic, causing a less vital cell morphology (siRNA was labeled with AF647 dyes; nuclei were stained with DAPI and cell membranes were labeled with FITC-wheat germ agglutinin).

## 2.4 Conclusion

In our research we investigated the different complexation and aggregation mechanism between polycationic nanocarriers and DNA or siRNA on the atomic and molecular scale. The novel synergic use of MD simulations, ITC and dye quenching assay provided an exceptionally clear depiction of the different hierarchical aspects which control the formation of polyplexes. It is well accepted that the positively charged surface of poly(ethylenimine) nanocomplexes induces not only increased cellular uptake through charge-mediated interactions<sup>26</sup> (Figure 5C) but also disadvantageous higher cytotoxicity (especially true for high N/P ratios). While researchers seek to balance toxicity and transfection efficiency, our investigation highlights the need to address the actual assembly of polyelectrolyte complexes and to optimize the formulation of siRNA complexes from a thermodynamic point of view. Our study based on poly(ethylenimine) as a model polycationic nanocarrier directs the attention to lower N/P ratios, which emerge as an unnoticed “blind spot” in polycationic siRNA delivery. All our results emphasized one point: lower N/P-ratios are especially effective for polycationic nanocarrier-based siRNA delivery. This could have broad implications for the delivery of siRNA as less toxic and yet efficient delivery systems have been the bottle-neck for the translation of this promising approach into the clinical arena. We recommend to the scientific community working in the area of polycationic siRNA delivery to study the actual assembly of self-assembled nanocarriers and thus to consider low N/P ratios, which could be particularly important for siRNA delivery but have been disregarded in previous studies.

## 2.5 Materials and Methods

**Materials.** Hyperbranched polyethylenimine (hy-PEI) 25kDa was obtained from BASF. Poly(ethylene glycol) mono-methyl ether (mPEG) (5kDa) and  $\epsilon$ -caprolactone were purchased from Fluka (Taufkirchen, Germany). Beetle Luciferin, heparin sodium salt and all other chemicals were obtained from Sigma–Aldrich (Steinheim, Germany). Luciferase-encoding plasmid (pCMV-Luc) (LotNo.: PF461-090623) was amplified by The Plasmid Factory (Bielefeld, Germany). Negative control sequence, hGAPDH-DsiRNA, and TYE546-DsiRNA were obtained from Integrated DNA Technologies (IDT, Leuven, Belgium).

**Molecular modeling and MD simulations.** The binding of nucleic acid and PEI25kDa was modeled according to a reported validated strategy<sup>9, 27</sup>. The MD simulations were conducted according to previous studies<sup>9, 27-29</sup>.

**Isothermal titration calorimetry.** ITC was carried out with an iTC200 Micro Titration Calorimeter (Microcal, Inc., Northampton, MA, USA) according to our earlier report<sup>30, 31</sup>. The baseline (dilution energy) was recorded by titrating redundant amounts of polymer into water.

After integration and fitting of the binding isotherm of peaks with a single-site-binding assumption, the thermodynamic parameters enthalpy ( $\Delta H$ ), entropy ( $\Delta S$ ) and the dissociation constant  $K$  of binding were calculated.

**Dye quenching assay.** Dye quenching assays were conducted according to a previous study by Merkel et al.<sup>20</sup>

***In vitro* cell uptake and knockdown experiments.** SKOV3 cells were seeded with  $10^6$  cells per well in 6-wells 24 h prior to transfection and transfected with 50 pmol of siRNA. The mRNA was isolated 24 h after transfection (PureLink<sup>TM</sup> RNA Mini Kit, Invitrogen GmbH, Germany) and reverse transcribed to cDNA (First Strand cDNA Synthesis kit, Fermentas, Germany). RT-PCR was performed using QuantiFast<sup>TM</sup> SYBR<sup>®</sup> Green PCR Kits (Qiagen, Germany) and the Rotor-Gene 3000 RT-PCR thermal cycler (Corbett Research, Sydney, Australia). For confocal laser scanning microscopy, cells were incubated with nanocomplexes containing AF647 labeled siRNA for 4h and then fixed. Nuclei were stained with DAPI and cell membranes were labeled with FITC-wheat germ agglutinin (Invitrogen, Karlsruhe, Germany).

**Transmission electron microscopy.** Polyplexes were metalized during incubation with 0.005 M AgNO<sub>3</sub> for 2 hours at 25 °C. TEM measurements were performed using a JEM-3010 microscope (Jeol Ltd., Tokyo, Japan), operated at 300 kV, equipped with a high-resolution CCD camera for image recording.

**Statistics.** All analytical assays were conducted in replicates of three or four. Results are given as mean values $\pm$ standard deviation. Two way ANOVA and statistical evaluations were performed using Graph Pad Prism 4.03 (Graph Pad Software, La Jolla, USA).

## 2.6 Acknowledgements

The authors wish to acknowledge Dr. Ayse Kilic and Dr. Holger Garn (Institute of Laboratory Medicine and Pathobiochemistry, Philipps Universität Marburg) for use of the Rotor-Gene real time cycler, Eva Mohr (IPTB) for expert technical support in the cell culture, Michael Hellwig (Center of Material Science, Philipps Universität Marburg) for TEM imaging, Prof. Dr. Wolfgang Parak and Yu Xiang (Department of Physics, Philipps-Universität Marburg) for CLSM imaging and Dr. Dafeng Chu (Department of Pharmaceutics and Biopharmacy, Philipps Universität Marburg) for excellent discussions.

## 2.7 Supporting Informations

### S1. Binding and protection efficiency and stability against competing polyanions

Method

The stability of complexes against competing polyanions, represented by heparin, was evaluated by means of the change in fluorescence intensity obtained with the fluorescent intercalating probe Sybr® Gold. To study the effect of N/P-ratio on the stability of complexes, polyplexes were prepared in solutions at different N/P-ratio. 20  $\mu$ L heparin (150 000 IU/g, Serva, Pharm., USP XV2, Merck, Darmstadt, Germany) solution with a concentration of 1.5 IU/ $\mu$ mol siRNA was added into 200 $\mu$ L polyplex solution in each well of a 96-well plate (Perkin Elmer, Rodgau-Jügesheim) where each well contained 1  $\mu$ mol siRNA. After 20 min of incubation with the heparin solution at 25 °C, 20  $\mu$ L diluted Sybr® Gold solution (Invitrogen, Karlsruhe, Germany) were added. After another 20 min of incubation at 25 °C, fluorescence was directly detected with a fluorescence plate reader (BMG Labtech GMBH, Offenburg, Germany) at 495 nm excitation and 537 nm emission<sup>32</sup>.

## Results and Discussions

Sybr® Gold (Invitrogen) can be used to quantify purified DNA and RNA quickly and accurately and is widely used to investigate the molecular interaction properties between nucleic acids and gene delivery agents. Compared with gel-electrophoresis with EtBr, the Sybr Gold assay describes the affinity of polymer and nucleic acids in a more quantitative and sensitive way. Free nucleic acids, which are not condensed with polymers, can be quantified in an indirect approach with the Sybr® Gold assay. In these assays, we observed good condensation of siRNA even at low N/P ratios (Figure S1). PEI25k and PEG-PCL modified branched PEI25kDa showed complete condensation at N/P=2 and above, whereas the condensation of siRNA with PEG-PCL modified branched PEI25k was more efficient than with PEI25k. This can be explained by the higher affinity of hyPEI25k-PCL1500-PEG2k, which was also shown by isothermal titration calorimetry (ITC). The long PEG-PCL chain in hyPEI25k-PCL1500-PEG2k seems to be advantageous for complex formation with not only DNA, but also siRNA.

Heparin is a polyanion and can compete with nucleic acids for interaction with polycations. Polyplexes, which are formed only by electrostatic interaction, can be easily dissociated by the competing polyanion heparin. The results of the heparin assay showed a very interesting trend. The stability of the siRNA-polyplex did not increase regularly with an increase of the N/P-ratio. Based on the results of the Sybr® Gold assay, PEI25k was expected to have an increased protection of the siRNA at N/P=5 compared to N/P=2. However, the results of heparin assay showed that only 19.5% free siRNA was detected at N/P=2, whereas 47.8% free siRNA was observed at N/P=5. Hypothesizing that the siRNA reorganizes after N/P=1 and distributes into more distinct polyplexes, a lower energy level and more stable polyplexes would be obtained. Therefore the stability of the polyplexes and the protection of siRNA against the competing heparin polyanions are especially good at N/P=2. However, we assumed that at N/P=5, the “multi-molecular complex”

state is exceeded due to the excess of polymers and it is easier for the polyanions to reach the surface of the polyplex and to dissociate siRNA from the polyplex.

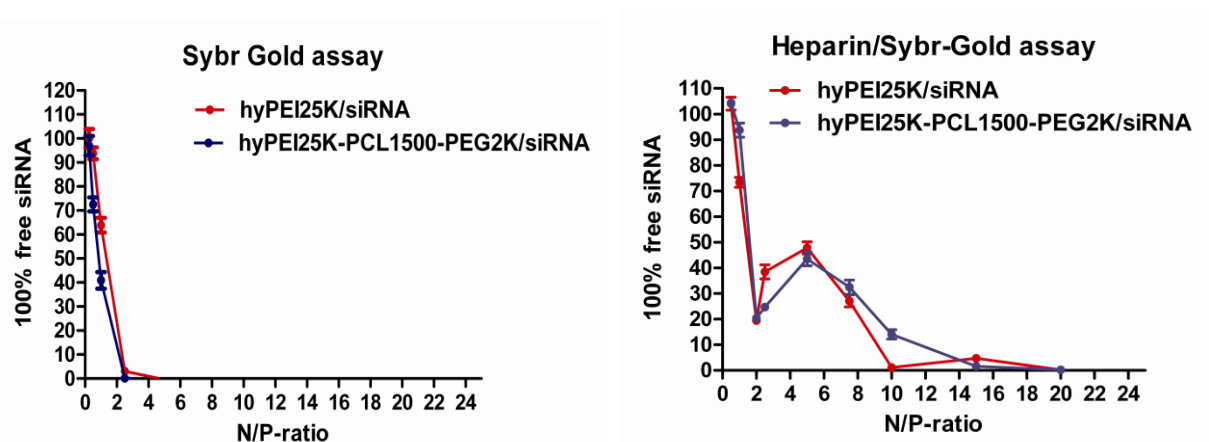


Figure S1: Sybr® Gold assay and heparin assay.

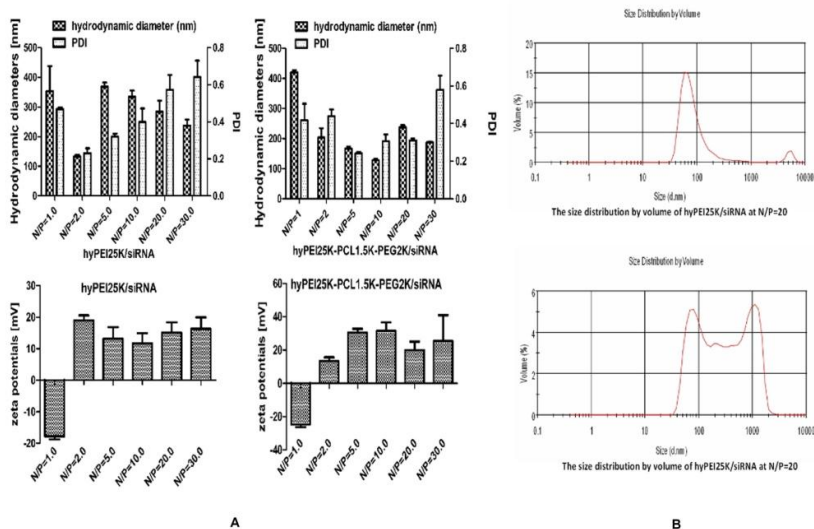
## S2. Dynamic light scattering and zeta potential analysis

Polyplexes were prepared with hGAPDH-DsiRNA or plasmid DNA as described above in 5% glucose solution at increasing N/P ratios and were measured as previously described in a disposable low volume UVette (Eppendorf, Wesseling–Berzdorf, Germany) using a Zetasizer Nano ZS (Malvern, Herrenberg, Germany). The measurement angle was 173° in back scatter mode. Zeta potentials were determined by laser Doppler anemometry (LDA) with the same samples after diluting 50  $\mu$ L of polyplexes with additional 500  $\mu$ L of glucose solution to a final volume of 550 $\mu$ L in a green zeta cuvette (Malvern, Herrenberg, Germany). Three samples were prepared for each N/P-ratio and three measurements were performed on each sample. Each measurement of size consisted of 15 runs of 10 s. Each measurement of zeta-potential consisted of 15–100 runs, which was set to automatic optimization by the software. Results are given as mean values (n=3) +/-SD.

With the increasing of N/P-ratio from 1 to 30, the size of DNA/polymer-polyplex decreased from 275 nm (N/P=1) to 101 nm (N/P=2) and remained stably below 100 nm at increased N/P-ratio. However, the size and surface charge of siRNA-polyplexes do not follow the trend of DNA-polyplexes: with increasing of the N/P-ratio, the polyplex size decreased at first to a minimum value and then increased again. For example, for polymer hyPEI25k, the smallest polyplexes were found at N/P-ratio 2 (133 nm), while for hyPEI25k-PCL1500-PEG2k, the minimum in size was observed at N/P-ratio 10 (128 nm). This difference can be explained by the different affinity of the polycations with siRNA, which was demonstrated by ITC. The K-value of hyPEI/siRNA ( $2.23E6 \pm 9.28E5$ ) was much higher than that of hyPEI25k-PCL1500-PEG2k/siRNA ( $2.80E5 \pm 7.40E4$ ). Due to the higher affinity of PEI25k, siRNA can be condensed into the smallest polyplexes at a low N/P-ratio. Interestingly, unlike polymer/DNA complexes, the size of

polymer/siRNA continues to increase if the N/P-ratio is further increased above the N/P ratio at which the smallest polyplexes were formulated. At higher N/P-ratios, the PDI was also much higher than the PDI at lower N/P-ratio.

Comparing the size distribution peaks based on volume at different N/P-ratios, we found that at N/P-ratio 2, 94.9% of the total polyplex distribution, had a mean size of 91.91 nm. If the N/P-ratio increased to 20, the characteristic peak of N/P-ratio 2 shifted only slightly, but contained only 35.5% of the polyplexes based on the volume distribution. Additionally, 15.4% of the polyplexes had a mean hydrodynamic diameter of 224.8 nm, and 12.1% of the polyplexes were found in a peak at 373.3 nm. Interestingly, in the dye quenching assay, almost no quenching could be observed at N/P 20. It was therefore assumed that individual polyplexes carried comparatively little siRNA at N/P 20, and that an excess of polymer was present as free polymer which can cause aggregation of polyplexes. As a result, we observed by dynamic light scattering a highly disperse distribution of peaks at N/P 20. Recent research of siRNA complexation by all-atom molecular dynamics simulations also reported that at a low charge ratio or N/P-ratio, all cationic polymers can bind to siRNA, but only a limited number of polymers can condense the siRNA at a high charge ratio.



### S3. *In vitro* transfection experiments with DNA

SKOV-cells were seeded with 0.2mL medium per well in 96-well plates (Nunc, Wiesbaden, Germany) at the density of 30,000 cells/mL. After 24h, 100µL medium (containing 10% serum) plus 25µL polymer/pDNA-complex containing 0.5µg pDNA (pCMVLuc, Plasmid Factory, Bielefeld, Germany) at different N/P-ratios were placed in each well. After 4h of incubation at 37.0°C in humidified atmosphere with 5% CO<sub>2</sub>, the medium was replaced with 200µL fresh medium containing 10% serum. After another 44h, cells were lysed in 100µL cell culture lysis



buffer (Promega, Mannheim, Germany) for 15min at 37 °C. A volume of 25µL of the cell lysate was added in each well of an opaque 96-well plate (Perkin Elmer, Rodgau-Jügesheim). Luciferase activity was quantified by injection of 50µL luciferase-assay-buffer, containing 10mM luciferin (Sigma–Aldrich, Taufkirchen, Germany). The resulting photons were measured as relative light units (RLU) with a plate luminometer (LumiSTAR Optima, BMG Labtech GmbH, Offenburg, Germany). Protein concentration was determined using a Bradford BCA assay (BioRad, Munich, Germany).

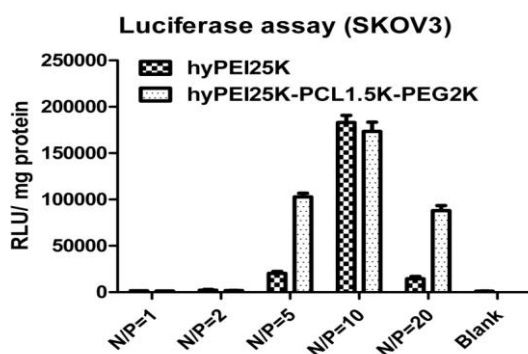


Figure S3: plasmid DNA transfection efficiency of hyPEI25kDa and copolymer hyPEI25k-PCL1.5k-PEG2k.

## 2.8 References

1. Riehemann, K.; Schneider, S. W.; Luger, T. A.; Godin, B.; Ferrari, M.; Fuchs, H., Nanomedicine--challenge and perspectives. *Angew Chem Int Ed Engl* **2009**, *48* (5), 872-97.
2. Petros, R. A.; DeSimone, J. M., Strategies in the design of nanoparticles for therapeutic applications. *Nature Reviews Drug Discovery* **2010**, *9* (8), 615-627.
3. Lollo, C. P.; Banaszczyk, M. G.; Chiou, H. C., Obstacles and advances in non-viral gene delivery. *Curr Opin Mol Ther* **2000**, *2* (2), 136-42.
4. Park, T. G.; Jeong, J. H.; Kim, S. W., Current status of polymeric gene delivery systems. *Advanced Drug Delivery Reviews* **2006**, *58* (4), 467-486.
5. Fire, A.; Xu, S.; Montgomery, M. K.; Kostas, S. A.; Driver, S. E.; Mello, C. C., Potent and specific genetic interference by double-stranded RNA in *Caenorhabditis elegans*. *Nature* **1998**, *391* (6669), 806-11.
6. Ferrari, M., Cancer nanotechnology: opportunities and challenges. *Nat Rev Cancer* **2005**, *5* (3), 161-71.
7. Zhang, L.; Gu, F. X.; Chan, J. M.; Wang, A. Z.; Langer, R. S.; Farokhzad, O. C., Nanoparticles in medicine: therapeutic applications and developments. *Clin Pharmacol Ther* **2008**, *83* (5), 761-9.
8. Steuber, H.; Czodrowski, P.; Sotriffer, C. A.; Klebe, G., Tracing changes in protonation: a prerequisite to factorize thermodynamic data of inhibitor binding to aldose reductase. *J Mol Biol* **2007**, *373* (5), 1305-20.
9. Pavan, G. M.; Danani, A.; Pricl, S.; Smith, D. K., Modeling the Multivalent Recognition between Dendritic Molecules and DNA: Understanding How Ligand "Sacrifice" and Screening Can Enhance Binding. *Journal of the American Chemical Society* **2009**, *131* (28), 9686-9694.
10. Pavan, G. M.; Kostianen, M. A.; Danani, A., Computational Approach for Understanding the Interactions of UV-Degradable Dendrons with DNA and siRNA. *Journal of Physical Chemistry B* **2010**, *114* (17), 5686-5693.

11. Doni, G.; Kostianen, M. A.; Danani, A.; Pavan, G. M., Generation-Dependent Molecular Recognition Controls Self-Assembly in Supramolecular Dendron-Virus Complexes. *Nano Letters* **2011**, *11* (2), 723-728.
12. Gary, D. J.; Puri, N.; Won, Y. Y., Polymer-based siRNA delivery: Perspectives on the fundamental and phenomenological distinctions from polymer-based DNA delivery. *Journal of Controlled Release* **2007**, *121* (1-2), 64-73.
13. Arnott, S., Principles of Nucleic-Acid Structure - Saenger, W. *Nature* **1984**, *312* (5990), 174-174.
14. Noy, A.; Perez, A.; Lankas, F.; Javier Luque, F.; Orozco, M., Relative flexibility of DNA and RNA: a molecular dynamics study. *J Mol Biol* **2004**, *343* (3), 627-38.
15. Pavan, G. M.; Albertazzi, L.; Danani, A., Ability to adapt: different generations of PAMAM dendrimers show different behaviors in binding siRNA. *J Phys Chem B* **2010**, *114* (8), 2667-75.
16. Merkel, O. M.; Mintzer, M. A.; Librizzi, D.; Samsonova, O.; Dicke, T.; Sproat, B.; Garn, H.; Barth, P. J.; Simanek, E. E.; Kissel, T., Triazine dendrimers as nonviral vectors for in vitro and in vivo RNAi: the effects of peripheral groups and core structure on biological activity. *Mol Pharm* **2010**, *7* (4), 969-83.
17. Koch, C.; Heine, A.; Klebe, G., Tracing the Detail: How Mutations Affect Binding Modes and Thermodynamic Signatures of Closely Related Aldose Reductase Inhibitors. *Journal of Molecular Biology* **2011**, *406* (5), 700-712.
18. Doni, G.; Kostianen, M. A.; Danani, A.; Pavan, G. M., Generation-dependent molecular recognition controls self-assembly in supramolecular dendron-virus complexes. *Nano Lett* **2011**, *11* (2), 723-8.
19. Zheng, M.; Liu, Y.; Samsonova, O.; Endres, T.; Merkel, O.; Kissel, T., Amphiphilic and biodegradable hy-PEI-g-PCL-b-PEG copolymers efficiently mediate transgene expression depending on their graft density. *Int J Pharm* **2011**.
20. Merkel, O. M.; Beyerle, A.; Librizzi, D.; Pfestroff, A.; Behr, T. M.; Sproat, B.; Barth, P. J.; Kissel, T., Nonviral siRNA delivery to the lung: investigation of PEG-PEI polyplexes and their in vivo performance. *Mol Pharm* **2009**, *6* (4), 1246-60.
21. Van Rompaey, E.; Engelborghs, Y.; Sanders, N.; De Smedt, S. C.; Demeester, J., Interactions between oligonucleotides and cationic polymers investigated by fluorescence correlation spectroscopy. *Pharmaceutical Research* **2001**, *18* (7), 928-936.
22. Park, J. W.; Bae, K. H.; Kim, C.; Park, T. G., Clustered magnetite nanocrystals cross-linked with PEI for efficient siRNA delivery. *Biomacromolecules* **2011**, *12* (2), 457-65.
23. Wu, Y.; Wang, W. W.; Chen, Y. T.; Huang, K. H.; Shuai, X. T.; Chen, Q. K.; Li, X. X.; Lian, G. D., The investigation of polymer-siRNA nanoparticle for gene therapy of gastric cancer in vitro. *International Journal of Nanomedicine* **2010**, *5*, 129-136.
24. Dimitrova, M.; Affolter, C.; Meyer, F.; Nguyen, I.; Richard, D. G.; Schuster, C.; Bartenschlager, R.; Voegel, J. C.; Ogier, J.; Baumert, T. F., Sustained delivery of siRNAs targeting viral infection by cell-degradable multilayered polyelectrolyte films. *Proc Natl Acad Sci U S A* **2008**, *105* (42), 16320-5.
25. Urban-Klein, B.; Werth, S.; Abuharbeid, S.; Czubayko, F.; Aigner, A., RNAi-mediated gene-targeting through systemic application of polyethylenimine (PEI)-complexed siRNA in vivo. *Gene Ther* **2005**, *12* (5), 461-6.
26. Godbey, W. T.; Wu, K. K.; Mikos, A. G., Size matters: molecular weight affects the efficiency of poly(ethylenimine) as a gene delivery vehicle. *J Biomed Mater Res* **1999**, *45* (3), 268-75.

- 27.Merkel, O. M.; Zheng, M.; Mintzer, M. A.; Pavan, G. M.; Librizzi, D.; Maly, M.; Hoffken, H.; Danani, A.; Simanek, E. E.; Kissel, T., Molecular modeling and in vivo imaging can identify successful flexible triazine dendrimer-based siRNA delivery systems. *J Control Release* **2011**, *153* (1), 23-33.
- 28.Pavan, G. M.; Mintzer, M. A.; Simanek, E. E.; Merkel, O. M.; Kissel, T.; Danani, A., Computational Insights into the Interactions between DNA and siRNA with "Rigid" and "Flexible" Triazine Dendrimers. *Biomacromolecules* **2010**, *11* (3), 721-730.
- 29.Jensen, L. B.; Mortensen, K.; Pavan, G. M.; Kasimova, M. R.; Jensen, D. K.; Gadzhyeva, V.; Nielsen, H. M.; Foged, C., Molecular characterization of the interaction between siRNA and PAMAM G7 dendrimers by SAXS, ITC, and molecular dynamics simulations. *Biomacromolecules* **2010**, *11* (12), 3571-7.
- 30.Klebe, G.; Steuber, H.; Czodrowski, P.; Sotriffer, C. A., Tracing changes in protonation: A prerequisite to factorize thermodynamic data of inhibitor binding to aldose reductase. *Journal of Molecular Biology* **2007**, *373* (5), 1305-1320.
- 31.Klebe, G.; Koch, C.; Heine, A., Tracing the Detail: How Mutations Affect Binding Modes and Thermodynamic Signatures of Closely Related Aldose Reductase Inhibitors. *Journal of Molecular Biology* **2011**, *406* (5), 700-712.

## Chapter 3

### **AMPHIPHILIC AND BIODEGRADABLE hy-PEI-g-PCL-b-PEG COPOLYMERS EFFICIENTLY MEDIATE TRANSGENE EXPRESSION DEPENDING ON THEIR GRAFT DENSITY**

Published in International Journal of Pharmaceutics, Theme Issue “Non-viral gene medicine”.  
(2011) 427, 80-7.

**Mengyao Zheng<sup>1</sup>, Yu Liu<sup>1</sup>, Olga Samsonova<sup>1</sup>, Thomas Endres, Olivia Merkel, and Thomas Kissel\***

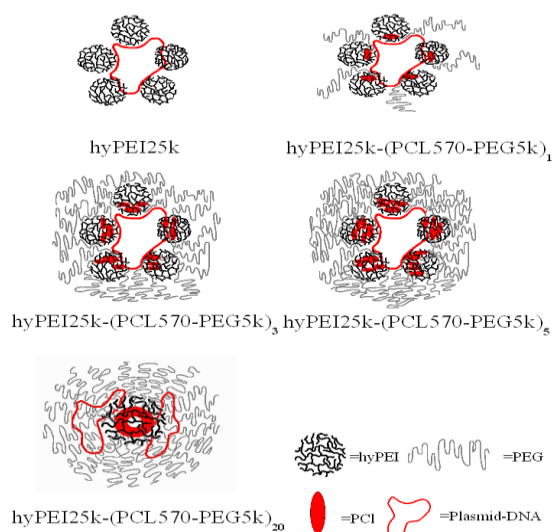
<sup>1</sup>Both authors contributed equally to this work.

#### **Author contributions**

T. K. guided and directed the research. Y. L. synthesized and characterized the polymers. M. Z. designed the measurements and carried out all of the biological and biophysical experiments. M. Z. and O. M. M. analysed the experimental data.

### 3.1 Abstract

Novel biodegradable amphiphilic copolymers hy-PEI-g-PCL-b-PEG were prepared by grafting PCL-b-PEG chains onto hyper-branched poly(ethylene imine) as non-viral gene delivery vectors. Our investigations focused on the influence of graft densities of PCL-b-PEG chains on physico-chemical properties, DNA complexation and transfection efficiency. We found that the transfection efficiencies of these polymers increased at first towards an optimal graft density ( $n=3$ ) and then decreased. The buffer-capacity-test showed almost exactly the same tendency as transfection efficiency. Cytotoxicity (MTT-assay) depended on the cooperation of PEG molecular weight and graft density of PCL-b-PEG chains. With increasing the graft density, cytotoxicity, zeta-potential, affinity with DNA, stability of the polyplexes and CMC-values were reduced strongly and regularly. Increasing the excess of polymer over DNA was shown to result in a decrease of the observed particle size to 100–200 nm. The application of these copolymers in siRNA transfection will be also under investigation and efficient transfection efficiency is expected with polymer hyPEI25K-(PCL570-PEG5K)<sub>3</sub> and polymer hyPEI25K-(PCL570-PEG5K)<sub>5</sub>.



Graphical Abstract: Schematic conformation of polyplexes from hyPEI25k-(PCL570-PEG5k)<sub>n</sub>: at graft densities of 1 to 5, PEG-PCL chains stay in separated blocks; but it was assumed to form a continuous corona at  $n=20$ .

**Keyword:** Transfection; Non-viral gene delivery; Biodegradable copolymer; Hyper-branched poly(ethylene imine) (hyPEI); Graft density; Buffer-capacity

### 3.2 Introduction

Thanks to advances in molecular biology and genomic research, numerous diseases have been given a genetic identity for which gene therapy may provide a possible treatment (Pawliuk et al., 2001; von Laer et al., 2006; Wong et al., 2006). For viral gene delivery techniques, viruses can be transformed into gene-delivery vehicles by replacing parts of the genome of a virus with a therapeutic gene (Pack et al., 2005). But viral vectors could induce cancer (Check, 2002; Hacein-Bey-Abina et al., 2003), and initiate an immunogenic response which has led to a fatal outcome (Marshall, 2000). Instead of viral gene delivery techniques, non-viral gene delivery

techniques have been investigated, which are considered as a safer, less pathogenic and immunogenic gene delivery alternative (Wong et al., 2007). Studies demonstrated that polymeric vectors might be advantageous over viruses and liposomes (Merdan et al., 2002) for gene delivery, regarding safety, immunogenicity, mutagenicity and production costs (Han et al., 2000).

Hyper-branched polyethylenimine (hy-PEI) is one of the most successfully used cationic polymers for gene delivery both *in vitro* and *in vivo* (Boussif et al., 1995; Godbey et al., 1999). HyPEI can condense DNA via electrostatic interaction to particles with sizes compatible with cellular uptake while providing steric protection from nuclease degradation (Bielinska et al., 1997). HyPEI has a unique property of endosomal buffering capacity due to protonable amino groups. This function causes osmotic swelling and subsequent endosomal disruption (Boussif et al., 1995), thus permitting the escape of endocytosed materials. However, PEI has a relatively high cytotoxicity due to the high density of cationic groups, especially at high molecular weights (Fischer et al., 1999; Kunath et al., 2003). PEI-PEG copolymers are less toxic than PEI (Sung et al., 2003). However they are not able to condense DNA into small particles less than 200 nm, which is critical for cell uptake and transfection efficiency (Park et al., 2005; Pun et al., 2004). Another drawback of PEI-PEG are the non-biodegradable bonds between PEI and PEG chains. Polymers that are not eliminated from the circulation may accumulate in tissues and cells. To resolve this problem, biodegradable hy-PEI-g-(PCL-b-PEG)<sub>n</sub> copolymers were synthesized (Shuai et al., 2003). Poly(caprolactone) (PCL) acts as a linker between PEI and PEG to increase the biodegradability of the copolymers. Hydrophobic PCL improves also the overall permeability of the complexes through the cell membranes. Another advantage of PCL is the shielding of the positive charges and the condensation of the DNA into small complexes of 100 nm (Han et al., 2001; Kono et al., 2005; Tian et al., 2007; Wang et al., 2002).

The copolymers hy-PEI-g-(PCL-b-PEG)<sub>n</sub> have been studied so far as potential gene delivery systems (Liu et al., 2009; Shuai et al., 2003). These investigations were limited to the discussion of the influence of PEI, PCL and PEG chain lengths. Nevertheless, the influence of graft density has not been studied systematically. In this report, a panel of hyPEI<sub>25K</sub>-(PCL<sub>570</sub>-PEG<sub>5k</sub>)<sub>n</sub> block copolymers was synthesized to elucidate the effect of graft density on physicochemical properties, DNA complexation and biological activities as non-viral gene delivery vectors. It is

commonly believed that the molecular weight of PEI most suitable for gene transfer ranges between 5 and 25 kDa. Higher molecular weights lead to increased cytotoxicity (Fischer et al., 2003), presumably due to aggregation to huge clusters of the cationic polymer on the outer cell membrane, which thereby induce necrosis (Freshney, 2005). To study their physicochemical properties and complexation with DNA, measurements of size and zeta-potential, heparin-assay, critical micelle concentration (CMC) and buffer-capacity were performed. The physico-chemical properties of these complexes were then compared with *in vitro* results of cytotoxicity tests (MTT), confocal laser scanning microscopy (CLSM) and transfection experiments. These results provide a basis for the rational design of block copolymers as gene delivery systems.

### 3.3. Materials and Methods

#### Materials

Hy-PEI with molecular weight of 25 kDa was obtained from BASF. Poly (ethylene glycol) mono-methyl ether (mPEG) (5 kDa) and  $\epsilon$ -caprolactone were purchased from Fluka (Taufkirchen, Germany), and all other chemicals were obtained from Sigma-Aldrich (Steinheim, Germany). Hy-PEI-PCL-mPEG was synthesized as reported previously (Liu et al., 2009). DNA from herring testes (Type XIV, 0.3-6.6 MDa, 400-10 000 bp) was from bought from Sigma (Steinheim, Germany), and Luciferase-Plasmid (pCMV-Luc) (Lot No.:PF461-090623) was amplified by The Plasmid Factory (Bielefeld, Germany).

#### Polyplex formation

All complexes of DNA and polymer were prepared freshly before use. Luciferase-Plasmid and DNA from herring testes were stored at -20 °C. Before use, 5% glucose solution and other buffer solutions were filtered freshly through 0.20  $\mu$ m pore sized filters (Nalgene® syringe filter, Sigma–Aldrich, Taufkirchen, Germany). The volume of a 1 mg/mL (based on hyPEI25k) polymer stock solution required for a certain N/P ratio (=Nitrogen/Phosphorus-ratios) was calculated as follows (Liu et al., 2009):

$$V_{\text{DNA}} = (C_{\text{copolymer}} * V_{\text{copolymer}} * 330) / (C_{\text{DNA}} * 43 * \text{N/P})$$

$C_{\text{copolymer}}$  = the concentration of the stock copolymer

$C_{DNA}$  = the concentration of the stock DNA solution

A certain amount of polymer stock solution was diluted with 5% glucose solution or other buffer solutions to a final volume of 50  $\mu\text{L}$ , which was mixed with an equal volume of diluted DNA aliquots in microcentrifuge tubes by pipetting (IKA, Stauffen), and incubated for 20 min before use for complex and equilibrium formation.

### **Cell culture**

Cells were seeded at a density of  $3.5 \times 10^3$  cells/cm<sup>2</sup> in dishes (10 cm diameter, Nunclon Dishes, Nunc, Wiesbaden, Germany) and incubated at 37 °C in humidified 5% CO<sub>2</sub> atmosphere (CO<sub>2</sub>-Incubator, Integra Biosciences, Fernwald, Germany). Medium (Dulbecco's modified Eagle medium, supplemented with 10% serum) was exchanged every 2 days. Cells were split after 7 days, when confluence was reached.

### **Measurement of size and zeta-potential**

Three buffer-solutions (5% glucose, pH 6.6; 10 mM TE-buffer, pH 9.0; 15 mM acetate-buffer, pH 5.5) were used for the measurement of size and zeta-potential, which were monitored with a Malvern Zetasizer Nano ZS (Malvern Instrument, Worcestershire, UK) at 25 °C. The measurement angle was 173 ° in backscatter mode. Following size measurements, zeta-potential measurements were performed with the same samples after diluting 50  $\mu\text{L}$  of polyplexes with additional 500  $\mu\text{L}$  of buffer solution to a final volume of 550  $\mu\text{L}$  with a DNA concentration of 1.82 ng/ $\mu\text{L}$ . Three samples were prepared for each N/P-ratio and three measurements were performed on each sample. Each measurement of size consisted of 15 runs of 10 sec. Each measurement of zeta-potential consisted of 15–100 runs, which was set to automatic optimization by the software.

### **Buffer-capacity**

Titration studies were performed to determine the buffer-capacity of the studied polymers. Therefore, 0.4 mL of aqueous polymer solution with the concentration of 2.5 mg/mL was titrated with standard 0.1 N HCl, until the pH of the polymer solutions decreased nearby pH=2.5. The pH-value was detected with a pH-meter (Hanna PH210 Microprocessor pH Meter) and an electrode (Inlab, Mettler Toledo, Schwerzenbach, Switzerland) at 25 °C.



### **Critical micelle concentration (CMC)**

In this experiment, the surface tension with increased polymer concentration in water was measured with a tensionmeter (Krüss Tensionmeter Control Panel; K11-MK3) at 25 °C. Data correlation with the polymer structure was performed using “Origin 7.0” (Origin-Labsoftware, Northampton, USA).

### **Heparin-assay**

The effect of heparin on the stability of complexes was evaluated by means of the change in fluorescence intensity obtained with the fluorescent intercalating probe sybr-gold (Creusat et al., 2010). To study the effect of pH on the stability of complexes, polyplexes were prepared in solutions with different pH and ionic strength. Heparin solution (150000 IE/g, Serva, Pharm., USP XV2, Merck, Darmstadt, Germany) was diluted to a concentration of 0.521 mg/mL. Increasing amounts (0 – 17.5 µL) of heparin were added to the 96-well plate (Perkin Elmer, Rodgau-Jügesheim) where each well contained 200 µL of polymer/HT-DNA-complexes at N/P 10. Subsequently, 20 µL diluted sybr-gold-solution (Invitrogen, Karlsruhe, Germany) were added. After 20 min of incubation at 25 °C, fluorescence was directly detected with a fluorescence plate reader (BMG Labtech GMBH, Offenburg, Germany) at 495 nm excitation and 537 nm emission.

### **MTT-assay**

*In vitro* cytotoxicity tests of the copolymers were performed by MTT-assays. Pure polymers were selected instead of DNA polyplexes to measure the cytotoxicity in a “worst case scenario” since it has been reported that the cytotoxicity was reduced when polymers were complexed with DNA (Godbey et al., 1999). The assays were performed as previously described (Liu et al., 2009). Briefly, L929 cells were seeded in 96-well cell culture-coated microtiter plates at the density of 8,000 cells/well and incubated in DMEM low glucose (PAA, Cölbe, Germany) supplemented with 10% fetal calf serum (Cytogen, Sinn, Germany) in humidified atmosphere with 5% CO<sub>2</sub> at 37 °C for 24 h prior to the treatment with polymer solutions of increasing concentration (from 9.77E-4 mg/mL to 0.5 mg/mL). After 24 h, the medium was replaced with 200 µL serum free medium and 20 µL 3-(4,5-dimethylthiazol-2-yl)-2,5-diphenyltetrazolium bromide (MTT, Sigma–Aldrich,

Germany) reaching a final concentration of 0.5 mg MTT/mL. Cells were incubated for another 4 h before 200  $\mu$ L of dimethylsulfoxide (DMSO) was added to dissolve the purple formazane product. The absorption was quantified using a plate reader (Titertek plus MS 212, ICN, Germany) at wavelengths of 570 nm and 690 nm. The IC<sub>50</sub> was calculated as the polymer concentration which inhibits growth of 50% of cells relative to non-treated control cells.

### **Confocal laser scanning microscopy (CLSM)**

MeWo-cells were seeded in 8 well-chamberslides (Lab-Tek; Rochester, NY, USA) at 50,000 cells/well and incubated for 24 h in DMEM high glucose (PAA, Cöbe, Germany) supplemented with 10% fetal calf serum (Cytogen, Sinn, Germany) in humidified atmosphere with 5% CO<sub>2</sub> at 37 °C. The DNA labeling steps were performed at room temperature and in the dark to protect fluorescent markers. YOYO-1 stock solution (Invitrogen, Karlsruhe, Germany) was diluted 50-fold with TE-buffer and 30  $\mu$ L of DAPI stock solution (6  $\mu$ g/mL, Molecular Probes, Eugene, OR, USA) was diluted with 1 mL PBS. Plasmid-DNA (pDNA) was incubated with YOYO-1 solution for 30 minutes at a weight ratio of 1:15. Complexes of YOYO-1-labeled pDNA were formed as usual by incubation with polymer solution at N/P 15 in 5% glucose solution for 20 minutes followed by addition of 25  $\mu$ L of polyplex solution, containing 0.5  $\mu$ g plasmid-DNA, to 375  $\mu$ L fresh culture medium with 10% FCS in each well. After incubation for 4 h, each chamber was washed twice with 0.5 mL PBS, and the cells were then fixed by incubating each chamber for 20 minutes with 0.5 mL of 4% paraformaldehyde in PBS (4% PFA). Subsequently, 100  $\mu$ L DAPI-solution was added per chamber and incubated for another 20 minutes in the dark. The cells were washed three times with 0.5 mL PBS before being fixed with Fluorsafe (Calbiochem, San Diego, USA) and covered with a No. 1.5 thickness cover slip (Menzel Gläser, Braunschweig, Germany). YOYO-1 labeled DNA was excited with a 488 nm argon laser, while DAPI-stained chromosomal DNA was excited with an enterprise laser with an excitation wavelength of 364 nm, and CLSM was performed by using a 385 nm long pass filter and a band-pass filter of 505–530 nm in the single-track mode (Axiovert 100 M and CLSM 510 Scanning Device; Zeiss, Oberkochen, Germany).

### ***In vitro* transfection experiments with DNA**

MeWo-cells were seeded in 48 well-plates (Nunc, Wiesbaden, Germany) at the density of 60,000 cells/well (0.4 mL medium/well) 24 h before transfection. On the day of transfection, 175  $\mu$ L medium (containing 10% serum) plus 25  $\mu$ L polymer/DNA-complex were placed in each well (containing 0.5  $\mu$ g pDNA per well). Polymer/DNA-complexes were prepared at different N/P-ratios. After 4 h of incubation at 37.0  $^{\circ}$ C, in humidified atmosphere with 5% CO<sub>2</sub>, the medium was replaced with fresh medium containing 10% serum. Luciferase activity was assayed 44 h after transfection. Cells were lysed in 100  $\mu$ L cell culture lysis buffer (Promega, Mannheim, Germany) for 15 minutes at 25  $^{\circ}$ C. Luciferase activity was quantified by injection of 50  $\mu$ L luciferase-assay-buffer, containing 10 mM luciferin (Sigma-Aldrich, Taufkirchen, Germany), to 25  $\mu$ L of the cell lysate. The relative light units (RLU) were measured with a plate luminometer (LumiSTAR Optima, BMG Labtech GmbH, Offenburg, Germany). Protein concentration was determined using a Bradford BCA assay (BioRad, Munich, Germany).

## Statistics

All analytical assays were conducted in replicates of three or four, as indicated. Results are given as mean values +/- standard deviation (SD). Two way ANOVA and statistical evaluations were performed using Graph Pad Prism 4.03 (Graph Pad Software, La Jolla, USA).

## 3.4. Results and Discussion

### Influence of polymer structure on the size and zeta-potential of polyplexes

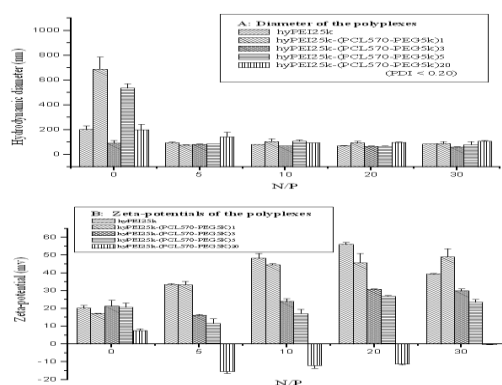


Fig. 1 A: Diameter of the polyplexes in 5% glucose solution at different N/P ratios. N/P 0= pure polymers in solution. B: Zeta potentials of the polyplexes in 5% glucose solution at different N/P ratios.

All copolymers were able to condense DNA into particles with sizes of 100–200 nm (Fig. 1A). No obvious size decrease was observed in 5% glucose when N/P ratio increased from 5 to 30. Under high ionic strength conditions (10 mM TE-buffer, pH 9.0; 15 mM acetate-buffer, pH 5.5), all copolymers formed larger complexes as compared to 5% glucose solution (Tab. SM 1). This result can be

explained by the shielding-effect of glucose molecules (Petersen et al., 2002). On the other hand, the polyplexes can aggregate in the buffer-solutions due to the reduced surface charge and lack of repulsion of the polymers (Petersen et al., 2002). The results of size measurements yielded comparable values as recently reported (Liu et al., 2009).

The zeta-potential was reduced with an increasing number  $n$  of PCL570-PEG5k segments, and was always highest in non-buffered glucose solution (Fig. 1A and Tab. SM 1). All polyplexes except hyPEI25k-(PCL570-PEG5k)<sub>20</sub> showed a positively charged surface at all buffer conditions. Due to the high graft density of hyPEI25k-(PCL570-PEG5k)<sub>20</sub>, the polymer loses its ability to condense DNA into a stable polyplexes as most positive charges of hyPEI are shielded, resulting in negatively charged polyplexes. It is assumed that the DNA remains only on the surface of this polymer (Scheme 1).

Interestingly, no further increase of the zeta-potential was observed when increasing the N/P ratio above 20, except for the polymer with graft density of 20. Therefore we hypothesize that for polymers with a graft density ranged between 1 and 5 at N/P 20 a polymer concentration is reached above which the additional polymer does not contribute to the condensation of DNA but is rather present as free polymer.

### Influence of polymer structure on the buffer-capacity

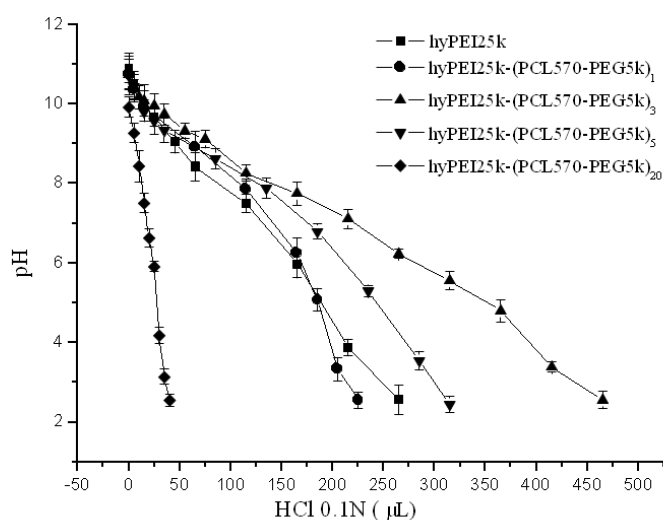


Fig. 2: Titration curve of aqueous polymer solution with standard 0.1 N HCl.

The most commonly used pH-sensitive excipients for gene delivery that exhibit the so-called “proton-sponge effect” are polymers such as PEI with protonatable amino groups with  $5 < pK_a < 7$  (Behr, 1997). The polymers with high buffer-capacity increase the ion concentration in the endosome and ultimately cause osmotic

swelling and rupture of the endosome membrane, which releases the polyplexes into the cytosol. Figure 2 shows the the buffer-capacity of the polymers which decreased in the following order:  $\text{hyPEI25k-(PCL570-PEG5k)}_3 > \text{hyPEI25k-(PCL570-PEG5k)}_5 > \text{hyPEI25K-(PCL570-PEG5k)}_1 = \text{hyPEI25k} > \text{hyPEI25k-(PCL570-PEG5k)}_{20}$ . With these results, it was shown that a low grafting degree of PEI with PCL-PEG segments can increase the accessibility of amines to be protonated, thereby increasing the buffer capacity. Thus, stability of the complexes could additionally be increased.

### **Influence of polymer structure on the CMC**

The critical micelle concentration (CMC) is defined as the concentration where the interfacial tension reached a minimum. It is extremely valuable not only to predict the micelle-forming capacity but also to determine the stability of the polymeric micelles, which was believed to play a crucial role in DNA transfection. In general, all amphiphilic polymers were able to form micelles at low concentrations (Tab. 1). For the copolymers with graft densities of 5 and 20, the CMC was reached at lower concentrations ( $8.7 \cdot 10^{-10}$  mol/L and  $4.6 \cdot 10^{-10}$  mol/L) in water. The results of CMC measurements in water were expected to be a function of the PCL molecular weight. Generally, increasing the amounts of hydrophobic segments decreases the CMC of copolymers. This principle could clearly be observed in our study where CMC-values decreased exponentially with the increase of PCL molecular weight, as shown in Figure 3. The tendency towards aggregation may also be affected by the presence of shielding components, for example glucose molecules or PEG chains in the copolymers, which may also decrease interactions between individual complexes as well as interactions between complexes and blood components in the systemic circulation (Petersen et al., 2002). Besides the shielding-effects of the PEG-PCL chains, the faster degradation of the polymers with higher graft density can also change the CMC tendency in base (Liu et al., 2010).

Tab. 1: CMC-values in water.

polymer	CMC in water (pH 7.0) (10E-9 mol/L)
hyPEI25k	none
hyPEI25k-(PCL570-PEG5k) <sub>1</sub>	16.76 ± 0.14
hyPEI25k-(PCL570-PEG5k) <sub>3</sub>	2.30 ± 0.11
hyPEI25k-(PCL570-PEG5k) <sub>5</sub>	0.87 ± 0.09
hyPEI25k-(PCL570-PEG5k) <sub>20</sub>	0.46 ± 0.02

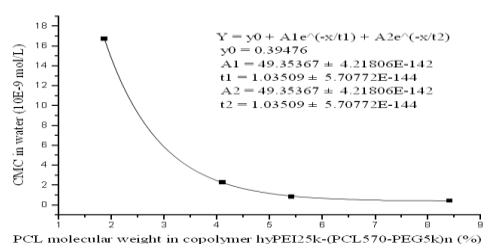


Fig. 3: The CMC-values decreased with the increase of the percentage of PCL molecular weight in the copolymers.

### Influence of polymer structure on the stability of polymer-DNA-complexes

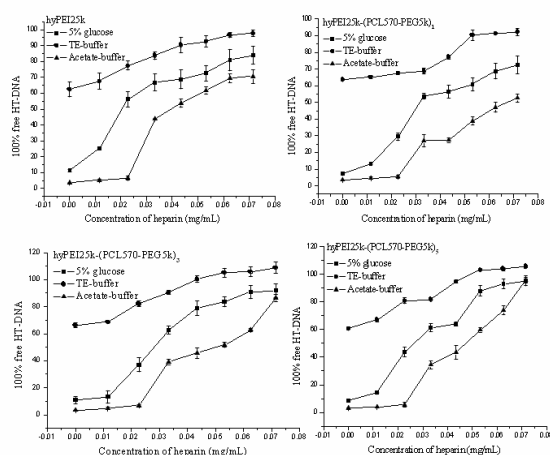


Fig. 4: DNA dissociation from complexes by heparin competition in different buffers.

Polymer/DNA-complexes, which are built due to electrostatic interaction, can be dissociated easily with the competing polyanion heparin (Moret et al., 2001). The release of DNA from complexes in the presence of heparin is summarized in Figure SM 1. The dissociation profiles all exhibit significant dependency on the heparin concentration. Another general trend is that all polymers display more stable complexes in acetate buffer as compared to other solutions.

Interestingly, hy-PEI25k-(PCL570-mPEG5k)<sub>1</sub>, released only 50% of the DNA load at 0.075 mg/ml heparin, the highest concentration tested. However, unstable complexes were obtained in TE buffer for all polymers. This can be explained by the fact that the amino groups in the polymers were protonated under acidic conditions, while deprotonated in TE buffer. Comparing the diagrams in Figure 4, no obvious difference was observed amongst the polymers in 5% glucose and TE buffer, while the stability of complexes was increased PEG-PCL-grafting in acetate buffer at low heparin concentrations. This may be caused by the shielding-effect of PCL-mPEG and a resulting inaccessibility for heparin. Although our data emphasize the importance of protonation of the polymer for stable interaction with DNA, a certain amount of lipophilic segments can even increase the stability as shown by hyPEI25k-(PCL570-PEG5k)<sub>1</sub>. Indeed, reduced complexation ability of copolymers may additionally facilitate the unpacking of the vector inside the cell, and a balance between DNA-complexation and DNA-release is necessary. Many reports described similar observations of increased transfection efficiency with reduction of positive charges (Banaszczyk et al., 1999; Schaffer et al., 2000).

### **Influence of polymer structure on the cytotoxicity**

To evaluate the cytotoxicity of hy-PEI-g-PCL-b-mPEG copolymers in L929 cells, MTT-assays were performed. Considering the IC<sub>50</sub> values, the cytotoxicity was clearly reduced with increasing of the graft density of the PCL570-PEG5k segments (Fig.5). PEG is very hydrophilic and considered to be safe by the FDA (Sung et al., 2003). By grafting PEG onto PEI, the toxicity of hyPEI25k is known to be reduced (Petersen et al., 2002). At the same time, the PCL segment is hydrophobic and shields the positive charges from hyPEI25K. On the other hand, the addition of PCL-segments increases also the degradation of the copolymers (Liu et al., 2010). It was interestingly found in Figure 6 that the IC<sub>50</sub>-values increased proportional as a function of the parameter: (percent of PEG molecular weight in copolymer) × (graft density n). This result provides a basis for the rational design of block copolymer with low cytotoxicity. But on the other hand, with the decrease of positive charges on the polymers, the stability of the polymer/DNA-complex and the interaction with negatively charged cell membranes can be reduced. It was therefore hypothesized that a low graft density would be advantageous for transfection.

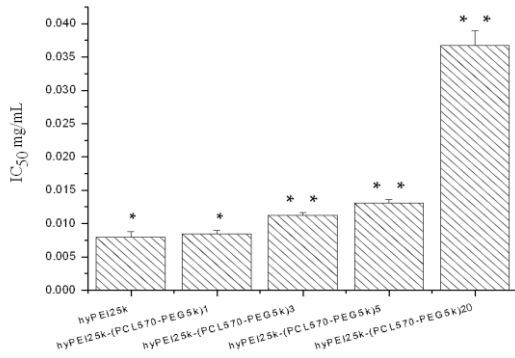


Fig. 5: IC<sub>50</sub>-values of each polymer as determined by MTT-assays in L929-cells.

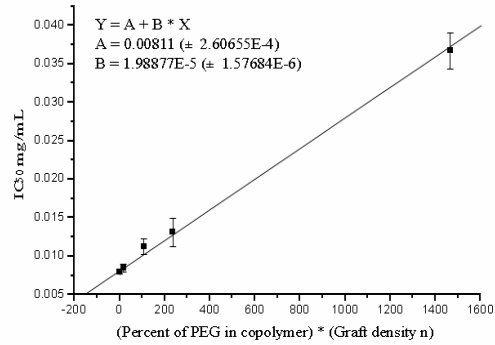


Fig. 6: PEG molecular weight and graft density of PCL-PEG chains both influence the cytotoxicity.

### Transfection experiments with plasmid-DNA

From the Figure 7, we found that the transfection efficiencies of these polymers increased at first towards an optimal graft density (n=3) and then decreased.

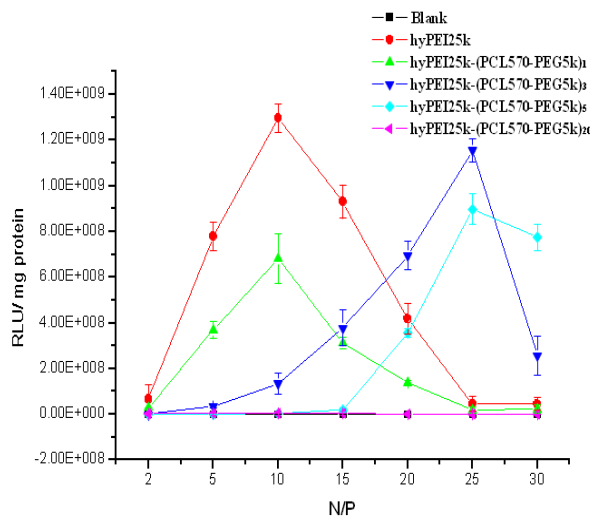


Fig. 7: Result of transfection of MeWo-cells in presence of serum in 48 well-plates.

showed comparable tendencies of transfection efficiency: the best N/P-ratio of transfection was 25. In case of N/P 25, the polymer with graft density 3 showed a 25.4 fold higher transfection efficiency than hyPEI25k. Due to the decrease of toxicity with increasing graft density, the optimal N/P-ratio was shifted for hyPEI25k-(PCL570-PEG5k)<sub>3</sub> and hyPEI25k-(PCL570-PEG5k)<sub>5</sub>. This shift additionally led to the hypothesis that polymers with little PEI content exhibit low transfection efficiency at low N/P-ratios but higher efficiencies than PEI at high N/P ratios. These properties rendered the two polymers with grafting densities of 3 and 5 promising candidates for *in vivo*



transfection. However, polymer hyPEI25k-(PCL570-PEG5k)<sub>20</sub> was, despite very low toxicity, always inefficient, and no obvious transfection was registered at any N/P-ratio. If the low transfection efficiency of hyPEI25k-(PCL570-PEG5k)<sub>20</sub> was due to the low buffer capacity described above, a treatment with chloroquine could increase the endosomal escape, and also the transfection of the polyplexes (Luthman and Magnusson, 1983). During the 4 h of incubation with the hyPEI25k-(PCL570-PEG5k)<sub>20</sub>/DNA-complex, the cells were treated with 50 µM, 100 µM, and 150 µM chloroquine. However, no increase in transfection efficiency was observed (data not shown). The low transfection efficiency of hyPEI25k-(PCL570-PEG5k)<sub>20</sub> can, however, be explained mainly by the negatively charged surface of hyPEI25k-(PCL570-PEG5k)<sub>20</sub>/DNA-complexes. The buffer capacity did in fact play an important role for complexes that were efficiently taken up. Copolymer hyPEI25k-(PCL570-PEG5k)<sub>3</sub> displayed a much higher buffer capacity than hyPEI25k or the other hyPEI-polymers, and the tendency of the buffer-capacity profiles was exactly the same as the one observed for transfection efficiency. These results are comparable with those of other authors. For instance, Jong et al., reported that polymers possessing better buffering capacity yield higher transfection efficiency (Jong, 2009).

### **Confocal laser scanning microscopy (CLSM)**

The CLSM-micrographs showed a clear trend of the cellular uptake efficiency from hyPEI25k to hyPEI25k-(PCL570-PEG5k)<sub>20</sub> (Fig.8). HyPEI25k clearly yielded more uptake of plasmid-DNA into the nucleus, the site of action, than into the cytosol. Cellular uptake of plasmid-DNA complexed by hyPEI25k-(PCL570-PEG5k)<sub>1</sub> was also clearly observed, but the fluorescence intensity of plasmid-DNA in nucleus was not as strong as observed with hyPEI25k. In case of hyPEI25k-(PCL570-PEG5k)<sub>3</sub> and hyPEI25k-(PCL570-PEG5k)<sub>5</sub>, the most pDNA remained in the cytosol, and only a low amount of pDNA could enter into the nucleus. After transfection with hyPEI25k-(PCL570-PEG5k)<sub>20</sub>, only very weak fluorescence of the pDNA was observed. We can conclude that the cell uptake was reduced clearly with an increasing number n of PCL570-PEG5k segments. This tendency of cell uptake agreed perfectly with the results of zeta-potential measurement. Due to their positive zeta-potentials, polyplexes could easily enter

the cells. And the negatively charged polyplexes hardly entered the cells, as shown with hyPEI25k-(PCL570-PEG5k)<sub>20</sub>/DNA-complexes (Wong et al., 2007).

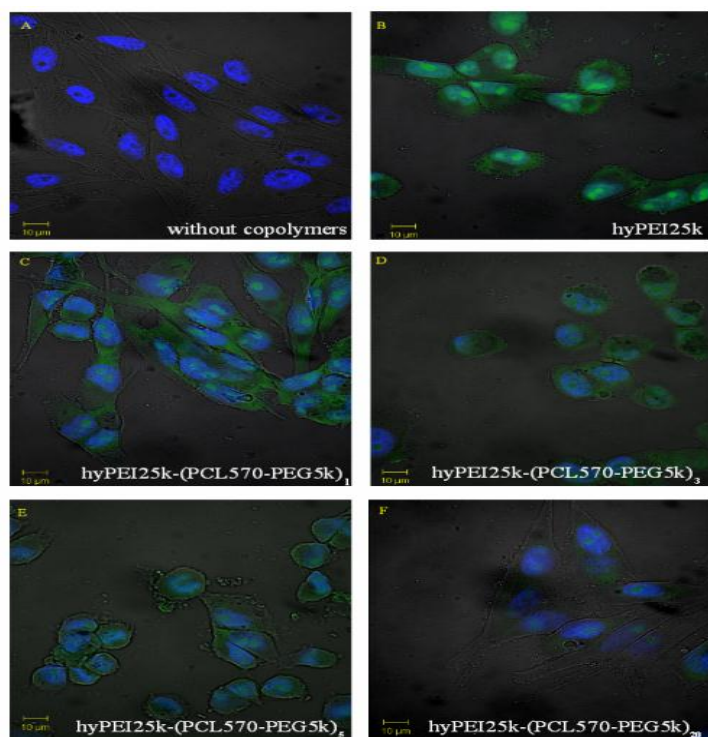


Fig. 8: Results of confocal laser scanning microscopy with MeWo-cells. A. Only MeWo-cells, without treatment with copolyplexes (Blue: nuclear; green: plasmid-DNA) and cellular uptake of B. pDNA complexed by polymer hyPEI25k, C. pDNA/hyPEI25k-(PCL570-PEG5k)<sub>1</sub> complexes, D. pDNA/hyPEI25k-(PCL570-PEG5k)<sub>3</sub> complexes, E. pDNA/hyPEI25k-(PCL570-PEG5k)<sub>5</sub> complexes, and F. pDNA/hyPEI25k-(PCL570-PEG5k)<sub>20</sub> complexes.

### 3.5. Conclusions

A general observation of our study was that with increasing graft density, toxicity, buffer-capacity and transfection efficiency increased at first until the graft density of 3, and then decreased. Cytotoxicity, zeta-potential, CMC-values, affinity with DNA and stability of the polyplexes were reduced upon increasing graft density. However, no correlation was shown between the sizes of polyplexes and transfection efficiencies. The results of the transfection experiments could be explained only by a combination of physico-chemical and biological parameters. Buffer-capacity, cytotoxicity and zeta-potential turned out to be the key factors for the explanation of the results of the gene transfer experiments. Whereas strong cytotoxicity is disadvantageous, a higher buffer-capacity was generally assumed to be advantageous for *in vitro* gene delivery since it enhances the endosomal escape of polyplexes. Of all the experimental results, buffer-capacity has almost exactly the same tendency as transfection efficiency. We therefore assume that in all processes of DNA transfection, the endosomal escape has a really important and rate-limiting role.

The zeta-potential of the complexes is also very important for the uptake of polyplexes. The high surface charges enhance the adhesion of the cationic complexes to the negatively charged cell membrane. Polymers with high buffer-capacity and zeta-potential but with low cytotoxicity showed high transfection activities and seemed to be most efficient as *in vitro* gene transfer vectors (e. g., hyPEI25k-(PCL570-PEG5k)<sub>3</sub>). *In vivo* experiments and the evaluation of the described polymers for siRNA delivery, such as elucidation of the structure of polyplexes are currently under way. Our results provide a basis for the optimization of the molecular structure of gene delivery vectors with higher buffer-capacity in the future.

### 3.6. Acknowledgments

We are grateful to Eva Mohr (Dept. of Pharmaceutics and Biopharmacy) for excellent technical support. MEDITRANS, an Integrated Project funded by the European Commission under the Sixth Framework (NMP4-CT-2006-026668), is gratefully acknowledged.

### 3.7. References

- Banaszczyk, M.G., et al., 1999. POLY-L-LYSINE-*GRAFT*-PEG COMB-TYPE POLYCATION COPOLYMERS FOR GENE DELIVERY. *Journal of Macromolecular Science, Part A: Pure and Applied Chemistry* 36, 1061 - 1084.
- Behr, J.-P., 1997. The Proton Sponge: a Trick to Enter Cells the Viruses Did Not Exploit. *CHIMIA International Journal for Chemistry* 51, 34-36.
- Bielinska, A.U., et al., 1997. The interaction of plasmid DNA with polyamidoamine dendrimers: mechanism of complex formation and analysis of alterations induced in nuclease sensitivity and transcriptional activity of the complexed DNA. *Biochim Biophys Acta* 1353, 180-190.
- Boussif, O., et al., 1995. A versatile vector for gene and oligonucleotide transfer into cells in culture and in vivo: polyethylenimine. *Proc Natl Acad Sci U S A* 92, 7297-7301.
- Check, E., 2002. A tragic setback. *Nature* 420, 116-118.
- Creusat, G., et al., 2010. Proton sponge trick for pH-sensitive disassembly of polyethylenimine-based siRNA delivery systems. *Bioconjug Chem* 21, 994-1002.
- Fischer, D., et al., 1999. A novel non-viral vector for DNA delivery based on low molecular weight, branched polyethylenimine: effect of molecular weight on transfection efficiency and cytotoxicity. *Pharm Res* 16, 1273-1279.
- Fischer, D., et al., 2003. In vitro cytotoxicity testing of polycations: influence of polymer structure on cell viability and hemolysis. *Biomaterials* 24, 1121-1131.
- Freshney, R.I., 2005. *Culture of Animal Cells: A Manual of Basic Technique*, 5th ed. Wiley-Liss, Wilmington, DE.
- Godbey, W.T., et al., 1999. Poly(ethylenimine) and its role in gene delivery. *J Control Release* 60, 149-160.
- Hacein-Bey-Abina, S., et al., 2003. LMO2-associated clonal T cell proliferation in two patients after gene therapy for SCID-X1. *Science* 302, 415-419.

Han, S., et al., 2001. Water-soluble lipopolymer for gene delivery. *Bioconjug Chem* 12, 337-345.

Han, S., et al., 2000. Development of biomaterials for gene therapy. *Mol Ther* 2, 302-317.

Jong, Y.C., 2009. Investigation of DNA Spectral Conformational Changes and Polymer Buffering Capacity in Relation to Transfection Efficiency of DNA/Polymer Complexes. *Journal of Pharmacy & Pharmaceutical Sciences* 12, 346-356.

Kono, K., et al., 2005. Transfection activity of polyamidoamine dendrimers having hydrophobic amino acid residues in the periphery. *Bioconjug Chem* 16, 208-214.

Kunath, K., et al., 2003. Low-molecular-weight polyethylenimine as a non-viral vector for DNA delivery: comparison of physicochemical properties, transfection efficiency and in vivo distribution with high-molecular-weight polyethylenimine. *J Control Release* 89, 113-125.

Liu, Y., et al., 2009. A new synthesis method and degradation of hyper-branched polyethylenimine grafted polycaprolactone block mono-methoxyl poly (ethylene glycol) copolymers (hy-PEI-g-PCL-b-mPEG) as potential DNA delivery vectors. *Polymer* 50, 3895-3904.

Liu, Y., et al., 2010. Degradation of Hyper-Branched Poly(ethylenimine)-graft-poly(caprolactone)-block-monomethoxyl-poly(ethylene glycol) as a Potential Gene Delivery Vector. WILEY-VCH Verlag, pp. 1509-1515.

Luthman, H., Magnusson, G., 1983. High efficiency polyoma DNA transfection of chloroquine treated cells. *Nucleic Acids Res* 11, 1295-1308.

Marshall, E., 2000. BIOMEDICINE:Gene Therapy on Trial. *Science* 288, 951-957.

Merdan, T., et al., 2002. Prospects for cationic polymers in gene and oligonucleotide therapy against cancer. *Adv Drug Deliv Rev* 54, 715-758.

Moret, I., et al., 2001. Stability of PEI-DNA and DOTAP-DNA complexes: effect of alkaline pH, heparin and serum. *J Control Release* 76, 169-181.

Pack, D.W., et al., 2005. Design and development of polymers for gene delivery. *Nat Rev Drug Discov* 4, 581-593.

Park, M.R., et al., 2005. Degradable polyethylenimine-alt-poly(ethylene glycol) copolymers as novel gene carriers. *J Control Release* 105, 367-380.

Pawliuk, R., et al., 2001. Correction of sickle cell disease in transgenic mouse models by gene therapy. *Science* 294, 2368-2371.

Petersen, H., et al., 2002. Polyethylenimine-graft-poly(ethylene glycol) copolymers: influence of copolymer block structure on DNA complexation and biological activities as gene delivery system. *Bioconjug Chem* 13, 845-854.

Pun, S.H., et al., 2004. Cyclodextrin-modified polyethylenimine polymers for gene delivery. *Bioconjug Chem* 15, 831-840.

Schaffer, D.V., et al., 2000. Vector unpacking as a potential barrier for receptor-mediated polyplex gene delivery. John Wiley & Sons, Inc., pp. 598-606.

Shuai, X., et al., 2003. Novel Biodegradable Ternary Copolymers hy-PEI-g-PCL-b-PEG: Synthesis, Characterization, and Potential as Efficient Nonviral Gene Delivery Vectors. *Macromolecules* 36, 5751-5759.

Sung, S.-J., et al., 2003. Effect of Polyethylene Glycol on Gene Delivery of Polyethylenimine. *Biological & Pharmaceutical Bulletin* 26, 492-500.

Tian, H., et al., 2007. Gene transfection of hyperbranched PEI grafted by hydrophobic amino acid segment PBLG. *Biomaterials* 28, 2899-2907.

von Laer, D., et al., 2006. Gene therapy for HIV infection: what does it need to make it work? *J Gene Med* 8, 658-667.

- Wang, D.-a., et al., 2002. Novel Branched Poly(Ethylenimine)-Cholesterol Water-Soluble Lipopolymers for Gene Delivery. *Biomacromolecules* 3, 1197-1207.
- Wong, L.F., et al., 2006. Lentivirus-mediated gene transfer to the central nervous system: therapeutic and research applications. *Hum Gene Ther* 17, 1-9.
- Wong, S.Y., et al., 2007. Polymer systems for gene delivery--Past, present, and future. *Progress in Polymer Science* 32, 799-837.

## Chapter 4

# ENHANCING IN VIVO CIRCULATION AND SIRNA DELIVERY WITH BIODEGRADABLE POLYETHYLENIMINE-GRAFT-POLYCAPROLACTONE-BLOCK-POLY(ETHYLENE GLYCOL) COPOLYMERS

Accepted by Biomaterials

**Mengyao Zheng<sup>a</sup>, Damiano Librizzi<sup>b</sup>, Ayşe Kılıç<sup>c</sup>, Yu Liu<sup>a,d</sup>, Harald Renz<sup>c</sup>, Olivia M. Merkel<sup>a,e,\*</sup>, Thomas Kissel<sup>a</sup>**

### **Author contributions**

T. K. guided and directed the research. O. M. M. designed the measurements. M. Z. carried out the dynamic light scattering/zeta potential analysis, SYBR<sup>®</sup> Gold assay, heparin assay, RT-PCR and CLSM. Y. L. synthesized and characterized the polymers. M. Z. and O. M. M. analysed the experimental data.

## 4.1 Abstract

The purpose of this study was to enhance the *in vivo* blood circulation time and siRNA delivery efficiency of biodegradable copolymers polyethylenimine-graft-polycaprolactone-block-poly(ethylene glycol) (hyPEI-g-PCL-b-PEG) by introducing high graft densities of PCL-PEG chains. SYBR<sup>®</sup> Gold and heparin assays indicated improved stability of siRNA/copolymer-complexes with a graft density of 5. At N/P 1, only 40% siRNA condensation was achieved with non-grafted polymer, but 95% siRNA was condensed with copolymer PEI25k-(PCL570-PEG5k)<sub>5</sub>. Intracellular uptake studies with confocal laser scanning microscopy and flow cytometry showed that the cellular uptake was increased with graft density, and copolymer PEI25k-(PCL570-PEG5k)<sub>5</sub> was able to deliver siRNA much more efficiently into the cytosol than into the nucleus. The *in vitro* knockdown effect of siRNA/hyPEI-g-PCL-b-PEG was also significantly improved with increasing graft density, and the most potent copolymer PEI25k-(PCL570-PEG5k)<sub>5</sub> knocked down 84.43% of the GAPDH expression. Complexes of both the copolymers with graft density 3 and 5 circulated much longer than unmodified PEI25kDa and free siRNA, leading to a longer elimination half-life, a slower clearance and a three- or fourfold increase of the AUC compared to free siRNA, respectively. We demonstrated that the graft density of the amphiphilic chains can enhance the siRNA delivery efficiency and blood circulation, which highlights the development of safe and efficient non-viral polymeric siRNA nanocarriers that are especially stable and provide longer circulation *in vivo*.

### Keywords

siRNA delivery

Biodegradable polycations

Non-viral polymeric nanocarrier

*In vivo* biodistribution and pharmacokinetics

SPECT imaging

## 4.2 Introduction

RNA interference (siRNA) promises great advantages for emerging therapeutic applications to silence disease genes [1, 2]. In contrast to the efficient and reliable siRNA-mediated gene silencing *in vitro*, only limited silencing of target gene expression *in vivo* has been achieved. One of the

reasons is that naked siRNA is very unstable in blood due to rapid enzymatic degradation, rapid excretion, and nonspecific uptake by the reticuloendothelial system [3]. Therefore, it is a formidable challenge to design and synthesize effective siRNA delivery systems, which are stable but biodegradable and long circulating *in vivo* [4].

Copolymers hy-PEI-g-(PCL-b-PEG)<sub>n</sub> are amphiphilic biodegradable non-viral polymeric gene delivery agents, which have shown a prominent gene delivery efficiency [5-7]. Positively charged polyethylenimine (PEI) is the functional component which condenses the genetic material due to electrostatic interactions and offers the buffer capacity with protonable amino groups to achieve successful endosomal escape of polyplexes [8, 9]. Hydrophobic poly(caprolactone) (PCL) increases the biodegradability of the copolymers and affects the hydrophilic–hydrophobic balance of the polymer to enhance uptake of the complexes through cell membranes [5, 6]. PEG has been widely used as a classical polymer to modify the surface of delivery systems like hydrophobic colloids [10] or other polymeric delivery agents such as polycation hy-PEI, resulting in decreased cytotoxicity, non-specific interaction of complexes with serum components and a prolonged blood circulation [11-14]. We hypothesize that the effect of PEG on prolonged circulating and the protection of siRNA with PCL-PEG chains depends not only on its content in a copolymer (length or percentage), but also on the structure or the shape of the amphiphilic copolymer. Therefore, we designed and synthesized a panel of biodegradable amphiphilic copolymers hy-PEI-g-PCL-b-PEG with different graft densities of PCL-PEG chains as polymer-based siRNA delivery systems. We expected that the PEG-PCL grafting degree would improve not only the gene silencing, but also the circulating time *in vivo*. In our study, the physicochemical properties of these siRNA/polymer-complexes were characterized with respect to particle size, zeta-potential, and stability against competing heparin anions. Real-Time-PCR and confocal laser scanning microscopy were used to measure the *in vitro* knock down efficiency and cell uptake. The siRNA delivery efficiency and biodistribution of these triblock amphiphilic copolymers under *in vivo* conditions was determined using single photon emission computed tomography (SPECT) imaging with <sup>111</sup>In radiolabelled siRNA [15] and fluorescently labeled copolymer. Our study provides us with an insight into advantageous structures and shapes of copolymers to promote the rapid development of safe and efficient non-viral polymeric siRNA delivery nanocarriers that are especially stable *in vivo*.



### **4.3 Methods and materials**

#### **Materials**

hy-PEI with a molecular weight of 25 kDa was obtained from BASF. Poly(ethylene glycol) mono-methyl ether (mPEG) (5kDa) and  $\epsilon$ -caprolactone were purchased from Fluka (Taufkirchen, Germany). Heparin sodium salt was from Sigma-Aldrich Laborchemikalien GmbH (Seelze, Germany) and all other chemicals were obtained from Sigma–Aldrich (Steinheim, Germany). hy-PEI-g-PCL-b-PEG was synthesized as reported previously [5, 6]. Lipofectamine™2000 (LF) was bought from Invitrogen (Karlsruhe, Germany). Amine-modified firefly luciferase DsiRNA with a C6-NH<sub>2</sub> linker at the 3' of the sense strand, negative control sequence, hGAPDH-DsiRNA, and TYE546-DsiRNA were obtained from Integrated DNA Technologies (IDT, Leuven, Belgium). Balb/c mice were bought from Harlan Laboratories (Horst, The Netherlands). The chelator 2-(4-isothiocyanatobenzyl)-diethylenetriaminepentaacetic acid (p-SCN-Bn-DTPA) was purchased from Macrocyclics (Dallas, TX, USA). The radioactive <sup>111</sup>InCl<sub>3</sub> was purchased from Covidien Deutschland GmbH (Neustadt a.d. Donau, Germany).

#### **Polyplex preparation**

Polyplexes were formed by diluting a calculated volume of 1 mg/mL polymer (based on PEI 25kDa) with 5% glucose solution in the first step. Equal volumes of diluted polymer and siRNA solution were mixed followed by vigorous pipetting before letting the polyplexes form at room temperature for 20 min. The N/P ratio (=nitrogen/phosphorus-ratios) was calculated as described earlier [6].

#### **Dynamic light scattering and zeta potential analysis**

Polyplexes were prepared with hGAPDH-DsiRNA as described above at different N/P ratios and measured in a disposable low volume UVette (Eppendorf, Wesseling–Berzdorf, Germany) using a Zetasizer Nano ZS (Malvern, Herrenberg, Germany). The measurements in 5% glucose solution were conducted in triplicates according to a previous work [16].

#### **SYBR® gold assay and heparin assay: binding and protection efficiency and stability against competing polyanions**

The ability of hy-PEI-g-PCL-b-PEG copolymers to condense siRNA into small polyplexes was studied in SYBR<sup>®</sup> Gold assays. Briefly, polyplexes were formed at different N/P ratios from 0 to 20. Polyplex solutions contained 1 µg hGAPDH-DsiRNA and the according amount of polymer in each well of FluoroNunc 96 well plates (Nunc, Thermo Fisher Scientific, Langenselbold, Germany). For heparin assays, polyplexes were prepared in solutions at different N/P-ratio like in the SYBR<sup>®</sup> Gold assay described above. Additionally, 20 µL heparin solution with a concentration of 1.5 IU/µmol siRNA was added to the polyplex solutions in each well of the 96-well plate (Perkin Elmer, Rodgau-Jügesheim) and the polyplex solutions were incubated for 20 min at 25°C, before 20 µL diluted SYBR<sup>®</sup> Gold solution were added. The measurement of fluorescence was conducted according to a previous study in quadruplets [17].

### **RT-PCR**

SKOV3 cells were used for knock down experiments and the Hs\_GAPDH silencing was measured with RT-PCR according to our previous work [18]. Briefly, 500,000 cells per well were seeded in 6-well-plates 24 h prior to transfection and transfected with 100 pmol of siRNA in triplicates. Real-Time PCR was performed using QuantiFast<sup>™</sup> SYBR<sup>®</sup> Green PCR Kit and Hs\_GAPDH and Hs\_ACTB\_2\_SG Primers (Qiagen, Germany) and the RotorGene3000 real-time PCR thermal cycler (Qiagen, Hilden, Germany).

### **Flow Cytometry**

SKOV3 cells were seeded in 24-well plates at a density of 60,000 cells per well 24h before transfection with polyplexes consisting of 50 pmol of Alexa488-labeled siRNA at N/P 5. Cells were incubated with the polyplexes in triplicates for 4h at 37 °C and were then washed with PBS buffer (with Ca<sup>2+</sup> and Mg<sup>2+</sup>). The fluorescence bound on the cell-surface was quenched by 5 min incubating with 0.4% trypan blue before the cells were trypsinized for 5 min and spun down in serum containing medium and fixed with CellFIX (BD Biosciences, San Jose, CA). Treated and untreated cells (as negative control) cells were measured using a FACSCantoII (BD Biosciences, San Jose, CA) with excitation at 488 nm and the emission filter set to a 530/30 bandpass. In each measurement, cells were gated to evaluate 10,000 viable cells, and the geometric mean fluorescence intensity (MFI) was calculated as the mean value of 3 independent measurements.

Data acquisition and analysis was performed using FACSDiva software (BD Biosciences, San Jose, CA) [17].

### **Confocal laser scanning microscopy (CLSM)**

For CLSM, polymers were first labeled with FITC as described before complexation with TYE546-DsiRNA [19] to detect polymer and siRNA in parallel. SKOV3 cells were seeded in 8 well-chamber slides (Lab-Tek; Rochester, NY, USA) 24h before transfection. For sample preparation and confocal microscopy on a Zeiss Axiovert 100 Microscope and a Zeiss LSM 510 scanning device (Zeiss, Oberkochen, Germany), steps and settings were chosen as previously described [20].

### **siRNA Radiolabeling and purification**

Amine-modified siRNA (IDT, Leuven, Belgium) was coupled with p-SCN-Bn-DTPA, radiolabeled with  $^{111}\text{InCl}_3$  and purified using Absolutely RNA miRNA columns (Agilent, Waldbronn, Germany) as described before [19].

### ***In vivo* imaging, pharmacokinetics and biodistribution**

Balb/c mice at the age of 6 weeks (about 20 g) were used for *in vivo* experiments. All animal experiments were carried out according to the German law of protection of animal life and were approved by an external review committee for laboratory animal care. Balb/c mice were anesthetized with xylazine and ketamine, and 5 animals per group were injected with polyplexes containing 35  $\mu\text{g}$  of radiolabelled siRNA and the corresponding amount of FITC labeled polymer at N/P 5. Complexes were injected i.v. into the tail vein. For the pharmacokinetics study, 25  $\mu\text{L}$  blood samples were drawn at different time points within two hours and measured using a Gamma Counter Packard 5005 (Packard Instruments, Meriden, CT). After 2h, biodistribution was recorded using three-dimensional SPECT and planar gamma camera imaging (Siemens AG, Erlangen, Germany). Finally, animals were sacrificed and the biodistribution in dissected organs was quantified using a Gamma Counter Packard 5005.

### **Flow cytometric quantification of cellular tissue uptake**

As described above, mice were injected with polyplexes containing 35  $\mu\text{g}$  siRNA and FITC labeled polymers at the N/P 5. Animals were sacrificed 2 h after injection, and the organs were dissected. The intracellular uptake within the organs was determined by flow cytometry. To obtain organ homogenates, lungs and livers were incubated in 2 mg/mL collagenase D solution (Roche, Mannheim, Germany) at 37  $^{\circ}\text{C}$  for 20 min before sieving the tissue through 100  $\mu\text{m}$  nylon cell strainers (BD Falcon, Heidelberg, Germany). Cells were then suspended in 10 mL of PBS and centrifuged at 350 g for 10 min. The cells were resuspended, once again centrifuged and resuspended in 500  $\mu\text{L}$  4% paraformaldehyde for flow cytometry. The internalization of fluorescently labeled polyplexes into lung and liver cells was measured on a FACSCanto™ II (BD Biosciences, San Jose, CA) with excitation at 488 nm and emission filter set to 530/30 bandpass. 10,000 viable cells were evaluated in each experiment and results are the mean values of 3 independent measurements.

## **Statistics**

Results are given as mean values and standard deviation (SD). Statistical evaluation, calculation of the AUC and two way ANOVA were performed using Graph Pad Prism 4.03 (Graph Pad Software, La Jolla, CA).

## **4.4 Results and discussion**

### **Polyplex size and zeta potential**

The hydrodynamic diameters and surface charges of the siRNA/copolymer-complexes are listed in Table 1. The polyplex sizes decreased with increasing N/P-ratios from 2 to 10. All copolymers were able to condense siRNA into polyplexes with sizes of 78–142 nm (Tab. 1) at N/P 5 or N/P 10 in 5% glucose solution. However, the polyplex size at N/P-ratio 2 was larger than at the other N/P-ratios, especially for the copolymer with graft density 1. This observation and the negative zeta potentials at N/P 2 indicate that siRNA is not fully condensed into the core of the micelle-like complexes. At N/P 5, all complexes revealed positive zeta potentials and rather narrow size distributions (PDI), especially in case of PEI25k-(PCL570-PEG5k)<sub>3</sub>. In a recent study, we investigated the binding behavior of siRNA and hy-PEI-g-PCL-b-PEG by molecular dynamic simulations, isothermal titration calorimetry and dye quenching assay (data not shown here). We

found that at low N/P ratios, siRNA complexation results in a more uniform and stable complex formation, which leads to increased siRNA delivery efficiency. This explains the lower PDI values as compared to N/P 10. Interestingly, amongst the three copolymers, PEI25k-(PCL570-PEG5k)<sub>5</sub> and PEI25k-(PCL570-PEG5k)<sub>3</sub> appeared to be most advantageous siRNA delivery agents, not only for *in vitro* but also for *in vivo* applications, according to the hydrodynamic diameter and surface properties. Both the hydrodynamic diameter and polydispersity of their siRNA complexes were lower than those of the polyplexes formed with PEI25k-(PCL570-PEG5k)<sub>1</sub>. The decreased size of those polyplexes despite higher molecular weight of the polymers can be explained by the micellar behavior of the more amphiphilic copolymers. Moreover, the narrow size distribution ( $0.23 < \text{PDI} < 0.31$ ) of the complexes is very important for biological activity and corresponds with what has been described as “coalesced” complexes before [20]. Additionally, the zeta potential of siRNA/ PEI25k-(PCL570-PEG5k)<sub>5</sub> was decreased as compared to the other copolymers, which reflects less positive charges on the surface of the complexes and thus avoids high toxicity [16], potentially less uptake into macrophages and therefore provides the prerequisites for prolonged circulation *in vivo*.

Table 1. Hydrodynamic diameters and surface charges of the siRNA/copolymer-complexes.

		Hydrodynamic diameter		Zeta-potential (mV)
		Size (nm)	PDI	
<b>PEI25k-(PCL570-PEG5k)<sub>1</sub></b>	<b>N/P2</b>	1079 ± 169.98	0.30 ± 0.01	-4.14 ± 0.62
	<b>N/P5</b>	123.2 ± 1.75	0.33 ± 0.01	19.97 ± 1.65
	<b>N/P10</b>	107.23 ± 1.85	0.32 ± 0.01	25.1 ± 1.11
<b>PEI25k-(PCL570-PEG5k)<sub>3</sub></b>	<b>N/P2</b>	114.8 ± 1.74	0.33 ± 0.02	-11.07 ± 0.35
	<b>N/P5</b>	93.56 ± 7.08	0.24 ± 0.02	13.87 ± 1.51
	<b>N/P10</b>	92.58 ± 1.92	0.40 ± 0.02	15.11 ± 4.02
<b>PEI25k-(PCL570-PEG5k)<sub>5</sub></b>	<b>N/P2</b>	211.47 ± 6.87	0.23 ± 0.01	-14.97 ± 1.16
	<b>N/P5</b>	142.0 ± 6.5	0.24 ± 0.01	7.04 ± 0.23
	<b>N/P10</b>	78.35 ± 4.62	0.31 ± 0.02	10.87 ± 0.49

### Binding and protection efficiency and stability against competing polyanions

The condensation efficiency of siRNA within the copolymers can be investigated by SYBR<sup>®</sup> Gold assays [21], which can quantify the amount of free or accessible siRNA that is able to bind SYBR<sup>®</sup> Gold. The SYBR<sup>®</sup> Gold assay revealed the different condensation abilities of the copolymers with different graft densities: the affinity of siRNA with the copolymers was increased with increasing N/P-ratio and siRNA could be condensed very well above N/P 5 with all of the copolymers. Compared with PEI25k-(PCL570-PEG5k)<sub>1</sub>, the copolymers with graft density 3 and 5 showed not only higher affinity to siRNA, but also the better protection against competing polyanions like heparin molecules. For example, only 40% siRNA was condensed with PEI25k-(PCL570-PEG5k)<sub>1</sub> at N/P 1, while about 95% siRNA was completely condensed with PEI25k-(PCL570-PEG5k)<sub>3</sub> and PEI25k-(PCL570-PEG5k)<sub>5</sub>.

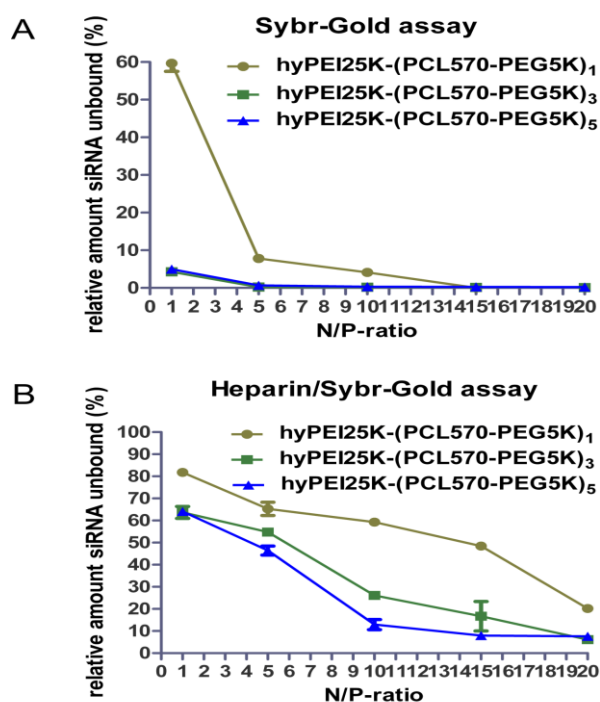


Fig. 1. In vitro stability of polyplexes of the siRNA/PEI25k-(PCL570-PEG5k)<sub>n</sub>-complexes as measured by (A) SYBR<sup>®</sup> Gold and (B) heparin assays.

the stability of the polyplexes was increased with increasing graft density [7] from 1 to 5. At N/P-ratio 10, after addition of heparin, 74% siRNA was condensed with PEI25k-(PCL570-PEG5k)<sub>3</sub> and 87% siRNA was condensed with PEI25k-(PCL570-PEG5k)<sub>5</sub>, while only 41% siRNA was condensed with PEI25k-(PCL570-PEG5k)<sub>1</sub>. We assumed that the PCL-PEG chains can increase the affinity of the amphiphilic copolymer with the 2'-O-methylated siRNA [17], and protect the siRNA very well from competing polyanions like heparin. In terms of stability, it is advantageous if the interaction with siRNA is not only of electrostatic nature but if hydrophobic forces that are not affected by competing polyanions stabilize the polyplexes. Interestingly, the previous stability study using these copolymers with plasmid DNA showed different results concerning stability: the stability of p-DNA/copolymer-complexes was decreased with an increase of the graft density, and the copolymer with graft density 1 showed the best protection of the p-DNA [16]. The copolymer with one PCL-PEG chain offered a better affinity to plasmid DNA than the other copolymers. This observation demonstrates that the entropic gain evidenced by ITC is indicative of the fact that inter-polyplex aggregations are controlled by hydrophobic forces. Indeed, a certain amount of lipophilic PCL can increase the affinity between copolymer with pDNA as shown by hyPEI25k-(PCL570-PEG5k)<sub>1</sub>, but with the increasing of graft density, reduced

The stability of polyplexes against competing polyanions is very important for gene delivery systems, especially for *in vivo* application since stability of the polyplexes can be strongly weakened in presence of serum [22]. The process of complexation of genetic material within polycations is entropy driven [23] and can be significantly impaired by the presence of other polyanions like heparin. The differences of the stability against polyanions were observed to be related to the graft density (Fig. 1). The higher grafted copolymers showed a better protection of the siRNA against heparin, and

stability of copolymers with pDNA was observed, which could be caused by the shielding-effect of PCL-mPEG segments. But different from pDNA, siRNA is locally more flexible in the case of local roll and tilt deformations [24] and more adaptable [25] in case of binding with a charged spherical polymer than DNA [26], which facilitates the uniform binding between the siRNA molecules and the polymers. Therefore, the complexation ability of the copolymer with siRNA is increased with the increasing of graft density.

### ***In vitro* cell uptake with CLSM and FACS**

The *in vitro* intracellular uptake was studied with confocal laser scanning microscopy qualitatively and flow cytometry quantitatively. The results of flow cytometry clearly revealed different cell uptake in the amount of siRNA as a result of the differently grafted copolymers, as shown in Fig. 3. Compared with PEI25kDa (3968.3 MFI), all of the amphiphilic copolymers showed an optimized cell uptake, especially in case of the copolymer with graft density 3 (8175.7 MFI). PEI25k-(PCL570-PEG5k)<sub>5</sub> seemed to showed reduced uptake as compared to PEI25k-(PCL570-PEG5k)<sub>3</sub>, which could be the result of the lower zeta potential. However, the differences between those two polymers were not significantly different. Our previous DNA delivery research with the same copolymers indicated the same tendency with the copolymer with graft density 3 displaying the best cell uptake and DNA transfection efficiency at N/P 25 [16].

However, flow cytometry quantifies the amount of fluorescently labeled genetic material not only in the cytosol, but also in the nucleus. Therefore, confocal laser scanning microscopy was performed additionally to detect differences in the subcellular distribution of the polyplexes made of differently grafted copolymers. The CLSM images of each treatment group are shown in Fig. 2: polyplexes formed with copolymer PEI25k-(PCL570-PEG5k)<sub>1</sub> seemed to be taken up only to a low extent, which corroborated the flow cytometry data. Interestingly, although the FACS had revealed a trend in favor of PEI25k-(PCL570-PEG5k)<sub>3</sub> over PEI25k-(PCL570-PEG5k)<sub>5</sub> polyplexes, nonetheless, more fluorescence of siRNA/ PEI25k-(PCL570-PEG5k)<sub>5</sub>-complexes was observed distributed in the cytoplasm of the transfected cells by confocal microscopy. This property is advantageous for siRNA delivery since the final target destination of siRNA is the cytoplasm, whereas plasmid DNA must be transported into the nucleus. In other words, to achieve a successful siRNA delivery, the siRNA must be delivered and released rapidly from its carrier upon



endosomal escape just in the cytoplasm, where the P-body (processing bodies: aggregates of translationally repressed mRNA-protein particles which associated with the translation repression and mRNA decay machinery) exist [27]. Moreover, PEI25k-(PCL570-PEG5k)<sub>5</sub> was one of the least toxic copolymers in our earlier study [16], due to the higher density of PCL-PEG chains and the stealth effect of the PEG layer. Generally, reduction in cytotoxicity is linked to reduced cell uptake, because both of the properties are based on the reduced interaction between polyplexes and cell surfaces. However, copolymers with higher graft densities showed optimized cell uptake of pDNA polyplexes into the cytosol and reduced cytotoxicity [16] at the same time. The surface charges of the siRNA/copolymer-complexes were also reduced with increasing graft density (Tab. 1), but the impact on DNA/copolymer-complexes was much stronger. Therefore, although the zeta potential of PEI25k-(PCL570-PEG5k)<sub>5</sub> complexes was reduced to a certain extent, they could still be taken up effectively into the SKOV3 cells. Additionally, the *in vivo* cell uptake study discussed below showed also an increased internalization of PEI25k-(PCL570-PEG5k)<sub>5</sub> complexes within tissue 2h after injection. Therefore, concerning the results of cell uptake, we found that the copolymer with the most PCL-PEG chains is more suitable for siRNA delivery than for DNA delivery.

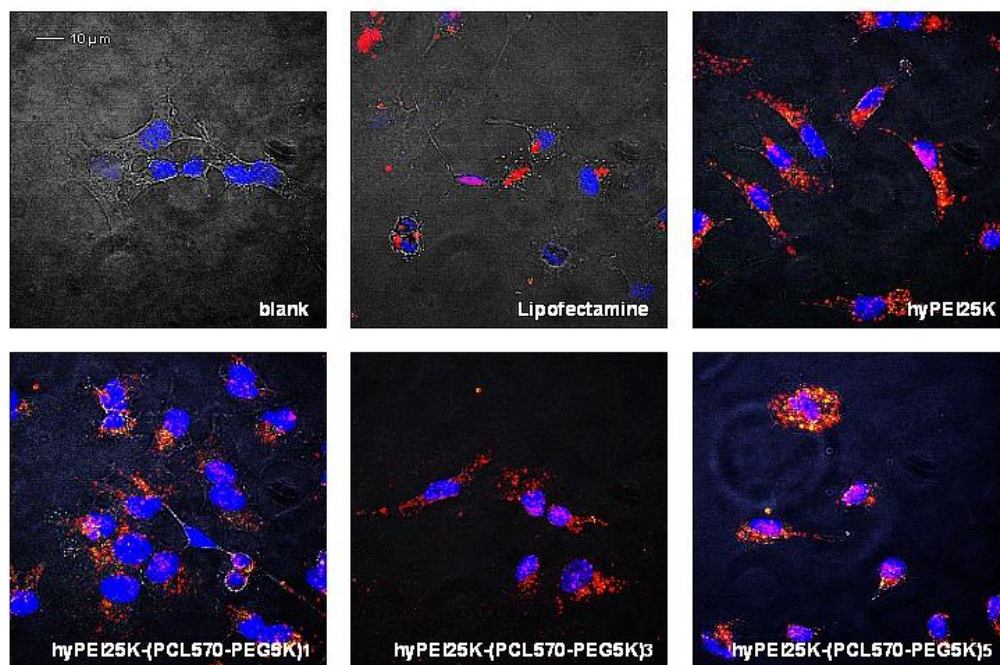


Fig. 2. Confocal images in SKOV3 cells 4 h after transfection showing the subcellular distribution of complexes made of Tye543-labeled siRNA (red) and FITC labeled polymer (green). Yellow spots indicate the colocalization of red siRNA and green polymer. DAPI-stained nuclei are shown in blue.

### Transfection efficiency

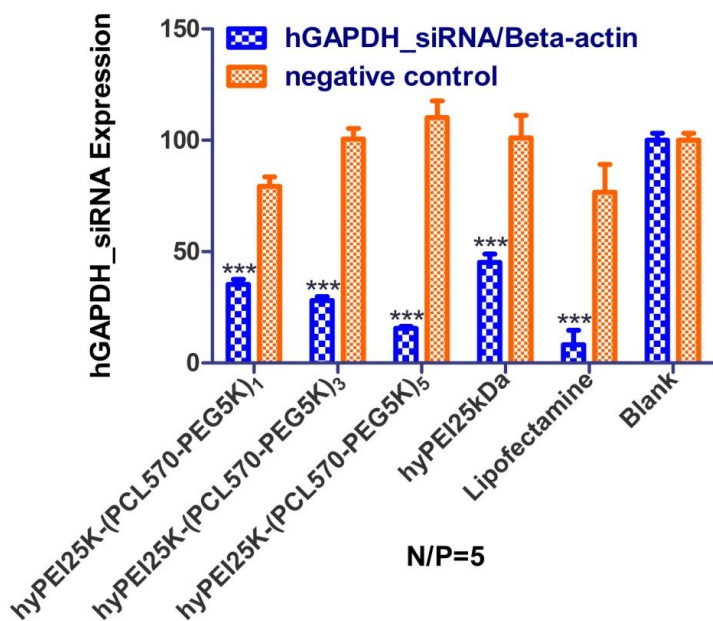


Fig. 4. Results of RT-PCR: knockdown effect of hGAPDH\_siRNA/copolymer-complexes in SKOV3 cells.

After determining the relationships between the physicochemical properties of the grafted copolymers and their uptake behavior, their siRNA transfection efficiency was measured *in vitro* using RT-PCR. Transfection reagent Lipofectamine™ (LF) was chosen as the positive control. LF is a commercially available DNA and siRNA transfectant; however the drawback, which is also reflected in Fig. 4 by the negative control bar of the LF-treated cells. In Fig. 4, the gene knockdown efficiency of the differently grafted copolymers was compared. As expected, the most potent copolymer for RNAi was PEI25k-(PCL570-PEG5k)<sub>5</sub> with the highest graft density which most significantly ( $***p < 0.001$ ) knocked down the GAPDH expression (16 residual expression), while the other copolymers with lower graft densities resulted in a weaker knockdown, for example 35.26% residual expression for PEI25k-(PCL570-PEG5k)<sub>1</sub> and 28.06% residual expression for PEI25k-(PCL570-PEG5k)<sub>3</sub>. In the case of PEI25k-(PCL570-PEG5k)<sub>5</sub>, the high knockdown efficiency most likely results from the combination of favorable intracellular distribution in the cytosol, the suitable size as well as the good stability and protection of siRNA against polyanions and the lowest cytotoxicity. In our previous research where we described these copolymers as gene delivery agents, PEI25k-(PCL570-PEG5k)<sub>3</sub> was the most promising copolymer for DNA delivery [16]. Based on the uptake results, polyplexes of PEI25k-(PCL570-PEG5k)<sub>3</sub> with siRNA were not readily translocated into the cytosol, but mostly into the nucleus, which is more suitable for DNA delivery [16]. Moreover, the less successful knockdown efficiency of PEI25k-(PCL570-PEG5k)<sub>3</sub> and PEI25k-(PCL570-PEG5k)<sub>1</sub> may be due, in part, to higher cytotoxicity as well as poor protection of siRNA against polyanions.

## Pharmacokinetics and biodistribution

The two most effective amphiphilic copolymers concerning the results of stability, *in vitro* cell uptake and knockdown efficiency, PEI25k-(PCL570-PEG5k)<sub>3</sub> and PEI25k-(PCL570-PEG5k)<sub>5</sub>, were investigated *in vivo* to evaluate their pharmacokinetics and biodistribution behavior as compared to polyplexes of PEI25kDa and naked siRNA. As measured by gamma scintillation counting of blood samples (Fig. 5), polyplexes made of both the grafted copolymers PEI25k-(PCL570-PEG5k)<sub>3</sub> and PEI25k-(PCL570-PEG5k)<sub>5</sub> were stable *in vivo* for at least 120 min and circulated longer than siRNA and PEI25kDa/siRNA polyplexes. As described earlier, complexes of unmodified PEI25kDa and siRNA dissociate easily upon intravenous administration and the polymer shows a strong first-pass effect in the liver [11, 17]. The pharmacokinetic profile of hy-PEI-complexed siRNA therefore strongly resembles that of free siRNA that is rapidly excreted upon injection [28]. While PEGylation of hy-PEI further destabilized siRNA complexes under *in vivo* conditions [22], we observed here that the amphiphilic triblock copolymers did not only show increased stability against competing heparin polyanions *in vitro* but were also more stable *in vivo* upon intravenous injection. This is reflected in longer circulation times, less steep alpha and beta elimination phases, and increased area under the curve (AUC) values which were calculated to analyze the differences in the circulation times of each load quantitatively (Fig. 5). The AUC of PEI25k-(PCL570-PEG5k)<sub>5</sub> and PEI25k-(PCL570-PEG5k)<sub>3</sub> complexed siRNA is almost four fold higher than that of PEI25kDa complexed or free siRNA (Supporting information). It can be hypothesized that the polyplexes made of PEI25k-(PCL570-PEG5k)<sub>3</sub> and PEI25k-(PCL570-PEG5k)<sub>5</sub> which display higher stability and decreased zeta potentials are less prone to dissociation and rapid uptake into macrophages. Thus, these polyplexes remain within the systemic circulation for a longer duration of time than instable complexes with high positive surface charge. Due to extended circulation times, they are eventually taken up into the liver as well (Fig. 6 and 7). However, since the cells types taking up those polyplexes in the liver were not differentially identified, it is not clear if the uptake was mediated by Kupffer cells.

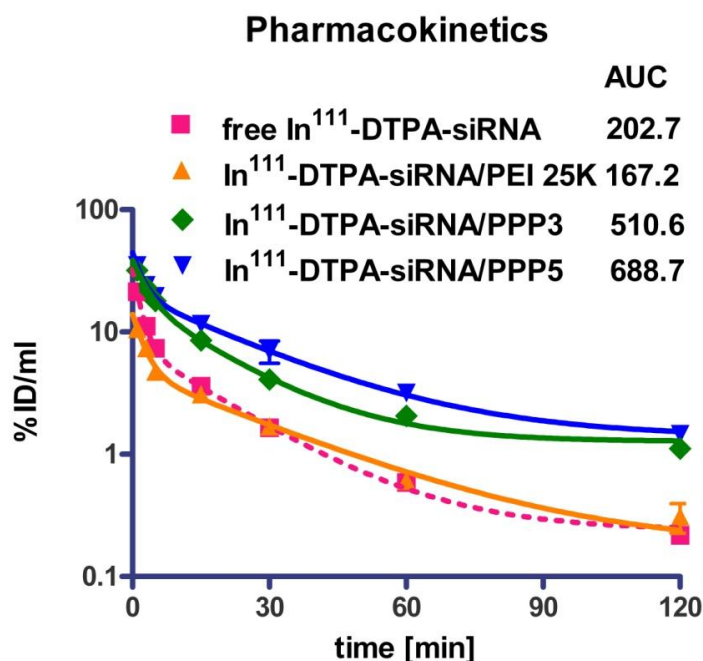


Fig. 5. Pharmacokinetics of siRNA polyplexes and free siRNA as measured by gamma scintillation counting of blood samples.

Accordingly, the deposition of the copolymers was studied two hours after injection as shown in Fig. 6. Although we hypothesized a decreased uptake into macrophages and thus into the reticuloendothelial system (RES) based on the pharmacokinetic profiles, Fig. 6 clearly shows an increased uptake of siRNA complexed with PEI25k-(PCL570-PEG5k)<sub>3</sub> and PEI25k-(PCL570-PEG5k)<sub>5</sub> into the liver and spleen. However, the uptake into the lung was increased as well. Since the flow cytometry results of the *in vitro* uptake of siRNA confirmed that the modified polymers were able to mediate better cell penetration and stronger internalization, these results are not very surprising. From the *in vitro* and *in vivo* results we conclude, that the amphiphilic character of the PEI25k-(PCL570-PEG5k)<sub>n</sub> polymers not only helps to form small and stable complexes but is also advantageous in terms of crossing biological membranes [29]. The increased uptake into the major organs (liver, lung, spleen) can be explained by the prolonged circulation times and the increased stability of the polyplexes. While free siRNA is rapidly excreted [28], and siRNA/PEI or siRNA/PEG-PEI complexes dissociate easily [22], in those cases the pharmacokinetic profiles of the siRNA show steep alpha and beta phases (Fig. 5), and most of the siRNA is eliminated before it can be taken up into the RES. The free polymers, however, are captured by macrophages in the RES, which was shown by disproportionately high uptake of PEI and PEG-PEI into the liver and spleen [22]. In case of “coalesced” polyplexes that are stable in circulation, we show here that the siRNA is stably encapsulated and that the intact complexes are slowly taken up into the RES over a longer period of circulation time. This is reflected in the less steep pharmacokinetic profiles that indicate the lack of rapid first pass in the liver (Figure 5).

Accordingly, the deposition of the copolymers was studied two hours after injection as shown in Fig. 6. Although we hypothesized a decreased uptake into macrophages and thus into the reticuloendothelial system (RES) based on the pharmacokinetic profiles, Fig. 6 clearly shows an increased uptake of siRNA complexed with PEI25k-(PCL570-PEG5k)<sub>3</sub> and PEI25k-(PCL570-PEG5k)<sub>5</sub> into the liver and spleen. However, the uptake into the lung was increased as well. Since the flow cytometry results of the *in vitro* uptake of siRNA confirmed that the modified polymers were able to mediate better cell penetration and stronger internalization, these results are not very surprising. From the *in vitro* and *in vivo* results we conclude, that the amphiphilic character of the PEI25k-(PCL570-PEG5k)<sub>n</sub> polymers not only helps to form small and stable complexes but is also advantageous in terms of crossing biological membranes [29]. The increased uptake into the major organs (liver, lung, spleen) can be explained by the prolonged circulation times and the increased stability of the polyplexes. While free siRNA is rapidly excreted [28], and siRNA/PEI or siRNA/PEG-PEI complexes dissociate easily [22], in those cases the pharmacokinetic profiles of the siRNA show steep alpha and beta phases (Fig. 5), and most of the siRNA is eliminated before it can be taken up into the RES. The free polymers, however, are captured by macrophages in the RES, which was shown by disproportionately high uptake of PEI and PEG-PEI into the liver and spleen [22]. In case of “coalesced” polyplexes that are stable in circulation, we show here that the siRNA is stably encapsulated and that the intact complexes are slowly taken up into the RES over a longer period of circulation time. This is reflected in the less steep pharmacokinetic profiles that indicate the lack of rapid first pass in the liver (Figure 5).

Table 2

	<b>AUC</b> [min%/ml]	<b>Alpha</b> [min]	<b>beta</b> [min]	<b>CL</b> [ml/min/kg]	<b>MRT</b> [min]	<b>V<sub>ss</sub></b> [ml/kg]
PEI25k/siRNA *	283.7±55.6	4.0±2.3	84.9±31.6	13.0±1.8	68.5±30.3	1056.3±160.8
Free siRNA*	1298.5±181.8	2.9±1.4	93.2±12.1	3.1±0.4	129.0±15.7	404.8±109.7
PEI25k-(PCL570-PEG5k) <sub>3</sub> /siRNA	528.9±67.0	0.249±0.130	0.024±0.012	0.168±0.016	35.9±13.9	8.2±1.4
PEI25k-(PCL570-PEG5k) <sub>5</sub> /siRNA	701.0±127.2	0.409±0.118	0.032±0.010	0.128±0.021	31.2±10.3	6.5±1.9

Kinetic parameters of siRNA polyplexes are listed in the table. AUC, area under the curve; alpha, half-life in alpha phase; beta, half-life in elimination (beta-) phase; CL, clearance; MRT, mean residence time; V<sub>ss</sub>, steady state volume of distribution.

(\* O.M. Merkel et al. / Journal of Controlled Release 138 (2009) 148–159) [22]

According to the *in vivo* biodistribution results, the lung, liver and spleen are the main target organs for deposition of siRNA after intravenous administration of the complexes. Since the measurement of radioactive siRNA deposition into organs, however, does not allow for differentiation between internalized siRNA and siRNA that is present in the interstitium, we measured cellular internalization after disruption of the extracellular matrix. Single cell suspensions were subjected to flow cytometry to quantify the intracellular uptake of fluorescently labeled polyplexes into the cells of the lung and liver. However, complete organ homogenates were investigated, and cells were not differentiated. It is therefore not clear if macrophages in the liver or lung played a predominant role or if other uptake mechanisms than phagocytosis were involved. It has been reported in the past that polyplexes that aggregate in the presence of serum can get stuck in the lung capillaries [30]. However, “coalesced” polyplexes [20] are less prone to aggregation, and the uptake into liver and lung tissue may be caused by endocytosis. While the *in vitro* uptake of PEI25k-(PCL570-PEG5k)<sub>3</sub> and PEI25k-(PCL570-PEG5k)<sub>5</sub> complexes was found to be not significantly different, complexes of PEI25k-(PCL570-PEG5k)<sub>5</sub> exhibited significantly increased internalization into lung and liver cells. These *in vivo* results, however, may be a result of the enhanced circulation time of PEI25k-(PCL570-PEG5k)<sub>5</sub> complexes. Additionally, Figure 6 also corroborates the trend of stronger uptake of PEI25k-(PCL570-PEG5k)<sub>5</sub> complexes into the major organs compared to PEI25k-(PCL570-PEG5k)<sub>3</sub>. This result is not surprising as in case of stable complexes the proportional uptake of carrier and load is expected to correlate. In case of

PEI-complexed and free siRNA, the overall recovery of siRNA in any of the organs is rather low due to the instability of the complexes and the rapid excretion of the siRNA. The deposition of the free polymer, in case of PEI 25kDa, however, was significantly higher [22].

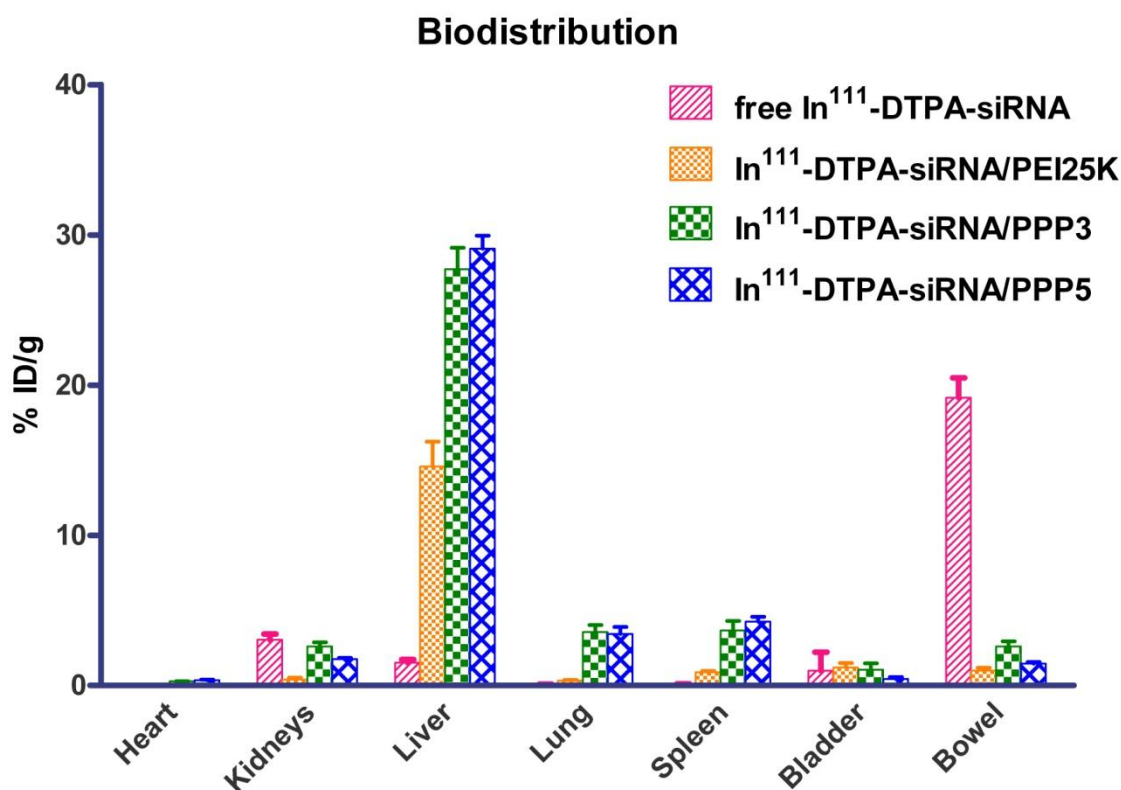


Fig. 6. Biodistribution of siRNA polyplexes and free siRNA 2 h after i.v. administration as measured by gamma scintillation counting of dissected organs.

#### 4.5 Conclusion

In this study, we synthesized a panel of hy-PEI-g-PCL-b-PEG amphiphilic copolymers with different graft densities of the PCL-PEG chains. Compared with copolymers of low graft density, the copolymers with high graft densities (3 and 5) showed not only a higher affinity with siRNA, a better protection against competing polyanions, but also an increased intracellular uptake into the cytosol, which was detected with confocal laser scanning microscopy and flow cytometry. Therefore, copolymers with higher graft density of PCL-PEG chains showed significant advantages as siRNA delivery agents concerning in vitro transfection and in vivo pharmacokinetics and biodistribution. In summary, we demonstrated that polymeric micelles, which are formed with amphiphilic block copolymers have advantages especially for in vivo siRNA delivery, and that the

graft density of the amphiphilic chains can enhance the blood circulation, which is a key parameter to promote the development of safe and efficient non-viral polymeric siRNA delivery *in vivo*.

#### 4.6 Acknowledgements

We are grateful to PD Dr. Helmut Hoeffken (Nuclear Medicine Department, University Hospital Marburg) for the generous use of equipment and facilities, and to Eva Mohr (Department of Pharmaceutics and Biopharmacy) for excellent technical support. MEDITRANS, an Integrated Project funded by the European Commission under the Sixth Framework (NMP4-CT-2006-026668) is gratefully acknowledged.

#### 4.7 References

1. Iorns E, Lord CJ, Turner N, Ashworth A. Utilizing RNA interference to enhance cancer drug discovery. *Nat Rev Drug Discov* 2007;6(7):556-568.
2. Shim MS, Kwon YJ. Efficient and targeted delivery of siRNA *in vivo*. *FEBS J* 2010;277(23):4814-4827.
3. Whitehead KA, Langer R, Anderson DG. Knocking down barriers: advances in siRNA delivery. *Nat Rev Drug Discov* 2009;8(2):129-138.
4. Grimm D, Kay MA. Therapeutic application of RNAi: is mRNA targeting finally ready for prime time? *J Clin Invest* 2007;117(12):3633-3641.
5. Shuai XT, Merdan T, Unger F, Wittmar M, Kissel T. Novel biodegradable ternary copolymers hy-PEI-g-PCL-b-PEG: synthesis, characterization, and potential as efficient nonviral gene delivery vectors. *Macromolecules* 2003;36(15):5751-5759.
6. Liu Y, Nguyen J, Steele T, Merkel O, Kissel T. A new synthesis method and degradation of hyper-branched polyethylenimine grafted polycaprolactone block mono-methoxyl poly (ethylene glycol) copolymers (hy-PEI-g-PCL-b-mPEG) as potential DNA delivery vectors. *Polymer* 2009;50(16):3895-3904.
7. Liu Y, Samsonova O, Sproat B, Merkel O, Kissel T. Biophysical characterization of hyper-branched polyethylenimine-graft-polycaprolactone-block-mono-methoxyl-poly(ethylene glycol) copolymers (hy-PEI-PCL-mPEG) for siRNA delivery. *J Control Release* 2011;153(3):262-268.
8. Grzelinski M, Urban-Klein B, Martens T, Lamszus K, Bakowsky U, Hobel S, et al. RNA interference-mediated gene silencing of pleiotrophin through polyethylenimine-complexed small interfering RNAs *in vivo* exerts antitumoral effects in glioblastoma xenografts. *Hum Gene Ther* 2006;17(7):751-766.
9. Werth S, Urban-Klein B, Dai L, Hobel S, Grzelinski M, Bakowsky U, et al. A low molecular weight fraction of polyethylenimine (PEI) displays increased transfection efficiency of DNA and siRNA in fresh or lyophilized complexes. *J Control Release* 2006;112(2):257-270.
10. Mosqueira VCF, Legrand P, Gulik A, Bourdon O, Gref R, Labarre D, et al. Relationship between complement activation, cellular uptake and surface physicochemical aspects of novel PEG-modified nanocapsules. *Biomaterials* 2001;22(22):2967-2979.

11. Merdan T, Kunath K, Petersen H, Bakowsky U, Voigt KH, Kopecek J, et al. PEGylation of poly(ethylene imine) affects stability of complexes with plasmid DNA under in vivo conditions in a dose-dependent manner after intravenous injection into mice. *Bioconjug Chem* 2005;16(4):785-792.
12. Kunath K, von Harpe A, Petersen H, Fischer D, Voigt K, Kissel T, et al. The structure of PEG-modified poly(ethylene imines) influences biodistribution and pharmacokinetics of their complexes with NF-kappa B decoy in mice. *Pharm Res* 2002;19(6):810-817.
13. Sung SJ, Min SH, Cho KY, Lee S, Min YJ, Yeom YI, et al. Effect of polyethylene glycol on gene delivery of polyethylenimine. *Biol Pharm Bull* 2003;26(4):492-500.
14. Sato A, Choi SW, Hirai M, Yamayoshi A, Moriyama R, Yamano T, et al. Polymer brush-stabilized polyplex for a siRNA carrier with long circulatory half-life. *J Control Release* 2007;122(3):209-216.
15. Merkel OM, Librizzi D, Pfestroff A, Schurrat T, Behe M, Kissel T. In vivo SPECT and real-time gamma camera imaging of biodistribution and pharmacokinetics of siRNA delivery using an optimized radiolabeling and purification procedure. *Bioconjug Chem* 2009;20(1):174-182.
16. Zheng M, Liu Y, Samsonova O, Endres T, Merkel O, Kissel T. Amphiphilic and biodegradable hy-PEI-g-PCL-b-PEG copolymers efficiently mediate transgene expression depending on their graft density. *Int J Pharm* 2011;427(1):80-87.
17. Merkel OM, Mintzer MA, Librizzi D, Samsonova O, Dicke T, Sproat B, et al. Triazine dendrimers as nonviral vectors for in vitro and in vivo RNAi: the effects of peripheral groups and core structure on biological activity. *Mol Pharm* 2010;7(4):969-983.
18. Endres T, Zheng M, Beck-Broichsitter M, Samsonova O, Debus H, Kissel T. Optimising the self-assembly of siRNA loaded PEG-PCL-IPEI nano-carriers employing different preparation techniques. *J Control Release* 2012.
19. Merdan T, Kunath K, Fischer D, Kopecek J, Kissel T. Intracellular processing of poly(ethylene imine)/ribozyme complexes can be observed in living cells by using confocal laser scanning microscopy and inhibitor experiments. *Pharm Res* 2002;19(2):140-146.
20. Merkel OM, Zheng M, Mintzer MA, Pavan GM, Librizzi D, Maly M, et al. Molecular modeling and in vivo imaging can identify successful flexible triazine dendrimer-based siRNA delivery systems. *J Control Release* 2011;153(1):23-33.
21. Merkel OM, Beyerle A, Librizzi D, Pfestroff A, Behr TM, Sproat B, et al. Nonviral siRNA delivery to the lung: investigation of PEG-PEI polyplexes and their in vivo performance. *Mol Pharm* 2009;6(4):1246-1260.
22. Merkel OM, Librizzi D, Pfestroff A, Schurrat T, Buyens K, Sanders NN, et al. Stability of siRNA polyplexes from poly(ethylenimine) and poly(ethylenimine)-g-poly(ethylene glycol) under in vivo conditions: effects on pharmacokinetics and biodistribution measured by fluorescence fluctuation spectroscopy and single photon emission computed tomography (SPECT) imaging. *J Control Release* 2009;138(2):148-159.
23. Bronich T, Kabanov AV, Marky LA. A thermodynamic characterization of the interaction of a cationic copolymer with DNA. *J Phys Chem B* 2001;105(25):6042-6050.
24. Noy A, Perez A, Lankas F, Javier Luque F, Orozco M. Relative flexibility of DNA and RNA: a molecular dynamics study. *J Mol Biol* 2004;343(3):627-638.
25. Pavan GM, Albertazzi L, Danani A. Ability to adapt: different generations of PAMAM dendrimers show different behaviors in binding siRNA. *J Phys Chem B* 2010;114(8):2667-2675.



- 26.Pavan GM, Kostianen MA, Danani A. Computational approach for understanding the interactions of UV-degradable dendrons with DNA and siRNA. *J Phys Chem B* 2010;114(17):5686-5693.
- 27.Wood MJA, Jagannath A. Localization of double-stranded small interfering RNA to cytoplasmic processing bodies is Ago2 dependent and results in up-regulation of GW182 and argonaute-2. *Mol Biol Cell* 2009;20(1):521-529.
- 28.Dykhhoorn DM, Palliser D, Lieberman J. The silent treatment: siRNAs as small molecule drugs. *Gene Ther* 2006;13(6):541-552.
- 29.Hsu CY, Hendzel M, Uludag H. Improved transfection efficiency of an aliphatic lipid substituted 2 kDa polyethylenimine is attributed to enhanced nuclear association and uptake in rat bone marrow stromal cell. *J Gene Med* 2010;13(1):46-59.
- 30.Malek A, Merkel O, Fink L, Czubyko F, Kissel T, Aigner A. In vivo pharmacokinetics, tissue distribution and underlying mechanisms of various PEI(-PEG)/siRNA complexes. *Toxicol Appl Pharmacol* 2009;236(1):97-108.

## Chapter 5

### MODULAR SYNTHESIS OF FOLATE CONJUGATED TERNARY

### COPOLYMERS:

### POLYETHYLENIMINE-GRAFT-POLYCAPROLACTONE-BLOCK-POLY(ETHYLENE GLYCOL)-FOLATE FOR TARGETED GENE DELIVERY

Published in Bioconjugate Chemistry, 2012 May 11. DOI: 10.1021/bc300025d

Li Liu<sup>†,‡,§</sup>, Mengyao Zheng<sup>†,‡</sup>, Thomas Renette<sup>‡</sup>, Thomas Kissel<sup>\*,‡</sup>

<sup>†</sup> Both authors contributed equally to this work.

#### Author contributions

T. K. guided and directed the research. M. Z. and L. L. designed the measurements. M. Z. carried out the SYBR<sup>®</sup> Gold assay, heparin assay, MTT and *in vitro* transfection experiment. L. L. synthesized and characterized the polymers. M. Z. and L. L. analysed the experimental data.

## 5.1 Abstract

Folate receptor (FR) is overexpressed in a variety of human cancers. Gene delivery vectors conjugated with folate as a ligand could possibly deliver gene materials into target tumor cells via FR-mediated endocytosis. This study addresses novel folate-conjugated ternary copolymers based on polyethylenimine-graft-polycaprolactone-block-poly(ethylene glycol) (PEI-*g*-PCL-*b*-PEG-Fol) as targeted gene delivery system using a modular synthesis approach including “click” conjugation of folate moieties with heterobifunctional PEG-*b*-PCL at PEG terminus and subsequently the introduction of PEI by a Michael addition between folate-PEG-*b*-PCL and PEI via active PCL terminus. This well controlled synthetic procedure avoids tedious separation of by-products. The structure of PEI-*g*-PCL-*b*-PEG-Fol was confirmed by <sup>1</sup>H NMR and UV spectra. DNA condensation of PEI-*g*-PCL-*b*-PEG-Fol was tested using a SYBR<sup>TM</sup> Gold quenching assay and agarose gel electrophoresis upon heparin competition assay. Although PEI-*g*-PCL-*b*-PEG-Fol could condense DNA completely at N/P ratio > 2, polyplexes of N/P ratio 10 with sizes at about 120 nm and positive zeta potentials were selected for further biological evaluations due to polyplex stability. An enhancement of cellular uptake of PEI-*g*-PCL-*b*-PEG-Fol/pDNA polyplexes was observed in FR over-expressing KB cells in comparison to unmodified PEI-*g*-PCL-*b*-PEG, through flow cytometry analysis and confocal laser scanning imaging. Importantly, this enhanced cellular uptake could be inhibited by free folic acid and did not occur in FR-negative A549 cells, demonstrating specific cell uptake by FR-mediated endocytosis. Furthermore, the transfection efficiency of PEI-*g*-PCL-*b*-PEG-Fol/pDNA polyplexes was increased approximately 14-fold in comparison to folate-negative polyplexes. Therefore, the PEI-*g*-PCL-*b*-PEG-Fol merits further investigation under *in vivo* conditions for targeting FR overexpressing tumors.

## 5.2 Introduction

Gene therapy has received increasing attention over the past two decades as a promising method for treating various inherited and acquired human diseases.<sup>1-3</sup> An efficient and safe delivery system that delivers the therapeutic genes into target cells is regarded as prerequisite for successful gene therapy. Recently, a large number of studies focused on the development of polymer-based non-viral gene delivery vectors due to their non-immunogenicity, low cost, physiochemical versatility and ease of manipulation.<sup>4, 5</sup> Among them, polyethylenimine

(PEI)-based delivery systems have emerged as one of the most successful and efficient candidates for gene delivery both *in vitro* and *in vivo*.<sup>6</sup> PEI is a cationic polymer with a high density of amines, which condense nucleic acids via electrostatic interaction into nano-scaled polyplexes. Importantly, the protonable amine group endowed PEI-containing polyplexes with efficient endosomal escape property through the proton-sponge mechanism, which was believed to be the main reason for the relatively high gene-transfer activity of PEI.<sup>6,7</sup> Nevertheless, the PEI-based gene delivery systems have suffered from relatively high toxicity, especially at high molecular weights, affecting their potential applications under *in vivo* conditions.

To decrease cytotoxicity and enhance gene transfection efficiency, many efforts relied on the modification of PEI either with hydrophilic segments such as poly(ethylene glycol) (PEG)<sup>8,9</sup>, or hydrophobic segments such as poly(L-lactide-*co*-glycolide)<sup>10</sup>, or other biocompatible compositions such as cyclodextrin<sup>11</sup>. Moreover, PEI derivatives have also been decorated with variety of targeting ligands<sup>12</sup> to generate gene delivery systems with targeting functionality for specific tissues/cells. For example, the folate receptor (FR) is known to be over-expressed in many types of carcinoma cells.<sup>13-15</sup> By conjugation with folate, the PEI-containing polyplexes were expected to target the folate receptor on cell surface and transfect specific cells by receptor-mediated endocytosis.<sup>16-23</sup>

In previous studies of our group, a series of ternary copolymers based on PEI-*g*-PCL-*b*-PEG were synthesized and investigated as potential gene delivery vectors.<sup>24-27</sup> The PEI-*g*-PCL-*b*-PEG copolymers were shown to be biodegradable and amphiphilic in character; hypothetically generating micelle-like polyplexes with excellent colloidal stability. Structure-function relationships suggested that higher graft densities of PCL-PEG led to decreased cytotoxicity and copolymers with short PCL segment displayed higher transfection efficiency *in vitro* compared with PEI 25kDa.<sup>25, 27</sup>

In this study, folate conjugated PEI-*g*-PCL-*b*-PEG was synthesized and examined for targeted gene delivery. It should be noted that the folate moiety was designed to be conjugated at the distal PEG end, instead of direct linkage to PEI.<sup>22</sup> This strategy provides more flexibility for the folate ligands via PEG spacers possibly improving their target binding efficacy. Therefore, to achieve the well-structured PEI-*g*-PCL-*b*-PEG-Folate copolymer, a modular synthesis procedure was designed, which involved the conjugation of folate moiety with heterobifunctional

PEG-*b*-PCL by click chemistry followed by a Michael addition between folate-PEG-*b*-PCL and PEI. The mild reaction conditions of click chemistry and Michael addition were beneficial to maintain the biological activity of folate and to avoid tedious cleaning procedures. The resulting copolymers were investigated regarding biophysical properties, DNA condensation and cytotoxicity. Furthermore, cell-uptake and transfection efficiency of PEI-*g*-PCL-*b*-PEG-Fol/pDNA complexes were evaluated *in vitro* in FR-positive KB cells to determine their potential as targeted gene delivery vehicles.

### 5.3 Experimental Section

**Materials.** Heterobifunctional poly(ethylene glycol) (HO-PEG-COOH, 3 kDa) was purchased from Rapp Polymere GmbH (Germany).  $\epsilon$ -Caprolactone from Fluka was distilled before use under vacuum over CaH<sub>2</sub>. Branched polyethylenimine (*hy*-PEI, 25kDa) was obtained from BASF. Folic acid, N-hydroxysuccinimide, dicyclohexylcarbodiimide and solvents were purchased from Acros. Propargylamine and acryloyl chloride were from Sigma-Aldrich. 1-azido-3-aminopropane was synthesized from 3-Bromopropylamine hydrobromide and sodium azide (Details in Supplement information). All other reagents for synthesis were obtained from Sigma-Aldrich and were used as received without further purification. Endotoxin-free luciferase-encoding plasmid DNA (pCMV-luc) was provided by Plasmid Factory (Bielefeld, Germany). SYBR<sup>TM</sup> Gold and YOYO-1 were obtained from Invitrogen.

**Synthesis of Azido-functionalized Folate.** Azido-functionalized folate was prepared by a method modified from the literature.<sup>28</sup> Folic acid (0.5 g, 1.135 mmol) was dissolved in DMSO (20 mL) containing triethylamine (0.25 mL). After addition of N-hydroxysuccinimide (NHS) (0.26 g, 2.2 equiv.), and dicyclohexylcarbodiimide (DCC) (0.25 g, 1.1 equiv.), the mixture was stirred at room temperature in the dark for 24 h. Then, 1-azido-3-aminopropane (0.24 g, 2 equiv.) was added into the mixture under stirring. The reaction was continued for another 24 h. After the precipitated side-product dicyclohexylurea (DCU) was removed by filtration, the product was precipitated in ethyl acetate and dried under vacuum. The crude product was purified by dissolving in 1M NaOH and precipitation by addition of 1M HCl. The precipitates were

collected by centrifugation, washed with EtOH/H<sub>2</sub>O (1:1) and dried under vacuum to give an orange-yellow product in 86% yield.

FT-IR ( $\nu$ , cm<sup>-1</sup>): 2800-3200, 2095 (-N<sub>3</sub>), 1682, 1602, 1506, 1297, 1236, 1174, 1126. <sup>1</sup>H NMR (*d*<sub>6</sub>-DMSO, 400M):  $\delta$  (ppm)= 11.37 (s, 1H, -CONHCHCOOH), 8.62 (s, 1H, PtC7H), 7.93-7.95 (d, 1H, PtC6-CH<sub>2</sub>NH-Ph), 7.79-7.80 (d, 1H, -CONHCHCOOH), 7.63-7.60 (d, 2H, Ph-C<sub>2</sub>H and Ph-C<sub>6</sub>H), 6.87 (br s, 2H, NH<sub>2</sub>), 6.62-6.59 (d, 2H, Ph-C<sub>3</sub>H and Ph-C<sub>5</sub>H), 4.46-4.44 (d, 2H, PtC6-CH<sub>2</sub>NH-Ph), 4.30-4.26 (m, 1H, -CONHCHCOOH), 3.44-3.39 (m, 2H, -CH<sub>2</sub>N<sub>3</sub>), 3.29 (br s, OH), 3.10-3.02 (m, 2H, -CONHCH<sub>2</sub>CH<sub>2</sub>CH<sub>2</sub>N<sub>3</sub>), 2.30-2.15 (m, 2H, -CH<sub>2</sub>CH<sub>2</sub>CONH), 2.05-1.85 (m, 2H, -CH<sub>2</sub>CH<sub>2</sub>CONH-), 1.60-1.56 (m, 2H, -CONHCH<sub>2</sub>CH<sub>2</sub>CH<sub>2</sub>N<sub>3</sub>). Pt = pteridine.

**Synthesis of PCL-*b*-PEG with Heterobifunctional Terminal Group (acrylate-PCL-*b*-PEG-alkyne).** PCL-*b*-PEG was firstly synthesized by ring-opening polymerization of  $\epsilon$ -caprolactone initiated from the hydroxyl end group of HO-PEG-COOH. Defined amounts of HO-PEG-COOH and caprolactone monomers were sealed in dry argon and stirred at 120 °C for 24 h with Sn(Oct)<sub>2</sub> (about 0.1% molar ratio of caprolactone) as catalyst.<sup>29</sup> The product was dissolved in chloroform and precipitated with cold methanol/ether (1/1, v/v). The precipitate obtained as HO-PCL-*b*-PEG-COOH was dried under vacuum for 24 h for the following modification. (Yield: 88%).

HO-PCL-*b*-PEG-COOH (0.3 mmol) was dissolved in dry dichloromethane (DCM) with NHS (0.6 mmol) and DCC (1.2 mmol). The mixture was stirred at 0 °C for 1 h and then at room temperature for 24 h, during which time the mixture became turbid due to DCU. Propargylamine (0.6 mmol) and triethylamine were added into the above mixture, and stirred under room temperature for another 24 h. The mixture was filtered to remove the precipitated DCU, and then precipitated in cold ether. The precipitates were dried under vacuum for 24 h to obtain HO-PCL-*b*-PEG-alkyne. (Yield: 79%).

Next, the terminal hydroxyl group of HO-PCL-*b*-PEG-alkyne (0.1 mmol) was coupled with acryloyl chloride (0.2 mmol) in dry toluene containing triethylamine (0.2mmol). The reaction mixture was stirred at 80 °C for 10 h, and then cooled to room temperature, filtered to remove triethylamine hydrochloride and precipitated in cold n-hexane. The precipitates were collected

and dried under vacuum overnight to produce heterobifunctional acrylate-PCL-*b*-PEG-alkyne. (Yield: 78%)

$^1\text{H}$  NMR ( $\text{CDCl}_3$ , 400M):  $\delta$  (ppm) = 5.7-6.5 (m,  $-\text{CH}=\text{CH}_2$ ), 4.25-4.20 (m,  $\text{NHCOCH}_2\text{CH}_2\text{CO}$ ), 4.07-4.01 (t,  $\text{COCH}_2\text{CH}_2\text{CH}_2\text{CH}_2\text{CH}_2\text{O}$ ), 3.82-3.80 (m, weak), 3.67-3.60 (s,  $\text{OCH}_2\text{CH}_2\text{O}$ ), 3.46-3.43 (m, weak), 2.32-2.28 (t,  $\text{COCH}_2\text{CH}_2\text{CH}_2\text{CH}_2\text{CH}_2\text{O}$ ), 2.23-2.21 (m,  $-\text{C}\equiv\text{CH}$ ), 1.68-1.60 (m,  $\text{COCH}_2\text{CH}_2\text{CH}_2\text{CH}_2\text{CH}_2\text{O}$ ), 1.42-1.33 (m,  $\text{COCH}_2\text{CH}_2\text{CH}_2\text{CH}_2\text{CH}_2\text{O}$ ).

#### **“Click” Conjugation of Azido-folate with PCL-*b*-PEG at PEG Terminal Alkyne.**

Azido-folate (0.12 mmol) and acrylate-PCL-*b*-PEG-alkyne (0.1 mmol) were dissolved in 15 mL aq.  $\text{NH}_4\text{HCO}_3$  (10 mM).  $\text{CuSO}_4$  (20 mol% to the azido group) and fresh sodium ascorbate solution (50 mol% to the azido group) were added, respectively. The mixture was stirred at room temperature for 24 h. Afterwards, the mixture was filtered through a 0.45  $\mu\text{m}$  filter. The clear solution was diluted with equal volume of saturated NaCl aqueous solution, and then extracted five times by DCM. The clear yellow DCM solution was concentrated by rotary evaporation and then precipitated in cold ether. The yellow product (acrylate-PCL-*b*-PEG-Fol) was dried under vacuum overnight. (Yield: 85 %).

$^1\text{H}$  NMR ( $d_6$ -DMSO, 400M):  $\delta$  (ppm)= 8.6, 7.8, 6.9, 6.6 (weak multiplets, folate terminus), 7.9 (s, weak, 1H, triazoles), 6.5-5.9 (m,  $-\text{CH}=\text{CH}_2$ ), 4.0-3.9 (t,  $\text{COCH}_2\text{CH}_2\text{CH}_2\text{CH}_2\text{CH}_2\text{O}$ ), 3.5-3.4 (s,  $\text{OCH}_2\text{CH}_2\text{O}$ ), 2.3-2.2 (t,  $\text{COCH}_2\text{CH}_2\text{CH}_2\text{CH}_2\text{CH}_2\text{O}$ ), 1.6-1.4 (m,  $\text{COCH}_2\text{CH}_2\text{CH}_2\text{CH}_2\text{CH}_2\text{O}$ ), 1.3-1.2 (m,  $\text{COCH}_2\text{CH}_2\text{CH}_2\text{CH}_2\text{CH}_2\text{O}$ ).

**Synthesis of PEI-*g*-PCL-*b*-PEG-Fol.** Hy-PEI (10  $\mu\text{mol}$ ) and acrylate-PCL-*b*-PEG-Fol (10  $\mu\text{mol}$  or 30  $\mu\text{mol}$ ) were dissolved in 3 mL of chloroform, respectively. The chloroform solution of folate-conjugated di-block copolymer was added drop wise into PEI solution at 40–45  $^\circ\text{C}$  and stirred for 24 h. Afterwards, the product was collected by solvent replacement (via methanol and water), dialyzed against water (Mw cut off 10,000) at 4 $^\circ\text{C}$  for 24 h and lyophilized to generate PEI-*g*-PCL-*b*-PEG-Fol. (Yield: 85 %).  $^1\text{H}$  NMR ( $\text{D}_2\text{O}$ , 400M):  $\delta$  (ppm)= 8.6, 8.0, 7.6, 6.8 (weak, folate terminus), 3.6 (s, strong,  $\text{OCH}_2\text{CH}_2\text{O}$ ), 1.6-1.2 (weak and broad,  $\text{COCH}_2\text{CH}_2\text{CH}_2\text{CH}_2\text{CH}_2\text{O}$ ).

The corresponding copolymers with non-folate conjugation were prepared from *hy*-PEI and acrylate-PCL-*b*-mPEG by a synthesis route reported previously.<sup>25</sup>

**Polymer Characterization.** FTIR was performed on a Nicolet FT-IR 510 P spectrometer (Thermo Fischer Scientific Inc., Waltham, MA, USA) in a range between 4000 and 400 cm<sup>-1</sup>. NMR analysis was carried out using a JEOL ECX-400 spectrometer (Japan) in ppm relatively to solvent signals.

**Folate Content in Copolymers determined by UV-vis Spectroscopy.** Folic acid and copolymers were dissolved in DMSO respectively, and measured by a UV-vis spectrometer (Pharmacia Biotech Ultrospec 3000, GE Healthcare) from 200 to 600 nm. Folic acid showed two typical absorbance peaks at 280 nm and 360 nm, respectively. The absorbance intensity at 360 nm was determined as a function of folic acid concentration, which showed a liner relation to folate concentration during  $(0.025-2.14) \times 10^{-7}$  mol/mL (Supporting information). The concentration of folate in PEI-*g*-PCL-*b*-PEG-Fol was calculated from the copolymer/DMSO solution with predetermined polymer concentration, according to the calibration curve made from free folic acid.

**Preparation of the Copolymer/DNA Complexes.** PEI-*g*-PCL-*b*-PEG-Fol was dissolved in water to prepare a stock copolymer solution of 1 mg/mL (based on *hy*-PEI 25k). All polymer stock solutions were filtered using disposable 0.22  $\mu$ m filters and then diluted with 5 % glucose solution. The DNA solution of 0.04 mg/mL was obtained by diluting 1 mg/mL stock solution with 5 % glucose solution. To prepare polyplexes, 50  $\mu$ L of DNA solution was taken and mixed with equal volume of copolymer solution at the appropriate concentration depending on the required N/P ratio by pipetting. Then the complexes were incubated at 25 °C for 20 min, followed by the corresponding characterizations.

**SYBR™ Gold Assay.** The complexation between copolymer and DNA was determined by the SYBR™ Gold quenching assay as previously reported.<sup>30</sup> Briefly, 100  $\mu$ L of polyplexes containing 2  $\mu$ g DNA were prepared at different N/P ratios in 96-well plate. After 20 minutes of



incubation at room temperature, 20  $\mu\text{L}$  diluted 4 $\times$ SYBR<sup>TM</sup> Gold solution was added and incubated for another 10 minutes in the dark. The fluorescence was directly detected with a fluorescence plate reader (BMG Labtech, Offenburg) at 495 nm excitation and 537 nm emission. Triplicate samples were investigated and the results were transformed into relative fluorescent intensity values ( $F_{\text{sample}}/F_{\text{free DNA}}$ ).

**Heparin Competition Assay.** The stability of polyplexes against heparin (a model molecule of competing polyanion) was assessed by agarose gel electrophoresis in TAE buffer (0.04 M Tris–acetate, 0.001 M EDTA, pH 7.4) containing 0.5 mg/mL ethidium bromide (EtBr). Heparin (150 000 IU/g, Serva, Pharm., USP XV2, Merck, Darmstadt, Germany) solution was added to reach a final heparin concentration of 0.5 mg/mL into the polyplex solution at different N/P-ratios. After 15 min of incubation with heparin, 25  $\mu\text{L}$  of polyplex solution containing 1.5  $\mu\text{g}$  DNA was loaded into the agarose gel wells and the agarose gels were run in TAE buffer for 45 min at 80 V using an Electro-4 electrophoresis unit (Thermo Electron, Waltham, MA, USA). The gels were recorded after irradiation with UV-light using a gel documentation system (BioDocAnalyze, Biometra, Göttingen, Germany).

**Size and zeta-potential analysis.** The size and zeta potential of the polyplexes were monitored by a dynamic light scattering (DLS) instrument (Zetasizer 3000HS, Malvern, Worcestershire, UK). Polyplexes were measured in a low volume cuvette (100  $\mu\text{L}$ ) firstly, and then zeta-potential measurements were performed on the samples prepared by diluting 100  $\mu\text{L}$  of polyplexes solution with additional 600  $\mu\text{L}$  of 5 % glucose solution to a final volume of 700  $\mu\text{L}$  in a transparent zeta cuvette. The samples were carried out in the standard clear capillary electrophoresis cell at 25  $^{\circ}\text{C}$ . Three measurements were performed on each sample.

**Cell culture.** Human epithelial nasopharyngeal carcinoma (KB) cells were gifts from Prof. P. S. Low's group (Purdue University) and continuously cultured in folate-free RPMI-1640 medium supplemented with 10 % fetal calf serum (FCS) at 37  $^{\circ}\text{C}$  in a humidified atmosphere containing 5 %  $\text{CO}_2$ . FR negative human lung epithelial carcinoma (A549) cells were obtained from DSMZ

(Braunschweig, Germany) and cultured in DMEM medium supplemented with 10 % FCS at 37 °C in a humidified atmosphere containing 5 % CO<sub>2</sub>.

**Cytotoxicity assay.** KB cells were seeded into 96-well plates at a density of  $8 \times 10^3$  cells/well. After 24 h, cell culture medium was aspirated and replaced by 200  $\mu$ L of serial dilutions of polymer stock solution in cell culture medium with FCS. The cells were then incubated for 24 hours at 37 °C. Afterwards, medium was replaced by medium without serum containing 0.5 mg/mL 3-(4,5-dimethylthiazol-2-yl)-2,5-diphenyl tetrazolium bromide (MTT). After 4 h incubation at 37 °C in the dark, medium was removed and then 200  $\mu$ L of DMSO was added to dissolve the formazan crystals formed by proliferating cells. After 15 min incubation with DMSO, measurement was performed using an ELISA reader (Titertek Plus MS 212, ICN, Eschwege, Germany) at a wavelength of 570 nm and 690 nm. Relative viability was calculated using wells with untreated cells as 100 % controls. Data are presented as mean values ( $\pm$ SD) of four experiments. The IC<sub>50</sub> values were calculated with Original 8 using Logistic fit.

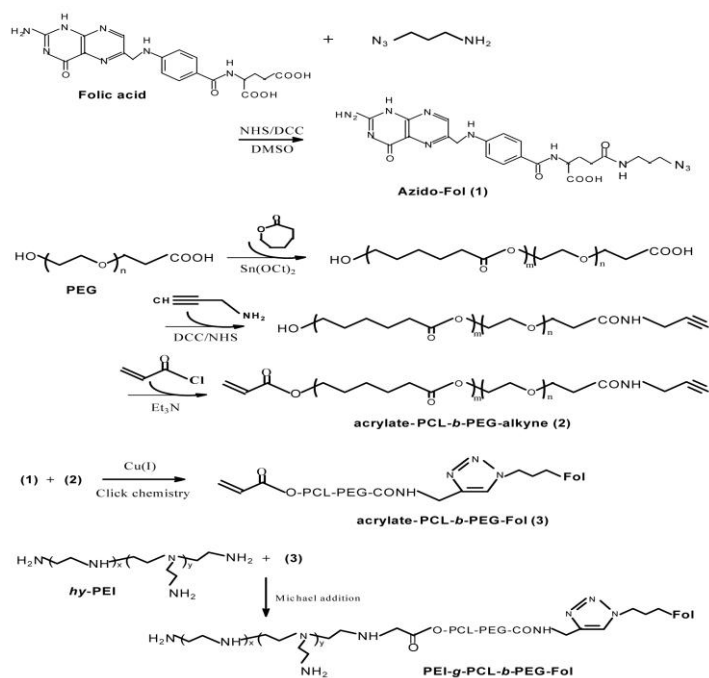
**Cellular Uptake by Flow Cytometry.** KB cells and A549 cells were seeded at a density of  $6 \times 10^4$  cells/well in 24 well plates 24 h prior to the experiment. Polymers including PEI 25kDa, PEI-g-PCL-*b*-mPEG (PCE3) and PEI-g-PCL-*b*-PEG-Fol (PCE3-F) were labeled with FITC in parallel assay. Polyplexes were prepared at N/P=10 using pCMV-Luc as described above. Cells were incubated with polyplexes containing 4  $\mu$ g DNA per well for 4 h at 37 °C. In free folate competition studies, the normal RPMI-1640 medium (containing 1 mg/L folic acid) was replaced as incubation medium 1 h before polyplexes added. Afterwards, cells were washed with PBS once and incubated with 0.4 % trypan blue solution for 5 min to quench extracellular fluorescence. Cells were washed again, detached using 100  $\mu$ L of trypsin and treated with 900  $\mu$ L of PBS solution containing 10 % FCS. Cells were then collected by centrifugation and resuspended in 300  $\mu$ L of Cellfix solution (BD Biosciences, San Jose, CA) for cell fixation. Cell suspensions were measured on a FACS Canto™ II (BD Biosciences, San Jose, CA) with excitation at 488 nm and emission filter set to 530/30 bandpass. 10,000 viable cells were evaluated in each experiment and results are the mean of 3 independent measurements.

**Confocal Laser Scanning Microscopy.** KB cells were seeded at a density of  $2 \times 10^4$  cells per well in 8 well chamber slides (Nunc, Wiesbaden, Germany) and allowed to grow for 24 h. Polyplexes were prepared at N/P=10 as described above using YOYO-1 labeled pCMV-Luc. Cells were incubated with polyplexes containing 1  $\mu\text{g}$  DNA per well in medium with FCS for 4 h at 37 °C. Subsequently, cells were washed with PBS, quenched with 0.4 % trypan blue solution, washed again with PBS, fixed using 4 % paraformaldehyde in PBS, DAPI stained and washed again with PBS. Finally, cells were embedded using FluorSave Reagent (Calbiochem, San Diego, CA). A Zeiss Axiovert 100 M microscope coupled to a Zeiss LSM 510 scanning device (Zeiss, Oberkochen, Germany) was used for confocal microscopy. For excitation of YOYO-1 fluorescence, an argon laser with an excitation wavelength of 488 nm was used. Fluorescence emission was detected using a 505–530 nm bandpass filter. Transmission images were obtained in the same scan.

***In vitro* Gene Transfection.** KB cells were seeded in 48 well plates ( $1.5 \times 10^4$  cells/well) 24 h prior to the experiment. Polyplexes were prepared at N/P=10 as described above using plasmid pCMV-luc. Medium was replaced by 200  $\mu\text{L}$  of fresh cell culture medium with 10% FCS, then 50  $\mu\text{L}$  of polyplexes (containing 1  $\mu\text{g}$  pDNA) were added in each well. For folate competition assay, normal RPMI1640 medium (containing 1mg/L folic acid) was replaced 1 h before polyplexes addition. After incubation for 4 h, the medium was exchanged and cells were cultured for another 44 h. Then cells were washed with PBS twice, lysed in 100  $\mu\text{L}$  cell culture lysis buffer for 15 min. Luciferase activity was quantified by injection of 50  $\mu\text{L}$  luciferase assay buffer, containing 10 mM luciferin, to 25  $\mu\text{L}$  of the cell lysate. The relative light units (RLU) were measured with a plate luminometer (LumiSTAR Optima, BMG Labtech GMBH, Offenburg, Germany). Protein concentration was determined using a Pierce BCA protein assay Kit (Thermo Scientific). All experiments were performed in triplicate and data were expressed in RLU per mg protein ( $\pm\text{SD}$ ).

**Statistics.** Significance between the means was tested by two way ANOVA and statistical evaluations using GraphPad Prism 4.03 (Graph Pad Software, La Jolla, USA).

## 5.4 Results and Discussion



Scheme 1. Synthesis strategy of PEI-g-PCL-b-PEG-Fol.

**Synthesis and characterization of PEI-g-PCL-*b*-PEG-Fol.** In most of the previously reported synthesis routes of folate-receptor targeted polycations, folate moieties were conjugated with polycation either directly<sup>22, 23, 31</sup> or via heterobifunctional PEG linker like HOOC-PEG-NH<sub>2</sub> through the amine-carboxyl reaction using NHS chemistry.<sup>18, 19</sup> NHS reactions are widely used in bioconjugations due to their mild reaction conditions, but

purification of the final product from excess NHS, by-product and solvent etc. may present considerable challenges. On the other hand, it was postulated that the rigid folate moiety attached at the distal end of flexible PEG chains would allow more efficient interaction and binding to folate receptor on the cell surface. But in the conventional HOOC-PEG-NH<sub>2</sub>/NHS strategy, random coupling between different PEG chains co-existed inevitably with PEG-Fol. The coupled PEG chains were difficult to separate and may also generate byproducts.

In this study, the folate-conjugated ternary copolymer of PEI-g-PCL-*b*-PEG-Fol was synthesized through a modular procedure as shown in Scheme1, which involved click conjugation of folate moiety with alkyne-terminated PCL-*b*-PEG, followed by the Michael addition between acrylate-terminated folate-PEG-*b*-PCL and PEI.

Firstly, the diblock copolymer of PCL-*b*-PEG was synthesized from heterobifunctional HO-PEG-COOH initiated from the hydroxyl group. The molecular weight of PCL block could be predetermined by the molar ratio of monomers to hydroxyl groups, which were confirmed by <sup>1</sup>H NMR analysis through the calculation of the integral intensity at 1.3-1.4 ppm (-COCH<sub>2</sub>CH<sub>2</sub>CH<sub>2</sub>CH<sub>2</sub>CH<sub>2</sub>O-, PCL) and 3.4-3.5 ppm (-CH<sub>2</sub>CH<sub>2</sub>O-, PEG) based on the known molecular weight of PEG. The obtained diblock copolymer HO-PCL-*b*-PEG-COOH was then

converted into alkyne end group at the PEG terminus and acrylate end group at the PCL terminus, respectively. The structures of intermediates in different steps were characterized by  $^1\text{H}$  NMR analysis (Figure S-3), where the appearance of signals belonging to alkyne and double bond was verified accordingly. Here, the heterobifunctional acrylate-PCL-*b*-PEG-alkyne was a key element for obtaining regioselectivity during synthesis. On one hand, the PEG-terminal alkyne was specific for conjugation with azido-folate through the copper(I)-catalyzed azide-alkyne click reaction. This cycloaddition reaction is well known for its high efficiency and selectivity under mild conditions, which has been applied in many bioconjugations of ligands or drugs to polymers.<sup>28, 32-34</sup> On the other hand, the PCL-terminal acrylate group was reactive to couple with the amino group of PEI according to a Michael addition under mild conditions afterward. This strategy avoided the risk of intersectional reactions between di-block copolymers. Importantly, both click conjugation and Michael addition were carried through under the mild conditions, which were advantageous to maintain the activity of folate in the objective material since folate is sensitive to light and heat.

Thereafter, the heterobifunctional acrylate-PCL-*b*-PEG-alkyne was transformed into folate terminated PCL-*b*-PEG-Fol via “click” cyclo-addition with azido-modified folate in weak basic aqueous solution (for water-soluble copolymer with short PCL block). The  $^1\text{H}$  NMR spectra in Figure 1 (a) verified the structure of acrylate-PCL-*b*-PEG-Fol with signal assignment. The successful conjugation of folate moiety onto PCL-*b*-PEG was further confirmed by UV spectra as shown in Figure 2. Two absorbance peaks appeared at 280 nm and 360 nm respectively for PCL-*b*-PEG-Fol, while its precursor PCL-*b*-PEG had no characteristic absorbance in this range. The content of folate conjugated in PCL-*b*-PEG-Fol was about  $2.1 \times 10^{-7}$  mol/mg, obtained on the basis of the standard curve using the UV absorbance at 360 nm as reference. This value is equivalent to the conjugation percent of folate onto PCL-*b*-PEG as about 95% (mol.%).

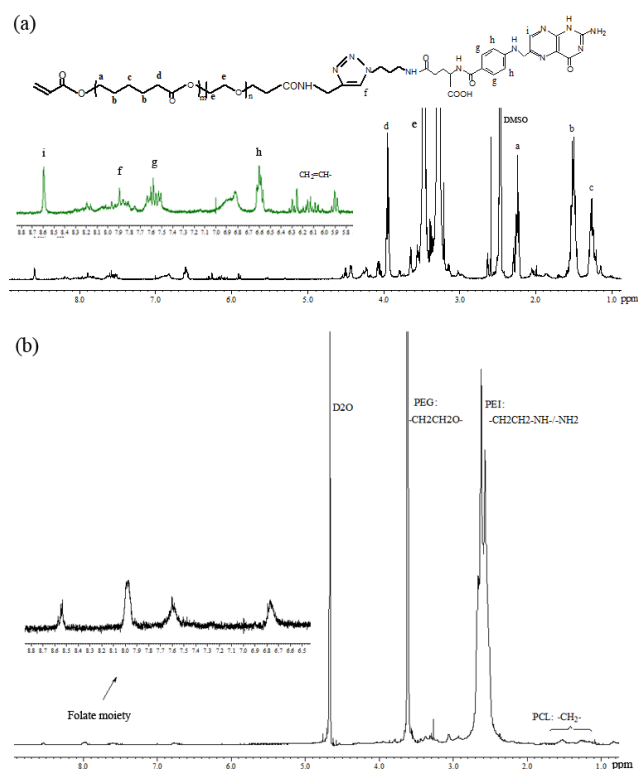


Figure 1.  $^1\text{H}$  NMR spectra of (a) Fol-PEG-b-PCL with terminal acrylate in  $d_6$ -DMSO and (b) PEI-g-PCL-b-PEG-Fol in  $\text{D}_2\text{O}$ .

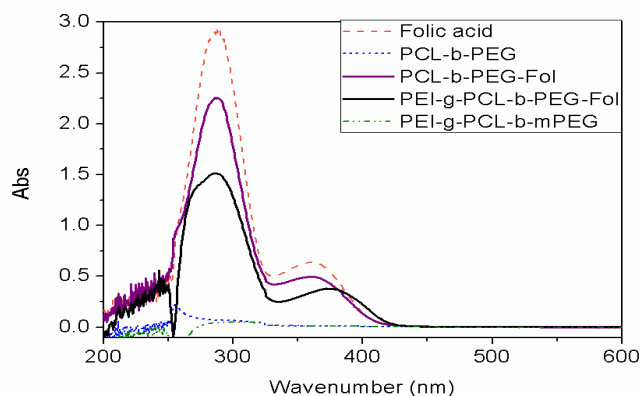


Figure 2. UV absorbance of folic acid solution, folate-conjugated copolymer solutions and control copolymer (without folate-conjugating) solutions in DMSO.

Finally, the acrylate-PCL-*b*-PEG-Fol was linked to *hy*-PEI via Michael addition between the active double bond and the amine group. Graft density of folate-conjugated branches could be predetermined by the feed ratio of acrylate-PCL-*b*-PEG-Fol to PEI. Figure 1 (b) showed the  $^1\text{H}$  NMR spectrum of the resulting copolymer PEI-*g*-PCL-*b*-PEG-Fol in  $\text{D}_2\text{O}$ , where the proton signals could be related to the PEI, PCL, PEG and folate moiety, respectively. Nevertheless, the peaks belonging to PCL segments were rather weak due to its hydrophobicity. The ratio of

integral  $-\text{CH}_2\text{CH}_2\text{O}-$  to integral  $-\text{CH}_2\text{CH}_2\text{NH}-$  was calculated to give the graft density, which coincided with the predetermined value. The compositions of synthesized PEI-*g*-PCL-*b*-PEG-Fol copolymers were summarized in Table 1. The folate content was obtained by the UV absorbance. Based on the previous investigations of PEI-*g*-PCL-*b*-PEG, those ternary copolymers with short PCL segment and low graft density showed potential as efficient gene delivery carriers, like *hy*PEI25k-(PCL570-mPEG5k)<sub>3</sub>.<sup>27</sup> Therefore, PEI-*g*-PCL-*b*-PEG-Fol copolymers with molecular weight of PCL at 570 and graft density of three was designed and synthesized successfully here for targeting purpose.

Table 1. Copolymers composition.

<sup>a</sup> Calculated from <sup>1</sup>H NMR spectra. <sup>b</sup> Calculated from the UV absorbance at 360 nm.

Sample name	Composition <sup>a</sup>	Folate content (mol/mg) <sup>b</sup>
<b>PCE3-F</b>	PEI25k-(PCL570-PEG3k-Fol) <sub>3</sub>	1.53 × 10 <sup>-8</sup>
<b>PCE3</b>	PEI25k-(PCL570-mPEG2k) <sub>3</sub>	/

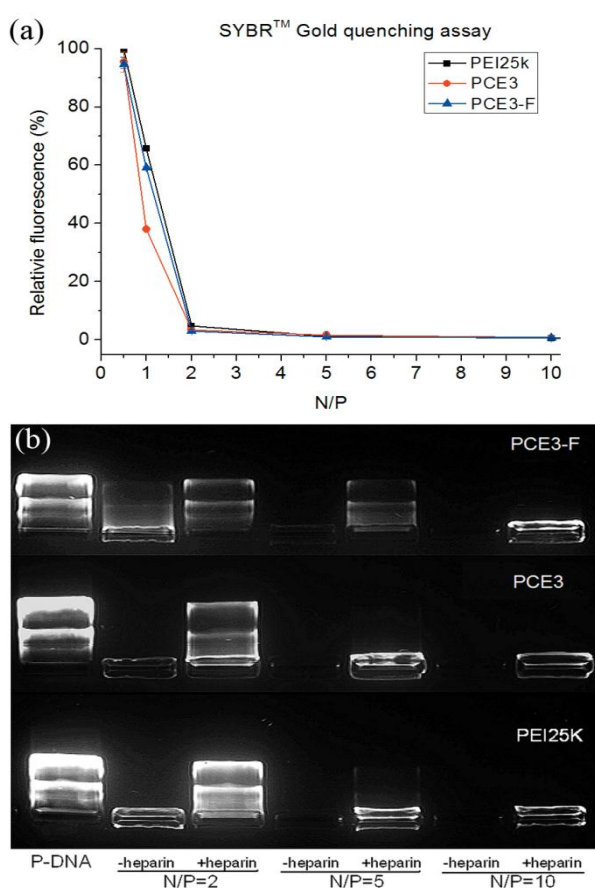


Figure 3. (a) Complexation of copolymers with pDNA measured by SYBR™ Gold quenching assay. (b) Agarose gel electrophoresis images of polyplexes at different N/P ratio treated with heparin.

### Complexation of PEI-g-PCL-*b*-PEG-Fol with DNA.

The DNA condensing capabilities of folate-conjugated copolymer (PCE3-F), non-folate-conjugated polymer (PCE3) and unmodified PEI 25kDa were investigated and compared by SYBR™ Gold quenching assay, as shown in Figure 3 (a). Generally, all the copolymers showed significant fluorescence quenching above N/P ratio of 2. This demonstrated that the copolymers could condense DNA efficiently above N/P ratio of 2. However, folate-conjugated copolymers exhibited less efficient nucleic acid-binding efficiency than the corresponding non-folate-conjugated PEI-g-PCL-*b*-PEG regarding the fluorescence quenching of polyplexes at N/P ratio of 1, indicating the weakening effect of folate ligands on the DNA-binding ability of copolymers to some extent. The binding affinity of copolymers with DNA originated from the electrostatic interaction between

negatively charged phosphates along nucleic acid and cationic PEI segments in copolymers. A sufficient condensation of DNA into polyplexes is a prerequisite to protect DNA from competing polyions, serum and enzyme, etc. To further investigate the stability of polyplexes, the heparin competition assay was performed by agarose gel electrophoresis. Figure 3 (b) showed that the polyplexes formed at N/P 2 could be dissociated to release DNA if treated with heparin (0.5 mg/mL). Stable polyplexes against heparin could be obtained when N/P ratio increased up to 5 for PCE3 and unmodified PEI 25kDa while till N/P 10 for the folate-conjugated PCE3-F copolymer. These results confirm the similar trends as the SYBR™ Gold quenching assay above, that the binding affinity between folate-conjugated copolymers and DNA is lower. An explanation could be that some folate ligands were buried inside the polyplexes during complexation due to the hydrophobic interaction between folate and PCL<sup>35</sup> or/and the hydrogen bonding interaction between folate and PEI. The interactions of buried folate ligands with positive PEI weakened electrostatic interactions between DNA and copolymers.



### Sizes and Zeta-potential of the Resulting Polyplexes.

The hydrodynamic diameters and zeta potentials of the polyplexes at different N/P ratios were shown in Figure 4. It presented a decreasing tendency on the hydrodynamic diameters with the increasing N/P ratio and an increasing one on the zeta-potentials. The size distribution was narrow ( $0.23 > PDI > 0.15$ ) for all polyplexes, except for PCE3-F at N/P 3 ( $PDI > 0.3$ ). At certain N/P ratio, the

PCE3-F/DNA polyplexes were found to have a somewhat larger sizes and lower zeta potentials than folate negative polyplexes (PCE3). This confirms the previous hypothesis that a few of folate ligands buried inside polyplexes would weaken the carrier-DNA interaction, resulting in looser and larger polyplexes. Generally, all polyplexes at N/P 10 were within the size range of 100-120 nm with no significant differences, which were selected for *in vitro* biological evaluations. Their zeta-potentials were positive in 35-40 mV.

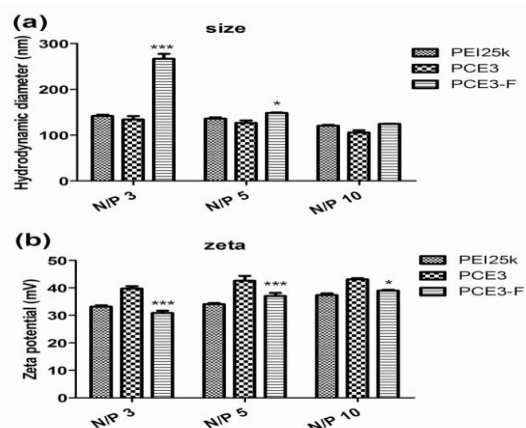


Figure 4. Hydrodynamic diameters and zeta-potentials of copolymer/pDNA polyplexes at different N/P ratio. (\*  $p < 0.05$ , \*\*\*  $p < 0.001$ )

### Biological Evaluations of PEI-g-PCL-b-PEG-Fol.

**Cytotoxicity.** The cytotoxicity of the ternary PEI-g-PCL-b-PEG copolymers with varying

PCL/PEG segment length and graft density was investigated in A549 cells and L929 cells previously.<sup>25, 27</sup> Reduction of the cytotoxicity was found to be a function of longer PCL and PEG block lengths as well as higher graft density due to the shielding of grafted neutral PCL-PEG segments to cationic PEI. This study focused on the folate-conjugated PEI-g-PCL-b-PEG copolymers for targeting purpose. The

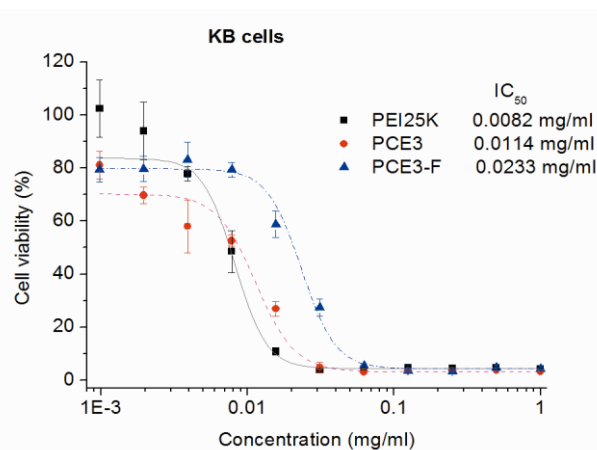


Figure 5. Cell viability of PEI-g-PCL-b-PEG-Fol and PEI-g-PCL-b-PEG copolymers in comparison with PEI 25kDa in KB cells.

cytotoxicity of PCE3-F copolymer was examined using FR-positive KB cells as shown in Figure 5, where the corresponding non-folate-conjugated copolymer PCE3 and unmodified PEI 25kDa were studied for comparison. Interestingly, the folate-conjugates PCE3-F exhibited less cytotoxicity than the non-folate-conjugates PCE3. The IC<sub>50</sub> value of PCE3-F was found to be 0.0233 mg/mL, about 2-fold to PCE3 and 3-fold to PEI 25kDa ( $p < 0.001$ ). The cytotoxicity of polycations like PEI was believed to result from their positive charge density. Some literature reported that FR-mediated targeting may increase the cytotoxicity of folate-conjugates due to greater interaction of materials with cells.<sup>36</sup> On the other hand, folate ligands could shield the positive charge of PEI, leading to a decreasing cytotoxicity of folate-conjugated copolymer. Then, the cytotoxicity of folate-conjugated PEI copolymer would rely on the competition of these two effects mentioned above. In this study, PCE3-F/DNA polyplexes were demonstrated with significant lower zeta potential than PCE3. Therefore, the shielding effect of folate moiety was predominating, resulting in a decreased cytotoxicity of PCE3-F than PCE3. There are also some literatures demonstrating no significant difference of the cytotoxicity between the folate-conjugated PEI-based copolymers and the non-folate ones.<sup>19, 22</sup>

**Cellular uptake of PEI-g-PCL-b-PEG-Fol/pDNA polyplexes.** To evaluate folate receptor

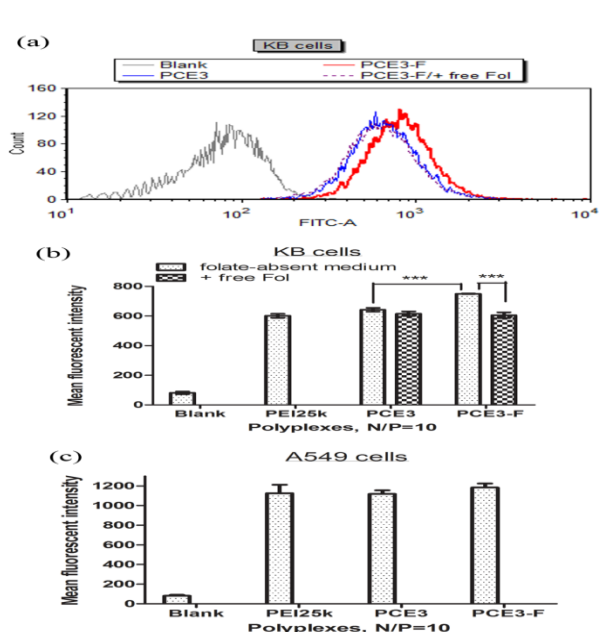


Figure 6. Quantitative determination of polyplexes cellular uptake by flow cytometry respectively in KB cells (a, b) and A549 cells (c), which are expressed as the mean fluorescent intensity of FITC-positive cells. (n=3, \*\*\*p < 0.001, using FITC-labeled polymer).

targeting efficiency, uptake of polyplexes was determined by flow cytometry. A panel of carrier materials (PCE3-F, PCE3 and PEI 25k) were fluorescently labeled using FITC and then used to prepare fluorescent polyplexes with pCMV-Luc and incubated with KB cells and A549 cells, respectively. As shown in Figure 6 (a), almost all the cells internalized fluorescent polyplexes after 4 h of incubation with FR-positive KB cells. Nevertheless, the amount of the internalized polyplexes, as determined from the mean fluorescent intensity [Figure 6 (b)], exhibited increased values for the

folate-conjugated polyplexes (PCE3-F) approximately 117% in comparison to folate-negative PCE3 polyplexes ( $p < 0.001$ ). Importantly, the competition experiments in the presence of free folate decreased the amount of the internalized PCE3-F/pDNA polyplexes down to 80% in KB cells ( $p < 0.001$ ). The control experiments performed in FR-negative A549 cells presented no distinct difference of the internalized polyplexes amount between PCE3-F and PCE3 [Figure 6 (c)]. Taken together, these results indicated significantly enhanced cell uptake of folate-conjugated polyplexes via FR-mediated endocytosis. Generally, reduction of cytotoxicity or zeta potential is usually linked to reduced cell uptake. Here, PEI-*g*-PCL-*b*-PEG-Fol copolymers with graft density 3 showed optimized cell uptake of pDNA polyplexes into cytosol and reduced cytotoxicity at the same time.

Furthermore, the FR-targeted gene delivery via PEI-*g*-PCL-*b*-PEG-Fol was confirmed using YOYO-1 labeled pDNA in KB cells. The results from flow cytometry (Figure S-5) were consistent with above that cell uptake of PCE3-F/pDNA polyplexes was higher than that of PCE3/pDNA polyplexes. The uptake and subcellular localizations of polyplexes inside KB cells were also examined by confocal laser scanning microscopy. In Figure 7, it could be visualized that the YOYO-1 labeled pDNA (Green) were distributed not only in the cytoplasm but also in the nuclei. The KB cells treated with PCE3-F/pDNA polyplexes showed brighter green fluorescence than those with PCE3/pDNA polyplexes, which again demonstrated increased uptake of polyplexes via PEI-*g*-PCL-*b*-PEG-Fol due to a specific FR interaction.

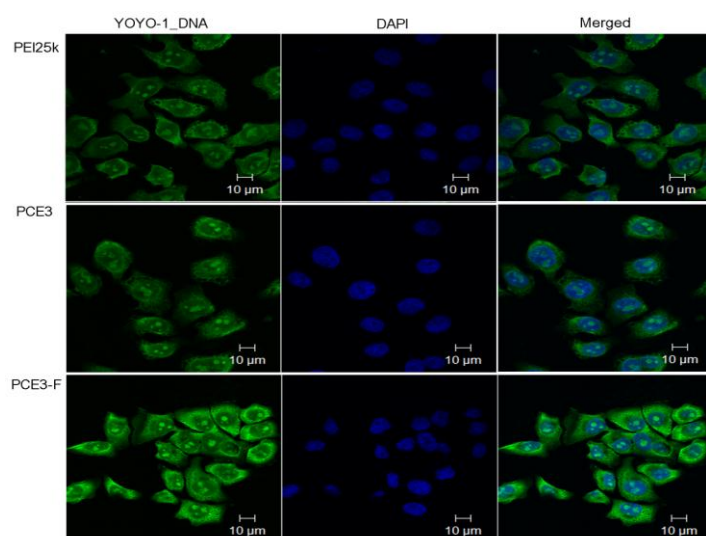


Figure 7. Confocal laser scanning microscopy of KB cells treated with polyplexes of PEI 25k, PEI-*g*-PCL-*b*-PEG and PEI-*g*-PCL-*b*-PEG-Fol. Cell nucleus were stained with DAPI (blue) and pDNA was labeled with YOYO-1 (green).

### ***In vitro* Gene Transfection.**

To further address targeted gene delivery effect of PEI-*g*-PCL-*b*-PEG-Fol, transfection efficiency of the PCE3-F/pDNA polyplexes at N/P ratio of 10 was tested in KB cells and compared to the corresponding PCE3/pDNA polyplexes. As shown in Figure 8, PEI-*g*-PCL-*b*-PEG-Fol (PCE3-F) displayed significant higher transfection efficiency approximately 14-fold than PCE3

( $p < 0.05$ ) in the folate-absent medium. Previous study have demonstrated that PEI<sub>25k</sub>-(PCL<sub>570</sub>-PEG<sub>5k</sub>)<sub>3</sub> is efficient with high transfection activities due to high buffer-capacity and zeta-potential.<sup>27</sup> Here, PCE3-F/pDNA polyplexes also exhibit high positive zeta potential.

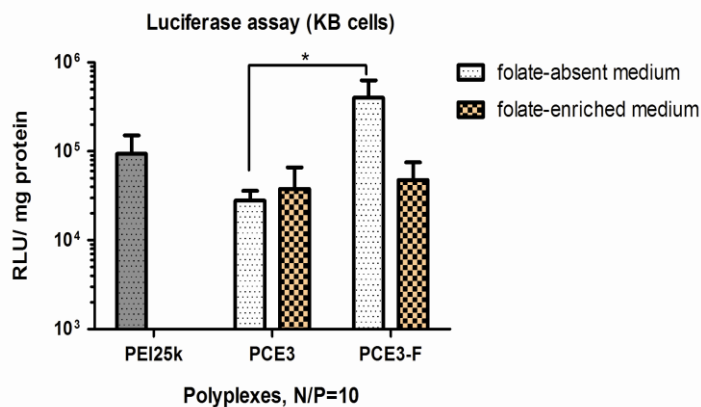


Figure 8. Transfection efficiency of PEI-*g*-PCL-*b*-PEG-Fol/pDNA polyplexes in comparison to PEI-*g*-PCL-*b*-PEG/pDNA polyplexes in KB cells at N/P ratio of 10, where PEI 25kDa/pDNA polyplexes as the control. (n=3, \* $p < 0.05$ )

Though it is a little lower than PCE3, the specific binding of folate-conjugated polyplexes due to folate/FR recognition enhanced cell uptake in KB cells as aforementioned. More importantly, the transfection efficiency of PCE3-F/pDNA polyplexes decreased to about 12% in the folate-enriched regular medium when the folate receptors on KB cell surface were occupied with free folate molecules. Consistently, the improvement of transfection efficiency for PEI-*g*-PCL-*b*-PEG-Fol could be attributed to the enhanced uptake of polyplexes by folate-mediated targeting to folate-receptors on the cell surface. These results are consistent with the previous reports showing the similar increase of transfection efficiency for folate-conjugated PEI-polyplexes in FR-positive cells, including Hela cells<sup>22</sup>, B16 cells<sup>23</sup> and KB cells<sup>19</sup>. Their transfection efficiency could additionally be blocked by excess free folic acid. Although cell type as well as copolymer structure account for difference in absolute values of transfection efficiency, here PCE3-F polyplexes exhibited enhanced gene transfection than PCE3 in KB cells, which was comparable with PEI 25kDa. Hence, the conjugation of folate molecules indeed endowed PEI-*g*-PCL-*b*-PEG-Fol to be a targeted gene vector for FR-positive cells.

## 5.5 Conclusions

Folate-conjugated ternary copolymer PEI-*g*-PCL-*b*-PEG-Fol was successfully synthesized by click cyclo-addition of azido-folate with heterobifunctional acrylate-PCL-*b*-PEG-alkyne, followed by Michael addition with PEI, for targeted gene delivery. Lower cytotoxicity was observed for PEI-*g*-PCL-*b*-PEG-Fol than PEI-*g*-PCL-*b*-PEG, which was much lower than unmodified PEI 25kDa. The cellular uptake of polyplexes was enhanced by PEI-*g*-PCL-*b*-PEG-Fol in FR over-expressing KB cells compared with those by PEI-*g*-PCL-*b*-PEG. Importantly, this enhancement was inhibited by free folic acid, while did not appear in FR-negative A549 cells. All these suggested the specific cell uptake of PEI-*g*-PCL-*b*-PEG-Fol/pDNA polyplexes via folate receptor-mediated endocytosis. Consequently, PEI-*g*-PCL-*b*-PEG-Fol/pDNA polyplexes revealed higher transfection than PEI-*g*-PCL-*b*-PEG/pDNA. Here, PEI-*g*-PCL-*b*-PEG-Fol is a novel kind of ternary copolymers with amphiphilicity, cationic property and folate-ligands, which endows them multifunctional prospect to co-delivery both gene and hydrophobic chemotherapeutic drug to target tumor tissue. Nevertheless, continued efforts still need to be considered to reduce nonspecific uptake and increase transfection efficiency further. Additional studies on gene transfection *in vivo* and utilizing these described folate-conjugated copolymers for targeted siRNA delivery are in proceeding.

**5.6 Acknowledgment.** Financial support of Dr. Liu, L. by the Alexander von Humboldt Foundation is gratefully acknowledged.

**5.7 Supporting Information Available.** Details of characterization of intermediate products, standard line of UV absorbance of folate solution and FACS data of polyplexes with YOYO-1 labeled pDNA in KB cells. This material is available free of charge via the Internet at <http://pubs.acs.org>.

## 5.8 REFERENCES.

- (1) Olefsky, J. M. (2000) Diabetes: Gene therapy for rats and mice. *Nature* 408, 420-421.

- (2) Merdan, T., Kopecek, J., and Kissel, T. (2002) Prospects for cationic polymers in gene and oligonucleotide therapy against cancer. *Adv. Drug Delivery Rev.* 54, 715-758.
- (3) Wagner, A. M., Schoeberlein, A., and Surbek, D. (2009) Fetal gene therapy: Opportunities and risks. *Adv. Drug Delivery Rev.* 61, 813-821.
- (4) Mintzer, M. A., and Simanek, E. E. (2008) Nonviral Vectors for Gene Delivery. *Chem. Rev.* 109, 259-302.
- (5) Pack, D. W., Hoffman, A. S., Pun, S., and Stayton, P. S. (2005) Design and development of polymers for gene delivery. *Nat. Rev. Drug Discov.* 4, 581-593.
- (6) Boussif, O., Lezoualc'h, F., Zanta, M. A., Mergny, M. D., Scherman, D., Demeneix, B., and Behr, J. P. (1995) A versatile vector for gene and oligonucleotide transfer into cells in culture and in vivo: polyethylenimine. *Proc. Natl. Acad. Sci.* 92, 7297-7301.
- (7) Behr, J.-P. (1997) The Proton Sponge: a Trick to Enter Cells the Viruses Did Not Exploit. *CHIMIA Int. J. Chem.* 51, 34-36.
- (8) Petersen, H., Fechner, P. M., Fischer, D., and Kissel, T. (2002) Synthesis, Characterization, and Biocompatibility of Polyethylenimine-graft-poly(ethylene glycol) Block Copolymers. *Macromolecules* 35, 6867-6874.
- (9) Petersen, H., Fechner, P. M., Martin, A. L., Kunath, K., Stolnik, S., Roberts, C. J., Fischer, D., Davies, M. C., and Kissel, T. (2002) Polyethylenimine-graft-Poly(ethylene glycol) Copolymers: Influence of Copolymer Block Structure on DNA Complexation and Biological Activities as Gene Delivery System. *Bioconjugate Chem.* 13, 845-854.
- (10) Lee, M., Kim, M., Jang, Y., Lee, K., Kim, T., Kim, S., Park, T., Kim, H., and Jeong, J. (2011) Polyethylenimine-g-poly(lactic-co-glycolic acid) as non-toxic micelle-type carrier for gene delivery. *Macromol. Res.* 19, 688-693.
- (11) Pun, S. H., Bellocq, N. C., Liu, A., Jensen, G., Machermer, T., Quijano, E., Schlupe, T., Wen, S., Engler, H., Heidel, J., and Davis, M. E. (2004) Cyclodextrin-Modified Polyethylenimine Polymers for Gene Delivery. *Bioconjugate Chem.* 15, 831-840.
- (12) Dachs, G., Dougherty, G., Stratford, I., and Chaplin, D. (1997) Targeting gene therapy to cancer: a review. *Oncol. Res.* 9, 313-25.
- (13) Salazar, M., and Ratnam, M. (2007) The folate receptor: What does it promise in tissue-targeted therapeutics? *Cancer Metast. Rev.* 26, 141-152.
- (14) Low, P. S., and Kularatne, S. A. (2009) Folate-targeted therapeutic and imaging agents for cancer. *Curr. Opin. Chem. Biol.* 13, 256-262.
- (15) Xia, W., and Low, P. S. (2010) Folate-Targeted Therapies for Cancer. *J. Med. Chem.* 53, 6811-6824.
- (16) Bennis, J. M., Maheshwari, A., Furgeson, D. Y., Mahato, R. I., and Kim, S. W. (2001) Folate-PEG-Folate-Graft-Polyethylenimine-Based Gene Delivery. *J. Drug Target.* 9, 123-139.
- (17) Liang, B., He, M. L., Xiao, Z. P., Li, Y., Chan, C. Y., Kung, H. F., Shuai, X. T., and Peng, Y. (2008) Synthesis and characterization of folate-PEG-grafted-hyperbranched-PEI for tumor-targeted gene delivery. *Biochem. Biophys. Res. Commun.* 367, 874-880.

- (18) Liang, B., He, M.-L., Chan, C.-y., Chen, Y.-c., Li, X.-P., Li, Y., Zheng, D., Lin, M. C., Kung, H.-F., Shuai, X.-T., and Peng, Y. (2009) The use of folate-PEG-grafted-hybranched-PEI nonviral vector for the inhibition of glioma growth in the rat. *Biomaterials* 30, 4014-4020.
- (19) Arote, R. B., Hwang, S. K., Lim, H. T., Kim, T. H., Jere, D., Jiang, H. L., Kim, Y. K., Cho, M. H., and Cho, C. S. (2010) The therapeutic efficiency of FP-PEA/TAM67 gene complexes via folate receptor-mediated endocytosis in a xenograft mice model. *Biomaterials* 31, 2435-2445.
- (20) He, M. L. (2009) The use of folate-PEG-grafted-hybranched-PEI nonviral vector for the inhibition of glioma growth in the rat. *Int. J. Mol. Med.* 24, 168.
- (21) Hwa Kim, S., Hoon Jeong, J., Chul Cho, K., Wan Kim, S., and Gwan Park, T. (2005) Target-specific gene silencing by siRNA plasmid DNA complexed with folate-modified poly(ethylenimine). *J. Controlled Release* 104, 223-232.
- (22) Cheng, H., Zhu, J. L., Zeng, X., Jing, Y., Zhang, X. Z., and Zhuo, R. X. (2009) Targeted Gene Delivery Mediated by Folate-polyethylenimine-block-poly(ethylene glycol) with Receptor Selectivity. *Bioconjugate Chemistry* 20, 481-487.
- (23) Yao, H., Ng, S. S., Tucker, W. O., Tsang, Y. K. T., Man, K., Wang, X. M., Chow, B. K. C., Kung, H. F., Tang, G. P., and Lin, M. C. (2009) The gene transfection efficiency of a folate-PEI600-cyclodextrin nanopolymer. *Biomaterials* 30, 5793-5803.
- (24) Shuai, X., Merdan, T., Unger, F., Wittmar, M., and Kissel, T. (2003) Novel Biodegradable Ternary Copolymers hy-PEI-g-PCL-b-PEG: Synthesis, Characterization, and Potential as Efficient Nonviral Gene Delivery Vectors. *Macromolecules* 36, 5751-5759.
- (25) Liu, Y., Nguyen, J., Steele, T., Merkel, O., and Kissel, T. (2009) A new synthesis method and degradation of hyper-branched polyethylenimine grafted polycaprolactone block mono-methoxyl poly(ethylene glycol) copolymers (hy-PEI-g-PCL-b-mPEG) as potential DNA delivery vectors. *Polymer* 50, 3895-3904.
- (26) Liu, Y., Samsonova, O., Sproat, B., Merkel, O., and Kissel, T. (2011) Biophysical characterization of hyper-branched polyethylenimine-graft-polycaprolactone-block-mono-methoxyl-poly(ethylene glycol) copolymers (hy-PEI-PCL-mPEG) for siRNA delivery. *J. Controlled Release* 153, 262-8.
- (27) Zheng, M., Liu, Y., Samsonova, O., Endres, T., Merkel, O., and Kissel, T. (2011) Amphiphilic and biodegradable hy-PEI-g-PCL-b-PEG copolymers efficiently mediate transgene expression depending on their graft density. *Int. J. Pharm. In Press, Corrected Proof*.
- (28) Lee, S. M., Chen, H. M., O'Halloran, T. V., and Nguyen, S. T. (2009) "Clickable" Polymer-Caged Nanobins as a Modular Drug Delivery Platform. *J. Am. Chem. Soc.* 131, 9311-9320.
- (29) Storey, R. F., and Sherman, J. W. (2002) Kinetics and Mechanism of the Stannous Octoate-Catalyzed Bulk Polymerization of Caprolactone. *Macromolecules* 35, 1504-1512.
- (30) Merkel, O. M., Mintzer, M. A., Librizzi, D., Samsonova, O., Dicke, T., Sproat, B., Garn, H., Barth, P. J., Simanek, E. E., and Kissel, T. (2010) Triazine Dendrimers as Nonviral Vectors for in Vitro and in Vivo RNAi: The Effects of Peripheral Groups and Core Structure on Biological Activity. *Mol. Pharmaceutics* 7, 969-983.
- (31) Jiang, H. L., Xu, C. X., Kim, Y. K., Arote, R., Jere, D., Lim, H. T., Cho, M. H., and Cho, C. S. (2009) The suppression of lung tumorigenesis by aerosol-delivered

- folate-chitosan-graft-polyethylenimine/Akt1 shRNA complexes through the Akt signaling pathway. *Biomaterials* 30, 5844-5852.
- (32) Parrish, B., and Emrick, T. (2006) Soluble Camptothecin Derivatives Prepared by Click Cycloaddition Chemistry on Functional Aliphatic Polyesters. *Bioconjugate Chem.* 18, 263-267.
- (33) Mindt, T. L., Muller, C., Stuker, F., Salazar, J. F., Hohn, A., Mueggler, T., Rudin, M., and Schibli, R. (2009) A "Click Chemistry" Approach to the Efficient Synthesis of Multiple Imaging Probes Derived from a Single Precursor. *Bioconjugate Chemistry* 20, 1940-1949.
- (34) van Dijk, M., Rijkers, D. T. S., Liskamp, R. M. J., van Nostrum, C. F., and Hennink, W. E. (2009) Synthesis and Applications of Biomedical and Pharmaceutical Polymers via Click Chemistry Methodologies. *Bioconjugate Chem.* 20, 2001-2016.
- (35) Valencia, P. M., Hanewich-Hollatz, M. H., Gao, W., Karim, F., Langer, R., Karnik, R., and Farokhzad, O. C. (2011) Effects of ligands with different water solubilities on self-assembly and properties of targeted nanoparticles. *Biomaterials* 32, 6226-6233.
- (36) Zheng, Y., Cai, Z., Song, X., Yu, B., Bi, Y., Chen, Q., Zhao, D., Xu, J., and Hou, S. (2009) Receptor mediated gene delivery by folate conjugated N-trimethyl chitosan in vitro. *Int. J. Pharm.* 382, 262-269.



## Chapter 6

# MOLECULAR MODELING AND IN VIVO IMAGING CAN IDENTIFY SUCCESSFUL HYPERFLEXIBLE TRIAZINE DENDRIMER-BASED SIRNA DELIVERY SYSTEMS

Published in The Journal of Control Release 2011, 153 (1), 23-33.

**Olivia M. Merkel<sup>a1\*</sup>, Mengyao Zheng<sup>a1</sup>, Meredith A. Mintzer<sup>b</sup>, Giovanni M. Pavan<sup>c</sup>, Damiano Librizzi<sup>d</sup>, Marek Maly<sup>c,e</sup>, Helmut H öffken<sup>d</sup>, Andrea Danani<sup>c</sup>, Eric E. Simanek<sup>f</sup>, and Thomas Kissel<sup>a</sup>**

<sup>1</sup>Both authors contributed equally to this work

### Author contributions

T. K. and E. E. S. guided and directed the research and directed the measurements. M. Z. carried out the measurement of size and zetapotential, CLSM, *in vitro* knockdown experiment. M. A. M. synthesized and characterized the polymers. M. Z. and O. M. M. analysed the experimental data.

## 6.1 Abstract

The aim of this study was to identify suitable siRNA delivery systems based on hyperflexible generation 2-4 triazine dendrimers by correlating physico-chemical and biological *in vitro* and *in vivo* properties of the complexes with their thermodynamic interaction features simulated by molecular modeling. The siRNA binding properties of the dendrimers in comparison to PEI 25 kDa were simulated, binding and stability were measured in SYBR Gold assays, hydrodynamic diameters and zeta potentials were investigated, and cytotoxicity was quantified. These parameters were paralleled with cellular uptake of the complexes and their ability to mediate RNAi. The radiolabeled complexes were administered intravenously, and their pharmacokinetic profiles and biodistribution were assessed invasively and non-invasively. All flexible triazine dendrimers formed thermodynamically more stable complexes than PEI. While PEI and generation 4 dendrimer interacted more superficially with siRNA, generation 2 and 3 virtually coalesced with siRNA. These dendriplexes were therefore more efficiently charge-neutralized than PEI complexes, reducing agglomeration. This was confirmed by results of hydrodynamic diameters (72.0 nm – 153.5 nm) and zeta potentials (4.9 mV – 21.8 mV in 10 mM HEPES) of the dendriplexes in comparison to PEI complexes (312.8 nm – 480.0 nm and 13.7 mV – 17.4 mV in 10 mM HEPES). All dendrimers, even generation 3 and 4, were less toxic than PEI, all dendriplexes were efficiently endocytosed and showed significant and specific luciferase knockdown in HeLa/Luc cells. Scintillation counting confirmed that the generation 2 triazine complexes showed more than twofold prolonged circulation times as a result of their good thermodynamic stability, whereas generation 3 complexes dissociated *in vivo*, and generation 4 complexes were captured by the reticulo-endothelial system due to their increased surface charge. Since molecular modeling helped to understand experimental parameters based on the dendrimers' structural properties and molecular imaging non-invasively predicted the *in vivo* fate of the complexes, both techniques can efficiently support the rapid development of safe and efficient siRNA formulations that are stable *in vivo*.

**Keywords:** Triazine dendrimers, RNA interference, molecular modeling, structure function relationship, physico-chemical characterization, *in vivo*, biodistribution, pharmacokinetics, SPECT imaging

## 6.2 Introduction

Dendrimers are increasingly employed for siRNA delivery. While PAMAM and its derivatives are most widely used [1], polypropylenimine (PPI) [2], dendritic poly-L-lysine (PLL) [3] and newer classes such as carbosilane dendrimers [4] and triazine dendrimers [5] are gaining more importance in the field of non-viral siRNA delivery. About 50 reports of dendrimer-mediated siRNA delivery can be found in the literature to date whereas only six studies describe *in vivo* results [2, 3, 5-8]. This can be understood as a consequence of the recent use of dendrimers for siRNA delivery needing further optimization in terms of efficiency versus toxicity to allow *in vivo* administration. Currently, the most relevant obstacle was seen in several studies where low generations of dendrimers were not able to condense siRNA into uniformly small complexes [9-11]. The use of higher generations such as 6 and 7 [1, 3, 9, 11-14], however, is often accompanied by an increase in toxicity [15]. Therefore, many structural modifications, e.g. carboxylate-terminated [16], acetylated [17], internally cationic and hydroxyl-terminated PAMAM dendrimers [18] were synthesized for enhanced biocompatibility, that, however, exhibited decreased *in vitro* efficiency [17, 18]. The lack of *in vitro* knockdown efficiency of PAMAM has been attributed to incomplete endosomal release of the siRNA [19] and nuclear localization of oligonucleotides [20]. In an earlier study, it was shown that endosomal release of siRNA can be modulated by introduction of short lipophilic C6-groups in the periphery of triazine dendrimers [5]. The alkylated generation 2 “rigid core” dendrimer efficiently mediating *in vitro* gene silencing, however, accumulated strongly in the lung after intravenous injection although hydrodynamic diameters of the complexes with siRNA were 103 nm as measured in buffer [5]. Since complex formation with the generation 3 rigid dendrimer did not lead to smaller dendriplexes (178 nm) and since dendrimer G3-1 had affected cell viability significantly stronger than G2-1 [21], this study focuses on a new panel of “hyperflexible” triazine dendrimers. Flexible triethanolamine core PAMAM dendriplexes of generation 7 were reported to exhibit almost no cytotoxicity in MTT and LDH assays [13], indicating that a flexible core may reduce the toxicity of higher generation dendrimers. Similarly, a flexible generation 2 triazine dendrimer F2-1 was previously shown to cause reduced hemolysis than G1-1, G2-1, and G3-1 rigid core analogues [21]. However, F2-1 was found to present a “collapsed” topology, leading to less interaction with siRNA than possible with the dendrimers that were actually expected to be more rigid [22] and formation of loosely associated large

agglomerates of 286 nm in size [5]. In an approach to enhance the interaction with and condensation of siRNA, new hyperflexible dendrimers of generation 2, 3, and 4 were synthesized and characterized in this study concerning computed siRNA binding characteristics. The results obtained from *in silico* simulations were compared with experimental physico-chemical parameters such as siRNA complexation, complex stability, size, and zeta potentials. Since these properties are expected to determine siRNA packaging, dendriplex endocytosis, unpackaging, stability in the blood stream and thus the RNAi efficiency of siRNA formulations [23], it was investigated if *in silico* results were able to predict the *in vitro* and *in vivo* performance of the dendriplexes and if radioactive *in vivo* imaging could support to identify efficient siRNA delivery systems.

### 6.3 Experimental Section

**Materials.** Poly(ethylene imine) (Polymin™, 25 kDa) was a gift from BASF (Ludwigshafen, Germany). Lipofectamine™2000 (LF) was bought from Invitrogen (Karlsruhe, Germany), Beetle Luciferin, and heparin sodium salt from Sigma-Aldrich Laborchemikalien GmbH (Seelze, Germany). 2'-O-Methylated 25/27mer DsiRNA targeting firefly luciferase (FLuc, sense: 5'-pGGUUCUGGAACAAUUGCUUUUAdCdA, antisense: 3'-mGmAmCCmAAmGGmACmCUmUGmUUmAAmCGAAAUGU), negative control sequence (NegCon, sense: 5'-pCGUAAUCGCGUAUAAUACGCGUdAdT, antisense: 3'-mCmAmGCmAAmUUmAGmCGmCmUAmUUmAUGCGCAUAp), TYE546- and 5'-sense strand C6-amine modified DsiRNA were obtained from Integrated DNA Technologies (IDT, Leuven, Belgium). Balb/c mice (6 weeks old) were bought from Harlan Laboratories (Horst, The Netherlands). The chelator 2-(4-isothiocyanatobenzyl)-diethylenetriaminepentaacetic acid (p-SCN-Bn-DTPA) was purchased from Macrocyclics (Dallas, TX, USA), SYBR® Gold from Invitrogen (Karlsruhe, Germany), and all chemicals used for synthesis were obtained from Sigma-Aldrich (St. Louis, MO).

**Synthesis of new triazine dendrimers.** The hyperflexible triazine dendrimers **F2-2**, **F3**, and **F4-2** used in this study were synthesized following a previously described divergent approach [21, 24]. The final products and all intermediate structures were characterized by <sup>1</sup>H and <sup>13</sup>C NMR spectroscopy, and mass spectrometry, as shown in the Supplementary data. For comparison,

generations 2, 3, and 4 were synthesized of which generation 2 and 4 bear the same periphery (Figure 1), previously designated as periphery number 2 [24].

**Molecular modeling.** The model for Dicer Substrate siRNA was constructed with the NAB module within the AMBER 11 suite of programs [25]. Since the study of multivalent molecular recognition that characterizes the complexation was subject of this study, the binding between siRNA and dendrimers in a 1:1 ratio was modeled according to a validated strategy previously reported for the binding of dendrons and dendrimers with DNA [26, 27] and siRNA [28]. The structures of F2-2, F3 and F4-2 were composed of different residues according to previous studies on similar dendrimers [22]. The model of random branched 25kDa PEI was created and pre-optimized using the Materials Studio (MS) software package (Accelrys). The total charges of F2-2, F3, F4-2 and PEI are +12, +24, +48 and +98, respectively, at pH 7.4 [29]. Each of the non-standard residues that compose the dendrimers was parameterized with the *antechamber* module of AMBER 11 following a well validated procedure previously adopted [31].

**Molecular dynamic simulations.** All simulations and data analyses were performed with the AMBER 11 suite of programs (*sander.MPI* and *pmemd.cuda* modules) [25]. The dendrimers were solvated in a TIP3P water box [30], minimized and then equilibrated by running 10 nanoseconds NPT molecular dynamics simulations, as described previously [22] to obtain a reliable configuration for PEI, F2-2, F3 and F4-2 in solution (Figure S1). The water molecules and counter ions were removed, and the polycations were placed in close proximity to the major groove of DsiRNA. The four complexes were re-solvated, the resulting molecular systems were minimized [22] and equilibrated for 20 ns in NPT periodic boundary condition at 300 K and 1 atm using a time step of 2 fs, the Langevin thermostat, and a 10 Å cut-off. To treat long-range electrostatic effects, the particle mesh Ewald (PME) approach was adopted [31], and the SHAKE algorithm was used to constrain all bonds involving hydrogen atoms. Each of the molecular dynamics runs were carried out using *parm99* all-atom force field [32] with NVIDIA Tesla 2050 GPU cards. The free energies of binding ( $G_{\text{bind}}$ ,  $H_{\text{bind}}$  and  $T S_{\text{bind}}$ ) were calculated according to the MM-PBSA approach [33] and the normal-mode analysis [34] on 100 MD frames taken from the equilibrated

MD trajectories according to previous studies on the interactions between dendrimers and nucleic acids [22, 28].

**Dendriplex formation.** Dendriplexes were formed as previously described by adding 25  $\mu\text{l}$  of a calculated concentration of dendrimer to an equal volume of 2  $\mu\text{M}$  siRNA followed by vigorous pipetting [5]. Both siRNA and dendrimers were diluted with an isotonic solution of 5% glucose unless otherwise described. The appropriate amount and “protonable unit” of each dendrimer to afford a certain N/P ratio, which is the excess of polymer amines (N) over siRNA phosphates (P), was calculated as previously described [21]. Polyplexes with PEI 25 kDa were formed as described above, and lipoplexes with LF with 1  $\mu\text{l}$  per 20 pmol were prepared as recommended by the manufacturer.

**SYBR Gold<sup>®</sup> Assay.** The ability of the three dendrimers to bind and protect siRNA was studied as previously reported and compared with PEI 25kDa [5]. Briefly, complexes of 1  $\mu\text{g}$  siRNA were prepared at different N/P ratios, incubated for 20 minutes before 50  $\mu\text{l}$  of a 1x SYBR<sup>®</sup> Gold solution was added and incubated for another 10 minutes in the dark. Free or accessible siRNA was quantified using a SAFIRE II fluorescence plate reader (Tecan Group Ltd, Männedorf, Switzerland) at 495 nm excitation and 537 nm emission wavelengths. The results are given as mean relative fluorescence intensity values (n=3) +/- the standard deviation (SD), where intercalation of free siRNA represents 100 % fluorescence, and non-intercalating SYBR<sup>®</sup> Gold in buffer represents 0 % remaining fluorescence.

**Heparin Competition Assay.** The stability of the dendriplexes against competing polyanions, such as the model molecule heparin, was studied as previously reported [5]. Briefly, dendriplexes were formed at N/P=5, incubated with 50  $\mu\text{l}$  of a 1x SYBR<sup>®</sup> Gold solution, and treated with increasing amounts of heparin for 20 minutes. Fluorescence was quantified as described above. Results are given as mean relative fluorescence intensity values (n=3) +/- SD, where free siRNA represents 100 % fluorescence, and SYBR<sup>®</sup> Gold in buffer represents 0 % fluorescence.

**Dynamic Light Scattering and Zeta Potential Analysis.** Dendriplexes of the various generations of hyperflexible triazine dendrimers and siRNA were characterized concerning their hydrodynamic diameters and zeta potentials, whereas PEI 25kDa served as control. Dendriplexes and PEI polyplexes were formed as described above in 5 % glucose, HEPES-buffered glucose (HBG: 5% glucose, 10 mM HEPES, pH 7.4) or 10 mM HEPES buffer at increasing N/P ratios and measured as previously described in a disposable low volume UVette (Eppendorf, Wesseling-Berzdorf, Germany) using a Zetasizer Nano ZS (Malvern, Herrenberg, Germany) [5]. Zeta potentials were determined by laser Doppler anemometry (LDA) after diluting the samples with 750  $\mu$ l of the equivalent solvent to a final volume of 800  $\mu$ l and transferring the suspensions into a green zeta cuvette (Malvern, Herrenberg, Germany). Results are given as mean values (n=3) +/- SD.

**Cell Culture.** HeLa cells stably expressing luciferase (HeLa/Luc) [35] were maintained at 100  $\mu$ g/ml hygromycin B in DMEM high glucose (PAA Laboratories, Cölbe, Germany) supplemented with 10 % fetal bovine serum (Cytogen, Sinn, Germany) in a humidified atmosphere with 5 % CO<sub>2</sub> at 37 °C, and seeded for experiments in antibiotics-free medium. L929 cells were cultured in antibiotics-free DMEM high glucose (PAA Laboratories, Cölbe, Germany) supplemented with 10 % fetal bovine serum (Cytogen, Sinn, Germany).

**Confocal laser scanning microscopy (CLSM).** As previously described, uptake and subcellular distribution of dendriplexes was investigated by confocal microscopy [5]. Briefly, HeLa/Luc cells were plated on 16-chamber slides and transfected 24 h later at N/P ratios of 10 and 20 with 25 pmol TYE-546-labeled siRNA per chamber in a total volume of 250  $\mu$ l. Cells transfected with free siRNA or Lipofectamine™2000 were used as negative and positive controls, respectively. After 4 h of incubation, cells were washed, fixed with 4% paraformaldehyde, counterstained with 4',6-diamidino-2-phenylindole (DAPI) (Molecular Probes, Invitrogen, Karlsruhe, Germany), and embedded with FluorSave (Calbiochem, Merck Biosciences, Darmstadt, Germany). For confocal microscopy on a Zeiss Axiovert 100 M microscope and a Zeiss LSM 510 scanning device (Zeiss, Oberkochen, Germany), lasers and filter settings were chosen as previously described [5].

**Transfection efficiency.** The ability of the different generation dendrimers to mediate RNA interference *in vitro* was quantified by luciferase knockdown in HeLa/Luc cells as previously reported [5]. Briefly, cells were seeded at a density of 15,000 cells per well in 48-well-plates and treated with dendriplexes of 50 pmol siRNA (siFLuc or siNegCon) and different N/P ratios 24 h after seeding. As positive controls, transfections were performed with Lipofectamine™2000. The medium was changed 4 hours post transfection, cells were incubated for another 44 h before they were washed with PBS buffer, lysed with CCLR (Promega) and assayed for luciferase expression on a BMG luminometer plate reader (BMG Labtech, Offenburg, Germany) [5]. Results are given as mean values (n=4) +/- SD.

**Radiolabeling and Purification.** Pharmacokinetics and biodistribution after i.v. injection were investigated with radiolabeled siRNA administered freely or as dendriplexes. Polyplexes formed with PEI 25kDa were administered as control. siRNA was labeled and purified as previously described [35, 36]. Briefly, amine-modified siRNA was reacted with p-Bn-SCN-DTPA at pH 8.5 for 3 h before it was precipitated in 10% sodium acetate and 70% ethanol overnight. After centrifugation for 5 min at 12,000 g, DTPA-coupled siRNA was dissolved in RNase free water, annealed in presence of <sup>111</sup>InCl<sub>3</sub> (Covidien Deutschland GmbH, Neustadt a.d. Donau, Germany) for 2 min at 94 °C, incubated for 30 min at room temperature and purified from free <sup>111</sup>InCl<sub>3</sub> by size exclusion chromatography (SEC) on PD-10 Sephadex G25 (GE Healthcare, Freiburg, Germany) and RNeasy spin column purification as described earlier [35].

### **In vivo Imaging, Pharmacokinetics and Biodistribution**

Circulation times and distribution within the body were determined as previously described [5]. Groups of 5 BALB/c mice were anesthetized intraperitoneally and injected with dendriplexes containing 35 µg of siRNA and the corresponding amount of dendrimer at N/P 5. Control animals received either free siRNA or PEI25kDa/siRNA polyplexes which were prepared and labeled as previously described [35]. Pharmacokinetics were assessed by retro-orbitally withdrawing blood samples, and biodistribution was recorded in three-dimensional SPECT and planar gamma camera images 2 h after injection using a Siemens e.cam gamma camera (Siemens AG, Erlangen, Germany) equipped with a custom built multiplexing multipinhole collimator and compared to



results of scintillation counting of dissected organs measured using a Gamma Counter Packard 5005 (Packard Instruments, Meriden, CT) [35].

**Statistics.** All analytical assays were conducted in replicates of three or four, as indicated and *in vivo* experiments included 5 animals per group. Results are given as mean values +/- standard deviation (SD). Two way ANOVA and statistical evaluations were performed using Graph Pad Prism 4.03 (Graph Pad Software, La Jolla, USA).

## 6.4 Results and Discussion

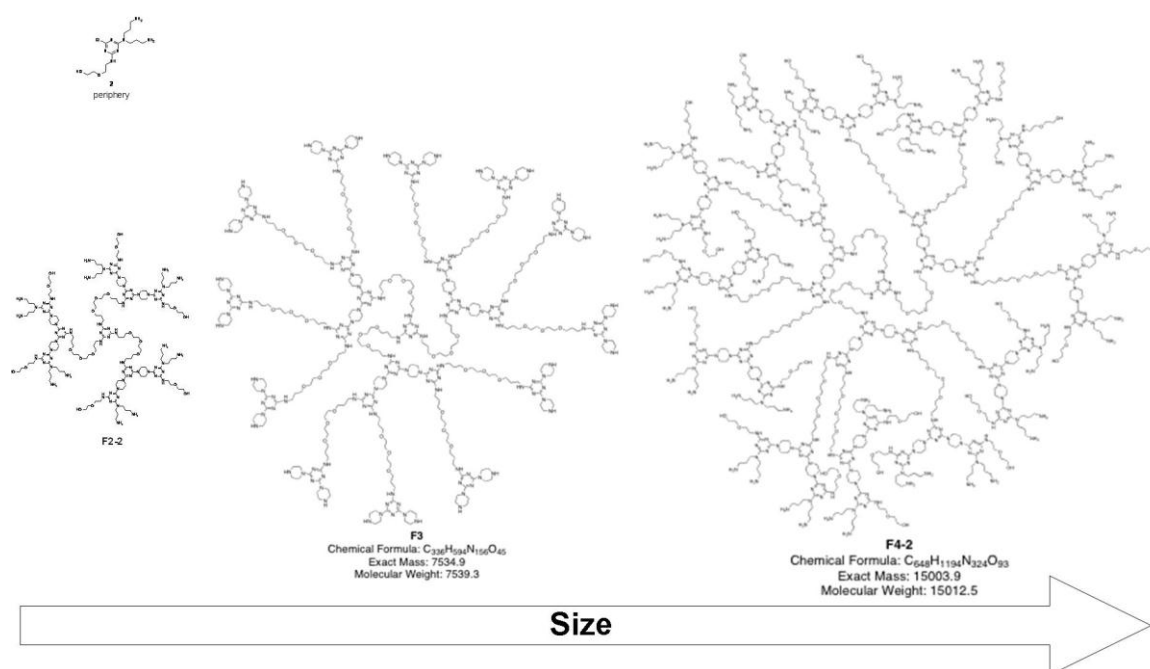


Figure 1. Structures of hyperflexible core triazine dendrimers F of generation number 2, 3 and 4. The monochlorotriazine from which the peripheral group 2 for generation 2 and 4 was obtained carries one hydroxyl groups and two amines.

**Nomenclature, Synthesis and Design Criteria of the Synthesized Dendrimers.** The nomenclature of the new dendrimers described in this manuscript was in line with previously described structures [21, 24] with respect to their generation, flexible core structure and surface group functionalities as shown in Figure 1. Previous investigations of gene delivery with triazine dendrimers had shown that flexibility is a key factor for promoting pDNA transfection [21] whereas different triazine dendrimers had been most efficient for siRNA delivery [5]. This difference was explained by the rigidity of siRNA in comparison to the rather flexible behavior of pDNA [22]. Since the “flexible” dendrimer F2-1 earlier reported as siRNA vector [5] was shown

to have a collapsed structure [22], it was shown that the peripheral groups had a stronger influence on the capacity of triazine dendrimers to deliver siRNA than the difference in flexibility between G2-1 and F2-1. Therefore, in this study a different periphery with a diethylene glycol instead of two ethylene glycol chains was investigated and the flexibility of the dendrimers was strongly increased by variation of the generation to achieve hyperflexible structures. The synthetic yields NMR and MS spectroscopic data for these new structures are provided in the Supporting Information. The composition of the panel is summarized in Figure 1. For the physicochemical and biological assays, branched poly(ethylene imine) of 25 kDa (PEI 25kDa) and/or LF were used as controls.

**Molecular dynamic simulations and energetic and structural analyses.** First, the solution phase structures were simulated as described above and shown in the Supplementary data (Figure S1). Subsequently, the binding affinity of the dendrimers and PEI towards partially 2'O-methylated siRNA was calculated as shown in Table 1. The binding energies were normalized per charge and expressed in kcal mol<sup>-1</sup> in order to allow direct comparison between the different polycations with respect to the averaged interaction of each surface group (Table 2). High enthalpic gain at a lower and unfavorable entropic loss is typical of electrostatic interactions with an overall gain in absolute free energy  $\Delta G$ . Although larger generations are expected to interact stronger with the nucleic acids, the normalized binding energies showed a different trend. This can be understood as a result of enhanced back folding of the peripheral groups with increasing generation. While the normalized  $\Delta G$  value for the assembly of F2-1 with unmodified GL3 siRNA was only -4.5 kcal mol<sup>-1</sup> [22], the binding of F2-2 to DsiRNA was comparably stronger with -9.1 kcal mol<sup>-1</sup> per amine which indicates additional hydrophobic interactions between the dendrimers and partially 2'O-methylated siRNA. Interestingly, F3 was the dendrimer with the lowest affinity to DsiRNA (-5.8 kcal mol<sup>-1</sup>) reaching only reduced enthalpic attraction at the same entropic cost as F2-2. This can be explained by the lack of primary amines in F3. Interestingly, all dendrimers showed similar enthalpic attraction towards DsiRNA slightly decreasing with generation ( $\Delta H$  of -13.4, -10.2, and -9.7 kcal/mol, respectively), while the entropic cost per charge in F4-2 was approximately half of that in F3 and F2-2. The binding with DsiRNA was therefore less entropically expensive for F4-2 than for F2-2 and F3, evidencing that F4-2 maintained higher residual flexibility during the binding

event, while F3 and F2-2 lost more degrees of freedom. The lower entropic cost of the complexation indicates that F4-2 interacts more superficially with DsiRNA, which is typically known from PAMAM dendrimers [28] and was also shown here for the interaction of DsiRNA with PEI. The normalized  $\Delta G$  value for PEI was the lowest among the tested panel. This indicates that PEI complexes are thermodynamically less stable than triazine dendrimer complexes, and that possibly not all charged amine groups are involved in a 1:1 complex with siRNA as a consequence of the sphere-like shape of solvated PEI. The entropic loss in all reactions was very well compensated by the enthalpic gain leading to thermodynamically stable complexes, even in case of PEI. From the normalized free energies, it was hypothesized that the stability of the complexes decreases in the following order: F2-2>F4-2>F3>PEI.

	<b>F2-2</b>	<b>F3</b>	<b>F4-2</b>	<b>PEI</b>
<b>H</b>	-161.3	-243.8	-466.5	-647.3
<b>-T S</b>	52.1	103.7	114.7	105.7
<b>G</b>	-109.2	-140.1	-351.7	-541.5

Table 1.  $\Delta G$  energies and the contributing potentials of the binding between dendrimers or bPEI 25 kDa and DsiRNA expressed in kcal mol<sup>-1</sup>.

	<b>F2-2</b>	<b>F3</b>	<b>F4-2</b>	<b>PEI</b>
<b>H</b>	-13.4	-10.2	-9.7	-6.6
<b>-T S</b>	4.3	4.3	2.4	1.1
<b>G</b>	-9.1	-5.8	-7.3	-5.5

Table 2.  $\Delta G$  energies and the contributing potentials of the binding between dendrimers or bPEI 25 kDa and DsiRNA normalized to energy per charged surface amine expressed in kcal mol<sup>-1</sup>.

Additionally, the models in Figure 2 help to understand the differences between the siRNA binding modalities of a globular molecule like PEI (Figure 2D) and flexible molecules like F2-2 and F3 (Figures 2A-B), while F4-2 holds an intermediate position. It is obvious that in PEI only on a limited part of the charged surface groups interact actively with siRNA while a larger part of charged amines is back folded. This assembly leads to a complex with a distinct PEI domain next

to a distinct siRNA domain shown in the upper panel of Scheme 1 and possible attachment of further PEI or siRNA molecules to the surface. Accordingly, it was previously hypothesized that complexes of PEI 25k and pDNA contain charge-neutralized regions but also patches of uncomplexed, positively and negatively charged areas leading to inter-particle electrostatic attractions [37]. The flexible dendrimers, however, exert both electrostatic and hydrophobic interaction with DsiRNA, which was assumed earlier [5], and form coalesced complexes that appear to be a single neutralized or barely charged entity as shown in the lower panel of Scheme 1. Interestingly, F4-2 deserves special attention since its binding behavior with DsiRNA results to be intermediate with respect to the one of the rigid PEI and the flexible F2-2.

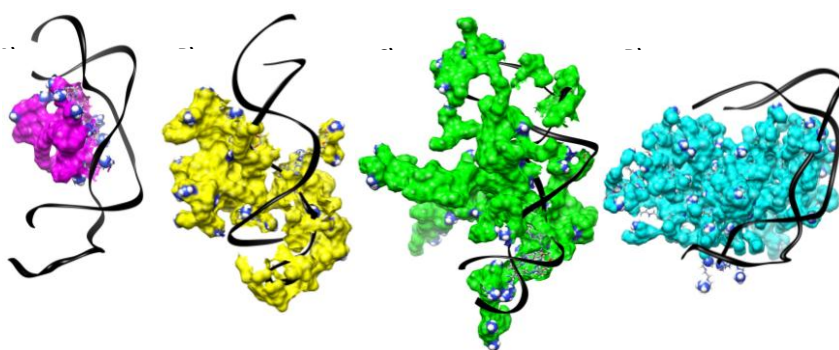
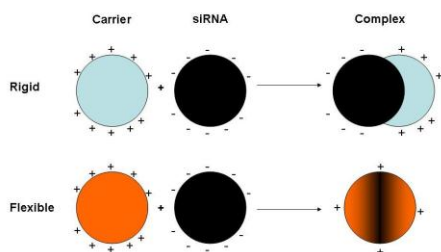


Figure 2. Equilibrated configurations (A) F2-2, (B) F3, (C) F4-2, and (D) PEI interacting with DsiRNA. Nucleic acids are represented as black ribbons and surface amines that carry a +1 charge are evidenced as spheres. Water molecules and counter ions are omitted for clarity.

This observation is supported by the thermodynamic values calculated above. According to this hypothetical scheme, PEI complexes aggregate over time, which has been described earlier for pDNA [37], and flexible triazine dendrimers coalesce with siRNA leading to “neutralization” of their opposite charges and avoidance of inter-dendriplex formation. Single, distinct units of complexes between flexible triazine dendrimers and pDNA were previously shown by AFM [21]. Since aggregation tendency of DNA-polyelectrolyte complexes as a result of the polymer structure was described in 1997 already [38], the simulated results of dendrimer interactions with DsiRNA as a function of flexibility and generation described here will be compared with experimental data in this study.



Scheme 1. Hypothesized interaction of rigid polycations with siRNA leading to complexes of charged patches and flexible polycations yielding coalesced complexes of essentially neutralized charge.

**Binding and protection efficiency and stability against competing polyanions.** To compare the hypothesized order of complex stability with experimental data, the binding affinity, siRNA protection and dendriplex stability were investigated in SYBR Gold assays [5]. The latter are developed from ethidium bromide displacement assays, which were found to yield DNA/polycation interaction profiles in agreement with thermodynamic microcalorimetry data [39] and allow to quantify siRNA available for intercalation of SYBR Gold. As shown in Figure 3A, the binding process was titrated by increasing the polycation concentration, specified as N/P ratio. The condensation of siRNA by PEI was very efficient and completely achieved at N/P 3, which is in line with previous reports [5, 40]. From the normalized binding enthalpy of a 1:1 PEI/siRNA complex, the complexation was expected to be less tight than the complexation of siRNA with flexible triazine dendrimers. However, the overall binding forces of PEI complexes were higher due to formation of multimolecular agglomerates. The condensation profile of F4-2 was comparable to that of PEI, while in F2-2 dendriplexes a fraction of 5% free siRNA remained accessible even at N/P 20, and F3 exhibited only low affinity towards siRNA as expected from the simulations. It was surprising that F2-2 dendriplexes, which were hypothesized to be most stable, seemed to condense siRNA to a lesser extent than F4-2 and F2-1 [5]. Apparently, the energetic values obtained in the simulations described above can predict the affinity of macromolecules whereas these numbers are not capable of predicting the spatial accessibility or the shielding and protection of siRNA. From the models in Figure 2, however, it can clearly be understood that a bulky molecule like F4-2 can mask siRNA more efficiently than a small dendrimer like F2-2. In case of the flexible dendrimers, the increase in generation to F4-2 helped the shielding of siRNA, as previously seen for pDNA [21], even though the increase in generation of the rigid dendrimer G3-1 improved its siRNA binding efficiency only marginally as compared to G2-1 [5]. The low affinity of F3 towards siRNA can be understood as a function of the lack of primary amines and is in line with previous observations that the condensation properties of triazine dendrimers are most importantly controlled by the end group modification rather than by the core structure [5]. The

poor condensation is also reflected in a low enthalpic attraction and high entropic loss of the F3 complex.

Since the stability of polyelectrolyte complexes is affected by the concentration of competing polyions [41], the presence of serum [36] and the interaction with negatively charged proteoglycans on the cell surface [42], stability of these complexes is one of the main factors determining the efficacy of non-viral vectors. Therefore, the thermodynamic stability of the complexes was compared with the experimental stability against the competing polyanionic model molecule heparin. As shown in Figure 3B, PEI complexes started to release siRNA at heparin concentrations of 0.25 IU per  $\mu\text{g}$  RNA. However, dendriplexes of F2-2 and F4-2 did not release siRNA up to 0.5 IU heparin per  $\mu\text{g}$  siRNA, which is comparable to dendriplexes of G2-1 [5], and were therefore more stable than PEI complexes at intermediate heparin concentrations. This can be explained by the additional hydrophobic interactions of triazine dendrimers with amphiphilic 2'-O-methylated DsiRNA previously assumed [5] and confirmed by simulation. These hydrophobic forces are not affected by competition with polyanions but are weaker than electrostatic forces and can not compensate for a lack of the latter. Therefore, both dendriplexes released about 90% of the load at 1 IU heparin per  $\mu\text{g}$  RNA where PEI complexes seemed to be more stable due to a very high amount of positive charges in the periphery of PEI and the possibility of a multimolecular assembly. Even though F2-2 complexes were hypothesized to be thermodynamically more stable than F4-2 complexes, their profiles were comparable in terms of stability against competing polyanions. Dendrimer F3, however, was hypothesized to have only low affinity towards siRNA, according to the *in silico* data, and formed loose complexes with over 90% accessible siRNA at N/P 5 as shown in Figure 3A. Therefore, bound siRNA was easily released by low concentrations of heparin, as shown in Figure 3B, leading to a gain in entropy. This data reinforced the previous assumption that a low number of protonated amines in the periphery would result in a lack of stability as shown for dendrimer G2-3 [5]. Taken together, the hypothesized inferior stability of F2-2 and F4-2 complexes over F3 based on the simulated energetic values was proven valid. Due to the fact that even the uncharged part of a dendrimer can shield encapsulated siRNA, the calculated differences in complex stability between F2-2 and F4-2 could not be confirmed by these assays.

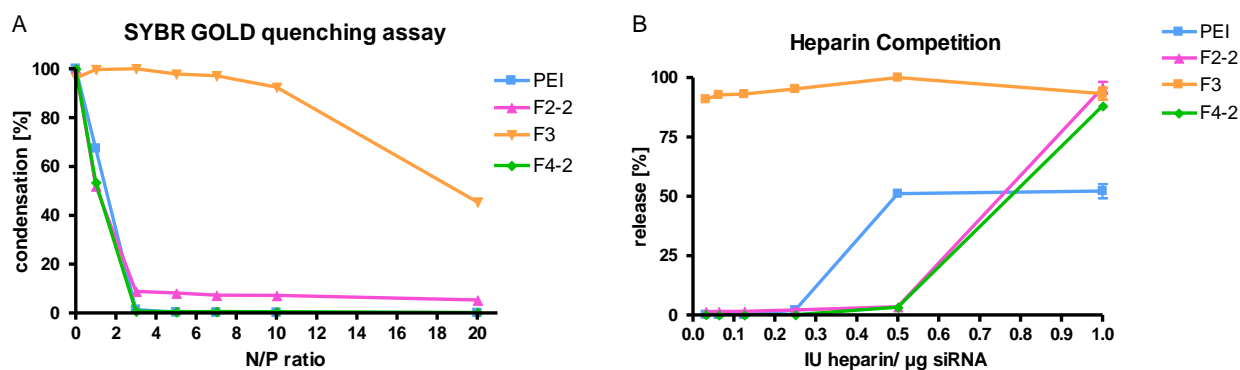


Figure 3A: Complexation behavior of dendrimers as measured by SYBR Gold intercalation of residual free siRNA at increasing N/P ratios. 3B: Release profiles of siRNA from polyelectrolyte complexes at N/P 5 as function of the concentration of heparin.

**Dendriplex Size and zeta potential.** Previously, siRNA complexes with triazine dendrimers were formed in isotonic glucose solution only [5]. To optimize the dendriplex formulation as a function of ionic strength and buffer capacity of the solvent [12], hydrodynamic diameters and zeta potentials were measured in glucose, HBG, and HEPES buffer as described above. PEI was highly efficient in condensing siRNA (Figure 3A), presumably due to the formation of multimolecular complexes. Figure 2D, shows that PEI is more rigid than the flexible dendrimers and only binds siRNA with a small share of its primary amines. As hypothesized earlier, this leads to distinct regions on the surface that are not charge-neutralized (Scheme 1) and thus to inter-polyplex attraction and aggregation, especially if incubated at 25 °C [37]. This hypothesis from Scheme 1 based on the simulations was proven right for PEI/siRNA complexes by the hydrodynamic diameters measured here. The aggregation tendency of the latter could be decreased if incubated at 0 °C (data not shown), which is in line with PEI/DNA complexes [37], and could also slightly be decreased with increasing N/P ratio if incubated at 25 °C, as shown in Figure 4A-C. The decreased aggregation tendency at higher N/P ratios can be understood as a result of electrostatic repulsion of complexes with increased zeta potential (Figure 4D-F). Interestingly, the size of the dendriplexes formed at room temperature at a certain N/P ratio was comparable for all dendrimers despite their different charge densities, different peripheries and strongly different condensation profiles. Only at N/P 20 in 5% glucose, F4-2 formed significantly smaller complexes than F2-2 and F3 (Figure 4A). The polydispersity was low for F2-2 and F3 formulations ( $0.12 < PDI < 0.35$ ) in contrast to F4-2 ( $0.19 < PDI < 0.44$ ) and PEI complexes ( $0.49 < PDI < 0.67$ ), indicating that the hypothesis of

differences in the interaction of rigid and flexible polycations with siRNA leading to multi-molecular PEI/siRNA agglomerates in contrast to coalesced dendriplexes shown in Figure 2 and Scheme 1 was right.

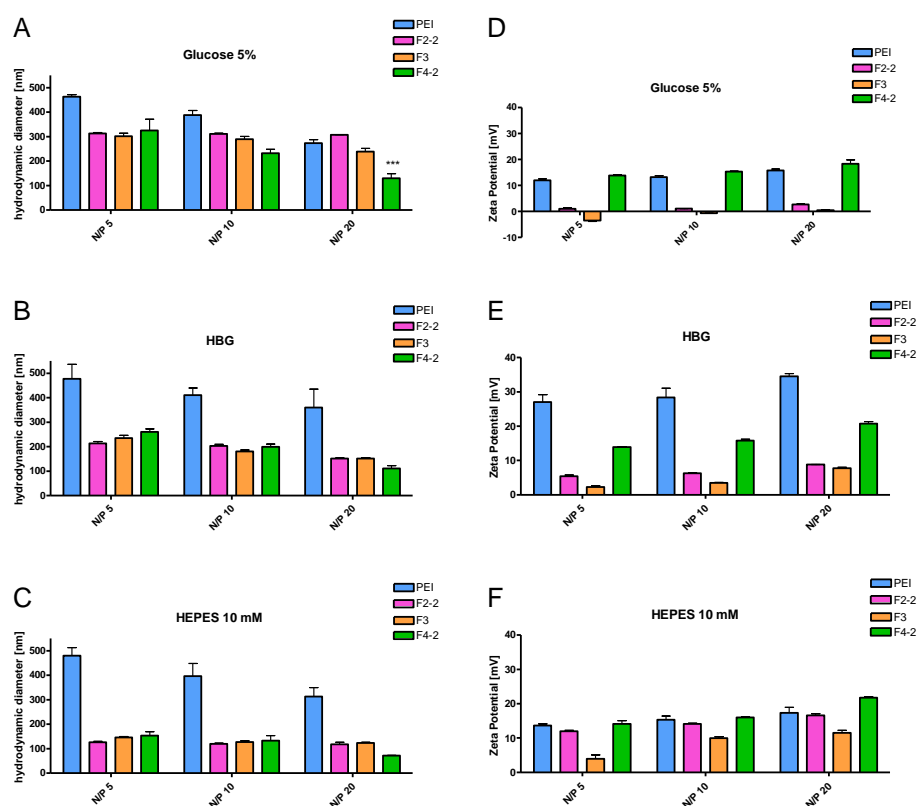


Figure 4. Hydrodynamic diameters and zeta potentials of dendrimer/siRNA complexes in comparison to PEI complexes as a function of solvent and N/P ratio.

The smallest particles (ca. 100 nm) were obtained in 10 mM HEPES, which was therefore used for dendriplex formulation for *in vitro* and *in vivo* assays. The advantage of low ionic strength media was previously described for the formulation of PAMAM dendriplexes of low generation [12]. The sizes obtained in 5% glucose were comparable to the size of F2-1 dendriplexes (286 nm) previously reported [5]. The zeta potentials measured in 5% glucose were in agreement with the condensation behavior shown in Figure 3A and the differences in charge neutralization hypothesized in Scheme 1 based on the simulations. While the siRNA was fully condensed into positively charged complexes by PEI and F4-2 at N/P 5 already, F2-2 complexes were almost neutral, and F3 complexes were negatively charged. While F2-2 and F3 coalesced with siRNA, F4-2 oriented some of its peripheral amines towards the surface of the dendriplex, as shown in Figure 2C, leading to higher zeta potential. As the charge density on the surface of F4-2



dendriplexes is much lower than on PEI complexes, and since F4-2 partially coalesces with and shields siRNA due to hydrophobic interactions, the positive charge of F4-2 complexes does not attract further siRNA molecules or F4-2 dendriplexes and does not lead to aggregation, confirmed by smaller sizes and lower PDI. Summed up, the models in Figure 2 in combination with the assembly hypothesized in Scheme 1 very well predicted size and surface charge of PEI and dendrimer complexes.

**Subcellular Distribution of Dendriplexes.** According to their toxicity profiles (Supplementary data Figure S2), all of the dendrimers were hypothesized to be suitable candidates for *in vitro* and *in vivo* siRNA delivery. Since physico-chemical parameters such as complex size [43], surface charge [17], and stability [36] determine the intracellular delivery of siRNA, uptake efficiency of the dendriplexes was compared with their simulated and experimentally determined properties. For comparison, uptake of PEI complexes at N/P 10, lipoplexes made of Lipofectamine, and free siRNA was investigated as shown in Figure 5A. As expected, free siRNA was not taken up into HeLa cells whereas lipoplexes showed very efficient uptake which was comparable to that of F2-2 complexes both at N/P 10 and N/P 20. Dendriplexes made of F2-1, however, were reported to be bound to the outer cell membrane after transfection [5] resulting in higher toxicity of F2-1 compared to F2-2 [21]. The new periphery reported here may therefore be advantageous for siRNA delivery and endocytosis of the dendriplexes. Since it was previously shown that polymeric siRNA complexes easily release their load in presence of serum [36], the great efficiency of F2-2 complexes can be explained by their thermodynamic stability which was best among the panel simulated. F3, which showed the lowest affinity (Figure 2B), lowest stability (Figure 3B), was least toxic due to the absence of primary amines (Figure S2) and had the lowest zeta potential (Figure 4D-F), mediated the poorest uptake of siRNA. The inefficiency of F3 was therefore fully in line with the *in silico* data and the previously reported reduced uptake of siRNA due to decreased surface charge and cytotoxicity of acetylated PAMAM derivatives [17]. The uptake of F4-2 complexes seemed to be reduced compared to F2-2 which may be explained by the lower thermodynamic stability of F4-2 complexes as compared to F2-2 complexes or the higher cytotoxicity (Figure S2). Additionally, F4-2 complexes showed uptake into distinct spots which may be an indication of incomplete endosomal release of the siRNA inside the cells as reported for

siRNA complexes of PAMAM and Tat-conjugated PAMAM [19], SuperFect and guanylated F2-1g complexes [5].

**Transfection Efficiency.** Since all dendriplexes were efficiently internalized into HeLa/Luc cells, it was checked if the simulated data also corroborated their capacity to knockdown luciferase expression in the same cell line. All dendriplexes mediated RNAi depending on the N/P ratio with some formulations achieving effects comparable to Lipofectamine (LF). While the latter showed considerable off-target effects in cells treated with lipoplexes of the negative control sequence, as shown in Figures 5B-D, dendrimers F2-2 and F3 maintained strong transfection efficiency with low or very low toxicity and off-target effects. The correlation between efficiency and toxicity has always been a major drawback of non-viral vectors [44] and was only recently reported to be overcome by disulfide cross-linked low molecular weight PEI for gene delivery [45] and conjugation of  $\beta$ -CD onto PAMAM for siRNA delivery [46]. Other modifications of dendrimers, however, such as internal quaternization in addition to a hydroxyl periphery of PAMAMs led to poor biological activity [18]. With hyperflexible triazine dendrimers, efficient luciferase knockdown was achieved even with the least toxic dendrimer F3, which supports the hypothesis of efficiency of flexible dendrimers at reduced toxicity reported for G7 triethanolamine core PAMAM dendriplexes [13]. The efficiency of F3 complexes was lower than that of F2-2 but surprising taking into account that F3 did not efficiently protect siRNA from intercalation of SYBR Gold. However, F3 complexes were small and monodisperse (Figure 4A-C) and were therefore endocytosed to a certain degree (Figure 5A). However, increasing signs of off-target effects were observed for flexible triazine dendrimers as a function of increasing amounts of primary amines.

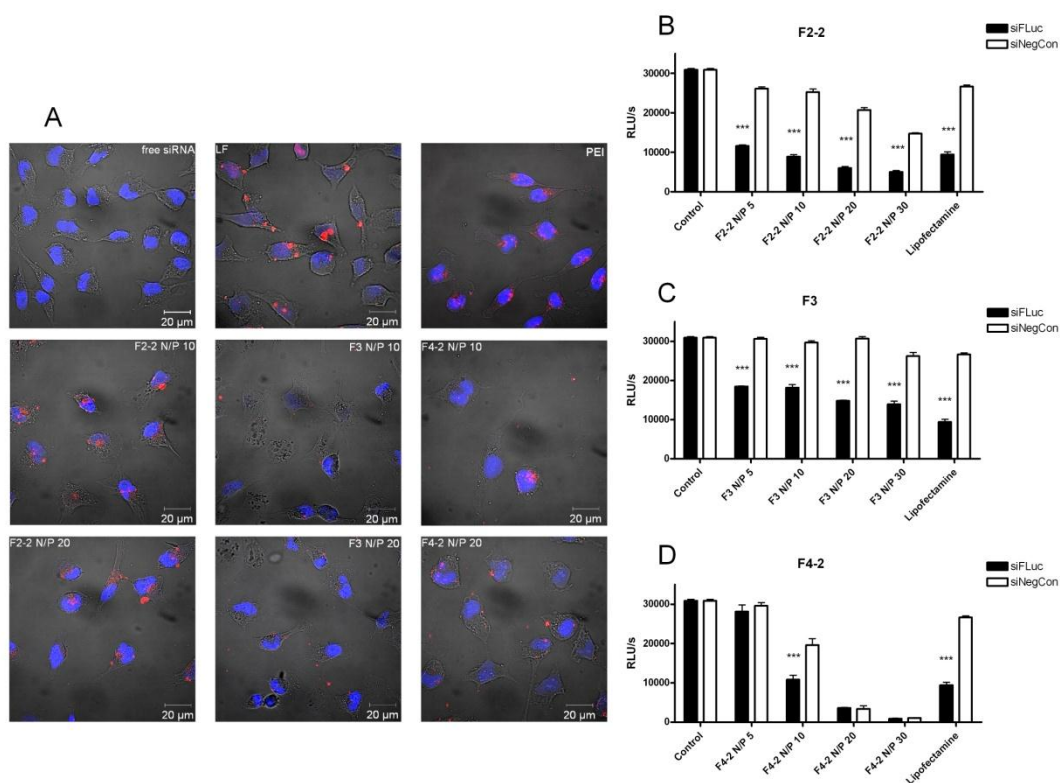


Figure 5A. Confocal images showing the subcellular distribution of complexes made of Tye543-labeled siRNA (red) following cellular uptake in HeLa/Luc cells 4 hours after transfection. DAPI-stained nuclei are shown in blue. 5B-D. Knockdown of luciferase expression by dendrimer-siFLuc complexes in HeLa/Luc cells in comparison to dendriplexes with siNegCon (\*\*p < 0.01, \*\*\*p < 0.001).

At N/P 20, the toxicity of F2-2 complexes was comparable to LF. However, since small and stable complexes were even obtained at much lower N/P ratios, such as 5 and 10, these formulations were highly efficient in downregulating luciferase expression at no effect of the non-specific siRNA sequence. Due to its higher amount of primary amines and lower IC<sub>50</sub> value, F4-2 led to considerable cell death and off-target effects at N/P 20 and 30. At lower N/P ratios, F4-2 complexes were less efficient than F2-2 which was fully in line with the simulated lower thermodynamic stability, reduced intracellular uptake, and hypothetically insufficient endosomal release. Stability [36], formation of larger aggregates with low generation dendrimers [9-11], nuclear localization [20], and incomplete endosomal release of the siRNA [19] were reported to be the major hurdles for polymeric and dendritic vectors. Concerning the panel of triazine dendrimers investigated here, sufficient stability as predicted for F2-2 by simulation of the thermodynamic binding profiles and tolerable toxicity appeared to be the determining factors.

**Biodistribution and Pharmacokinetics.** Since all dendrimer formulations successfully mediated RNAi *in vitro* with negligible toxicity at N/P 5, all of them qualified for *in vivo* experiments. As SPECT imaging of *in vivo* administration of radiolabeled siRNA was previously reported to predict pharmacokinetics and biodistribution with good correlation to results obtained by scintillation counting [35], the same technique was employed to gain insight into the *in vivo* performance of hyperflexible dendriplexes. To date, information on biodistribution of dendritic siRNA carriers is limited to a study of surface-engineered PPI where *ex vivo* fluorescence imaging and confocal laser scanning microscopy (CLSM) was employed to investigate the organ distribution of fluorescently labeled siRNA [2] and a second study that performed CLSM to trace the fluorescently labeled G4 cystamine-core PAMAM-based carrier [7]. The only report on pharmacokinetics of dendrimer-complexed siRNA investigated radioactively labeled siRNA and rigid triazine dendrimers and described strong lung accumulation of radioactively and fluorescently labeled siRNA [5]. As can be seen in Figure 6A and Movie 1 (Supporting Information), F2-2 dendriplexes did not accumulate in the lung, but in the liver, the kidneys and to some extent in the bowel due to partial hepatobiliary excretion of amphiphilic DsiRNA [5]. Although F3 complexes were stable enough in 10% serum containing medium to mediate RNAi *in vitro*, these complexes dissociated *in vivo* as previously described for PEI complexes [36] leading to quantitative excretion of free siRNA via the bowel and the bladder (Figure 6B and Movie 2). Interestingly, F4-2 complexes seemed to be most stable under *in vivo* conditions with very strong uptake of radiolabeled siRNA into the liver, some excretion into the bladder and no noticeable excretion of free siRNA via the bowel (Figure 6C and Movie 3).

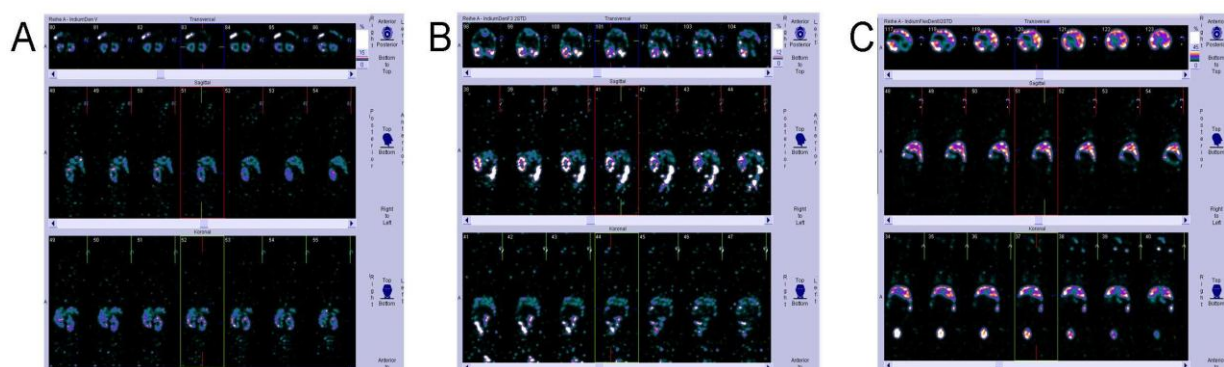


Figure 6. Three-dimensional biodistribution of A. F2-2-siRNA-dendriplexes, B. F3-siRNA-dendriplexes, and C. F4-2-siRNA-dendriplexes 2 hours after i.v. administration as registered by SPECT imaging.

These results were confirmed by scintillation counting of dissected organs as shown in Figure 7A. Dendriplexes made of dendrimer F2-2 showed a higher signal in the heart 2 h after injection which is in line with significantly prolonged circulation times (Figure 7B). Their advantageous pharmacokinetics reflected in a more than twofold increased AUC versus free siRNA (Figure 7B) can be explained by reduced uptake into the reticulo-endothelial system (RES) which results from lower surface charge of F2-2 complexes compared to PEI or F4-2 complexes. Although F2-2 complexes were expected to be most stable, the SYBR Gold assay showed that some siRNA was still accessible for intercalation. This finding corroborates the considerable amount of 9.8% of the injected dose (ID) which was excreted as free siRNA via the bowel and 5.3% ID cleared through the kidneys. All other formulations led to rapid clearance from the blood pool as shown by low AUC values (167.2-276.7 %ID\*min/ml), as previously reported for native siRNA [47]. Both free siRNA and siRNA formulated with F3 were mostly cleared into the bowel and the bladder. The similarity of the pharmacokinetic profiles and the deposition of free siRNA and siRNA/F3 complexes into the bowel is a strong indication of instability which was hypothesized due to simulated thermodynamic data and the results from the SYBR Gold assay. F4-2 complexes, however, were not rapidly cleared from the blood stream because of instability but because of extensive capture by the RES. In fact, the uptake of 52.1% of the injected siRNA is a sign of enhanced stability compared to PEI complexes, PEG-PEI complexes [36] and rigid triazine dendriplexes [5]. This strong uptake of siRNA into the liver was previously reported for surface-engineered PPI-based siRNA complexes [2] and was exploited for knockdown of ApoB in healthy C57BL/6 mice with poly-L-lysine-based vectors [3] or G3 tetra-oleoyl lysine dendrimers bound to the hydrophobic surface of single-walled carbon nanotubes (SWNT) [8]. While the spleen took up additional 7.0% ID of F4-2 formulated siRNA, only 0.7% ID accumulated in the kidneys and 2.3% ID were found in the bowel. As reported earlier, PEI complexes dissociated in the liver which was the only organ in which PEI-formulated siRNA accumulated. This is strongly in line with previous reports [36], and the differences of RES capture are in line with the different interaction of rigid and flexible polycations with siRNA as hypothesized based on the simulations. Radiolabeled siRNA complexed with PEI 25k showed the same pharmacokinetic profile as free siRNA and siRNA complexed with F3, indicating the instability of both complexes as hypothesized from the thermodynamic values.

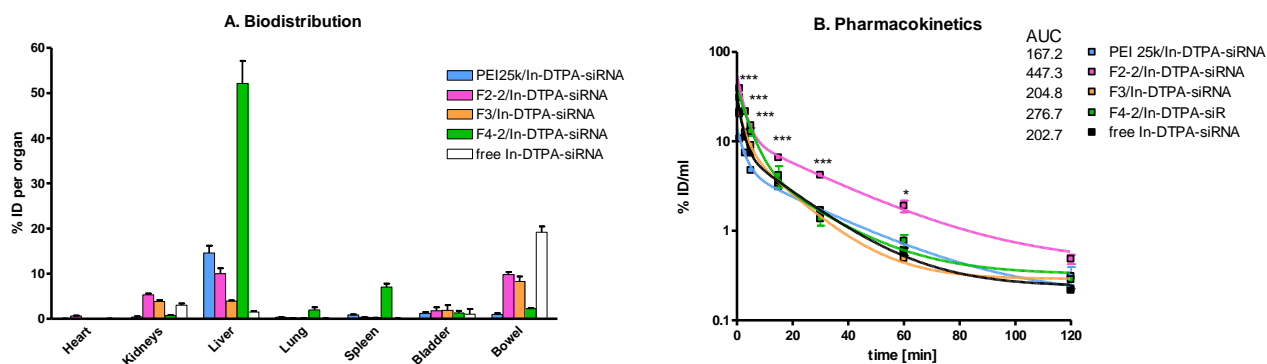


Figure 7A. Biodistribution, 7B. Pharmacokinetics and AUC values in %ID\*min/ml of siRNA-dendriplexes and polyplexes as measured by gamma scintillation counting of organ and blood samples.

## 6.5 Conclusions

Although dendrimers are increasingly used as non-viral vectors for siRNA delivery, the influence of dendrimer flexibility on *in vitro* and *in vivo* performance has not systematically been investigated. Molecular modeling approaches have been reported to explain the interactions of dendrimers with nucleic acids, but the predictive power of this kind of simulations has not been challenged. In this study, simulated thermodynamic results were compared with experimental data which showed that the predicted trend held true. Especially the aggregation tendency of PEI complexes in comparison to dendriplexes could be well explained, and the resulting internalization and transfection efficiency of the dendriplexes were in line with the predicted order of stability. However, as shown in the SYBR Gold assays, the simulated data does not account for differences in the shielding of siRNA by polycations. Although F2-2 was simulated to form the most stable complexes with siRNA, PEI and F4-2 most efficiently protected siRNA from intercalation with SYBR Gold. The lack of protection of siRNA in F2-2 and F3 complexes is reflected by the partial excretion of free siRNA via the bowel and kidneys upon intravenous administration. In contrast to PEI complexes, dendriplexes of F4-2 were very stable *in vivo*. As predicted by the simulations, complexes of the more rigid PEI and F4-2 with non-charge neutralized patches were captured by the RES to a higher extent than F2-2 and F3 complexes. This accumulation may however be exploited for liver targeting in the future, or local administration that circumvents the uptake into the liver may be considered. In this study, it became obvious that results from molecular modeling

approaches very well explain physico-chemical parameters and the *in vitro* behavior of dendriplexes. These attributes, in turn, determine *in vivo* behavior such as stability in presence of serum or uptake into the RES. Since *in vivo* conditions, however, involve the complex interplay of dendriplexes with serum, cells, organs and metabolism, the prediction of the *in vivo* performance of dendriplexes can not solely be simulated but should be supported by methods such as *in vivo* imaging. If combined, however, molecular modeling and *in vivo* imaging very well represent the *in vitro* and *in vivo* performance of non-viral vectors for siRNA delivery as shown in this study. Further validation of *in silico* data by isothermal titration calorimetry is currently under way.

## 6.6 Acknowledgments

We are grateful to Brian Sproat (IDT/Chemconsilium) for supplying the siRNA within MEDITRANS and to Eva Mohr (Dept. of Pharmaceutics and Biopharmacy) and Ulla Cramer (Dept. of Nuclear Medicine) for excellent technical support. MEDITRANS, an Integrated Project funded by the European Commission under the Sixth Framework (NMP4-CT-2006-026668), is gratefully acknowledged. EES and MAM thank the N.I.H. (R01 GM 65460). MM acknowledges the Czech national project OC10053.

## 6.7 References

- [1] J. Zhou, J. Wu, N. Hafdi, J.P. Behr, P. Erbacher, L. Peng, PAMAM dendrimers for efficient siRNA delivery and potent gene silencing, *Chem Commun (Camb)*, (2006) 2362-2364.
- [2] O. Taratula, O.B. Garbuzenko, P. Kirkpatrick, I. Pandya, R. Savla, V.P. Pozharov, H. He, T. Minko, Surface-engineered targeted PPI dendrimer for efficient intracellular and intratumoral siRNA delivery, *J Control Release*, 140 (2009) 284-293.
- [3] K. Watanabe, M. Harada-Shiba, A. Suzuki, R. Gokuden, R. Kurihara, Y. Sugao, T. Mori, Y. Katayama, T. Niidome, *In vivo* siRNA delivery with dendritic poly(L-lysine) for the treatment of hypercholesterolemia, *Mol Biosyst*, 5 (2009) 1306-1310.
- [4] N. Weber, P. Ortega, M.I. Clemente, D. Shcharbin, M. Bryszewska, F.J. de la Mata, R. Gómez, M.A. Muñoz-Fernández, Characterization of carbosilane dendrimers as effective carriers of siRNA to HIV-infected lymphocytes, *Journal of Controlled Release*, 132 (2008) 55-64.
- [5] O.M. Merkel, M.A. Mintzer, D. Librizzi, O. Samsonova, T. Dicke, B. Sproat, H. Garn, P.J. Barth, E.E. Simanek, T. Kissel, Triazine Dendrimers as Nonviral Vectors for *in Vitro* and *in Vivo* RNAi: The Effects of Peripheral Groups and Core Structure on Biological Activity, *Mol Pharm*, 7 (2010) 969-983.

- [6] I.D. Kim, C.M. Lim, J.B. Kim, H.Y. Nam, K. Nam, S.W. Kim, J.S. Park, J.K. Lee, Neuroprotection by biodegradable PAMAM ester (e-PAM-R)-mediated HMGB1 siRNA delivery in primary cortical cultures and in the postischemic brain, *J Control Release*, 142 (2010) 422-430.
- [7] A. Agrawal, D.H. Min, N. Singh, H. Zhu, A. Birjiniuk, G. von Maltzahn, T.J. Harris, D. Xing, S.D. Wolfenden, P.A. Sharp, A. Charest, S. Bhatia, Functional delivery of siRNA in mice using dendriworms, *ACS Nano*, 3 (2009) 2495-2504.
- [8] J. McCarroll, H. Baigude, C.S. Yang, T.M. Rana, Nanotubes functionalized with lipids and natural amino acid dendrimers: a new strategy to create nanomaterials for delivering systemic RNAi, *Bioconjug Chem*, 21 (2010) 56-63.
- [9] X.C. Shen, J. Zhou, X. Liu, J. Wu, F. Qu, Z.L. Zhang, D.W. Pang, G. Quelever, C.C. Zhang, L. Peng, Importance of size-to-charge ratio in construction of stable and uniform nanoscale RNA/dendrimer complexes, *Org Biomol Chem*, 5 (2007) 3674-3681.
- [10] R.L. Juliano, Intracellular delivery of oligonucleotide conjugates and dendrimer complexes, *Ann N Y Acad Sci*, 1082 (2006) 18-26.
- [11] Y. Inoue, R. Kurihara, A. Tsuchida, M. Hasegawa, T. Nagashima, T. Mori, T. Niidome, Y. Katayama, O. Okitsu, Efficient delivery of siRNA using dendritic poly(L-lysine) for loss-of-function analysis, *J Control Release*, 126 (2008) 59-66.
- [12] A.P. Perez, E.L. Romero, M.J. Morilla, Ethylenediamine core PAMAM dendrimers/siRNA complexes as in vitro silencing agents, *Int J Pharm*, 380 (2009) 189-200.
- [13] X.X. Liu, P. Rocchi, F.Q. Qu, S.Q. Zheng, Z.C. Liang, M. Gleave, J. Iovanna, L. Peng, PAMAM dendrimers mediate siRNA delivery to target Hsp27 and produce potent antiproliferative effects on prostate cancer cells, *ChemMedChem*, 4 (2009) 1302-1310.
- [14] Q. Yuan, E. Lee, W.A. Yeudall, H. Yang, Dendrimer-triglycine-EGF nanoparticles for tumor imaging and targeted nucleic acid and drug delivery, *Oral Oncol*, 46 (2010) 698-704.
- [15] S. Svenson, Dendrimers as versatile platform in drug delivery applications, *European Journal of Pharmaceutics and Biopharmaceutics*, 71 (2009) 445-462.
- [16] R. Jevprasesphant, J. Penny, R. Jalal, D. Attwood, N.B. McKeown, A. D'Emanuele, The influence of surface modification on the cytotoxicity of PAMAM dendrimers, *Int J Pharm*, 252 (2003) 263-266.
- [17] C.L. Waite, S.M. Sparks, K.E. Uhrich, C.M. Roth, Acetylation of PAMAM dendrimers for cellular delivery of siRNA, *BMC Biotechnology*, 9 (2009).
- [18] M.L. Patil, M. Zhang, O. Taratula, O.B. Garbuzenko, H. He, T. Minko, Internally cationic polyamidoamine PAMAM-OH dendrimers for siRNA delivery: effect of the degree of quaternization and cancer targeting, *Biomacromolecules*, 10 (2009) 258-266.
- [19] H. Kang, R. DeLong, M.H. Fisher, R.L. Juliano, Tat-conjugated PAMAM dendrimers as delivery agents for antisense and siRNA oligonucleotides, *Pharmaceutical Research*, 22 (2005) 2099-2106.
- [20] M.L. Patil, M. Zhang, S. Betigeri, O. Taratula, H. He, T. Minko, Surface-modified and internally cationic polyamidoamine dendrimers for efficient siRNA delivery, *Bioconjug Chem*, 19 (2008) 1396-1403.
- [21] O.M. Merkel, M.A. Mintzer, J. Sitterberg, U. Bakowsky, E.E. Simanek, T. Kissel, Triazine dendrimers as nonviral gene delivery systems: effects of molecular structure on biological activity, *Bioconjug Chem*, 20 (2009) 1799-1806.



- [22] G.M. Pavan, M.A. Mintzer, E.E. Simanek, O.M. Merkel, T. Kissel, A. Danani, Computational insights into the interactions between DNA and siRNA with "rigid" and "flexible" triazine dendrimers, *Biomacromolecules*, 11 (2010) 721-730.
- [23] W.R. Sanhai, J.H. Sakamoto, R. Canady, M. Ferrari, Seven challenges for nanomedicine, *Nat Nanotechnol*, 3 (2008) 242-244.
- [24] M.A. Mintzer, O.M. Merkel, T. Kissel, E.E. Simanek, Polycationic triazine-based dendrimers: effect of peripheral groups on transfection efficiency, *New J Chem*, 33 (2009) 1918-1925.
- [25] D.A. Case, T.A. Darden, T.E. Cheatham III, C.L. Simmerling, J. Wang, R.E. Duke, R. Luo, R.C. Walker, W. Zhang, K.M. Merz, B. Robertson, B. Wang, S. Hayik, A. Roitberg, G. Seabra, I. Kolossvary, K.F. Wong, F. Paesani, J. Vanicek, J. Liu, X. Wu, S. Brozell, T. Steinbrecher, H. Gohlke, Q. Cai, X. Ye, J. Wang, M.-J. Hsieh, G. Cui, D.R. Roe, D.H. Mathews, M.G. Seetin, C. Sangui, V. Babin, T. Luchko, S. Gusarov, A. Kovalenko, P.A. Kollman, AMBER 11, in, University of California, San Francisco, 2010.
- [26] S.P. Jones, G.M. Pavan, A. Danani, S. Pricl, D.K. Smith, Quantifying the Effect of Surface Ligands on Dendron-DNA Interactions: Insights into Multivalency through a Combined Experimental and Theoretical Approach, *Chemistry*, 16 (2010) 4519-4532.
- [27] G.M. Pavan, A. Danani, S. Pricl, D.K. Smith, Modeling the multivalent recognition between dendritic molecules and DNA: understanding how ligand "sacrifice" and screening can enhance binding, *J Am Chem Soc*, 131 (2009) 9686-9694.
- [28] G.M. Pavan, L. Albertazzi, A. Danani, Ability to adapt: different generations of PAMAM dendrimers show different behaviors in binding siRNA, *J Phys Chem B*, 114 (2010) 2667-2675.
- [29] J. Suh, H.J. Paik, B.K. Hwang, Ionization of Poly(ethylenimine) and Poly(allylamine) at Various pH's, *Bioorganic Chemistry*, 22 (1994) 318-327.
- [30] W.K. Jorgensen, M.J. Rice, Morphology of a very extensible insect muscle, *Tissue Cell*, 15 (1983) 639-644.
- [31] T. Darden, D. York, L. Pedersen, Particle mesh Ewald: An  $N \log(N)$  method for Ewald sums in large systems, *The Journal of Chemical Physics*, 98 (1993) 10089-10092.
- [32] W.D. Cornell, P. Cieplak, C.I. Bayly, I.R. Gould, K.M. Merz, D.M. Ferguson, D.C. Spellmeyer, T. Fox, J.W. Caldwell, P.A. Kollman, A Second Generation Force Field for the Simulation of Proteins, Nucleic Acids, and Organic Molecules, *Journal of the American Chemical Society*, 117 (1995) 5179-5197.
- [33] J. Srinivasan, T.E. Cheatham, P. Cieplak, P.A. Kollman, D.A. Case, Continuum Solvent Studies of the Stability of DNA, RNA, and Phosphoramidate-DNA Helices, *Journal of the American Chemical Society*, 120 (1998) 9401-9409.
- [34] I. Andricioaei, M. Karplus, On the calculation of entropy from covariance matrices of the atomic fluctuations, *The Journal of Chemical Physics*, 115 (2001) 6289-6292.
- [35] O.M. Merkel, D. Librizzi, A. Pfestroff, T. Schurrat, M. Behe, T. Kissel, In vivo SPECT and real-time gamma camera imaging of biodistribution and pharmacokinetics of siRNA delivery using an optimized radiolabeling and purification procedure, *Bioconjug Chem*, 20 (2009) 174-182.
- [36] O.M. Merkel, D. Librizzi, A. Pfestroff, T. Schurrat, K. Buyens, N.N. Sanders, S.C. De Smedt, M. Behe, T. Kissel, Stability of siRNA polyplexes from poly(ethylenimine) and poly(ethylenimine)-g-poly(ethylene glycol) under in vivo conditions: effects on pharmacokinetics and biodistribution measured by Fluorescence Fluctuation Spectroscopy and Single Photon Emission Computed Tomography (SPECT) imaging, *J Control Release*, 138 (2009) 148-159.

- [37] V.K. Sharma, M. Thomas, A.M. Klibanov, Mechanistic studies on aggregation of polyethylenimine-DNA complexes and its prevention, *Biotechnol Bioeng*, 90 (2005) 614-620.
- [38] M.X. Tang, F.C. Szoka, The influence of polymer structure on the interactions of cationic polymers with DNA and morphology of the resulting complexes, *Gene Ther*, 4 (1997) 823-832.
- [39] T. Ehtezazi, U. Rungsardthong, S. Stolnik, Thermodynamic analysis of polycation-DNA interaction applying titration microcalorimetry, *Langmuir*, 19 (2003) 9387-9394.
- [40] O.M. Merkel, A. Beyerle, D. Librizzi, A. Pfestroff, T.M. Behr, B. Sproat, P.J. Barth, T. Kissel, Nonviral siRNA delivery to the lung: investigation of PEG-PEI polyplexes and their in vivo performance, *Mol Pharm*, 6 (2009) 1246-1260.
- [41] V.A. Izumrudov, T.K. Bronich, M.B. Novikova, A.B. Zezin, V.A. Kabanov, Substitution reactions in ternary systems of macromolecules, *Polymer Science U.S.S.R.*, 24 (1982) 367-378.
- [42] A.L. Bolcato-Bellemin, M.E. Bonnet, G. Creusat, P. Erbacher, J.P. Behr, Sticky overhangs enhance siRNA-mediated gene silencing, *Proc Natl Acad Sci U S A*, 104 (2007) 16050-16055.
- [43] I. Mellman, Endocytosis and molecular sorting, *Annu Rev Cell Dev Biol*, 12 (1996) 575-625.
- [44] S. Hong, P.R. Leroueil, E.K. Janus, J.L. Peters, M.M. Kober, M.T. Islam, B.G. Orr, J.R. Baker, Jr., M.M. Banaszak Holl, Interaction of polycationic polymers with supported lipid bilayers and cells: nanoscale hole formation and enhanced membrane permeability, *Bioconjug Chem*, 17 (2006) 728-734.
- [45] M. Breunig, U. Lungwitz, R. Liebl, A. Goepferich, Breaking up the correlation between efficacy and toxicity for nonviral gene delivery, *Proc Natl Acad Sci U S A*, 104 (2007) 14454-14459.
- [46] T. Tsutsumi, H. Arima, F. Hirayama, K. Uekama, Potential Use of Dendrimer/ $\alpha$ -Cyclodextrin Conjugate as a Novel Carrier for Small Interfering RNA (siRNA), *Journal of Inclusion Phenomena and Macrocyclic Chemistry*, 56 (2006) 81-84.
- [47] D.M. Dykxhoorn, D. Palliser, J. Lieberman, The silent treatment: siRNAs as small molecule drugs, *Gene Ther*, 13 (2006) 541-552.

## Chapter 7

# DESIGN AND BIOPHYSICAL CHARACTERIZATION OF BIORESPONSIVE DEGRADABLE POLY(DIMETHYLAMINOETHYL METHACRYLATE) BASED POLYMERS FOR IN VITRO DNA TRANSFECTION

Published in Biomacromolecules. 2012 Feb 13;13(2):313-22. Epub 2012 Jan 17.

Yi Zhang,<sup>†§</sup> Mengyao Zheng,<sup>‡§</sup> Thomas Kissel,<sup>\*‡</sup> Seema Agarwal<sup>\*\*†</sup>

<sup>§</sup>Both authors contributed equally to this work

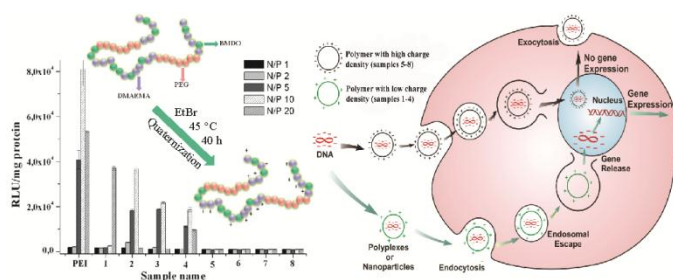
### Author contributions

T. K. and S. A. guided the research. M. Z. and Y. Z. directed the measurements. Y. Z. synthesized and characterized the polymers and M. Z. carried out the SYBR<sup>®</sup> Gold assay, heparin competition assay, MTT assay, CLSM and in vitro transfection. M. Z. and Y. Z. analysed the experimental data.

## 7.1 Abstract

Water soluble, degradable polymers based on poly(*N,N*-dimethylaminoethyl methacrylate) (PDMAEMA) with low cytotoxicity and good p-DNA transfection efficiency are highlighted in this article. To solve the non-degradability issue of PDMAEMA, new polymers based on DMAEMA and 5,6-benzo-2-methylene-1,3-dioxepane (BMDO) for gene transfection were synthesized. A poly(ethylene oxide) (PEO) azo-initiator was used as free-radical initiator. PEGylation was performed to improve water solubility and to reduce cytotoxicity of the polymers. The resulting polymers contain hydrolysable ester linkages in the backbone and were soluble in water even with very high amounts of ester linkages. These degradable copolymers showed significantly less toxicity with a MTT assay using L929 cell lines and demonstrated promising DNA transfection efficiency when compared with the gold standard poly(ethyleneimine). Bioresponsive properties of the corresponding quaternized DMAEMA based degradable polymers were also studied. Although the quaternized DMAEMA copolymer showed enhanced water solubility, it was inferior in gene transfection and toxicity as compared to the unquaternized copolymers.

**KEYWORDS:** gene transfection; degradable; cyclic ketene acetal; dimethyl aminoethyl methacrylate



## 7.2 Introduction

Gene therapy is a highly promising approach for the potential treatment of genetic and inherited diseases.<sup>1,2</sup> Substantial research has already been carried out in the last few decades on the development of gene delivery vectors.<sup>3-5</sup> In spite of the high transfection efficiency of viral gene vectors, there is an ever increasing amount of number of literature on the use of non-viral gene delivery vehicles for gene therapy. This is to overcome the basic drawbacks of viral vectors

which are immune response, limitations in the size of inserted DNA, difficulty in large scale pharmaceutical grade production etc.<sup>6</sup> Some non-viral DNA delivery systems include pure plasmid DNA, lipoplexes (DNA complexed with cationic lipids), polyplexes (nucleic acid complexes with polycations and encapsulated DNA in degradable polymer matrices). For example, cationic polymers show the ability to form polyplex with DNA by electrostatic interactions due to its polyanionic character.<sup>7-11</sup> An example of a frequently studied polycation for this purpose is polyethyleneimine (PEI), a gold standard with buffering properties (at physiological pH only 25% of the amine groups are protonated) but with the major drawback of cytotoxicity (half maximal inhibitory concentration ( $IC_{50}$ ) =  $\sim 8 \mu\text{g}\cdot\text{ml}^{-1}$ ).<sup>12</sup> Recently, attention has been given to poly(*N,N*-dimethylaminoethyl methacrylate) (PDMAEMA) as a non-viral gene delivery system with buffering capacity and less cytotoxicity ( $IC_{50}$  =  $\sim 40\mu\text{g}\cdot\text{ml}^{-1}$ ) (pKa = 7.5). This polymer is prepared by radical polymerization of the corresponding vinyl monomer. It was shown for the first time in 1996 by Hennink et al. that PDMAEMA is an interesting vector for designing of a gene transfection system.<sup>13</sup>

PDMAEMA contains tertiary amines for the complexation of DNA and reaches 90% of the transfection efficiency of PEI (branched PEI 25 kDa). Since then, several aspects of this transfection reagent have been modified i.e. the role of molecular weight, polyplex size and transfection parameters, pH, ionic strength, temperature, viscosity, polymer/plasmid-DNA (p-DNA) ratio and the presence of stabilizers on transfection efficiency of PDMAEMA.<sup>14-18</sup> Despite so much research, the key problem of polycations like PEI and PDMAEMA is their non-biodegradable nature, notable toxicity and the need for further improvement of transfection efficiency.

Vinyl polymers like PDMAEMA, which can be easily synthesized by radical polymerization, could be further designed to meet these requirements. Recently, Oupicky et al. reported PDMAEMA copolymers with reducible –S-S- disulfide linkages using reversible addition fragmentation transfer (RAFT) polymerization with comparable cytotoxicity and gene transfection efficiency like homo PDMAEMA for the first time.<sup>19</sup> Unfortunately, no data (*in vivo* or *in vitro*) regarding biodegradation behavior was provided.

To solve the non-degradability issue of PDMAEMA, we recently showed the possibility of forming a degradable and less toxic PDMAEMA by introducing ester linkages into the

PDMAEMA backbone. We consider radical-ring-opening polymerization of cyclic ketene acetals a promising method for introducing degradable ester linkages into the polymer backbone, which can be used to develop new gene transfection systems. Cyclic ketene acetals are the isomers of the corresponding cyclic lactones and can undergo radical addition at the vinyl double bond with subsequent ring-opening leading to the formation of polyesters. Free-radical copolymerization of cyclic ketene acetal 5,6-benzo-2-methylene-1,3-dioxepane (BMDO), with *N,N*-dimethylaminoethyl methacrylate (DMAEMA) can lead to the formation of degradable PDMAEMA with ester linkages in the backbone.<sup>20</sup> The polymers were not soluble in water, therefore quaternization with alkyl bromide was carried out. Regardless of copolymer composition, all of the polymers were less cytotoxic than PEI and showed very high cell viability. Unfortunately, the system showed poor transfection efficiency which could be due to the strong interactions between the positively charged units and DNA. Therefore, further improvement was implemented in this system by designing a polymer avoiding quaternization of PDMAEMA. Small poly(ethylene glycol) (PEG) hydrophilic blocks were introduced onto degradable PDMAEMA units to enhance water solubility and reduce the cytotoxicity.<sup>21,22</sup> Again, simple free radical chemistry was used for this purpose and a poly(ethylene oxide) (PEO) macro-azo-initiator was used. The success of this concept is highlighted in this work by giving details about synthesis, cytotoxicity, polyplex formation and gene transfection.

### 7.3 Experimental Part

**Materials.** PEO macro-azo-initiator (WAKO Company  $M_n = 24$  kDa, PEG block =  $6000 \text{ g}\cdot\text{mol}^{-1}$ ) and bromoethane (Acros, 99%) were used as received. DMAEMA (Acros) was passed through a basic alumina column to remove the inhibitor. Dimethylformamide (DMF), chloroform, pentane and methanol were distilled before use. BMDO was synthesized according to our previous report.<sup>23</sup> Luciferase-Plasmid (pCMV-Luc) (LotNo.: PF461-090623) was amplified by The Plasmid Factory (Bielefeld, Germany). All other chemicals were obtained from Sigma–Aldrich (Steinheim, Germany) and used as received.

**Instrumentation.**  $^1\text{H}$  (400,13 MHz) and  $^{13}\text{C}$  (100,21 MHz) spectra were recorded on a Bruker DRX-400 spectrometer. Tetramethylsilane was used as internal standard. The molecular weight of the polymers were measured with size exclusion chromatography at 25 °C with 1 liner PSS

suprema Max 1000 Å column and a differential refractive index detector (SECcurity RI, PSS). 0.3 mol·L<sup>-1</sup> formic acid in water was used as an eluent at a flow rate of 0.5 mL·min<sup>-1</sup>. An SECcurity 1100 (PSS) pump was used for the experiment. Linear poly 2-vinylpyridine was used for calibration. The injected volume was 100 µL and the polymer concentration was 1 mg·mL<sup>-1</sup>.

#### **Copolymerization of DMAEMA and BMDO with PEO Azo-initiator (general procedure).**

As an example for polymerization reactions, the procedure for the synthesis of sample 4 is described below. All of the sample names and monomer feed ratios are shown in Table 1 and Table 2.

The monomer BMDO (0.99 g, 6.1 mmol) was dissolved in DMAEMA (0.1 mL, 0.59 mmol) in a predried Schlenk tube under an argon atmosphere. The reaction mixture was degassed by three freeze-pump-thaw cycles. The PEO azo-initiator with PEG 6000 block (0.41 g, 6.8·10<sup>-2</sup> mmol) was added to the still frozen solution. The Schlenk tube was closed, evacuated and refilled with argon three times. This reaction mixture was placed immediately in a preheated oil bath at 70 °C for 24 h. Then the Schlenk tube was taken out of the oil bath and shock cooled in an ice bath. The reaction mixture was diluted with chloroform and precipitated in 200 mL of pentane which yielded a white precipitate. This white polymer was washed with a small amount of water then dissolved in chloroform and precipitated in pentane again. This procedure was repeated twice and then purified by dialysis against water. The final copolymer was dried under a vacuum at 40 °C for 48 h.

**Quaternization Reaction of Poly(PEO-co-(BMDO-co-DMAEMA)) Copolymers.** 200 mg copolymer (samples 1-4) were dissolved in 20 mL chloroform at room temperature in a flask. 0.5 mL methanol and 2 mL ethylbromide were added to the copolymer solution. The flask was placed in a preheated oil bath at 45 °C for 40 h. Afterwards, the solvent was evaporated using a rotary evaporator. The residue was dissolved again in methanol and precipitated in pentane. This product was then purified by repeatedly dissolving in methanol and precipitating in pentane. The final product was dried at 40 °C under vacuum for 48 h.

**Hydrolytic Degradability.** In general, 100 mg copolymer was dissolved in a flask containing 10 mL of 5 wt-% KOH in distilled water. This mixture was kept at room temperature for 48 h. Then, 10 mL 10 wt-% HCl was added. This mixture was extracted with chloroform. The aqueous

phase was dried with a freeze dryer for 3 days. The remaining solid was then characterized with NMR spectroscopy.

**Enzymatic Degradability.** 200 mg copolymer was solved in PBS buffer (0.1 M, pH = 7.4) and Lipase from *Pseudomonas Cepacia* ( $10 \text{ mg}\cdot\text{mL}^{-1}$ ) with a  $0.2 \text{ mg}\cdot\text{mL}^{-1}$   $\text{NaN}_3$  solution. This mixture was then placed at  $37 \text{ }^\circ\text{C}$  with shaking for different time. Then the mixture was dried with a freezer dryer for 5 days. The remaining solid was also characterized with NMR spectroscopy and GPC.

**Cell Culture.** L929 mouse fibroblasts cells (human adenocarcinoma) for MTT assay and luciferase assay were seeded at a density of  $5.0\cdot 10^3 \text{ cells}\cdot\text{cm}^{-2}$  in dishes (10 cm diameter, Nunclon Dishes, Nunc, Wiesbaden, Germany). The incubation condition was at  $37 \text{ }^\circ\text{C}$  in a humidified 8.5%  $\text{CO}_2$  atmosphere ( $\text{CO}_2$ -Incubator, Integra Biosciences, Fernwald, Germany).<sup>24</sup> The medium was exchanged every 3 days. Cells were split after 5 days when confluence was reached.

**Cytotoxicity Test using MTT Assay.** The cell viability test (MTT assay) was performed according to the method of Mosmann.<sup>25</sup> Polymer solutions were prepared in a serum supplemented tissue culture medium (Dulbecco's modified Eagle's medium, supplemented with 10% serum, without antibiotic) containing  $2\cdot 10^{-3} \text{ M}$  glutamine and was sterile filtered ( $0.2 \text{ }\mu\text{m}$ , Schleicher&Schüll, Dassel, Germany).

24 h before the MTT assay, L929 cells ( $8000 \text{ cells}\cdot\text{well}^{-1}$ ) were seeded into 96-well plates (Nunc, Wiesbaden, Germany). On the day of MTT assay, the culture medium was replaced by  $200 \text{ }\mu\text{L}$  of a serially diluted polymer medium solution with a different concentration. After a further 24 h of incubation at  $37 \text{ }^\circ\text{C}$ , the cell culture medium was replaced with  $200 \text{ }\mu\text{L}$  medium containing  $20 \text{ }\mu\text{L}$  sterile filtered MTT (3-(4,5-dimethyl-thiazol-2-yl)-2,5-diphenyl tetrazolium bromide) (Sigma, Deisenhofen, Germany) stock solution in phosphate buffered saline (PBS) ( $5 \text{ mg}\cdot\text{mL}^{-1}$ ) in each well. The final concentration of MTT in each well was  $0.5 \text{ mg}\cdot\text{mL}^{-1}$ . After a 4 h incubation at  $37 \text{ }^\circ\text{C}$  in the dark, the medium was removed and  $200 \text{ }\mu\text{L}$  of DMSO was added in each well to dissolve the purple formazane product. The measurement was performed spectrophotometrically with an ELISA reader (Titertek Plus MD 212, ICN, Eschwege, Germany) at wavelengths of 570 nm and 690 nm. The calibration of the spectrometer to zero absorbance was performed using a culture medium without cells and to 100% absorbance was performed using control wells containing



standard cell culture medium but without polymer. The relative viability (%) related to the control wells containing the cell culture medium without polymer was calculated by the following equation:

$$\text{Relative cell growth} = ((A\ 570)\ \text{test} - (A\ 690)\ \text{test}) / ((A\ 570)\ \text{control} - (A\ 690)\ \text{control}) \quad (1)$$

Polyethyleneimine (PEI 25 kDa, BASF, Germany) was used as a positive control. The IC<sub>50</sub> was calculated using the Boltzman sigmoidal function from Microcal Origin1 v 7.0 (OriginLab, Northampton, USA). It shows the polymer concentration, which inhibits growth of half of the cells relative to non-treated control cells. The statistical analysis was conducted in a quadruplicate per group. Statistical evaluation was done using the program Sigma Stat 3.5. The one way ANOVA with Bonferroni t-test was performed for all of the MTT data.

**Preparation of Nanoparticles for Samples 3 and 4.** Nanoparticles of the samples 3 and 4 were prepared by a solvent displacement technique.<sup>26</sup> 10 mg polymer was dissolved in 1 mL of acetone or acetonitrile. Under magnetic stirring, 0.5 mL of the obtained solution was injected with an injection needle (0.6•30 mm) into 5 mL of distilled water at a constant flow rate (8.0 mL•min<sup>-1</sup>). After the injection, the suspension was stirred for about 2 h under reduced pressure to remove the organic solvent. The resulting suspension contained 1 mg•mL<sup>-1</sup> polymer concentration.

**Preparation of Polyplex with Copolymer.** A 5% glucose solution and p-DNA (plasmid-DNA) for physicochemical-experiments was used for the polyplex formation. 5% glucose is an isotonic solution. In the buffer-solutions, the surface charges of the polymers are reduced due to the higher ionic strength, and the polyplexes aggregates to larger agglomerates due to the lack of repulsion.<sup>21</sup> In terms of dimension, complex formation in a glucose solution is most suitable for transfection.<sup>27</sup> All solutions were filtered with 0.20 µm pore sized filters (Nalgene syringe filter, Sigma–Aldrich, Taufkirchen, Germany). 50 µL of p-DNA solution (40 ng•µL<sup>-1</sup>) were placed in a micro centrifuge tube. The volume of a 1 mg mL<sup>-1</sup> (based on hy-PEI 25 kDa) polymer stock solution (samples 1, 2 and 5-8) or suspension (samples 3, 4) required for a certain N/P ratio was calculated by following equation:<sup>22</sup>

$$V_{\text{DNA}} = (C_{\text{copolymer}} \times 10\ \mu\text{L} \times 330) / (C_{\text{DNA}} \times 157 \times \text{N/P})$$

C<sub>copolymer</sub> = concentration of the stock copolymer

C<sub>DNA</sub> = concentration of the stock DNA solution

A certain amount of polymer stock solution was diluted with buffer-solution to a final volume of 50  $\mu\text{L}$  in a micro centrifuge tube. The 50  $\mu\text{L}$  polymer aliquots were mixed with 50  $\mu\text{L}$  diluted p-DNA aliquots and then incubated for 30 min at room temperature for complexation and equilibrium formation.

**Zeta Potential and Size Measurements.** The zeta potential and size measurements of the polyplexes were monitored with Malvern Zetasizer Nano ZS (Marvern Instrument, Worcestershire, UK). The viscosity (0.88 mPa•s) and the refractive index (1.33) of distilled water at room temperature (RT) was used for data analysis. The measurement angle was 173° in backscatter mode. This polyplex solution was prepared and incubated at RT for 30 min before measurement. Subsequently, zeta-potential measurements were performed with the same samples after diluting 50  $\mu\text{L}$  of polyplexes with an additional 500  $\mu\text{L}$  of 5% glucose solution to a final DNA concentration of 1.82 ng• $\mu\text{L}^{-1}$  and a final volume of 550  $\mu\text{L}$ . A low volume cuvette (100  $\mu\text{L}$ ) was used for the size measurements, and the measurements of zeta potential were carried out in the standard clear capillary electrophoresis cell at room temperature. Three samples were prepared for each N/P ratio, and three measurements were performed on each sample. Each measurement of size consisted of 15 runs for 10 sec. Each measurement of zeta potential consisted of 60 runs, which was set to automatic optimization by the software.

**Confocal Laser Scanning Microscopy (CLSM).** 24 h before of the cell uptake experiment, L929-cells were seeded into 8 well-chamberslides (Lab-Tek, Rochester, NY, USA) at a seeding density of 50,000 cells•well<sup>-1</sup>. in a DMEM low glucose (PAA, Cölbe, Germany) medium, which contained 10% fetal calf serum (Cytogen, Sinn, Germany) . Before complexation with the copolymer, p-DNA was at first labeled with YOYO-1 (Invitrogen, Karlsruhe, Germany) at a weight ratio of 1:15 at room temperature for 30 min in the dark to protect fluorescent markers. The YOYO-1 labeled p-DNA was condensed with polymer at N/P 15 in a 5% glucose solution, and the polyplexes were incubated for another 20 min at room temperature. 25  $\mu\text{L}$  polyplex solution containing 0.5  $\mu\text{g}$  p-DNA and 375  $\mu\text{L}$  medium with 10% FCS were added in each well. The well-chamberslides were incubated for 4 h at 37 °C in a humidified 8.5% CO<sub>2</sub> atmosphere. After incubation, the cells were washed with a 0.5 mL PBS buffer and then fixated by 20 min of incubation with 0.1 mL of 4% paraformaldehyde in PBS. 30  $\mu\text{L}$  of a 6  $\mu\text{g}\cdot\text{mL}^{-1}$  DAPI solution (Invitrogen, Karlsruhe, Germany) was diluted with 1 mL a PBS buffer. Then 100  $\mu\text{L}$  DAPI

solutions were filled into each chamber for 20 min of incubation in the dark. Afterwards, the cells were washed again three times with a 0.5 mL PBS buffer before being fixated with Fluorsafe (Calbiochem, San Diego, USA) and covered with a No.1.5 thickness cover slip (Menzel Gläser, Braunschweig, Germany). The CLSM measurements were performed with a 385  $\mu\text{L}$  long pass filter and a band pass filter of 505-530 nm in the single-track mode (Axiovert 100M and CLDM 510 Scanning Device; Zeiss, Oberkochen, Germany). The excitation of YOYO-1 labeled DNA was performed with a 488 nm argon laser while the excitation of DAPI-stained chromosomal DNA was performed with an enterprise laser with an excitation wavelength of 364 nm.

***In Vitro* Transfection.** L929 cells were seeded with a density of 30000 cells $\cdot\text{mL}^{-1}$  in 96-well-plates (Nunc, Wiesbaden, Germany) 24 h before transfection. Each well contained 6000 cells in 0.2 mL medium. The preparation of the polyplex solution was described above. 25  $\mu\text{L}$  of polyplex solution and 175  $\mu\text{L}$  of the medium (10% serum content) were placed in each well (0.5  $\mu\text{g}$  p-DNA content). The well plates were incubated for 4 h at 37  $^{\circ}\text{C}$  under an 8.5%  $\text{CO}_2$  atmosphere. After 44 h, the cell medium was exchanged, and the cells were lysed in a 100  $\mu\text{L}$  cell culture lysis buffer (Promega, Mannheim, Germany) for 15 min at 37  $^{\circ}\text{C}$ . The quantification of luciferase activity was determined by injecting a 50  $\mu\text{L}$  luciferase assay buffer, containing 10 mM luciferin (Sigma-Aldrich, Taufkirchen, Germany), into 25  $\mu\text{L}$  of cell lysate. The relative light units (RLU) were measured with a plate luminometer (LumiSTAR Optima, BMG Labtech GmbH, Offenburg, Germany). The protein concentration was determined using a Bradford BCA assay (BioRad, Munich, Germany). The measurement of the transfection activity was performed according to the protocol provided by Promega (Madison, WI, USA). The statistical analysis was conducted in quadruplicate per group. Statistical evaluation was done using the program Sigma Stat 3.5. The One way ANOVA with Bonferroni t-test was performed for all the transfection data.

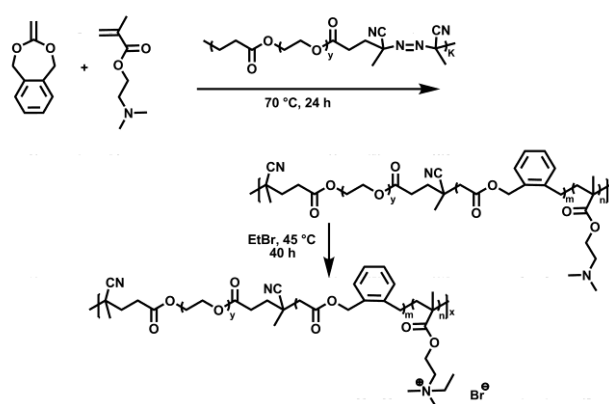
**SYBR Gold<sup>®</sup> Assay.** The polymer/p-DNA complexes were prepared at N/P = 0.25, 0.5, 1, 2, 4, 6, 8, 10 in 96 well-plates as described. 200  $\mu\text{L}$  dilutions of polymers containing 0.5  $\mu\text{g}$  DNA for the SYBR Gold<sup>®</sup> assay were performed in a water solution. After 20 min of incubation at room temperature, 20  $\mu\text{L}$  of diluted SYBR Gold<sup>®</sup> solution (5  $\mu\text{L}$  stock solution was diluted in 12.5 mL water) was added to each well and incubated for another 20 min. SYBR Gold<sup>®</sup> is light sensitive, and this experiment should be protected from direct light as much as possible. The fluorescence

was directly detected using a fluorescence plate reader (BMG Labtech, Offenburg) at 495 nm excitation and 537 nm emission. Data was analyzed with “Origin 7.0”.

**Heparin Competition Assay.** Briefly, polyplexes were prepared in solutions at different N/P-ratios like the SYBR Gold<sup>®</sup> assay. Additionally, a 20  $\mu$ L heparin (150 000 IU/g, Serva, Pharm., USP XV2, Merck, Darmstadt, Germany) solution with a concentration of 0.5 mg/mL was added into a 200  $\mu$ L polyplex solution in each well of the 96-well plate (Perkin Elmer, Rodgau-Jügesheim), where each well contained 0.5  $\mu$ g p-DNA. After a 20 min incubation of the heparin at 25°C, 20  $\mu$ L of the diluted SYBR Gold<sup>®</sup> solution (Invitrogen, Karlsruhe, Germany) were added. The measurement was performed in the same manner as for the SYBR Gold<sup>®</sup> assay.

## 7.4 Results and Discussion

Free radical polymerization of cyclic ketene acetal BMDO and vinyl monomer DMAEMA was performed with different monomer ratios in the feed at 70 °C for 24 h. PEO macro-azo-initiator with PEO 6 kDa block was used to start the reaction. The molecular weight of the PEO azo-initiator was 24 kDa. A schematic illustration of the reaction is given in Scheme 1.



Scheme 1: Synthesis route for the formation of the poly(PEG-co-(BMDO-co-DMAEMA)) and poly(PEG-co-(BMDO-co-DMAEMA))•EtBr.

The copolymer composition was determined by NMR. In the <sup>1</sup>H NMR spectrum, the characteristic peaks from both comonomers (BMDO and DMAEMA) and the PEG block from initiator were seen. The peak assignments are given in Figure 1. The signal at 3.6 ppm resulted from the PEG block (-OCH<sub>2</sub>- peak numbers 21, 22 in Fig. 1). The 2.2 ppm signal could be assigned to the two methyl groups of DMAEMA (peak 8 in Fig. 1). Aromatic signals and -OCH<sub>2</sub>- of BMDO were seen around 7 and 5 ppm, respectively (peaks 5 and 1 in Fig. 1). In the

$^{13}\text{C}$  NMR (not shown here), there was no peak observed around 110 ppm. This proved that the complete ring opening mechanism of BMDO formed ester units.<sup>23,28</sup> Peaks 1, 8, 21 and 22 were used to determine the final copolymer composition. Different copolymers with varied amounts of ester units could be synthesized by simply changing the amount of BMDO in the feed (Table 1).

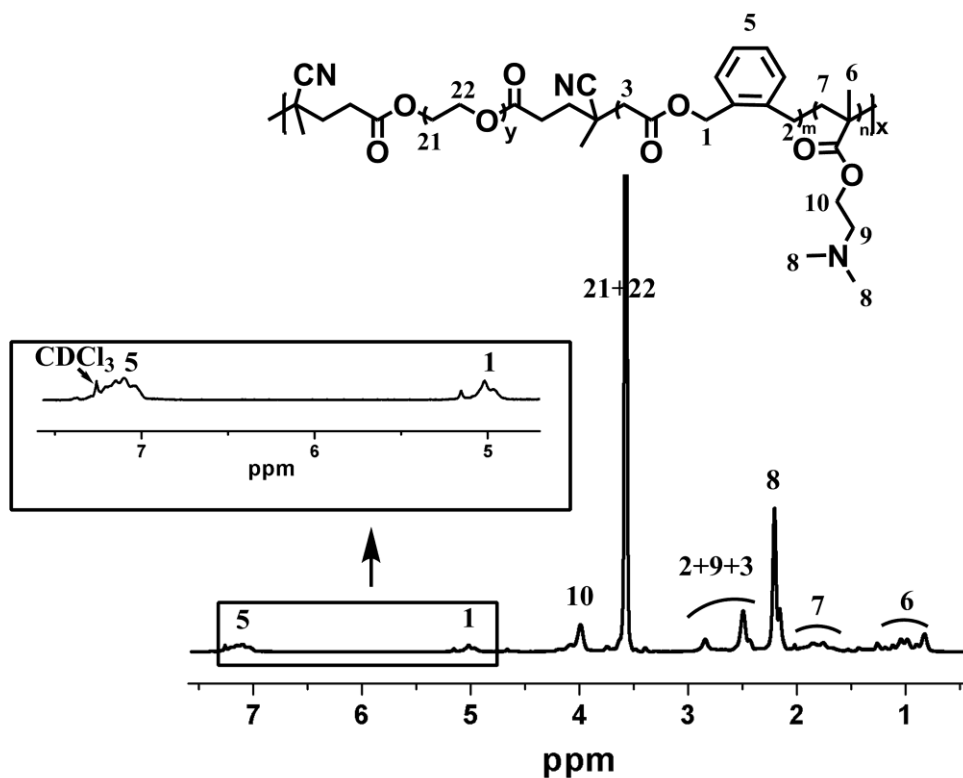


Figure 1.  $^1\text{H}$  NMR spectrum of the copolymer  $\text{p}(\text{PEG-co-poly}(\text{BMDO-co-DMAEMA}))$  with 4 mol-% BMDO in the feed (Sample 2, Table 1).

Table 1. Synthesis of the p(PEG-co-poly(BMDO-co-DMAEMA)) copolymers with PEO macro-azo-initiator at 70 °C for 24 h.

Sample Name	Feed ratio	Poylmer composition		Yield [%]	Solubility
	molar ratio	BMDO:DMAEMA	BMDO:DMAEMA		
1 <sup>a</sup>	0 : 100	0 : 100		43	Water
2	10 : 90	4 : 96		70	Water
3	50 : 50	16 : 84		45	Water <sup>b</sup>
4	90 : 10	45 : 55		32	Acetonitrile

<sup>a</sup> This reaction was carried out for 50 min; <sup>b</sup> Maximum solubility in water 0.5 mg•mL<sup>-1</sup>.

The presence of PEG blocks from the initiator in the polymer chains increased the hydrophilicity of these new copolymers and showed an improvement in the solubility behavior in water. In our previous work, the random copolymer poly(BMDO-co-DMAEMA) showed limitations for use as a gene transfection system due to insolubility in water and water miscible solvents like acetonitrile.<sup>20</sup> The use of a PEO macro-azo-initiator led to improved solubility of all of the copolymers both in water and acetonitrile, even with high amounts of BMDO (Table 1).

The copolymers (Samples 1-4; Table 1) were further quaternized with ethylbromide via SN<sub>2</sub> substitution. The properties of quaternized polymers are tabulated in the Table 2. After quaternization, the solubility of the copolymer was further improved significantly. All copolymers (even the polymer with BMDO: DMAEMA 45 : 55 molar ratio) could be solved in water immediately.

Table 2. Quaternization reaction of the p(PEG-co-(BMDO-co-DMAEMA)) with ethyl bromide at 45 °C for 40 h.

Sample	Copolymer composition	Quaternized Sample	Quaternization Yield	$M_n$	$M_w^a$	Solubility
	molar ratio BMDO:DMAEMA		[%]	[kDa]		H <sub>2</sub> O <sup>b</sup>
1	0 : 100	5	100	54	322	+
2	4 : 96	6	100	46	127	+
3	16 : 84	7	100	26	67	+
4	45 : 55	8	92	13	36	+

<sup>a</sup>  $M_n$ ,  $M_w$  were determined with water GPC; <sup>b</sup> + means soluble.

The <sup>1</sup>H NMR spectrum after the quaternization reaction showed the shifting of peaks 8 and 9 to a lower magnetic field (Figure 2). The addition of the ethyl groups (-CH<sub>2</sub>-) and -CH<sub>3</sub> protons (23, 24 in Fig 2) was also observed at a high magnetic field. The degree of quaternization was calculated using the integrals of the two methyl groups on the nitrogen atom of DMAEMA. The quaternization reaction for most of the polymers was quantitative (Table 2). The molecular weight and yield of the copolymer decreased with the increase of BMDO content. The copolymers showed molecular weights between 13 kDa and 60 kDa. The polydispersity of the polymers was high. This could be due to the formation of different multiblock copolymers with PEG block and block of a copolymer of BMDO-co-DMAEMA or amphiphilic nature of the block copolymers. Poly(PEG-co-(BMDO-co-DMAEMA•EtBr)) copolymer contained a hydrophilic part, PEO, a hydrophobic part, BMDO, and the positively charged PDMAEMA-EtBr.

This combination is a challenge for the column system and could lead to broad signal.

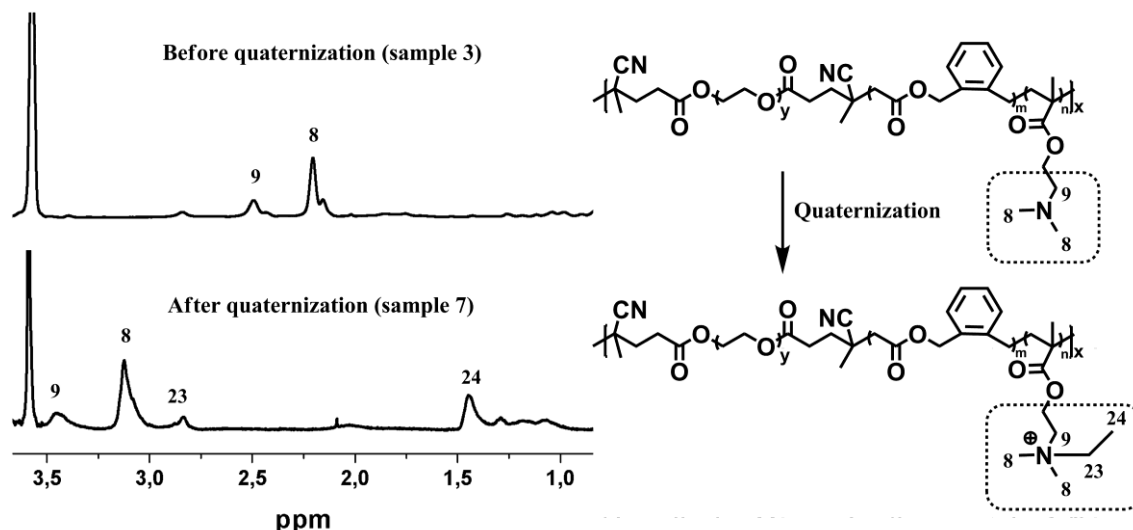


Figure 2. Comparison of NMRs of sample 3 and sample 7 (molar ratio of DMAEMA:BMDO is 15:85) before and after quaternization reaction.

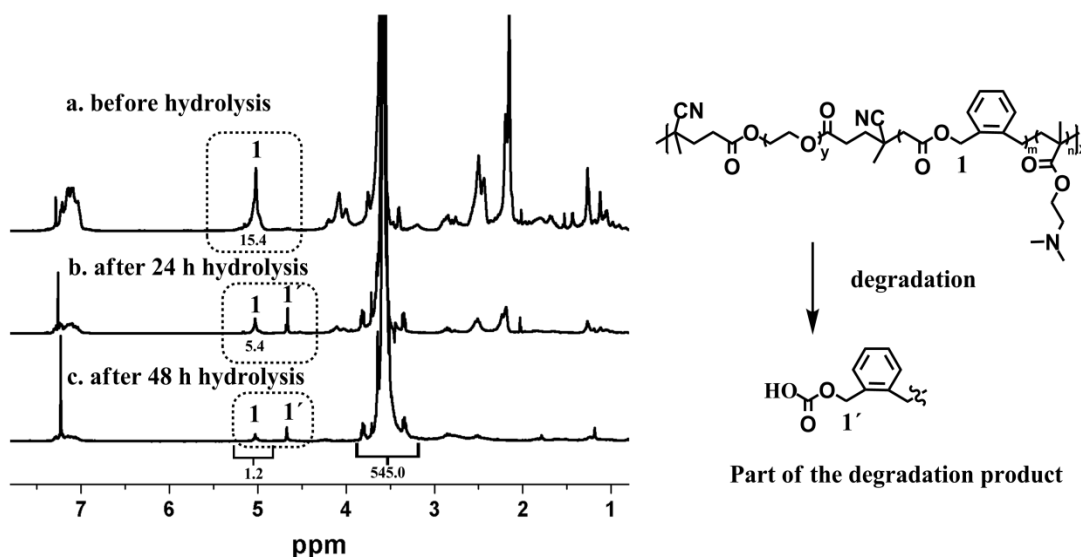


Figure 3.  $^1\text{H}$  NMR spectrum in  $\text{CDCl}_3$  before and after hydrolysis of poly(PEG-co-(BMDO-co-DMAEMA)) (sample 4): a) before hydrolysis of the copolymer with molar ratio of BMDO:DMAEMA = 45:55; b) after 24 h hydrolysis in 5 wt-% KOH solution; c) after 48 h hydrolysis in 5 wt-% KOH solution.

The hydrolytic degradation behavior of the new copolymers was studied under basic ( $\text{pH} = 9$ ) and enzymatic conditions. The degradation rate was determined by comparing peak integrals before and after hydrolysis as shown for sample 4 (Figure 3). Proton 1 at 5 ppm showed the characteristic proton peak in proximity to the ester bond of BMDO units. In Figure 3, the reduced intensity of the proton 1 signal after 24 h degradation could be observed. After 24 h, around 65% and after 48 h, nearly 93% of the ester bond was hydrolyzed.



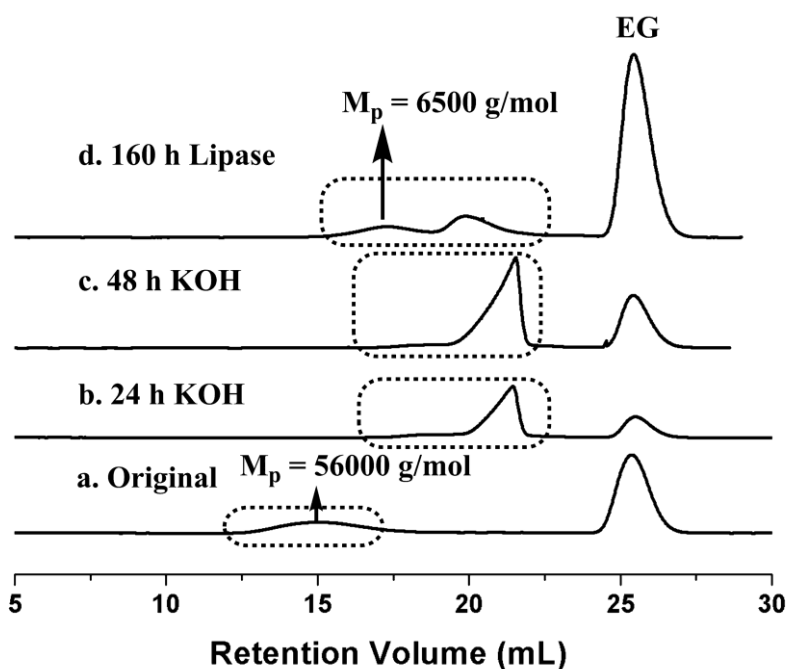


Figure 4. GPC overlays of poly(PEG-co-(BMDO-co-DMAEMA)) (sample 7, mol ratio of BMDO:DMAEMA = 16:84) a) GPC result before basic hydrolysis; b) after 24 h of basic hydrolytic degradation with 5 wt-% KOH; c) after 48 h of basic hydrolytic degradation with 5 wt-% KOH; d) after 160 h degradation with 10 mg•mL<sup>-1</sup> Lipase (from *Pseudomonas cepacia*) solution.

For the quaternized polymer (samples 5-8), the decrease of molecular weight could be observed directly via GPC. The molecular weight of the basic and enzymatic degradation products of sample 7 are shown in Figure 4. The overlay of the GPC results showed a shift in the retention volume. After 24 h of basic hydrolysis, the synthesized block copolymer was completely degraded to the low molecular weight range, which was already in the exclusion volume of the column. A significant signal in the oligomer range around 6 kDa was seen. This was the molecular weight of the PEG block left over after degradation. The SEC results showed also a clear shift to the small molecular range after 160 h degradation with an enzyme (Lipase from *Pseudomonas cepacia*) at 37 °C. A bimodal molecular curve was obtained after degradation. Because of the bimodality of the GPC curve, the  $M_p$  value of the curve was determined for comparison. The higher  $M_p$  is around 6500 g•mol<sup>-1</sup>. This also showed the molecular weight of the PEG block. The smaller molecular weight is already out of the resolution range of the column. Sample 7 had the least ester content and could still be rapidly degraded to oligomers because of the random addition of BMDO in the polymer.

The cytotoxicity of all of the synthesized copolymers was tested using L929 cells. The cell viability of the synthesized copolymer was compared with a PEI 25 kDa as the standard. A

polymer concentration between  $0.01 \text{ mg}\cdot\text{mL}^{-1}$  and  $1 \text{ mg}\cdot\text{mL}^{-1}$  was tested. The  $\text{IC}_{50}$  values are shown in a bar diagram (Figure 5). The statistical analysis shows the “probability of obtaining a test statistic” (P value) to be smaller than 0.001. Sample 4 shows the highest cell viability so we compared all the MTT result with sample 4. The statistical analysis shows also a small p value, smaller than 0.001, which indicated a good test result.

All of the synthesized copolymers have higher  $\text{IC}_{50}$  values than PEI 25 kDa, especially the unquaternized copolymers (samples 1-4). For example, sample 4 showed an  $\text{IC}_{50}$  value of  $0.18 \text{ mg}\cdot\text{mL}^{-1}$ , which was 22 times higher than PEI 25 kDa. All of the quaternized copolymers (samples 5-8) have higher cell viability than the unquaternized copolymers because of the more positively charged surface. Sample 8 showed an  $\text{IC}_{50}$  value of  $0.12 \text{ mg}\cdot\text{mL}^{-1}$ , which was 15 times higher than PEI 25 kDa.

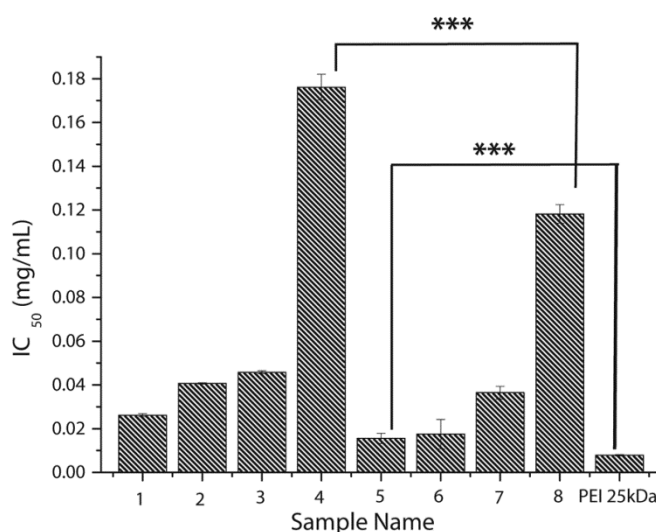


Figure 5.  $\text{IC}_{50}$  doses for different poly(PEG-co-(BMDO-co-DMAEMA)) polymers and the standard PEI 25kDa.\*\*\* means a P value smaller than 0.001.

The micrographs show the cell morphology comparison after 4 h and 24 h treatment with  $0.03 \text{ mg}\cdot\text{mL}^{-1}$  of the polymer samples 6-8 and PEI 25 kDa (Figure 6). The micrographs of the L929 cells demonstrate the higher viability of the cells treated with the BMDO copolymer as opposed to those treated with PEI. Sample 6 (pictures a and e) and PEI 25 kDa (pictures d and h) showed comparable cell morphology, while samples 7 and 8 show higher cell density and viability. After 20 further hours of incubation, the viability in all cases decreased, but the differences between samples 7 and 8 as opposed to samples 6 and PEI remained. Whereas for sample 6 and the PEI 25kDa, the cell viability was almost zero after 24 h, sample 7 showed a

reduced viability and sample 8 showed a minimal decrease in viability. All of these results clearly show significantly reduced toxicity of the polymers compared to the accepted gold standard PEI 25kDa.

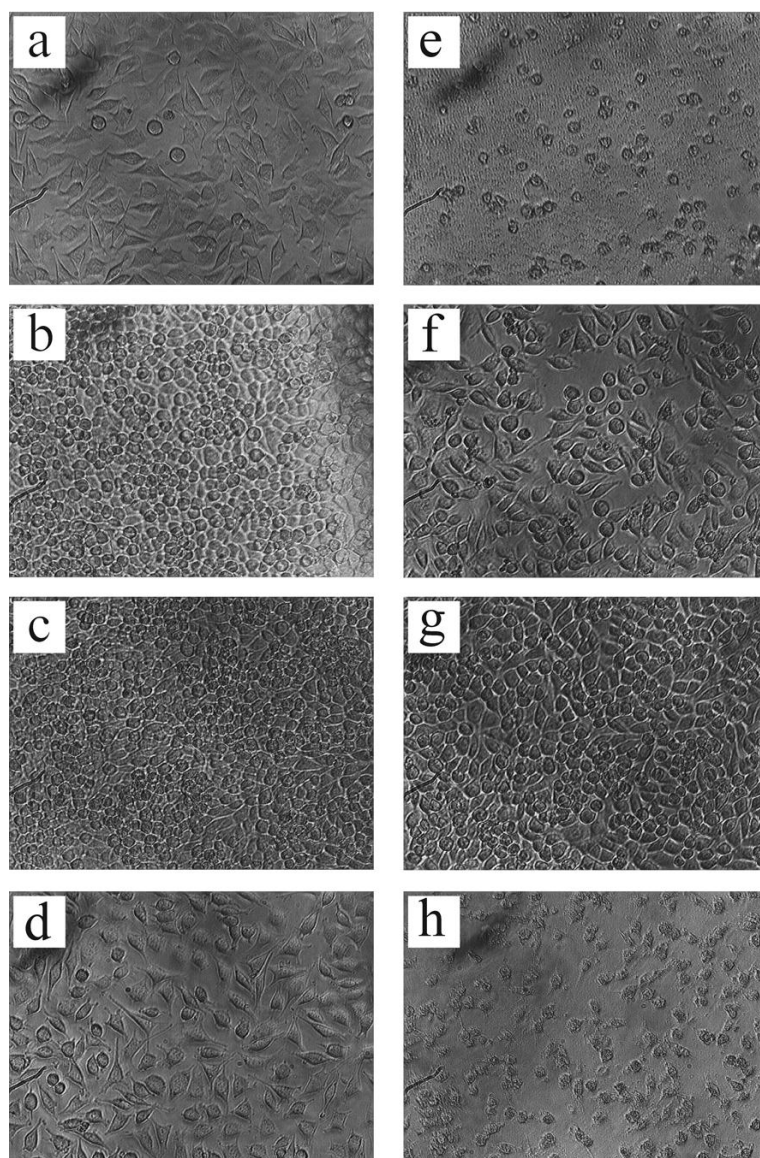


Figure 6. 40×Micrographs of the L929 cells, which were incubated with polymers for 4 h and 24h, respectively. The concentration of the polymers was  $0.03 \text{ mg}\cdot\text{mL}^{-1}$ . a) with sample 6 for 4 h; b) with sample 7 for 4 h; c) with sample 8 for 4 h; d) with PEI 25 kDa for 4 h; e) with sample 6 for 24 h; f) with sample 7 for 24 h; c) with sample 8 for 24 h; d) with PEI 25 kDa for 24 h.

The hydrodynamic diameters of the polymer with a p-DNA complex at different N/P ratio were measured at room temperature (Figure 7). This size measurement was performed for all of the stable polyplexes at N/P ratios between 0 and 20. It has been reported that the acceptable size of polyplex for endocytosis are less than 250 nm.<sup>29,30</sup>

The polydispersities of the polyplexes were all smaller than 0.3. All of the polyplex sizes were less than 250 nm, and had already reached this size at an N/P ratio of 5. The size of the polyplex depends on the N/P ratios and the polymer composition. With the increase of the N/P ratio, the polyplex size decreased. With the increase of the PEG and BMDO part, the polyplex size

decreased as expected. That can be explained by the shielding effect of PEG.<sup>29</sup> According to the hydrodynamic size of the polyplexes, these copolymers are suitable candidates for gene transfections.

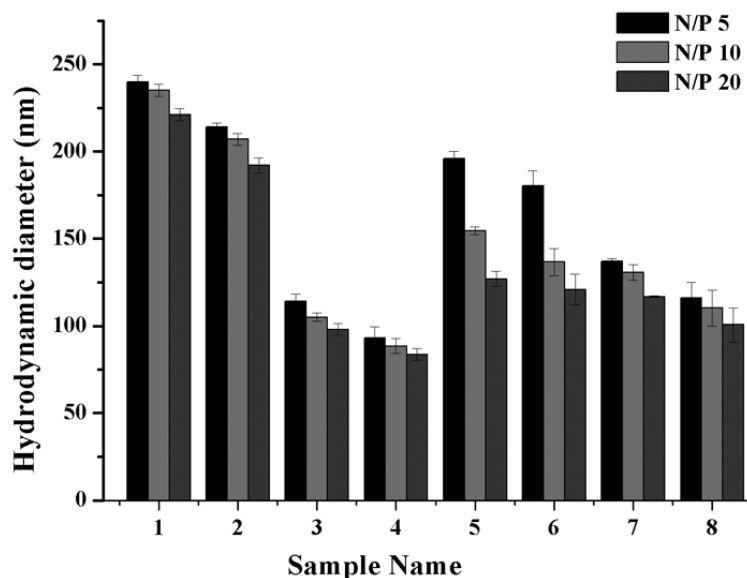


Figure 7. Size of polyplexes formed with plasmid DNA (samples 1-8) at different N/P ratios by DLS (dynamic light scattering) measurement.

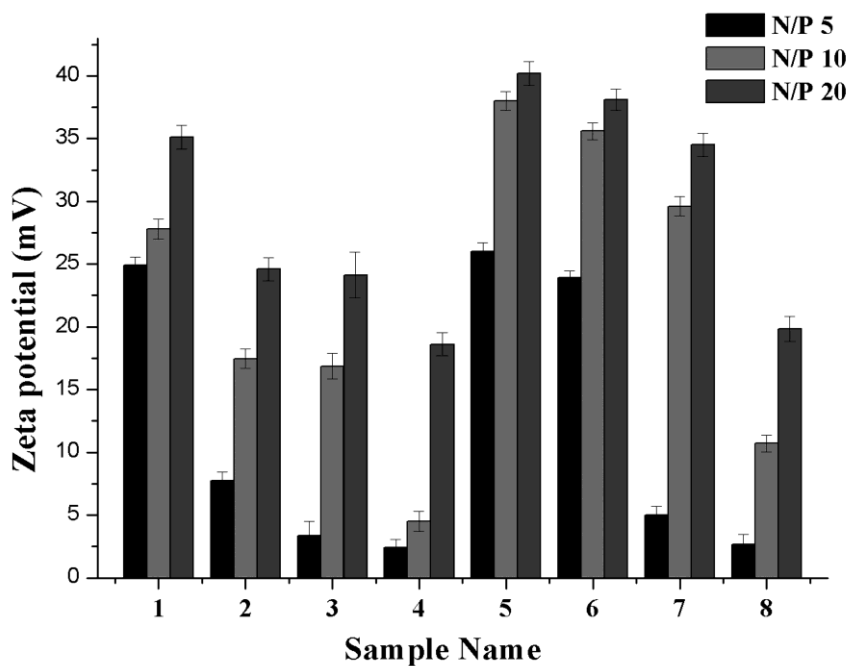


Figure 8. The zeta potential of polyplexes (samples 1-8 with plasmid DNA) at different N/P ratios. Values are the means of 6 runs.

The zeta potential of the polyplex was determined at the N/P ratios of 5, 10, and 20 (Figure 8). The zeta potential increased with the increasing N/P ratio. The polyplex with quaternized

polymer poly(PEG-co-(BMDO-co-DMAEMA))•EtBr showed higher zeta potential than the unquaternized polymer poly(PEG-co-(BMDO-co-DMAEMA)). All of the p-DNA polyplexes had positive surface charges which are considered to facilitate uptake by negatively charged cell membranes.<sup>30,31</sup>

For DNA transfection, the polyplex should be internalized into the cells. The CLMS was performed to see if the polyplex was able to reach the nucleus. CLSM images of the L929 cells incubated with fluorescence labeled copolymer p(PEO-co-(BMDO-co-DMAEMA)) DNA complexes for 4 h are shown in Figure 9.

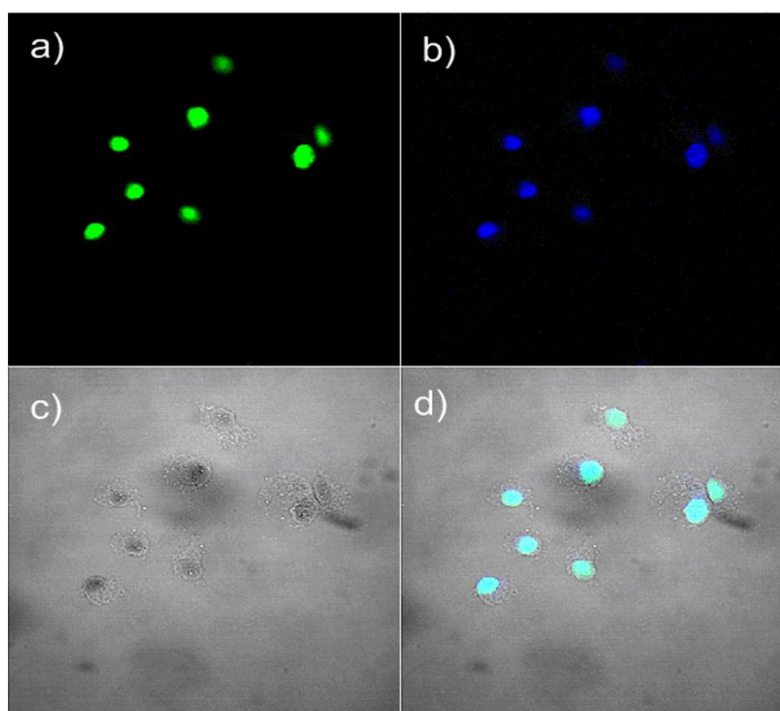


Figure 9. Confocal images with L929 cells for sample 8 at N/P ratio 10: a) p-DNA was labeled with YOYO and showed in green; b) DAPI-stained nuclei are shown in blue; c) background without any fluorescence detection; d) overlay of the YOYO-stained p-DNA and DAPI-stained nuclei.

According to the CLSM pictures for sample 8, the high efficiency of cellular uptake could be observed (Figure 9). All of the polyplexes with p-DNA were internalized into the cells nuclei. High fluorescence intensity of plasmid-420 DNA in the nucleus could be observed. This proves that the synthesized copolymer was a promising candidate for DNA transfection.

Transfection experiments with plasmid-DNA were performed with all the DMAEMA based polymers (samples 1-8) (Figure 10). PEI 25kDa was used as the positive control for this experiment. First we compared the synthesized polymer transfection efficiency with PEI 25kDa. Then we compared the transfection efficiency at N/P 5 for all the samples. The statistical analysis

for the unquaternized polymers shows the P value to be smaller than 0.01, which indicated a relative good test results.

All of the unquaternized polymers (samples 1-4) showed successful transfection and the same tendency. The p-DNA transfection efficiency increased with the increasing of N/P ratio until a best N/P ratio and decreased after the best transfection efficiency was reached. At N/P 1, almost no polymers showed significant transfection, even PEI 25kDa, because at N/P 1, the p-DNA could not be condensed completely within the polycations. Surprisingly, sample 2 with the 4% BMDO began to show low transfection while the other polymers were silent. Samples 1 and 2 have the advantage of a higher DEMAEMA concentration and, therefore, the higher density of positive charges for condensing the negatively charged p-DNA. Compared to samples 3 and 4, they showed a better transfection in the luciferase experiment. However, sample 1 only showed a good transfection efficiency at a higher N/P 20 because the polyplexes of this polymer with p-DNA were larger than the others and the size was only less than 230 nm if the N/P ratio was over 10. Compared to samples 1, 2 and 4, sample 3 showed the best transfection at N/P 5, which is a standard for animal testing, at which the polymers were not yet so toxic. The particle size of the polyplex with sample 3 was also relatively low and was even under 120 nm at N/P 5. Additionally, sample 3 had a lower surface charge than samples 1 and 2, which offers a long term circulation in the blood in the *in vivo* experiment. The ester bond in BMDO could be degraded under basic and enzymatic condition. Sample 3 had a higher BMDO content than samples 1 or 2, which means more potential biodegradability than sample 1 or 2. Therefore, although the *in vitro* luciferase assay showed no greater p-DNA transfection efficiency with sample 3 than samples 1 and 2, we believe that sample 3 will be a highly potent gene delivery agent.

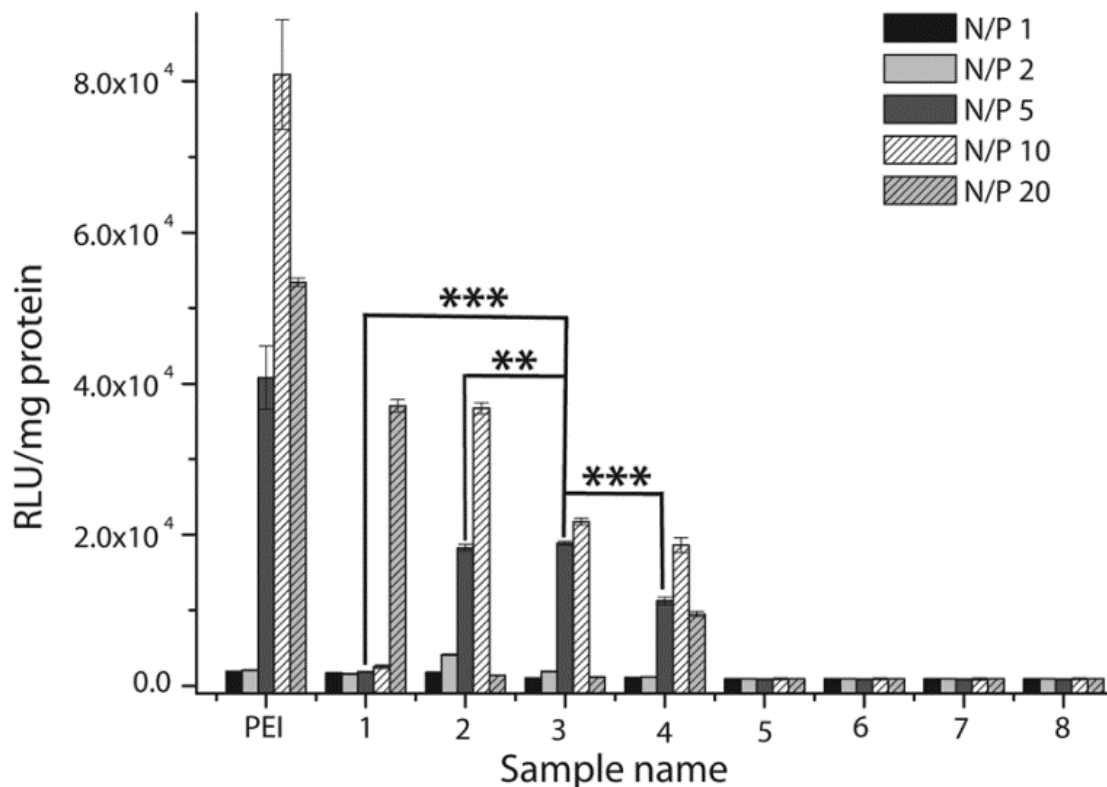


Figure 10. Transfection result of plasmid-DNA-polymer-complexes with L929 cells at different N/P ratio. \*\*\*means a P value smaller than 0.001, \*\* means a P value smaller than 0.01.

It is known that the molecular weight, rigidity and charge density of the pDMAEMA influence the transfection efficiency.<sup>32</sup> All of these physical properties could be regulated to balance the protection and release of the DNA. Among these factors, the stability of polyplexes was believed to play a more important role than others.<sup>33</sup> The stability of the polyplex is dependent on the charge density of the polymer. From the zeta potential, we saw that the quaternized samples (samples 5-8) showed, in general, a higher zeta potential than unquaternized samples (samples 1-4). The CLSM result showed that all of the quaternized copolymer polyplexes (samples 6-8) reached the cell nucleus. The cytotoxicity of the quaternized polymers was higher than the unquaternized polymer due to the higher density of the positive charges on the polymer surface. A high density of positive charges on the polymer surface may cause very strong electrostatic interactions, which may lead to polyplexes that are too stable to release plasmid DNA into the cytosol or into the cell nucleus, therefore no expression of the target gene could be observed. That could be the reason for the completely negative transfection results for the quaternized polymer samples. The quaternized samples had a much higher charge density than the unquaternized samples. That led to a much more stable complex with DNA and higher toxicity of the polymers.

To analyze the stability of the polyplexes, a further SYBR Gold® and heparin competition assay was performed.

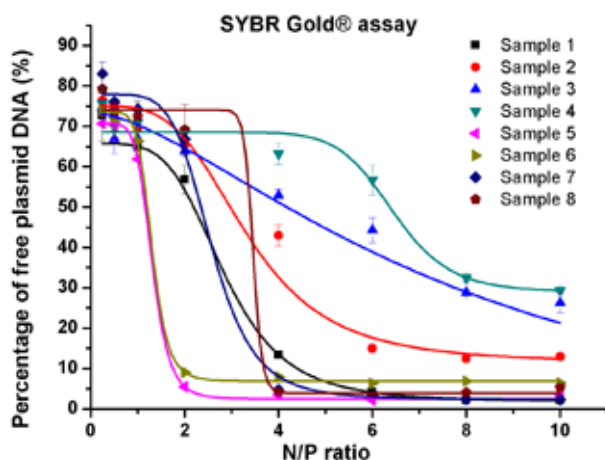


Figure 11. Complexation behavior of p(PEG-co-(BMDO-co-DMAEMA) (samples 1-8) measured by SYBR Gold® intercalation of residual free plasmid DNA increasing N/P ratio.

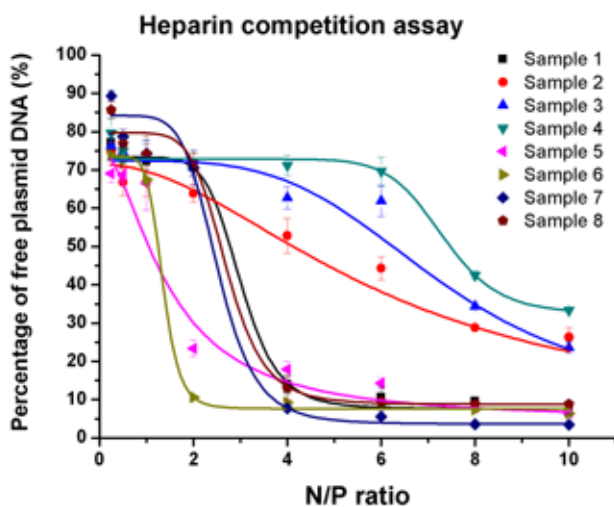


Figure 12. Release profiles of plasmid DNA from polyplex of samples 1-8 by increasing N/P ratio.

The SYBR® Gold assay showed the different condensation abilities of the polymers with plasmid-DNA. The affinity of plasmid-DNA with a polymer was increased by increasing the DEMAEMA content, and plasmid DNA could be condensed very well from N/P 6 with all of the quaternized polymers (samples 5, 6, 7, 8) (Figure 11). Compared to the quaternized polymer, the condensation ability with plasmid DNA of the unquaternized polymers was lower. However, sample 1 also showed good condensation with plasmid DNA up to N/P = 6 because of the high



DEMAEMA content, although it was unquaternized and had a less positive surface charge. The other unquaternized polymers (samples 2, 3, 4) could not completely reach a complete p-DNA condensation with an increasing N/P ratio, especially sample 4. The stability of polyplexes against competing polyanions is also an important parameter for a gene delivery system, especially for *in vivo* experiment, because the stability of the polyplexes can be strongly weakened by the presence of serum in blood.<sup>34</sup> The process of gene material complexation within polycations is entropy driven and can be significantly impaired by the presence of other polyions like heparin.<sup>35</sup> Differences in the stability against polyions were found to follow the same trend as the Sybr gold assay, but the polyplexes formed with quaternized copolymers were less impaired by heparin (Figure 12). That means the condensation of the plasmid DNA with quaternized copolymers was complete. The plasmid DNA was very difficult to be released if delivered into the nuclei. Therefore, no successful transfection was observed in the *in vitro* transfection experiment for the quaternized polymers, in contrast to the successful transfection with unquaternized polymers (Figure 13).

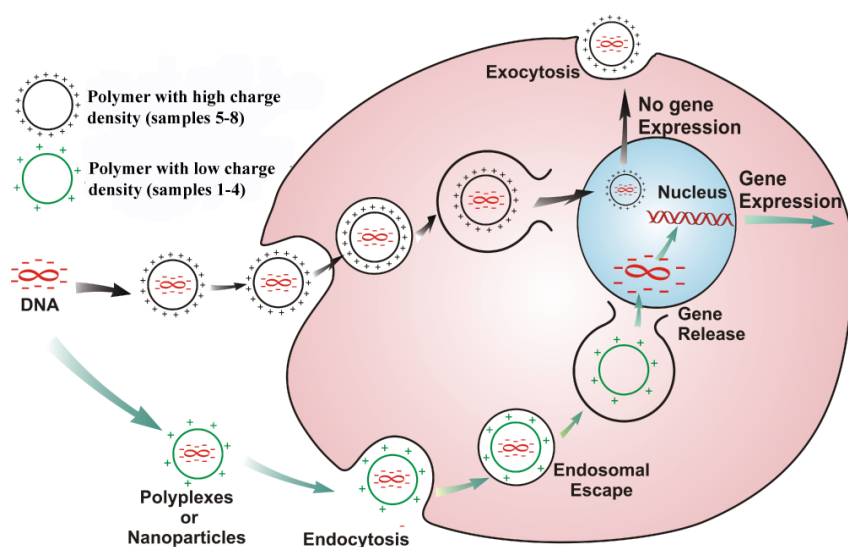


Figure 13. *In vitro* pDNA transfection mechanism with the synthesized polymer p(PEG-co-(BMDO-co-DMAEMA) (samples 1-4) and p(PEG-co-(BMDO-co-DMAEMA)•EtBr (samples 5-8).

## 7.5 Conclusions

Novel degradable and biocompatible poly(PEG-co-(BMDO-co-DMAEMA) for gene transfection were successfully synthesized via free radical polymerization. The solubility and the IC<sub>50</sub> values of the copolymers were significantly improved by bringing hydrophilic PEG blocks into the polymer backbone. The toxicity of all the polymers was much lower than the positive control

PEI. The unquaternized copolymers showed a higher cell viability than the quaternized copolymers as well as positive results in p-DNA transfection.

## 7.6 References

- (1) Dalglish, A. *Gene Ther.* **1997**, *4*, 629-630.
- (2) Anderson, W. F. *Science* **1992**, *256*, 808-813.
- (3) Fakhrai, H.; Dorigo, O.; Shawler, D. L.; Lin, H.; Mercola, D.; Black, K. L.; Royston, I.; Sobol, R. E. *Proc. Natl. Acad. Sci. U.S.A.* **1996**, *93*, 2909-2914.
- (4) Spear, M. A.; Herrlinger, U.; Rainov, N.; Pechan, P.; Weissleder, R.; Breakefield, X. O. *J. NeuroVirol.* **1998**, *4*, 133-147.
- (5) Takamiya, Y.; Short, M. P.; Ezzeddine, Z. D.; Moolten, F. L.; Breakefield, X. O.; Martuza, R. L. *J. Neurosci. Res.* **1992**, *33*, 493-503.
- (6) Azzam, T.; Domb, A. J. *Curr. Drug Delivery* **2004**, *1*, 165-193.
- (7) Kabanov, A. V.; Felgner, P. L.; Seymour, L. J. In *Self-assembling complexes for gene delivery - From Laboratory to Clinical Trial*; Wiley: NY, 1998; pp. 115-167.
- (8) Felgner, P. L.; Heller, M. J.; Lehn, P.; Behr, J. P.; Szoka, J. F. C. In *Am. Chem. Soc.*; Oxford University Press: Washington, USA, 1996; pp. 177-190.
- (9) Garnett, M. C. *Crit. Rev. Ther. Drug Carrier Syst.* **1999**, *16*, 147-207.
- (10) Rolland, A. In *Advanced Gene Delivery*; Harwood Academic Publishers: The Netherlands, 1999; pp. 103-190.
- (11) Chesnoy, S.; Huang, L. *STP Pharma Sci.* *9*, 5-12.
- (12) Neu, M.; Fischer, D.; Kissel, T. *J. Gene Med.* **2005**, *7*, 992-1009.
- (13) Cherng, J. Y.; Wetering, P. van de; Talsma, H.; Daan, J. A. C.; Hennink, W. E. *Pharm. Res.* **1996**, *13*, 1038-1042.
- (14) Arigita, C.; Zuidam, N. J.; Crommelin, D. J. A.; Hennink, W. E. *Pharm. Res.* **1999**, *16*, 1534-1541.
- (15) Van de Wetering, P.; Cherng, J. Y.; Talsma, H.; Hennink, W. E. *J. Controlled Release* **1997**, *49*, 59-69.
- (16) Jones, R. A.; Poniris, M. H.; Wilson, M. R. *J. Controlled Release* **2004**, *96*, 379-391.
- (17) Verbaan, F. J.; Klein Klouwenberg, P.; Van Steenis, J. H.; Snel, C. J.; Boerman, O.; Hennink, W. E.; Storm, G. *Int. J. Pharm.* **2005**, *304*, 185-192.
- (18) Cherng, J. Y.; Talsma, H.; Verrijck, R.; Crommelin, D. J.; Hennink, W. E. *Eur. J. Pharm. Biopharm.* **1999**, *47*, 215-224.
- (19) You, Y.-Z.; Manickam, D. S.; Zhou, Q.-H.; Oupick y, D. *J. Controlled Release* **2007**, *122*, 217-225.
- (20) Agarwal, S.; Ren, L.; Kissel, T.; Bege, N. *Macromol. Chem. Phys.* **2010**, *211*, 905-915.
- (21) Petersen, H.; Fechner, P. M.; Martin, A. L.; Kunath, K.; Stolnik, S.; Roberts, C. J.; Fischer, D.; Davies, M. C.; Kissel, T. *Bioconjugate Chem.* **2002**, *13*, 845-854.
- (22) Zheng, M.; Liu, Y.; Samsonova, O.; Endres, T.; Merkel, O.; Kissel, T. *Int. J. Pharm.* **2011**.
- (23) Wickel, H.; Agarwal, S. *Macromolecules* **2003**, *36*, 6152-6159.
- (24) Samsonova, O.; Pfeiffer, C.; Hellmund, M.; Merkel, O.; M.; Kissel, T. *Polymers* **2011**, *3*, 693-718.
- (25) Mosmann, T. *J. Immunol. Methods* **1983**, *65*, 55-63.

- (26) Beck-Broichsitter, M.; Thieme, M.; Nguyen, J.; Schmehl, T.; Gessler, T.; Seeger, W.; Agarwal, S.; Greiner, A.; Kissel, T. *Macromol. Biosci.* **2010**, *10*, 1527-35.
- (27) Merkel, O. M.; Zheng, M.; Mintzer, M. A.; Pavan, G. M.; Librizzi, D.; Maly, M.; Höffken, H.; Danani, A.; Simanek, E. E.; Kissel, T. *J. Controlled Release* **2011**, *153*, 23-33.
- (28) Wickel, H.; Agarwal, S.; Greiner, A. *Macromolecules* **2003**, *36*, 2397-2403.
- (29) Liu, Y.; Steele, T.; Kissel, T. *Rapid Commun.* **2010**, *31*, 1509-1515.
- (30) Kunath, K.; Merdan, T.; Hegener, O.; Häberlein, H.; Kissel, T. *J. Gene Med.* **2003**, *5*, 588-599.
- (31) Grayson, A. C. R.; Doody, A. M.; Putnam, D. *Pharm. Res.* **2006**, *23*, 1868-1876.
- (32) Grigsby, C. L.; Leong, K. W. *J. R. Soc., Interface* **2010**, *7*, 67-82.
- (33) Mao, S.; Neu, M.; Germershaus, O.; Merkel, O.; Sitterberg, J.; Bakowsky, U.; Kissel, T. *Bioconjugate Chem.* **2006**, *17*, 1209-1218.
- (34) Merkel, O. M.; Librizzi, D.; Pfestroff, A.; Schurrat, T.; Buyens, K.; Sanders, N. N.; De Smedt, S. C.; B é M.; Kissel, T. *J. Controlled Release* **2009**, *138*, 148-159.
- (35) Bronich, T.; Kabanov, A. V.; Marky, L. a *J. Phys. Chem. B* **2001**, *105*, 6042-6050.

## 8 SUMMARY

### 8.1 Summary

In this thesis, biodegradable non-viral polymeric nucleic acids delivery vectors were characterized concerning biophysicochemical parameters.

In the first part of this research (*chapter 2*), to answer the questions: why the principle of DNA transfection cannot be directly applied for siRNA transfection, we investigated the complexation and aggregation mechanism of nucleic acids/polycations on the atomic and molecular scale. The MD and ITC data showed us the different nature and the different hierarchical mechanism related polycation-siRNA and polycation-pDNA complexes. The results of dye quenching assays indicated a biphasic behavior of siRNA binding with polycations where molecular reorganization of the siRNA within the polycations occurred at lower N/P-ratios (nitrogen/phosphorus). Additionally, heparin assays showed that the stability of siRNA/polymer complexes is especially good at a rather lower N/P-ratio of 2. Interestingly, with the following study of the relationship between nucleic acids/polycations aggregation mechanism and *in vitro* siRNA delivery efficiency, which is performed by RT-PCR and CLSM, we found that the copolymer showed the best knockdown effect with siRNA at N/P=2. All our results emphasized one point: lower N/P-ratios are especially effective for polycationic nanocarrier-based siRNA delivery, because siRNA aggregation results in a more uniform and stable complex formation at low N/P ratios already, which lead to increased siRNA delivery efficiency. This could have broad implications for the delivery of siRNA as less toxic and yet efficient delivery systems have been the bottle-neck for the translation of this promising approach into the clinical arena.

In *chapter 3*, novel biodegradable amphiphilic copolymers hy-PEI-g-PCL-b-PEG were prepared by grafting PCL-b-PEG chains onto hyper-branched poly(ethylene imine) as non-viral gene delivery vectors. With the question: how can the graft densities of PCL-b-PEG chains influence the *in vitro* DNA delivery efficiency, our study began with the characterization of physico-chemical properties and expected that with the introducing of the grafted PCL-b-PEG chains, the *in vitro* DNA delivery efficiency with the grafted PCL-b-PEG chains could be improved. In the following study, no correlation was shown between the sizes of polyplexes and transfection efficiencies, while

buffer-capacity, cytotoxicity and zeta-potential turned out to be the key factors for the explanation of the results of the gene transfer experiments. Of all the experimental results, buffer-capacity has almost exactly the same tendency as transfection efficiency. We therefore assume that in all processes of DNA transfection, the endosomal escape has a really important and rate-limiting role. This opens new perspectives to advance the rational design of new gene delivery systems.

The further investigation of these biodegradable grafted amphiphilic copolymers hy-PEI-g-(PCL-b-PEG)<sub>n</sub> as potential siRNA delivery vectors was showed in *chapter 4*, which is the direct continuation of *Chapter 3*. The purpose in this section was to enhance the *in vivo* blood circulation time and siRNA delivery efficiency of biodegradable copolymers polyethylenimine-graft-polycaprolactone-block-poly(ethylene glycol) (hyPEI-g-PCL-b-PEG) by introducing high graft densities of PCL-PEG chains. The questions which this work was based on, such as zeta size, siRNA complexation efficiency, siRNA protection against competing polyanions, *in vitro* RNAi, pharmacokinetic issues of *in vivo* administered siRNA, *in vivo* biodistribution and *in vivo* stability of polyelectrolyte complexes are elucidated. Our study indicated that the effect of PEG on prolonged circulating depends not only on its content in a copolymer (length or percentage), but also on the structure or the shape of the amphiphilic copolymer. We demonstrated that polymeric micelles, which are formed with amphiphilic block polymers have advantages especially for *in vivo* siRNA delivery, and that the graft density of the amphiphilic chains can enhance the blood circulation, which is a key parameter to promote the development of safe and efficient non-viral polymeric siRNA delivery *in vivo*.

Although the copolymers hy-PEI-g-(PCL-b-PEG)<sub>n</sub> showed positive results as pDNA and siRNA delivery vectors in *chapter 3 and 4*, the delivery of gene materials with these non-targeted copolymers is achieved mainly passively by the passive targeting. Therefore, to optimize these polymeric gene delivery vectors with targeting function, in *chapter 5*, folate conjugated PEI-g-PCL-b-PEG was examined for targeted gene delivery. Lower cytotoxicity was observed for PEI-g-PCL-b-PEG-Fol than PEI-g-PCL-b-PEG and the cellular uptake of polyplexes was enhanced by PEI-g-PCL-b-PEG-Fol in FR over-expressing KB cells compared with those by PEI-g-PCL-b-PEG. Importantly, this enhancement was inhibited by free folic acid, while did not appear in FR-negative A549 cells. All these suggested the specific cell uptake of PEI-g-PCL-b-PEG-Fol/pDNA polyplexes via folate receptor-mediated endocytosis. Consequently,

PEI-*g*-PCL-*b*-PEG-Fol/pDNA polyplexes revealed higher transfection than PEI-*g*-PCL-*b*-PEG/pDNA. Additional studies on gene transfection *in vivo* and utilizing these described folate-conjugated copolymers for targeted siRNA delivery are in proceeding.

In *Chapter 6*, the novel siRNA delivery systems based on hyperflexible generation 2-4 triazine dendrimers was identified by correlating physico-chemical and biological *in vitro* and *in vivo* properties of the complexes with their thermodynamic interaction features simulated by molecular modeling and the influence of dendrimer flexibility has systematically been investigated and discussed. In this study, molecular modeling helped to understand experimental parameters based on the dendrimers' structural properties and molecular imaging non-invasively predicted the *in vivo* fate of the complexes, both techniques can efficiently support the rapid development of safe and efficient siRNA formulations that are stable *in vivo*.

In *Chapter 7*, novel degradable and biocompatible poly(PEG-*co*-(BMDO-*co*-DMAEMA) for gene transfection were successfully characterized. The physicochemical properties and *in vitro* pDNA delivery efficiency of these polymers were characterized. The unquaternized copolymers showed higher cell viability than the quaternized copolymers as well as positive results in p-DNA transfection.

## 8.2 Perspectives

In continuation of the projects described, a number of further developments are possible. *Chapter 2* is the about study of the complexation and aggregation mechanism of nucleic acids/polycations on the atomic and molecular scale. Although we have introduced the novel synergistic use of molecular modeling, molecular dynamics simulation, isothermal titration calorimetry and other characterization techniques, the novel research methods for the binding and aggregation mechanism of nucleic acids/polycations are still needed. For example, more detection about the nucleic acids localization with in polyplexes will also be very necessary, which depends exactly on the new development of microscopical methods.

In *chapter 3*, the copolymers were designed to decrease the toxicity of hyPEI. But after the study of buffer-capacity, we find that the endosomal escape has really a very important role of all of the

gene material delivery process. And a design or optimization of the molecule structure for a higher buffer-capacity might be very meaningful in the future.

*Chapter 3-5* described the copolymer  $\text{hy-PEI-g-(PCL-b-PEG)}_n$  as novel gene delivery vectors. In these studies, only copolymers with short PCL segments (weight of 570) were studied. It is still very interesting to discuss the influence of long PCL segments in this structure.

In *chapter 5*, folate conjugated PEI-g-PCL-b-PEG showed improved targeted pDNA delivery. These targeted vectors described above are certainly investigating for siRNA delivery *in vitro* and *in vivo*, which is especially meaningful for the development of pulmonary siRNA delivery.

Moreover, cationic quantum dots (QDs) is a promising method to study the intracellular trafficking, unpacking, and gene silencing. In the following study about the the intracellular trafficking and unpacking mechanism, gene delivery vectors can be labeled with QDs. Fluorescence resonance energy transfer (FRET) can be achieved between fluorescence-labeled siRNA and QDs-conjugated polymers in the complex. If the siRNA is not condensed within the polymeric vectors, the FRET effect should not be detected anymore, which describes indirectly the unpacking or release of the siRNA from the polymers.

These multifunctional gene delivery systems with higher siRNA protection and loading efficiency, better biocompatibility and transfection efficiency, targeting effect and long circulating time is still challenging the area in cancer gene delivery. The “magic bullet” vision of Paul Ehrlich over 100 years ago is beginning to be realized, and with continued research and development.

### **8.3 Zusammenfassung**

In der vorliegenden Arbeit wurden neue bioabbaubare Polymere für den Transport von Nucleinsäuren bezüglich ihrer biophysikochemischen Eigenschaften charakterisiert. Im ersten Teil dieser Arbeit (Kapitel 2) untersuchten wir die Komplexbildung und den Aggregationsmechanismus von Nucleinsäuren mit Polykationen auf atomarer und molekularer Ebene unter Verwendung der molekularen Modellierung, molekulardynamischen Simulation, isothermen Titrationskalorimetrie und anderen Charakterisierungsmethoden, um die Frage zu beantworten, warum ein guter pDNA-Vektor nicht unbedingt eben so gut für siRNA funktioniert. Diese Daten zeigten uns sehr unterschiedliche natürliche Eigenschaften und den hierarchischen Mechanismus der Komplexbildung von Polykationen/siRNA und Polykationen/pDNA. Mit der folgenden

Untersuchung der Beziehung zwischen dem Nukleinsäuren/Polykationen-Aggregationsmechanismus und der in-vitro-siRNA-Delivery-Effizienz, konnten wir zeigen, dass niedrige N/P-Verhältnisse (Stickstoff/Phosphat) exzellente siRNA-Delivery-Effizienz ermöglichen, dies wurde aber in den bisherigen Untersuchungen für siRNA-Transfektion mit Polykationen vernachlässigt.

In Kapitel 3 wurden neue bioabbaubare, amphipathische Copolymere hy-PEI-g-PCL-b-PEG durch die Kupplung von PCL-b-PEG-Ketten auf dem hyper-verzweigten Poly(ethylenimin) als nicht-virale Gentransfer-Vektoren charakterisiert. Der Einfluss der Kupplungsdichten von PCL-b-PEG-Ketten auf physikalisch-chemische Eigenschaften, DNA-Komplexierung und Transfektionseffizienz wurde untersucht und diskutiert. In dieser Studie wurde keine Korrelation zwischen den Größen der Polyplexe und Transfektionseffizienz gezeigt, während sich die Puffer-Kapazität, Zytotoxizität und Zeta-Potential als die entscheidenden Faktoren für Erklärung der Ergebnisse der Gentransfektion erwiesen. Von allen experimentellen Ergebnissen, zeigte die Puffer-Kapazität fast genau die gleiche Tendenz wie die Transfektionseffizienz. Wir gehen daher davon aus, dass in allen Prozessen der DNA-Transfektion, der „endosomal escape“ eine wichtige und geschwindigkeitsbestimmende Rolle spielt.

Weitere Untersuchungen dieser biologisch abbaubaren amphipathischen Copolymere hy-PEI-g-(PCL-b-PEG)<sub>n</sub> als potentielle siRNA-delivery Vektoren wurden in Kapitel 4 berichtet. Der Zweck der Untersuchungen dieses Kapitels war, die *in vivo* Blutzirkulationszeit und die siRNA Transfektionseffizienz der bioabbaubaren Copolymere hy-PEI-g-(PCL-b-PEG)<sub>n</sub> zu erhöhen. Unsere Studie zeigte, dass die Wirkung von PEG auf längere Blutzirkulationszeit nicht nur vom prozentualen Inhalt in einem Copolymer abhängt, sondern auch von der Struktur oder Form des Copolymers. Die Polymere-Mizellen, die mit amphipathischen Blockpolymeren entstehen, haben Vorteile für siRNA Transfektion z.B. effektive *in vivo* siRNA Transfektion und verlängerte Blutzirkulation. Im Kapitel 5, wurde das mit der Folsäure konjugierte Polymer PEI-g-PCL-b-PEG-Fol bezüglich seiner biophysikochemischen Eigenschaften charakterisiert. Geringere Zytotoxizität wurde bei PEI-g-PCL-b-PEG-Fol beobachtet. Die zelluläre Aufnahme wurde durch die Kupplung von Folsäure verbessert. Wichtig ist, dass diese Verbesserung durch freie Folsäure gehemmt wurde, und dass diese Verbesserung auch nicht in Folat-Rezeptor-negativen A549-Zellen beobachtet wurde. Alle Daten bestätigen die Aufnahme der



PEI-g-PCL-b-PEG-Fol/pDNA Polyplexe über Folat-Rezeptor-vermittelte Endozytose. Die *in vitro* DNA Transfektionseffizienz wurde deutlich erhöht durch die Kupplung von Folsäure. Die zusätzlichen Untersuchungen *in vivo* und Nutzung dieser beschriebenen Folat-konjugierten Copolymeren für gezielte siRNA Transfektion sind in Bearbeitung.

In Kapitel 6 wurden hyperflexible Triazin-Dendrimere der Generationen 2-4 als neuartige siRNA-Delivery-Systeme bezüglich ihrer physikalisch-chemischer und biologischer *in vitro* und *in vivo* Eigenschaften untersucht und diskutiert. In diesem Kapitel wurden die thermodynamische Eigenschaften durch molekulare Modellierung simuliert, und der Einfluss der Flexibilität wurde systematisch untersucht und diskutiert.

In Kapitel 7 wurden neuartige bioabbaubare und biokompatible Polymere der Zusammensetzung Poly (PEG-co-(BMDO-co-DMAEMA)) für die Gen-Transfektion erfolgreich bezüglich ihrer physikalisch-chemischen und *in vitro* biologischen Eigenschaften charakterisiert. Die quarternierten Copolymere zeigten niedrige Zytotoxizität als die quarternisierten Copolymere sowie positive Ergebnisse in der DNA-Transfektion *in vitro*.

Weiterentwicklungen der beschriebenen nicht-virale Gen-Transfektion-Systeme sind immer denkbar. In Kapitel 2 haben wir die Komplexbildung und den Aggregationsmechanismus von Nucleinsäuren mit Polykationen auf atomarer und molekularer Ebene untersucht. In diesem Projekt wurden molekulare Modellierung, molekulardynamische Simulation, isotherme Titrationskalorimetrie und andere Charakterisierungsmethoden angewendet. Trotzdem besteht immer Bedarf für neue Untersuchungsmethoden zur Charakterisierung der pDNA- oder siRNA-Lokalisierung innerhalb der Komplexe. Es ist daher sinnvoll, neue mikroskopische Methoden weiterzuentwickeln.

In Kapitel 3 haben wir anhand der Untersuchung des Einflusses der Kupplungsdichten von PCL-b-PEG-Ketten auf physikalisch-chemische Eigenschaften, DNA-Komplexbildung und Transfektionseffizienz gefunden, dass der „endosomal escape“ eine sehr wichtige Rolle für die Gen-Transfektion spielt. Und ein Design oder eine Optimierung des Polymers mit einer höherer Puffer-Kapazität könnte sich in Zukunft als sehr sinnvoller weisen.

In Kapitel 3-5 werden die Copolymer hy-PEI-g-(PCL-b-PEG)<sub>n</sub> als neuartige Transfektionpolymere beschrieben. In dieser Untersuchung wurden nur Copolymere mit kurzen PCL-Segmenten

(Gewicht von 570 Da) untersucht. Es wäre daher noch sehr interessant, den Einfluss der langen PCL-Segmente in dieser Struktur zu diskutieren.

In Kapitel 5 wurden Folsäure-gekoppelte PEI-g-PCL-b-PEG-Konjugate charakterisiert, und verbesserte pDNA Transfektion wurde beobachtet im Vergleich mit unmodifiziertem Polymer. Die beschriebenen Vektoren mit Targeting-Liganden sind sicherlich wert, Weiter *in vivo* für siRNA untersucht zu werden, welches besonders sinnvoll wäre für die Entwicklung der Gentransfektion in der Lunge.

Kationische Quantenpunkte (QDs) können für die weitere Untersuchung der siRNA-Freisetzung benutzt werden. Der Fluoreszenz-Resonanz-Energie-Transfer (FRET) Effekt zwischen fluoreszenzmarkierter siRNA und mit QDs geladenen Polymeren könnte nachgewiesen werden, wenn die siRNA innerhalb der Polymere kondensiert wird.

Diese multifunktionalen Gen-Transport-Systeme mit höherer siRNA-Verkapselung und höherem Schutz-Effizienz, besserer Biokompatibilität und Transfektionseffizienz sowie zusätzlichem Targeting-Effekt und langer Blutzirkulation sind jedoch eine Herausforderung für das Gebiet der Genetherapie innerhalb der Krebsforschung. Die “magic bullet” Vision von Paul Ehrlich vor über 100 Jahren beginnt sich bei fortgesetzter Forschung und Entwicklung zu verwirklichen.

## 9 APPENDICES

### 9.1 Abbreviations

2'OMe	2'O-Methoxy-
AFM	Atomic Force Microscopy
ANOVA	Analysis of Variance
AUC	Area under the Curve
CLSM	Confocal Laser Scanning Microscopy
DLS	Dynamic Light Scattering
DTPA	Diethylenetriaminepentaacetic Acid
dsRNA	Double-Stranded RNA
EGFP	Enhanced Green Fluorescent Protein
EPR	Enhanced Permeability and Retention
FACS	Fluorescence Assisted Cell Sorting
FITC	Fluorescein-Isothiocyanate
FOL	folate acids
HEPES	2-[4-(2-Hydroxyethyl)-1-piperazinyl]ethanesulfonic Acid
IC <sub>50</sub>	Half-Inhibitory Concentration
LMW	Low Molecular Weight
MTT	3-(4,5-Dimethylthiazol-2-yl)-2,5-diphenyltetrazolium Bromide
N/P	Nitrogen to Phosphate Ratio
PBS	Phosphate Buffered Saline
PCR	Polymerase Chain Reaction
pDNA	Plasmid DNA
PAMAM	Polyamidoamine
PEG	Polyethyleneglycol
PEI	Polyethylenimine
PDI	Polydispersity Index
PLGA	poly(lactic- <i>co</i> -glycolic acid)
RISC	RNA Induced Silencing Complex

RNAi

RNA Interference

siRNA

Short Interfering RNA

SPECT

Single Photon Emission Computed Tomography

## 9.2 List of Publications

### 9.2.1 Articles

1. Zheng, M. Y.; Liu, Y.; Samsonova, O.; Endres, T.; Merkel, O.; Kissel, T., Amphiphilic and biodegradable hy-PEI-g-PCL-b-PEG copolymers efficiently mediate transgene expression depending on their graft density. *International Journal of Pharmaceutics* **2012**, *427* (1), 80-87.  
(contributed equally first authors)
2. Zheng, M.; Pavan, G. M.; Neeb, M.; Schaper, K., A.; Danani, A.; Klebe, G.; Merkel, M. O.; Kissel, T.: Targeting the blind spot of polycationic nanocarrier-based siRNA delivery (*Submitted to ACS Nano*, **2012**)
3. Zheng, M.; Merkel, M. O.; Librizzi, D.; Kilic, A.; Liu, Y.; Renz, H.; Kissel, T.: Enhancing in vivo long-circulating and siRNA delivery efficiency of biodegradable high grafted hy-PEI-g-PCL-b-PEG copolymers (*Accepted by Biomaterials*, **2012**)
4. Zhang, Y.; Zheng, M.; Kissel, T.; Agarwal, S., Design and biophysical characterization of bioresponsive degradable poly(dimethylaminoethyl methacrylate) based polymers for in vitro DNA transfection. *Biomacromolecules* **2012**, *13* (2), 313-22.  
(contributed equally first authors)
5. Liu, L.; Zheng, M.; Renette, T.; Kissel, T., Modular Synthesis of Folate Conjugated Ternary Copolymers: Polyethylenimine-graft-Polycaprolactone-block-Poly(ethylene glycol)-Folate for Targeted Gene Delivery. *Bioconjug Chem* **2012**.  
(contributed equally first authors)
6. Merkel, O. M.; Zheng, M. Y.; Mintzer, M. A.; Pavan, G. M.; Librizzi, D.; Maly, M.; Hoffken, H.; Danani, A.; Simanek, E. E.; Kissel, T., Molecular modeling and in vivo imaging can identify successful flexible triazine dendrimer-based siRNA delivery systems. *Journal of Controlled Release* **2011**, *153* (1), 23-33.  
(contributed equally first authors)
7. Merkel, O. M.; Zheng, M.; Debus, H.; Kissel, T., Pulmonary gene delivery using polymeric nonviral vectors. *Bioconjug Chem* **2011**, *23* (1), 3-20.
8. Endres, T.; Zheng, M.; Beck-Broichsitter, M.; Kissel, T., Lyophilised ready-to-use formulations of PEG-PCL-PEI nano-carriers for siRNA delivery. *Int J Pharm* **2012**, *428* (1-2), 121-4.

9. Endres, T.; Zheng, M.; Beck-Broichsitter, M.; Samsonova, O.; Debus, H.; Kissel, T., Optimising the self-assembly of siRNA loaded PEG-PCL-IPEI nano-carriers employing different preparation techniques. *J Control Release* **2012**.
10. Merkel, O. M.; Beyerle, A.; Beckmann, B. M.; Zheng, M. Y.; Hartmann, R. K.; Stoger, T.; Kissel, T. H., Polymer-related off-target effects in non-viral siRNA delivery. *Biomaterials* **2011**, 32 (9), 2388-2398.
11. Mattheis, C.; Zheng, M. Y.; Agarwal, S., Closing One of the Last Gaps in Polyionene Compositions: Alkyloxyethylammonium Ionen as Fast-Acting Biocides. *Macromolecular Bioscience* **2012**, 12 (3), 341-349.
12. Zheng, M.; Kissel, T.; Agarwal, S.: Gentherapie ohne Nebenwirkung-Neuartige Biopolymere helfen bei der Gentransfektion  
*Laborpraxis*, Juni, **2011**

## 9.2.2 Poster Presentations

Mengyao Zheng, Yu Liu, Olga Samsonova, Thomas Endres, Olivia Merkel, and Thomas Kissel: Amphiphilic and biodegradable hy-PEI-g-PCL-b-PEG copolymers efficiently mediate transgene expression depending on their graft density, Jahrestagung der Deutschen Pharmazeutischen Gesellschaft e.V., Braunschweig, Germany, 4-6 October 6, 2010

Olivia Merkel, Mengyao Zheng, Meredith Mintzer, Giovanni Pavan, Damiano Librizzi, Eric Simanek, Thomas Kissel: Molecular modeling and in vivo imaging can identify successful flexible triazine dendrimer-based siRNA delivery systems, Controlled Release Society Local Chapter Meeting Germany , Jena, Germany, 15-16 March, 2011

Li Liu, Mengyao Zheng, Markus Benfer, Thomas Kissel: Multifunctional nano carrier based on PEI-g-PCL-b-PEG-folate for targeted gene delivery. the 3rd European Science Foundation Summer School" Nanomedicine 2011 ", Lutherstadt Wittenberg, Germany, 19-24 June 2011

Mengyao Zheng, Olivia M. Merkel, Damiano Librizzi, Thomas Kissel: Enhancing in vivo long-circulating and siRNA delivery efficiency of biodegradable high grafted hy-PEI-g-PCL-b-PEG copolymers, International Conference on Nanoscience & Technology, China 2011, Beijing, China, 7-9 September, 2011

Mengyao Zheng, Li Liu, Damiano Librizzi, Thomas Renette, Olivia M. Merkel, Thomas Kissel: Folate conjugated copolymer (Fol-PEG-PCL-hyPEI) for efficient and targeted in vitro and in vivo siRNA delivery, Controlled Release Society Local Chapter Meeting Germany, Wuerzburg, Germany, March 29-30, 2012

### **9.2.3 Lectures**

Mengyao Zheng, Olivia Merkel, Manuel Neeb, Michael Hellwig, Thomas Kissel: Structural Conformations and Nucleic Acid Location within Amphiphilic hy-PEI-PCL-mPEG Complexes as Non-Viral Vectors, Lecture, Controlled Release Society Local Chapter Meeting Germany, Jena, Germany, March 15-16, 2011

### **9.2.4 Abstracts**

Li Liu, Mengyao Zheng, Markus Benfer, Thomas Kissel: Multifunctional nano carrier based on PEI-g-PCL-b-PEG-folate for targeted gene delivery. the 3rd European Science Foundation Summer School "Nanomedicine 2011", Lutherstadt Wittenberg, Germany, 19-24 June 2011

Mengyao Zheng, Olivia M. Merkel, Damiano Librizzi, Thomas Kissel: Enhancing in vivo long-circulating and siRNA delivery efficiency of biodegradable high grafted hy-PEI-g-PCL-b-PEG copolymers, International Conference on Nanoscience & Technology, China 2011, Beijing, China, 7-9 September, 2011

Mengyao Zheng, Li Liu, Damiano Librizzi, Thomas Renette, Olivia M. Merkel, Thomas Kissel: Folate conjugated copolymer (Fol-PEG-PCL-hyPEI) for efficient and targeted in vitro and in vivo siRNA delivery, Controlled Release Society Local Chapter Meeting Germany, Wuerzburg, Germany, March 29-30, 2012

Mengyao Zheng, Yu Liu, Olga Samsonova, Thomas Endres, Olivia Merkel, and Thomas Kissel: Amphiphilic and biodegradable hy-PEI-g-PCL-b-PEG copolymers efficiently mediate transgene expression depending on their

graft density, 8th World Meeting on Pharmaceutics, Biopharmaceutics and Pharmaceutical Technology, Istanbul, Turkey 19<sup>th</sup> to 22<sup>nd</sup> March, 2012

### 9.3 Curriculum Vitae

#### Persönliche Daten

Name: Mengyao Zheng  
Geburtsdatum: 17.02.1983  
Geburtsort: Beijing, China  
Staatsangehörigkeit: Chinesisch  
Anschrift: Wehrdaer Weg 3, 35037 Marburg  
E-Mail: [mengyao\\_zheng@hotmail.com](mailto:mengyao_zheng@hotmail.com)

#### Ausbildung und Berufspraxis

Jul. 2001	Abitur, Gymnasium, Beijing, China (Note: sehr gut)
Sep. 2001 – Apr. 2003	Peking Pädagogische Universität (China), Fachbereich Chemie
Apr. 2004 – Jul. 2004	Philipps-Universität Marburg, Fachbereich Chemie
Oct. 2004 – Oct. 2009	Philipps-Universität Marburg Fachbereich Pharmazie
Feb. 2009	Wahlpflichtpraktikum, Institut für Pharmazeutische Chemie, Philipps-Universität, Marburg: Isolierung und Charakterisierung rekombinanter RNA- und DNA-Polymerasen
Oct. 2009	2. Abschnitt der Pharmazeutischen Prüfung
Sep. 2010	Diplomverteidigung (Note: sehr gut)
Jan. 2010-jetzt	Promotion; Wissenschaftliche Mitarbeiterin im Institut für Pharmazeutische Technologie und Biopharmazie, Philipps-Universität Marburg

## 9.4 Danksagung

Mein ganz besonderer Dank gilt meinem Doktorvater Herrn Prof. Dr. Thomas Kissel.

Vor allem möchte ich mich für das mir entgegengebrachte Vertrauen und Ermutigungen bedanken, wodurch ich mich selbst weiterentwickeln konnte. Ihre immer wieder überraschende Ideen, interessante Diskussionen sowie Ihr großer Erfahrungsschatz haben bewirkt, dass mir den Weg in die Forschung gebahnt. Von Ihnen habe ich gelernt, wie wichtig die Kreativität und Leidenschaft für die Forschung sind. Auf der anderen Seite, man muss auch dazwischen selbst denken und Erfahrungen sammeln, um das nicht realistische Konzept und den unnötigen Fehler zu vermeiden. Herr Prof. Dr. Thomas Kissel stellt uns immer wertvolle gute Fragen, welche, in meiner Meinung, noch wichtiger als die Lösungen selbst sind. Ich möchte mich auch für alle die Freiheiten und die großartige Unterstützung bedanken, die ich zwischen meine Promotion genießen durfte.

Mein besonderer Dank gilt außerdem Frau Prof. Olivia M. Merkel. Frau Merkel hat mich eine Vielzahl an Methoden beigebracht. Für die überraschende Ideen, interessante Diskussionen sowie hilfreiche Unterstützung vom ersten bis zum letzten Tag möchte ich mich ganz besonders herzlich bei Frau Merkel bedanken. Ihre Kreativität, Aktivität, Forschungsleidenschaft und Durchführungsfähigkeit beeindruckten mich sehr.

Herrn Prof. Dr. Carsten Culmsee möchte ich einerseits für die Erstellung des Zweitgutachters, andererseits aber auch für die offene Unterhaltung und Vorschlägen bezüglich weiterer Karriereentwicklung nach dem 2. Staatsexam bedanken.

Außerdem möchte ich mich ganz besonders herzlich bei Herrn Prof. Andreas Greiner und Frau Prof. Seema Agarwal (Makromolekulare Chemie, Marburg) für das tolle Zusammenarbeit und Forschungsstipendium bedanken. Bei Frau Prof. Seema Agarwal möchte ich mich herzlich für die Synthese und viele interessante Ideen und Diskussionen bedanken. Zusätzlich bedanke ich mich auch bei der gesamten Gruppe für die äußerst gastfreundliche Aufnahme am Institut.

Mein besonderer Dank gilt außerdem Herrn Prof. Andreas K. Schaper und Herrn Michael Hellwig (Center of Material Science, Philipps Universität Marburg) for TEM imaging.

Bei Herrn Prof. Dr. Gerhard Klebe, Herrn Manuel Neeb und Herrn Dr. Adam Biela, möchte ich mich für die Nutzung von ITC-Geräten und die Unterstützung in Fragen und Diskussionen bedanken.



Bei Herrn Prof. Dr. Wolfgang Parak, Yu Xiang und Raimo Hartmann (Department of Physics, Philipps-Universität Marburg) möchte ich mich für die Unterstützung CLSM imaging bedanken.

Herzlich danken möchte ich auch Herrn Prof. Dr. Harald Renz, Herrn Dr. Holger Garn (Institute of Laboratory Medicine and Pathobiochemistry, Philipps Universität Marburg) und Frau Dr. Agnieszka Turowska sowie der gesamten Gruppe am BMFZ für die freundliche Aufnahme im Institut und für die lehrreiche und interessante Zusammenarbeit. Ohne die vielen etablierten Untersuchungsmethoden, die Aufarbeitung einer Vielzahl von Organproben sowie das Anfertigen mikroskopischer Präparate, wäre die Durchführung der *in vivo* Experimente nicht möglich gewesen.

Ganz besonders möchte ich mich bei Herrn Damiano Librizzi (Institut für Nuklearmedizin, Uni-Marburg) bedanken, die Tage und Nächte mit uns durchgearbeitet hat, um die *in vivo* Versuche möglich zu machen.

Bei Herrn Prof. Dr. Roland Hartmann, Herrn Dr. Arnold Grünweller, möchte ich mich für die Nutzung von Geräten und die Unterstützung in molekularbiologischen Fragen bedanken.

Mein Dank gilt besonders Frau Ayse Kilic für die Zusammenarbeit bezüglich Messung von FACS sowie der Transfektion in den T-Zellen. Ohne die vielen etablierten Untersuchungsmethoden, wäre die Durchführung der Experimente nicht möglich gewesen. Ebenso möchte ich mich für die vielen Diskussionen mit Frau Ayse Kilic bedanken, die mir oftmals neue Perspektiven eröffnet haben.

Ganz besonders möchte ich mich bei Herrn Dr. Giovanni M. Pavan für die ausgezeichnete Molecular dynamics simulation und weitere interessante Diskussion bedanken.

Allen Mitgliedern des Instituts für pharmazeutische Technologie und Biopharmazie bin ich zu größtem Dank verpflichtet. Ich danke Frau Eva Mohr für ihre Arbeit in der Zellkultur sowie die Organisation der Bestellungen für die Unterstützung in allen Fragen nach den Zellen.

Weiterhin möchte ich meinen Kollegen Julia Michaelis, Nadja Bege, Moritz Beck-Broichsitter, Markus Benfer, Heiko Debus, Thomas Endres, Tobias Lehardt, Dr. Dafeng Chu, Dr. Yu Liu, Dr. Li Liu, Nan Zhao, Thomas Renette, Susanne Rösler, Christoph Schweiger, Eyas Dayyoub und für die vielen gemeinsamen Stunden in der Uni und für die gemeinsamen Freizeitaktivitäten und Freundschaft ganz herzlich danken. Besonders hervorheben möchte ich die ehemaligen Kollegen Frau Dr. Olga Samsonova für die Vorstellung einigen Forschungsmethoden am Anfang meiner Promotion.

Von tiefstem Herzen möchte ich mich bei meiner Familie für die immerwährende Unterstützung,  
ihren Glauben an mich und ihre Liebe bedanken.